DRIVING FORCES OF TDP-43 PHASE TRANSITIONS AND THEIR PHYSIOLOGICAL AND PATHOLOGICAL CONSEQUENCES IN CELLS

Lara Aletta Gruijs da Silva

Graduate School of Systemic Neurosciences

LMU Munich

Dissertation at the
Graduate School of Systemic Neurosciences
Ludwig-Maximilians-Universität München

March, 2022

Supervisor
Prof. Dr. Dorothee Dormann
Institut für Molekulare Physiologie
Johannes Gutenberg-Universität Mainz, Biozentrum

First Reviewer: Prof. Dr. Dorothee Dormann
Second Reviewer: Dr. Bettina Schmid

Date of Submission: 11th March, 2022
Date of Defense: 21st June, 2022

I Table of content

II List of Abbreviations

Abbreviation	Description
ALS	Amyotrophic lateral sclerosis
ATP	Adenosine triphosphate
C9orf72	Chromosome 9 open reading frame 72
CK1δ or ε	Casein kinase 1 delta or epsilon
CK2	Casein kinase 2
CNS	Central nervous system
CTD	Carboxy terminal domain
CTFs	C-terminal TDP-43 fragments
DPRs	Dipeptide repeat proteins
FTD	Frontotemporal dementia
FUS	Fused in sarcoma
G3BP1	Ras GTPase activating protein (SH3 domain) binding protein 1 (also G3BP stress granule assembly factor 1)
hnRNP	Heterogeneous nuclear ribonucleoprotein
IDP	Intrinsically disordered protein
IDRs	Intrinsically disordered regions
LARKS	Low-complexity, aromatic-rich, kinked segments
LCD	Low complexity domain
LCRs	Low-complexity regions
LLPS	Liquid-liquid phase separation
lncRNA	Long noncoding RNAs

MADD	MAP Kinase Activating Death Domain
MALAT1	Metastasis Associated Lung Adenocarcinoma Transcript 1
MAPT	Microtubule-associated protein tau
MLO	Membraneless organelle
NEAT1	Nuclear-enriched abundant transcript 1
NLS	Nuclear localization signal
NTD	N-terminal domain or amino terminal domain
OPTN	Optineurin
PABP-1	Poly-A binding protein-1
POLDIP3 or SKAR	DNA Polymerase Delta Interacting Protein 3
PrLD	Prion-like domain
PTMs	Post-translational modifications
RBP	RNA-binding protein
RGG	Arginine (R) – glycine (G) - glycine (G)
RNP	Ribonucleoprotein
RRM	RNA recognition motif
SG	Stress granule
SLiMs	Short linear motifs
SOD1	Superoxide dismutase 1
SORT1	Sortilin 1
STAG2	Stromal Antigen 2
STMN2	Stathmin-2

TARDBP	TAR DNA binding protein
TDP-43	TAR DNA-binding protein of 43 kDa
TIA-1	T-cell-restricted intracellular antigen 1
TNIK	TRAF2 And NCK Interacting Kinase
TTBK1 or 2	Tau tubulin kinase 1 or 2
UBQLN2	Ubiquilin-2
UPS	Ubiquitin-proteasome system
VCP	Valosin containing protein

III List of Figures

Note that all pictures were created using Biorender.

IV Publications of the thesis

Sedimentation assays to assess the impact of post-translational modifications on phase separation of RNA-binding proteins in vitro and in cells

Lara A. Gruijs da Silva, Dorothee Dormann

Springer Nature, Methods in Molecular Biology (MiMB) series, chapter in an upcoming volume titled “Phase-Separated Biomolecular Condensates”.

Status: Accepted, In press

Disease-linked TDP-43 hyperphosphorylation suppresses TDP-43 condensation and aggregation

Lara A. Gruijs da Silva, Francesca Simonetti, Saskia Hutten, Henrick Riemenschneider, Erin L. Sternburg, Lisa M. Pietrek, Jakob Gebel, Volker Dötsch, Dieter Edbauer, Gerhard Hummer, Lukas S. Stelzl, Dorothee Dormann

The EMBO Journal (2022) e108443, doi: 10.15252/embj.2021108443

Post-translational modifications on RNA-binding proteins: accelerators, brakes, or passengers in neurodegeneration?

Erin L. Sternburg, Lara A. Gruijs da Silva, Dorothee Dormann

Review in Trends in Biochemical Sciences (2022) volume 47, doi: 10.1016/j.tibs.2021.07.004.

1 Summary

TDP-43 is a well-recognized RNA-binding protein (RBP) with a prion-like low complexity domain (LCD). It is known for being the main component of pathological aggregates in amyotrophic lateral sclerosis (ALS) and frontotemporal dementia (FTD) patients, and TDP-43 aggregates closely correlate with neurodegeneration. It is believed that the formation of pathological RBP-containing inclusions occurs as a result of aberrant liquid-liquid phase separation (LLPS) in membraneless organelles (MLOs), such as stress granules, where RBPs can reach high concentrations and consequently undergo a liquid-to-solid phase transition and form solid RBP inclusions. A highly recognized feature of TDP-43-positive aggregates is the hyperphosphorylation of serine residues in the C-terminal LCD of TDP-43. Antibodies specific for C-terminal TDP-43 phosphorylation sites only identify pathological inclusions, but not physiological nuclear TDP-43, therefore hyperphosphorylation is considered to be a pathological hallmark of TDP-43 proteinopathies and largely assumed to promote TDP-43 aggregation. To date, no molecular studies have been done focusing on how this disease-linked PTM alters TDP-43 phase separation and aggregation. Hence, the aim of this thesis was to address the role of C-terminal hyperphosphorylation on TDP-43 LLPS and subsequent aggregation.

In my thesis work, I established two simple methods, sedimentation assays *in vitro* and in cells, that based on the protein solubility allowed me to analyze the phase separation behavior of TDP-43 in the presence or absence of phosphorylation. Moreover, I could show that Casein kinase 1δ-mediated TDP-43 hyperphosphorylation or C-terminal phosphomimetic mutations strongly suppress TDP-43 phase separation and aggregation *in vitro*, and increase the dynamics and liquidity of TDP-43 condensates. This behavior was observed due to enhanced solvation of phosphomimetic residues that reduced homotypic interactions of TDP-43 low-complexity domains. Additionally, I could show that phosphomimetic substitutions do not interfere with nuclear import, localization or some RNA regulatory functions of TDP-43 in cells, but reduce the accumulation of TDP-43 in membraneless organelles, such as stress granules and stress induced nuclear bodies, and enhance its solubility in HeLa and neuronal cells. These data raise the hypothesis that TDP-43 hyperphosphorylation could be a protective cellular response to enhance TDP-43 solubility and counteract its aggregation.

2 Introduction

2.1 The ALS and FTD disease spectrum

Amyotrophic lateral sclerosis (ALS) also known as Lou Gehrig's disease is a neurodegenerative disease with an incidence of 1 to 2 per 100,000 per year and prevalence of 4 to 8 per 100,000 individuals (Logroscino *et al,* 2010). This disease syndrome is characterized by the progressive degeneration of both upper and lower motor neurons in the brain and spinal cord (Rowland & Shneider, 2001) (Figure 1). The primary clinical presentations of ALS are normally described as two defined types of onsets based on a patient's primary motor symptoms: the spinal or limb-onset disease, with muscle weakness and spasticity of the upper and lower limbs, and the bulbar-onset disease, with speech and swallowing complications (Kiernan *et al,* 2011) . After disease onset, ALS patients have an average survival of 2 to 5 years with respiratory failure as the main cause of death (Kiernan *et al,* 2011). Like other neurodegenerative diseases, ALS has so far remained uncurable. So far, Riluzole is the only approved drug for ALS patients, which has a limited but positive effect on patient survival (Lacomblez *et al,* 1996). This effect is considered to take place through the inhibition of glutamate release and consequent reduction of excitotoxicity in neurons (Doble, 1996; Wang *et al,* 2004b). Apart from this drug treatment, ALS therapy is mainly based on symptom management, nutrition, and respiratory assistance (van Damme *et al,* 2017).

Initially, ALS was considered a pure neuromuscular disease that affects the upper and lower motor neurons. However, neurological and pathological evidences emerged in the past decade showing that ALS patients not only present motor but also develop non-motor symptoms such as cognitive complications (van Es *et al,* 2017). Owing to the degeneration of frontal and temporal cortical neurons in the central nervous system (CNS), patients typically manifest perturbation in behavior and language functions (Figure 1). This cognitive deterioration has been reported to some degree in ~50% of the ALS cases during their disease progression. About 10% of these cases gather the clinical features of concomitant frontotemporal dementia (FTD) (van Damme *et al,* 2017), known by a subset of severe symptoms such as inappropriate social behavior, loss of self-control and severe apathy along with personality changes (Siddique & Siddique, 2021). Moreover, patients displaying both ALS and FTD show shortened life span when compared to pure ALS or FTD patients (Olney *et al,* 2005).

FTD is one of the most common dementias besides Alzheimer´s disease, with a prevalence of 15 to 22 per 100.000 individuals per year (Onyike & Diehl-Schmid, 2013). There are two major subsets of FTD based on the patients' clinical phenotypes. Some develop behavioral decline (behavioral variant, bvFTD), while others present language dysfunction (primary progressive aphasia, PPA) (Warren *et al,* 2013). After disease onset, a substantial proportion of FTD patients typically survive for over a decade and eventually die due to secondary complications (Warren *et al,* 2013; van Engelen *et al,* 2020). Like for ALS, there are currently no effective therapies for the treatment or halt of FTD (Elia *et al,* 2020).

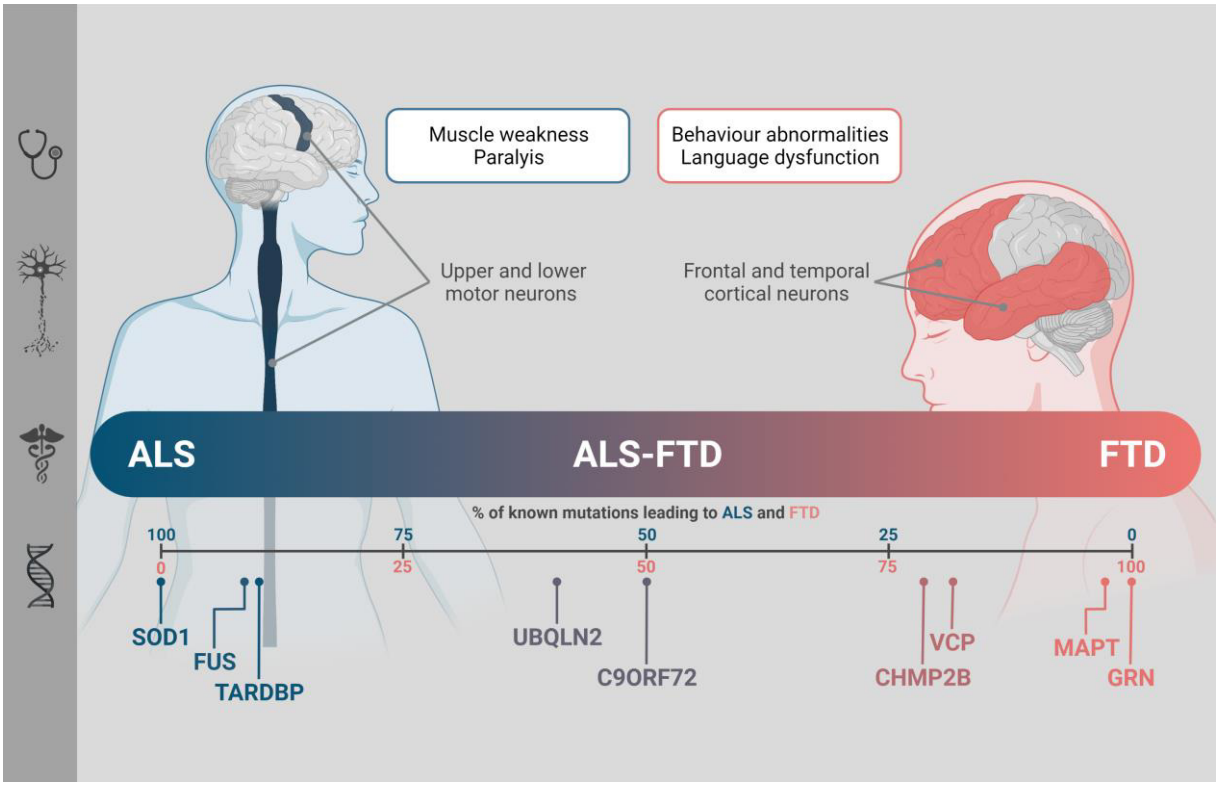

Figure 1. Clinical and genetic overlap of ALS and FTD.

ALS (in blue) and FTD (in red) correspond to extreme ends of a continuous neurodegenerative syndrome with overlapping clinical phenotypes. The symbols on the left from top to bottom represent: the clinical phenotypes, affected neurons, the disease spectrum, and the implicated genetic mutations. ALS, amyotrophic lateral sclerosis; FTD, frontotemporal dementia; *SOD1*, *superoxide dismutase 1*; *FUS*, *fused in sarcoma*; *TARDBP*, *TAR DNA binding protein; UBQLN2*, *ubiquilin-2*; *C9orf72*, *chromosome 9 open reading frame 72*; *CHMP2B*, *charged multivesicular body protein 2B*; *VCP*, *valosin containing protein*; *MAPT*, *microtubule-associated protein tau*; *GRN*, *granulin*.

Interestingly, not only do some ALS patients show FTD-like symptoms, as described before, but also nearly 15% of FTD patients develop clear motor neuron signs and are diagnosed with ALS (Lomen-Hoerth *et al,* 2002).

This clinical overlap as well as the common genetic, pathological and biochemical features of ALS and FTD (described below) built evidence of a disease spectrum with overlapping characteristics.

2.2 Genetic contribution to ALS and FTD

A minority of ALS patients (~10%) develop familial disease (fALS) linked to the presence of specific gene mutations in the family. Yet, 90% of all ALS cases fall into the sporadic (sALS) category where no mendelian inheritance pattern can be detected, though in 5-10% of the sporadic cases causative mutations have been identified (Hardiman *et al,* 2017).

In 1993, the first ALS gene was identified with the discovery of mutations in the cytosolic *superoxide dismutase 1* (*SOD1*) gene (Rosen *et al,* 1993). Since then, several other genes have been implicated in familial ALS (Figure 1). Mutations in the *chromosome 9 open reading frame*

72 (*C9ORF72*) (DeJesus-Hernandez *et al,* 2011; Renton *et al,* 2011), *SOD1* (Rosen *et al,* 1993), *TAR DNA binding protein* (*TARDBP*) (Kabashi *et al,* 2008; Sreedharan *et al,* 2008) and *fused in sarcoma* (*FUS*) (Kwiatkowski *et al,* 2009; Vance *et al,* 2009) genes account for the most common mutated genes in ALS cases.

FTD, on the other hand, has a stronger genetic contribution with approximately 50% of the patients showing a familial history (Rohrer *et al,* 2009; Ling *et al,* 2013). The most frequent genetic causes of FTD are: mutations in *microtubule-associated protein tau* (*MAPT*) (Hutton *et al,* 1998), *granulin* (*GRN*) (Mackenzie *et al,* 2006) or *C9orf72* (DeJesus-Hernandez *et al,* 2011; Renton *et al,* 2011) genes (Figure 1).

Among the ALS and FTD associated genes, several functional subsets can be distinguished. Some genes encode for proteins known to function in RNA metabolism, others have functions in the protein quality control machinery or regulate the cytoskeletal dynamics in axon motor neurons. Even so, for most genetic variants the mechanism behind pathology remains puzzling and still needs to be determined. Most of the genetic mutations consist of missense substitutions, apart from the expansion of an intronic hexanucleotide repeat in the *C9orf72* gene. The latter, as mentioned before, is the major genetic cause of both ALS and FTD, and strongly correlated with the combined ALS/FTD phenotypes, further supporting the disease spectrum concept of both diseases. ALS/FTD patients carrying this genetic variant can have hundreds or even thousands of hexanucleotide repeats in the *C9orf72* gene, while healthy individuals usually only carry 2-22 repeats (Renton *et al,* 2011; DeJesus-Hernandez *et al,* 2011). Apart from *C9orf72*, there are also other common genetic causes that are rarer, e.g. mutations in the *ubiquilin-2* (*UBQLN2*) gene (Deng *et al,* 2011) (Figure 1).

Curiously, individual genetic mutations (e.g. *C9orf72* repeat expansion) may lead to different phenotypes and diseases (e.g. ALS, FTD, ALS/FTD, Alzheimer´s disease phenotypes and atypical Parkinsonism) (Boer *et al,* 2020; Cacace *et al,* 2013; Jiao *et al,* 2013; DeJesus-Hernandez *et al,* 2011). The mechanism behind these divergent effects is not clear, although there is evidence that genetics might interplay with environmental factors. Indeed, ALS has long been recognized as a multistep and multifactorial disease, where genetic mutations can be considered as triggers of the degenerative process, but cannot alone fully explain the pathologic process (Chiò *et al,* 2018; Vucic *et al,* 2020). This highlights the possible impact of epigenetic and environmental factors in ALS pathogenesis, yet not much information is available about possible implicated elements (Boer *et al,* 2020). Nevertheless, genetic studies and identification of genetic variants are an important piece to understand ALS pathology and the biological mechanisms behind it.

Besides causative mutations there are genetic modifiers that can increase ALS susceptibility or modify clinical phenotypes. The most well known in this category is *ataxin-2* (*ATXN2*), where the presence of intermediate polyglutamine expansions increase the risk of developing ALS (Elden *et al,* 2010).

2.3 Neuropathological phenotypes in ALS and FTD

One of the differences between ALS and FTD is the degree of brain tissue loss. In FTD, the degree of brain tissue loss is substantial, predominantly in the frontal and temporal lobes (Broe *et al,* 2003), while in ALS this is not so obvious, with only ~25% of patients showing atrophy in the motor cortex region (Chen & Ma, 2010).

The detection of protein aggregates or inclusions has long been established as a pathological hallmark in many neurodegenerative diseases, including ALS and FTD (Forman *et al,* 2004). In ALS, the normally nuclear TAR DNA-binding protein 43 (TDP-43), is often mislocalized and found accumulated in cytoplasmic inclusions in nearly all remaining motor neurons of most sALS cases, and some fALS patients (ALS-TDP, 97%) (Arai *et al,* 2006; Neumann *et al,* 2006) (Figure 2). The only exception is observed in ALS cases with SOD1 or FUS mutations, which instead feature SOD1 (ALS-SOD1, 2%) or FUS (ALS-FUS) positive aggregates (Mackenzie *et al,* 2007; Tan *et al,* 2007; Vance *et al,* 2009; Kwiatkowski *et al,* 2009) (Figure 2). In extremely rare ALS cases, other RNA binding proteins (RBPs), such as hnRNP A1 and hnRNP A2, have also been detected in pathological inclusions (Kim *et al,* 2013). In FTD one of the most commonly observed aggregated protein is also TDP-43 (FTD-TDP, ~50%), which shows a similar prevalence as Tau aggregates (FTD-Tau, ~50) (Figure 2). The remaining small portion of FTD neuropathological subtypes feature inclusions positive for FUS (FTD-FUS, ~9%) or ubiquitin-proteasome system markers (FTD-UPS, ~1%) (Lee *et al,* 2011) (Figure 2).

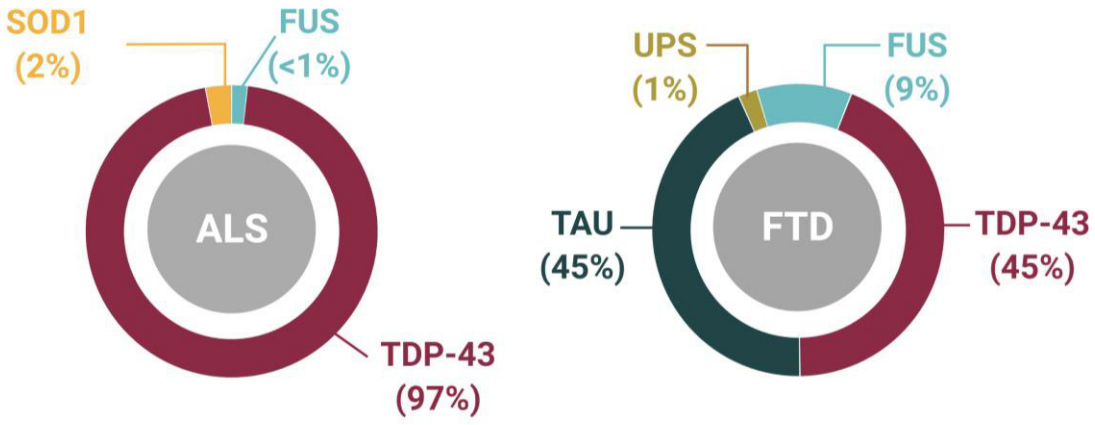

Figure 2. Pathological overlap and major proteins found aggregated in ALS and FTD.

Both ALS and FTD patients feature TDP-43 or FUS positive inclusions, with TDP-43 aggregates being the main pathological feature in both diseases. ALS and FTD diseases are named according to the main deposited protein, e.g. ALS-TDP, ALS-SOD, ALS-FUS, FTD-TDP, FTD-Tau, FTD-FUS. In a few cases of FTD, the main accumulated protein is unknown, therefore these cases are categorized as FTD-UPS, to indicate that aggregates are so fare only labelled by markers of the ubiquitin-proteasome system (UPS) (Mackenzie *et al,* 2010).

In addition to TDP-43 pathology, ALS and FTD patients with *C9orf72* hexanucleotide repeat expansion also show additional pathological features (Al-Sarraj *et al,* 2011; Stewart *et al,* 2012;

Vatsavayai *et al,* 2016). These features occur in the form of nuclear RNA foci, which result from bidirectional, sense (GGGGCC) and antisense (GGCCCC), transcription of hexanucleotide repeats (Lee *et al,* 2013; Haeusler *et al,* 2014), and cytosolic protein aggregates, positive for dipeptide repeat proteins (DPRs, namely glycine-arginine (GR), proline-arginine (PR), glycine-alanine (GA), glycine-proline (GP) and proline-alanine (PA)), which result from unconventional non-ATG translation of the expanded nucleotide repeats (Gendron *et al,* 2013; Ash *et al,* 2013; Gitler & Tsuiji, 2016).

Besides the main protein component of pathological aggregates, which as described above define the different neuropathological subtypes of ALS and FTD, inclusions are commonly positive for markers of both the proteasome and autophagy degradation systems, such as ubiquitin and p62 (Neumann *et al,* 2006; Arai *et al,* 2006; Forman *et al,* 2006; Bäumer *et al,* 2010; Neumann *et al,* 2009b; Al-Sarraj *et al,* 2011). Additionally, pathological inclusions positive for TDP-43 and FUS were also shown to co-localize with certain stress granule (SG) marker proteins. For instance, TDP-43 inclusions in ALS cases were shown to contain TIA1, PABP-1 and Staufen, while PABP-1 and eIF3 were found in TDP-43-positive inclusions in FTD patients (Bentmann *et al,* 2013). Inclusions in both ALS-FUS and FTD-FUS patients were demonstrated to be positive for eIF4G and PABP-1 (Dormann *et al,* 2010; Bäumer *et al,* 2010), but FUS-positive inclusions immunoreactive for TIA1 were only described in FTD-FUS cases (Fujita *et al,* 2008).

2.4 TDP-43 pathology in ALS and FTD

The identification of TDP-43 as an aggregating protein in ALS and FTD in 2006 was one of the major discoveries linking the two diseases (Arai *et al,* 2006; Neumann *et al,* 2006). In these studies, the authors discovered that TDP-43 is the major component of intracellular pathogenic aggregates in neurons and glia cells of ALS and FTD postmortem samples (Figure 3).

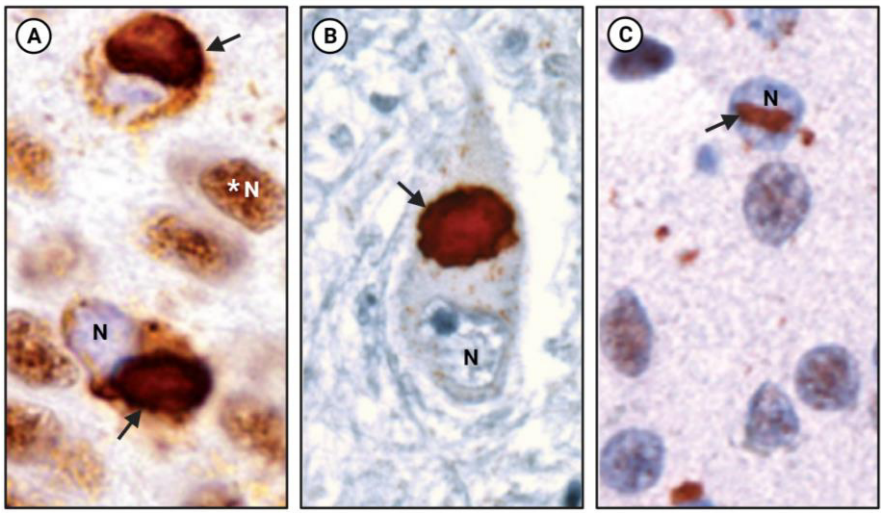

Figure 3. TDP-43 pathological inclusions in ALS and FTD.

In healthy conditions TDP-43 is mainly localized in the nucleus (*N). TDP-43 immunohistochemistry of *postmortem* patient samples of FTD brain neurons (A) and ALS motor neurons (B) showing cytoplasmic TDP-43 inclusions in the affected brain regions (arrows). (C) More rarely, TDP-43 inclusions can also be found in nuclei neurons (see arrow pointing to an intranuclear inclusion, N = nucleus). Figure (A) adapted from (Lee *et al,* 2011) and (B) and (C) from (Mackenzie *et al,* 2010) with permission from *Springer Nature* and *Elsevier*.

Remarkably, both familial and sporadic forms of ALS and FTD present pathological inclusions that are highly enriched in ubiquitinated, hyperphosphorylated and cleaved forms of TDP-43, predominantly observed in the cytosol of neuronal and glial cells (Arai *et al,* 2006; Neumann *et al,* 2006) (Figure 4). Additionally, TDP-43 deposition typically comes along with TDP-43 clearance from the nucleus, implying that both loss of nuclear TDP-43 functions and cytoplasmic gain-of-functions may contribute to neurotoxicity and consequent disease onset and progression (Robberecht & Philips, 2013).

Besides ALS and FTD, TDP-43 pathology has also been described in other neurodegenerative diseases (Cook *et al,* 2008). For instance, approximately 50% of Alzheimer´s disease cases also display TDP-43 pathology, which thus corresponds to the third most prevalent proteinopathy observed in Alzheimer patient brains (Arai *et al,* 2009). TDP-43 positive inclusions have also been reported as a prominent pathological feature in many cases of Parkinson and Huntington diseases (Gao *et al,* 2018).

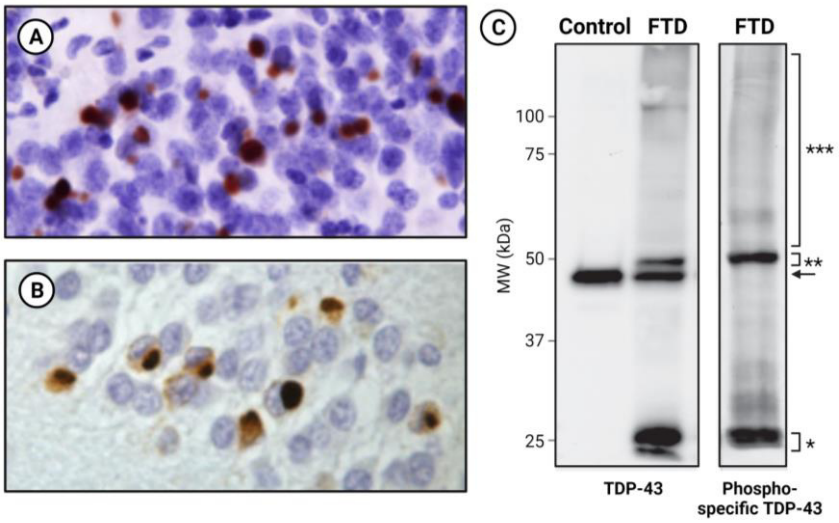

Figure 4. TDP-43 pathology and its biochemical signature.

TDP-43 immunohistochemistry of FTD-TDP *postmortem* patient brain samples showing ubiquitin (A) and phospho-TDP-43 (B) positive inclusions. (C) Immunoblot analysis of urea fractions isolated from postmortem brain tissue, displaying characteristic features of FTD-TDP that are not detected in controls. Typical pathological hallmarks include: a band of approximately 25 kDa (*) that corresponds to TDP-43 C-terminal fragments, a 45 kDa (**) band that corresponds to hyperphosphorylated TDP-43 and a high-molecular-weight smear (***) that corresponds to polyubiquitinated TDP-43. The arrow indicates the 43 kDa band that corresponds to unmodified TDP-43, which is present in both controls and in FTD-TDP patients. Immunoblot with a phospho-specific antibody (C, right) against phosphorylated serine residues 409 and 410 shows only the hyperphosphorylated pathological TDP-43. Figure (A) adapted from (Arai *et al,* 2006), (B) from (Neumann *et al,* 2009a) and (C) from (Mackenzie *et al,* 2010) with permission from *Elsevier* and *Springer Nature*.

The molecular mechanisms driving pathological aggregation of TDP-43 remains poorly understood, one possibility can be genetic mutations in TARDBP (see next section) or other genes (see section 2.2), hence likely different mechanisms contribute to driving it.

2.5 TARDBP gene mutations

Approximately 50 different missense mutations have been identified in the *TARDBP* gene in both familial and sporadic cases of ALS and FTD (Boer *et al,* 2020) (Figure 5). Notably, *TARDBP* mutations are a rare cause of dominant ALS with or without FTD and even more rare for FTD alone. These mutations are predominantly clustered in exon 6 of *TARDBP* which encodes for the glycine rich C-terminal domain of the protein. These mutations have been proposed to have diverse effects on the TDP-43 protein, such as: increase its propensity to aggregate; alter its protein stability; modify its protein-protein interactions; alter its subcellular localization (Buratti, 2015). Moreover, they were also shown to cause cytotoxicity in various animal models (Stallings *et al,* 2010; Ritson *et al,* 2010; Kabashi *et al,* 2010; Zhou *et al,* 2010). Together these diverse effects suggest that TARDBP mutations can trigger both toxic gain of function as well as loss of function mechanisms which may contribute to disease pathogenesis.

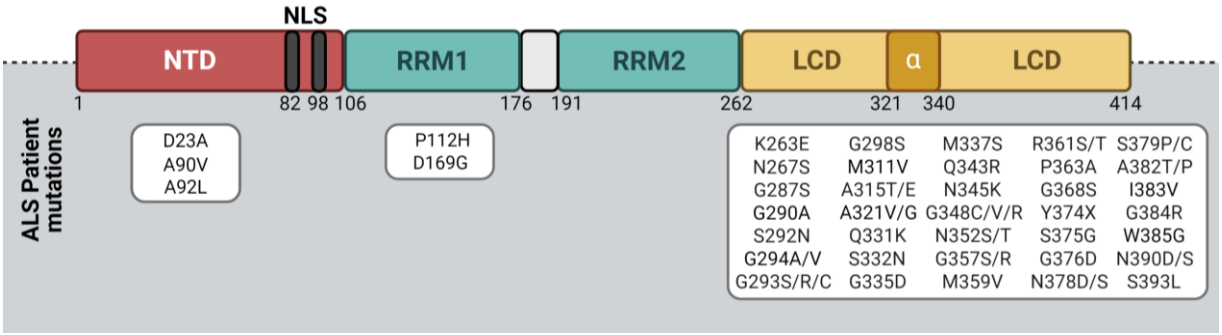

Figure 5. TDP-43 disease-causing mutations.

Top: simple schematic representation of TDP-43 domain structure. Bottom: TDP-43 ALS patient mutations and their distribution throughout the different protein domains. NTD, N-terminal domain; NLS, nuclear localization signal; RRM, RNA recognition motif; LCD, low complexity domain; α, alpha-helix. Figure adapted from (Sternburg *et al,* 2022) with journal author rights by *Elsevier*.

2.6 TDP-43 structure and physiological functions

TDP-43, as mentioned before, is the major aggregating protein in ALS and FTD patients. Therefore, research on TDP-43´s physiological and pathological functions has become of an important focus in the ALS and FTD field (e.g. how does TDP-43 aggregate and how is this process linked to neurodegeneration).

TDP-43 is an abundant and ubiquitously expressed protein predominantly localized in the nucleus. The protein is highly conserved in mammals and invertebrates and encoded by the *TARDBP* gene on chromosome 1 (Ayala *et al,* 2005; Wang *et al,* 2004a). TDP-43 is a DNA and RNA binding protein (RBP) initially discovered for its ability to regulate the *HIV-1* gene expression, through the binding of TDP-43 to the *trans*-active response (TAR) DNA region of the *HIV-1* DNA sequence (Ou *et al,* 1995), therefore its name. Since then, TDP-43 has also been shown to bind more than 6000 different RNA species, including coding and non-coding RNAs. It preferential binds to their 3´untranslational (UTR) and intronic regions and regulates

almost all aspects of RNA metabolism (Polymenidou *et al,* 2011; Tollervey *et al,* 2011; Xiao *et al,* 2011).

The ability of TDP-43 to bind DNA and RNA is mediated by two nucleotide binding domains termed RNA recognition motif 1 and 2 (RRM1 and RRM2) (Ayala *et al,* 2005) (Figure 6), which are common in the heterogeneous nuclear ribonucleoprotein (hnRNP) family and allow the binding to nucleic acids (Busch & Hertel, 2012; Dreyfuss *et al,* 2002). The binding of TDP-43 to RNA/DNA molecules is specific for short UG/TG repeat regions (Buratti *et al,* 2001; Ayala *et al,* 2005; Lukavsky *et al,* 2013; Kuo *et al,* 2014). The RRM1 of the protein has been shown to be indispensable for binding to single-stranded RNA with at least five UG repeats, and this affinity enhances with repeat length (Ayala *et al,* 2005). On the other hand, the function of RRM2 remains still vague, since it seems to not have a substantial role in RNA interaction. In fact, its affinity to RNA has been shown to be two times lower than that of RRM1 (Kuo *et al,* 2014).

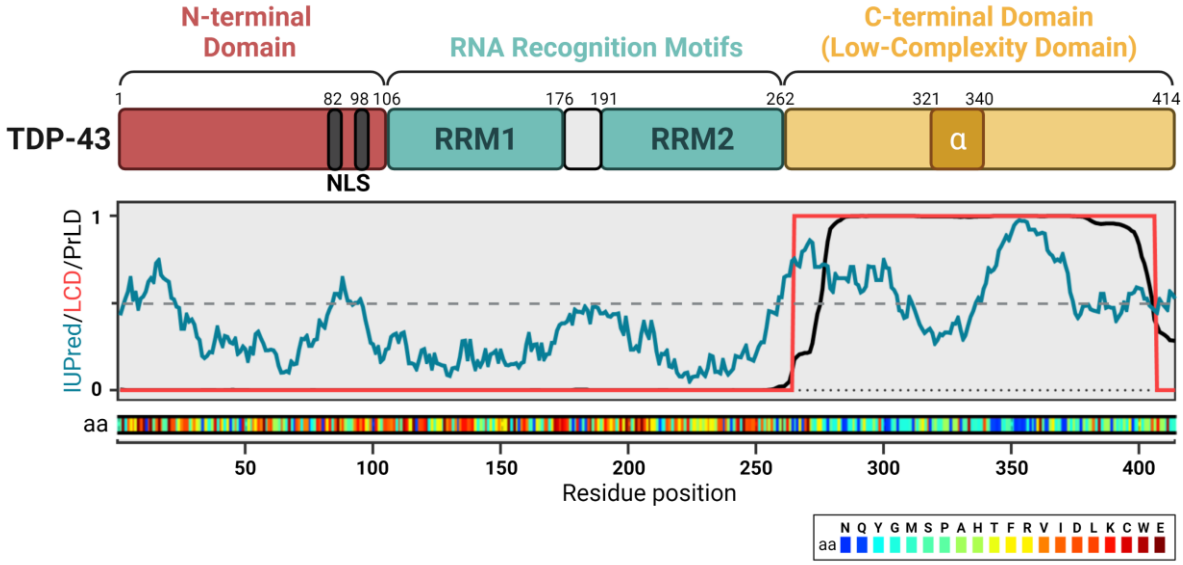

Figure 6. Schematic representation of TDP-43 domains and amino acid sequence patterns and features.

Top row: TDP-43 comprises several domains, a N-terminal domain (NTD), two RNA recognition motif domains (RRM1 and RRM2) and a C-terminal low complexity domain (LCD). Second row: (blue) prediction for intrinsically disordered regions using IUPred2A (Mészáros *et al,* 2018); (red) prediction for low-complexity regions (LCRs) using SEG, an algorithm based on amino acid segmentation (Wootton & Federhen, 1993); and (black) prediction for prion-like domains (PrLDs) using PLAAC (Lancaster *et al,* 2014). Third row: Colorful bars diagram showing the different amino acid composition of TDP-43 (color-coded as in the legend), an output from PLAAC predictor (Lancaster *et al,* 2014). NLS, nuclear localization signal; RRM, RNA recognition motif; α, alpha-helix; aa, amino acid.

Another important region for TDP-43 RNA associated functions is the glycine rich carboxy terminal domain (CTD) (Figure 6), which engages in protein-protein interactions with other RNA binding factors (Buratti *et al,* 2005). The abundance of glycine, serine, asparagine and glutamine acid residues and the consequent low amino acid variety gives this domain prion-

like and low complexity features (Figure 6). This region was also found to be responsible for TDP-43 recruitment into membraneless organelles (MLOs), such as stress granules (SGs) and ribonucleoprotein (RNP) transport granules (Freibaum *et al,* 2010; Bentmann *et al,* 2012) (Figure 7). In contrast to the RRMs, accepted as well folded domains, the CTD has two intrinsically disordered regions (Figure 6) separated by an alpha-helical structure shown to be involved in TDP-43 phase separation (Conicella *et al,* 2016) (see section 2.10 for further details). Furthermore, structural and functional experiments have shown that the TDP-43 amino terminal domain (NTD) mediates TDP-43 oligomerization (Chang *et al,* 2012; Afroz *et al,* 2017), which is required for TDP-43´s normal functions. Additionally, TDP-43 possesses a classical bipartite nuclear localization signal (NLS) in the NTD (Figure 6), which is recognized by the dimeric nuclear import receptor Importin α/β (Nishimura *et al,* 2010) and mediates TDP-43 nuclear import (Ayala *et al,* 2008; Ederle & Dormann, 2017).

TDP-43 plays a role in numerous molecular and cellular processes through its ability to regulate several aspects of RNA metabolism (Ratti & Buratti, 2016). As mentioned before TDP-43 was initially described as a transcription factor (Ou *et al,* 1995), yet its functions rapidly expanded to include regulation of pre-mRNA splicing, noncoding RNA processing, mRNA stability, mRNA transport and translation (Ratti & Buratti, 2016) (Figure 7).

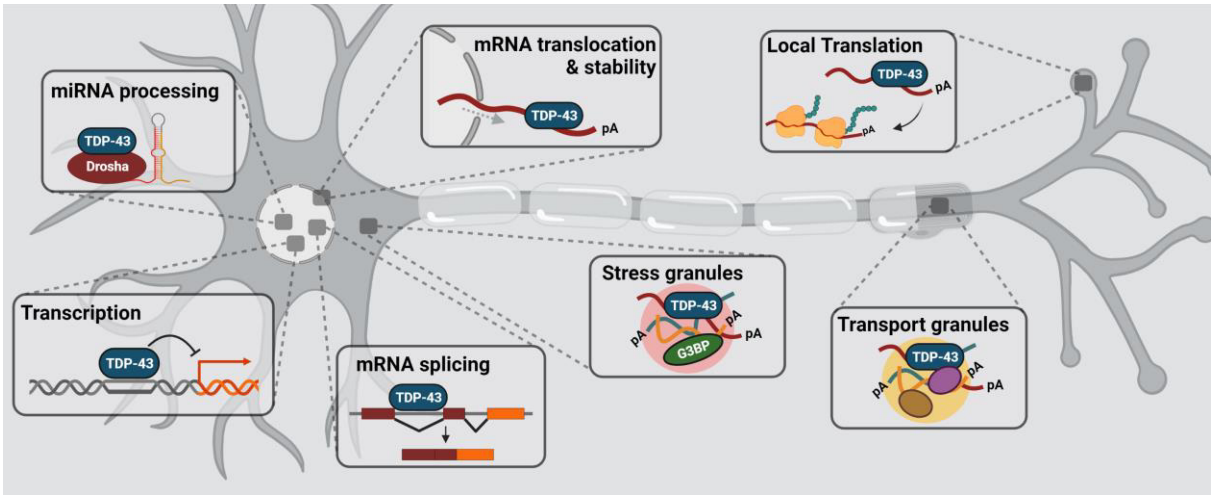

Figure 7. TDP-43 physiological functions.

TDP-43 participates in several mRNA related processes. In the nucleus, TDP-43 is involved in mRNA transcription and splicing regulation, as well as miRNA and lncRNA processing. In addition, TDP-43 is important for mRNA transport and stability. Even if predominantly located in the nucleus, TDP-43 is continuously shuttling between the nucleus and the cytoplasm. In the cytoplasm, TDP-43 participates in mRNA transport and translation as well as formation of stress granules (SGs) and ribonucleoprotein (RNP) transport granules.

The first involvement of TDP-43 in pre-mRNA splicing was described by (Buratti *et al,* 2001), with the finding that TDP-43 binds to UG repeats near the 3´splice site of the human cystic fibrosis transmembrane conductance regulator (*CFTR*) exon 9 and induces exon skipping. Meanwhile, many other direct TDP-43 splicing targets were identified in TDP-43 knockdown-based studies (e.g. *SKAR/POLDIP3*, *MADD*, *STAG2*, *SORT1* and *TNIK*) (Shiga *et al,* 2012; Fiesel *et al,* 2012; Polymenidou *et al,* 2011; Conti *et al,* 2015; Colombrita *et al,* 2015; Ratti &

Buratti, 2016; Fratta *et al,* 2018). Interestingly, among the splice targets of TDP-43 is also *TARDBP* mRNA, encoding for TDP-43 itself. This process allows TDP-43 to tightly regulate its own levels through an autoregulation feedback loop where splicing of an intron in its own 3´untranslated region directs its own transcript to nonsense mediated RNA degradation (Ayala *et al,* 2011; Polymenidou *et al,* 2011). Moreover, TDP-43 was also shown to repress the incorporation of cryptic exons into mRNA, avoiding cryptic exon interference with translation and consequent nonsense-mediated RNA decay (Ling *et al,* 2015). In fact, knockdown of TDP-43 was reported to induce aberrant processing of *stathmin-2* (*STMN2*) pre-mRNA, a microtubule-associated protein essential for normal axonal outgrowth and regeneration, by allowing the usage of a cryptic polyadenylation site that induces truncation of mRNAs encoding STMN2 (Melamed *et al,* 2019; Klim *et al,* 2019). More recently, TDP-43 depletion was also shown to induce robust inclusion of a cryptic exon within *UNC13A* (Ma *et al,* 2022; Brown *et al,* 2022), a well-known ALS/FTD risk gene essential for synaptic functions (van Es *et al,* 2009; Diekstra *et al,* 2014; Placek *et al,* 2019), causing nonsense-mediated decay and protein loss (Brown *et al,* 2022). In contrast to TDP-43 loss-of-function through aberrant inclusion of cryptic exons, splicing gain-of-function has also been described for certain C-terminal TDP-43 mutation variants (e.g. Q331K) in knock-in mouse models and patient-derived cells. This gain-of-function results from the skipping of constitutive exons, described as “skiptic exons”, which would normally be included in the mature mRNA. Interestingly, some examples of targeted genes are genes involved in the ubiquitin proteasome pathway (e.g. E3 Ubiquitin ligases), and the overall expression of these genes in C-terminal mutant TDP-43 models were shown to be downregulated, demonstrating that this induces changes in their expression levels (Fratta *et al,* 2018).

Besides controlling the fate of mRNAs, TDP-43 has also been shown to regulate the generation and processing of micro-RNAs (miRNA) and long noncoding RNAs (lncRNAs). Several studies have confirmed that TDP-43 depletion leads to the dysregulation of various miRNAs (Buratti *et al,* 2010; Kawahara & Mieda-Sato, 2012). In line with this notion, TDP-43 was found to control the levels and stability of Drosha and Dicer, two fundamental nucleases required for the miRNA maturation process, explaining how TDP-43 could affect miRNA biogenesis (Kawahara & Mieda-Sato, 2012; Freibaum *et al,* 2010). Additionally, TDP-43 was also shown to affect the expression of some lncRNAs, including MALAT1 (present in nuclear splicing speckles) and NEAT1 (vital for nuclear paraspeckle formation) (Tollervey *et al,* 2011).

Even though TDP-43 is predominantly localized in the nucleus, it can also be found in the cytosol where it exerts some of its RNA regulatory functions. One of these tasks is the regulation of mRNA stability. To this end, TDP-43 binds to the regulatory 3´UTR sequence of several mRNA transcripts and consequently controls their half-life (Sephton *et al,* 2011). Relevant examples include the human low molecular weight neurofilament (hNFL) (Strong *et al,* 2007) and the histone deacetylase HDAC6 (Fiesel *et al,* 2010) transcripts, which have crucial roles in neuronal viability.

TDP-43 is also known to play an important role in the transport of mRNAs into axons and dendrites, a fundamental process important for proper neuronal activity and synaptic plasticity (Wang *et al,* 2008; Alami *et al,* 2014).

Lastly, another emerging role of TDP-43 regards regulation of mRNA translation. There is evidence that TDP-43 participates in local translation at hippocampal neuron synapses, where TDP-43 behaves as a translational repressor (Wang *et al,* 2008). In line with this finding, a global proteomic study has revealed that TDP-43 interacts with several proteins of the translation machinery, such as ribosomal units and translation factors (Freibaum *et al,* 2010). A more recent study found that TDP-43 transports ribosomal protein mRNAs to regulate local translation in neuronal axons (Nagano *et al,* 2020).

Given all the different functions in mRNA metabolism and its high conservation throughout evolution, it is not surprising that TDP-43 has key roles in supporting cellular functions and survival. In fact, knockout of TDP-43 has been shown to be lethal during embryonic stages in transgenic mouse, zebrafish and fly models (Feiguin *et al,* 2009; Sephton *et al,* 2010; Kraemer *et al,* 2010; Schmid *et al,* 2013), supporting the idea that TDP-43 has an essential role during development.

2.7 Post-translational modifications of TDP-43 and their links to disease

More than 50% of all Eukaryotic proteins are, at some point during their life cycle (from translation to degradation), subjected to one or more modifications (Buratti, 2018). Protein post-translational modifications (PTMs) result normally from the addiction of a modifying chemical group that is covalently linked to an amino acid or are introduced by means of an enzymatic modification (Hoog & Mann, 2004). These PTMs can be reversible (e.g. phosphorylation, acetylation, and glycosylation) or irreversible (e.g. proteolysis). Nevertheless, all PTMs share the ability to quickly modify the structure and functional properties of proteins in reaction to cellular and environmental stimuli.

Likewise, TDP-43 undergoes a significant number of PTMs, such as phosphorylation, acetylation, oxidation, nitrosylation, ubiquitination, O-GlcNAcylation, and proteolysis (Figure 8) (reviewed in (Sternburg *et al,* 2022)). Most of them are linked to pathological TDP-43 and therefore a hallmark of TDP-43 proteinopathies (as mentioned before in section 2.4). Among them, proteolytic cleavage and consequent formation of C-terminal TDP-43 fragments (CTFs) of approximately 35 kDa and 25 kDa are one of the most common TDP-43 species observed in ALS and FTD brain inclusions (Igaz *et al,* 2008). In addition, aggregated CTFs are normally highly ubiquitinated and phosphorylated (Igaz *et al,* 2008). In cells and animal models CTFs have a high aggregate-prone nature, trapping essential cellular factors (e.g. transport factors) (Chou *et al,* 2018; Riemenschneider *et al,* 2021) and inducing cytotoxicity (Zhang *et al,* 2009; Yang *et al,* 2010).

Besides the main PTMs observed in ALS and FTD (TDP-43 hyperphosphorylation, ubiquitination and the formation of CTFs), there is evidence of more TDP-43 PTMs in disease. For instance, acetylated TDP-43 has also been identified in TDP-43 positive inclusions in ALS patient spinal cords (Cohen *et al,* 2015; Wang *et al,* 2017). Additionally, lysine acetylation within the RRM domains of TDP-43 (K136, K145 and K192) was shown to reduce RNA binding, which disrupts the regulation of TDP-43 RNA targets and leads to increased aggregation via

phase separation in cells (Cohen *et al,* 2015; Morato *et al,* 2020; Mann *et al,* 2019). Moreover, TDP-43 cysteine oxidation and nitrosylation have been observed in FTD patient brains (Cohen *et al,* 2012). In line with this observation, *in vitro* and in cell-based studies have shown that oxidative stress promotes TDP-43 cross-linking via disulphide bond and cysteine oxidation, which increases TDP-43 insolubility, aggregation and consequent neurotoxicity (Cohen *et al,* 2012; Pirie *et al,* 2021).

Apart from the described PTMs there is evidence that TDP-43 may also be subjected to additional PTMs (e.g. O-GlcNAcylation, sumoylation, etc.) (see www.phosphosite.org), although none of them have thus far been implicated in disease.

Also noteworthy is the fact that many disease-linked TDP-43 mutations modify known or putative PTM sites or create new ones (Figure 8), which could have an impact on the pathogenicity of the mutations.

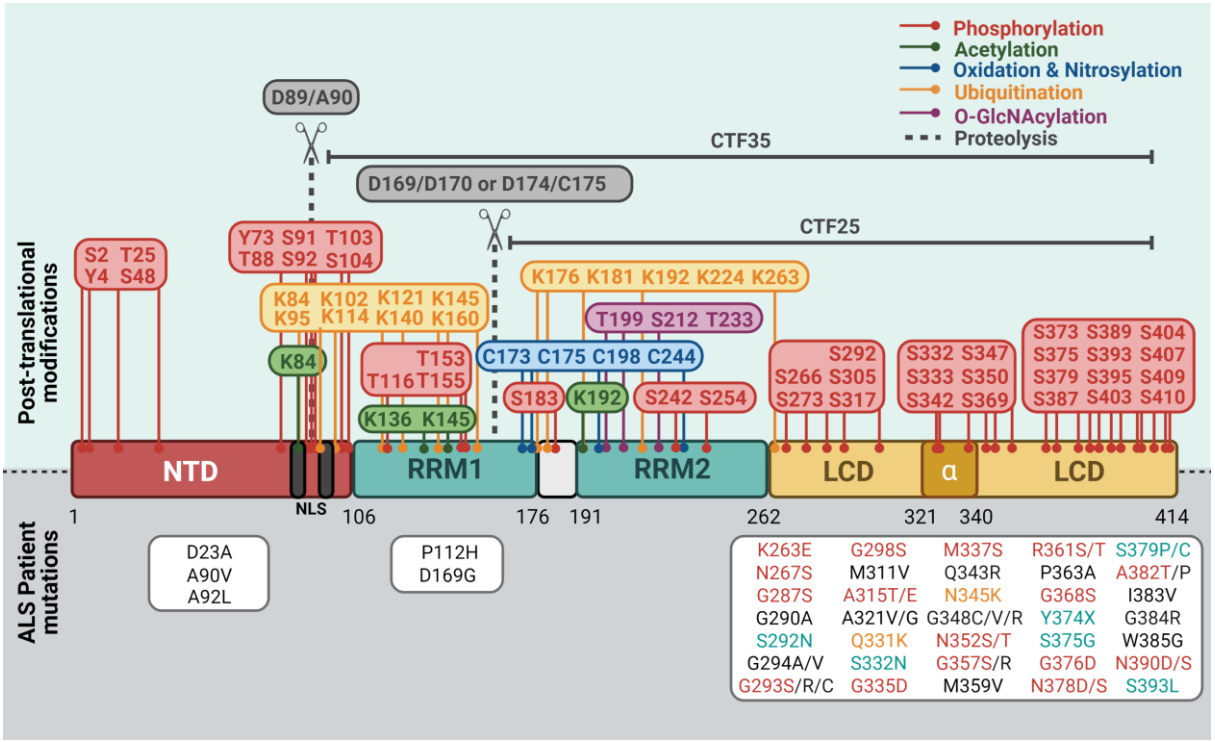

Figure 8. Post-translational modifications (PTMs) of TDP-43.

The top panel shows/lists all PTMs that have been mapped on TDP-43, most of these PTMs have been linked to disease. Phosphorylation and ubiquitination sites are from www.phosphosite.org. Acetylation sites are from (Cohen *et al,* 2015; Morato *et al,* 2020; Wang *et al,* 2017). Oxidation and nitrosylation sites are from (Cohen *et al,* 2012; Pirie *et al,* 2021). O-GlcNAcylation sites are from (Zhao *et al,* 2021). Proteolysis sites are from (Igaz *et al,* 2008; Igaz *et al,* 2009). The bottom panel highlights the ALS-linked TDP-43 mutations that create potential new acetylation or ubiquitination sites (in yellow), phosphomimetic or phosphorylation sites (in red) or delete potential phosphorylation sites (blue). NTD, N-terminal domain; NLS, nuclear localization signal; RRM, RNA recognition motif; LCD, low complexity domain; α, alpha-helix; CTF, C-terminal fragments. Figure adapted from (Sternburg *et al,* 2022) with journal author rights by *Elsevier*.

2.7.1 TDP-43 phosphorylation and responsible mediators

As mentioned before, atypical phosphorylation of TDP-43 has been identified as one of the most persistent and robust disease-linked PTMs and therefore is a key pathological hallmark of ALS and FTD spectrum diseases (Arai *et al,* 2006; Neumann *et al,* 2006; Hasegawa *et al,* 2008). In fact, phosphorylation of certain serine residues, such as S403/404 and S409/410, has been consistently identified in patients with TDP-43 pathology and is now used as a diagnostic tool to identify TDP-43 pathology in post-mortem brains of patients (Neumann *et al,* 2009a; Hasegawa *et al,* 2008; Inukai *et al,* 2008). TDP-43 has 8 tyrosine (Tyr, Y), 15 threonine (Thr, T) and 41 serine (Ser, S) residues that can potentially be phosphorylated (Figure 9). Indeed, further studies have reported several other serine residues being phosphorylated in disease. First, a mass spectrometry analysis of insoluble brain material of two ALS patients has revealed 17 phosphorylated S/T sites, of which 16 were located in the C-terminal LCD of the protein (Kametani *et al,* 2016). Additionally, several additional sites in the CTD were identified in ALS and FTD patients based on recognition with phospho-TDP-43-specific antibodies (Neumann *et al,* 2021; Neumann *et al,* 2009a) (Figure 9). Of these sites, S379, S403/404 and S409/410 have been consistently occurring and identified in disease by means of phosphorylation site-specific antibodies (Hasegawa *et al,* 2008), which detect pathological inclusions in patients, without detecting physiological nuclear TDP-43 (underlined sites in figure 9, bottom panel (red)). Taken all together, hyperphosphorylation of C-terminal serine residues in the LCD of TDP-43 has long been highlighted as one of the most common PTMs on pathological TDP-43.

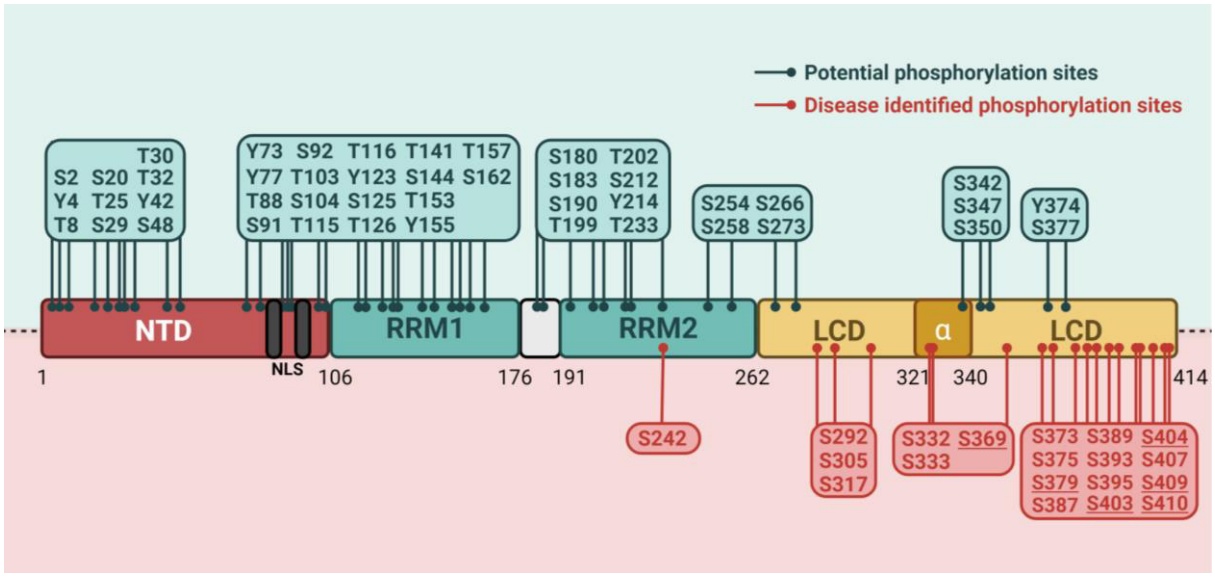

Figure 9. TDP-43 phosphorylation sites.

TDP-43 has 64 possible phosphorylation sites, and only a subset of the sites has so far been identified in ALS and FTD-TDP patients to be phosphorylated (bottom panel, red). Some of the modified sites in patients were identified using phosphorylation site-specific antibodies (underlined sites, bottom panel, red).

Moreover, approximately 20 of the disease-linked missense mutations have been identified to introduce a potential phosphorylation site (new Serine (S) or Threonine (T) residue), to delete

a phosphorylation site (elimination of S or tyrosine (Y) residue), or to create a phosphomimetic residue (Aspartic acid (D) and Glutamic acid (E)) (Figure 8, bottom panel), which may interfere with TDP-43 localization, aggregation, half-life, or protein-protein interactions and thus with protein fate (Buratti, 2015).

How TDP-43 phosphorylation is regulated during disease and which factors are responsible for it, is so far not clear. Nevertheless, six kinases have to date been shown to directly phosphorylate TDP-43 *in vitro*, in cultured cells, fly or *Caenorhabditis elegans*: casein kinase 1 delta (CK1δ) and epsilon (CK1ε), casein kinase 2 (CK2), tau tubulin kinase 1 (TTBK1) and 2 (TTBK2), cell division cycle 7 (CDC7) and p38α mitogen-activated protein kinase (MAPK) (Hasegawa *et al,* 2008; Nonaka *et al,* 2016; Kametani *et al,* 2009; Choksi *et al,* 2014; Carlomagno *et al,* 2014; Liachko *et al,* 2013; Liachko *et al,* 2014; Taylor *et al,* 2018; Aikio *et al,* 2021). In addition, dephosphorylation of TDP-43 has so far been reported by two phosphatases: calcineurin and protein phosphatase 1 (PP1) (Liachko *et al,* 2016; Gu *et al,* 2018). Some studies have found that, in cells and animal models, TDP-43 phosphorylation by CK1δ/ε or TTBK1/2 overexpression or calcineurin-mediated dephosphorylation inhibition cause aggregation of phosphorylated TDP-43, cytotoxicity and neurodegeneration (Nonaka *et al,* 2016; Choksi *et al,* 2014; Liachko *et al,* 2014; Taylor *et al,* 2018; Liachko *et al,* 2016). Consequently, the idea of using kinase inhibitors to counteract TDP-43 phosphorylation has been proposed as a possible therapeutic approach for TDP-43 proteinopathies such as ALS and FTD (Liachko *et al,* 2013; Salado *et al,* 2014; Martínez-González *et al,* 2020). In contrast to these findings, two other studies have shown that phosphomimetic mutations of Ser to aspartic acid (S2D or S5D) or glutamic acid residues (S5E) in C-terminal fragments of TDP-43 decrease aggregation propensity and toxicity in cells and transgenic *Drosophila* models (Li *et al,* 2011; Brady *et al,* 2011). The effect of phosphorylation on TDP-43 remains therefore, unclear, and largely controversial.

Generally unexplored is the understanding of the timing and the subcellular localization of TDP-43 phosphorylation during disease, but some studies in cellular models have demonstrated that TDP-43 insolubility and aggregation appears to precede TDP-43 phosphorylation (Li *et al,* 2011; Mann *et al,* 2019; Zhang *et al,* 2019; Dormann *et al,* 2009; Gasset-Rosa *et al,* 2019). This suggests that TDP-43 phosphorylation could be following TDP-43 insolubility and not the other way round, as proposed by the above mentioned studies.

2.8 Mechanisms of TDP-43 mislocalization and aggregation

2.8.1 Mechanisms of TDP-43 mislocalization to the cytoplasm

The detection of TDP-43 positive inclusions and mutations in the gene encoding for TDP-43 in ALS and FTD patients, support a causative role of TDP-43 dysfunction in these diseases. However, the reason why TDP-43 becomes mislocalized, dysfunctional and aggregated in these diseases is still not fully understood.

Normally, TDP-43 is predominantly found in the nucleus, yet pathological inclusions containing TDP-43 are mostly found in the cytosol (Neumann *et al,* 2006). This fact has given rise to the idea that possible defects in nuclear import of TDP-43 might be behind this pathological redistribution and might be responsible for increased TDP-43 concentrations in the cytosol (Dormann & Haass, 2011; Hutten & Dormann, 2020). How such a nuclear import defect could arise is not instantly obvious, given the fact that no mutations in the TDP-43 NLS have been observed, as is the case for example for FUS (Dormann *et al,* 2010; Vance *et al,* 2009; Kwiatkowski *et al,* 2009). Nevertheless, reduced levels or aggregation of nuclear import factors (e.g. Impα) have been reported in FTD-TDP-43 patients and proposed to contribute to TDP-43 mislocalization (Nishimura *et al,* 2010; Solomon *et al,* 2018). Additionally, various studies have linked the *C9orf72* repeat expansion with dysregulated nuclear transport (Jovičić *et al,* 2015; Zhang *et al,* 2015; Boeynaems *et al,* 2016; Solomon *et al,* 2018; Zhang *et al,* 2018; Hutten *et al,* 2020). For instance, unbiased genetic screens in yeast identified strong modulators of *C9orf72* toxicity, including a great number of modifier genes involved in nucleocytoplasmic transport (e.g. karyopherins, enzymes implicated in the Ran-mediated nucleocytoplasmic transport, and nuclear pore complex components) (Jovičić *et al,* 2015). Moreover, overexpression of some of these factors (e.g. Ran GTPase-activating protein 1 (RanGAP1) or importins) was shown to rescue *C9orf72* repeat expansion-induced toxicity, while downregulation enhanced toxicity in yeast and *Drosophila* models (Zhang *et al,* 2015; Boeynaems *et al,* 2016; Jovičić *et al,* 2016). These findings provide strong evidence that nucleocytoplasmic transport defects may play a critical role in disease initiation, by mislocalization and accumulation of RBPs in the cytoplasm. Nevertheless, once TDP-43 accumulates in the cytoplasm (e.g. by means of NLS mutations), TDP-43 remains soluble and homogeneously distributed (Ayala *et al,* 2011; Bentmann *et al,* 2012). This fact implies that mislocalization alone cannot cause TDP-43 aggregation. Therefore, in addition to transport defects, further steps are needed to explain this pathological cascade.

2.8.2 Stress granules as possible seeds of TDP-43 aggregates

Several studies have reported that disease-linked RBPs, such as TDP-43 and FUS, are recruited within stress-induced RNP granules called stress granules (SGs) upon cellular stress (Dormann *et al,* 2010; Bentmann *et al,* 2012; Liu-Yesucevitz *et al,* 2010). Moreover, TDP-43 and FUS aggregates in ALS and FTD patients were found to be frequently co-localized with SG marker proteins, such as TIA-1, G3BP1, PABP-1 (Bentmann *et al,* 2012; Dormann *et al,* 2010; Liu-Yesucevitz *et al,* 2010). These observations gave rise to the hypothesis that pathological RBP inclusions observed in these pathologies may evolve from SGs (Li *et al,* 2013).

SG formation is a sophisticated strategy of the cell to deal with several cellular stressors, such as heat/cold shock, osmotic and oxidative stress, hypoxia, viral infections, chemical exposures, UV irradiation, mitochondrial dysfunction and even aging (Anderson & Kedersha, 2006). SGs are formed temporarily in order to preserve energy and focus on cell survival and ultimate recovery. This way, during stress, cells are thought to repress the translation of mRNAs that are not essential for cell survival, through the condensation of most newly transcribed mRNAs and their associated RBPs into messenger ribonucleoprotein particles (mRNPs) (Li *et al,* 2013). Certain mRNAs that encode for chaperones or repair enzymes avoid being trapped in SGs in order to be preferentially translated during stress and help the cell to cope with stress (Kedersha *et al,* 2013; Anderson & Kedersha, 2006). SGs contain several components of the translational machinery and there is evidence that they function towards translation suppression. Some typical components are translational initiation factors (eIF family), 40S ribosomal subunits, poly-A mRNAs, SG nucleating RBPs (e.g. G3BPs, TIA-1), factors important for translational silencing, mRNA localization or degradation (e.g. Staufen) (Buchan & Parker, 2009), and passive clients recruited by their bound mRNAs (e.g. TDP-43, FUS, hnRNPs) (Bowden & Dormann, 2016).

SGs are dynamic and reversible compartments distinct from insoluble inclusions, that readily dissolve again upon recovery of stress. This way, when stress dissipates, all confiscated mRNAs and translation machinery are released and can return to their normal functions. On the other hand, persistent SGs have also been shown to be cleared by autophagy (Buchan *et al,* 2013; Maxwell *et al,* 2021).

Interestingly, it has been observed that the TDP-43 inclusions in ALS and FTD patients also contain protein markers of SGs (e.g. TIA-1, poly-A binding protein-1(PABP-1), G3BP1) (Volkening *et al,* 2009; Liu-Yesucevitz *et al,* 2010; Bentmann *et al,* 2012; McGurk *et al,* 2014). Based on this it has been hypothesized that SGs might be the precursors of pathological inclusions observed in ALS and FTD and other neurodegenerative diseases. Also supporting this idea, pathological FUS or SOD1 inclusions in ALS and FTD (Dormann *et al,* 2010; Bentmann *et al,* 2012; Miao & St Clair, 2009) and Tau positive inclusions in FTD and Alzheimer´s disease (Vanderweyde *et al,* 2012; Vanderweyde *et al,* 2016; Apicco *et al,* 2018) have likewise been shown to be positive for several SGs markers. Moreover, various studies demonstrated that NLS mutations that lead to cytosolic mislocalization of TDP-43 or FUS greatly enhance recruitment of these RBPs into SGs (Bentmann *et al,* 2012; Dormann *et al,* 2010). These mutations can trigger altered binding of SG components (e.g. G3BP1) as well as boost the number and size of SGs (Baron *et al,* 2013; Vance *et al,* 2013; Dewey *et al,* 2011; McDonald *et al,* 2011). These studies suggest that mislocalized TDP-43 and FUS can alter SG dynamics, possibly by engaging and trapping certain SG components, which may ultimately contribute to ALS and FTD pathology (Bowden & Dormann, 2016). Besides high concentration of these RBPs in SGs, additional potential triggers of aberrant SG dynamics and SG solidification could be genetic mutations, persistent stress, defects in the protein quality control (PQC) machinery or altered PTMs, by means of aberrant liquid-to-solid phase transitions (Note that this topic will be discussed in more detail in section 2.9.4).

Taken together, a nuclear transport defect (first pathological hit) followed by stress and SG formation (second pathological hit) and consequent recruitment of TDP-43 into SGs, may be required for formation of the typical TDP-43 pathology, raising the hypothesis that TDP-43 mislocalization and aggregation evolves via a “Two hit model” as suggested by (Dormann & Haass, 2011) (Figure 10).

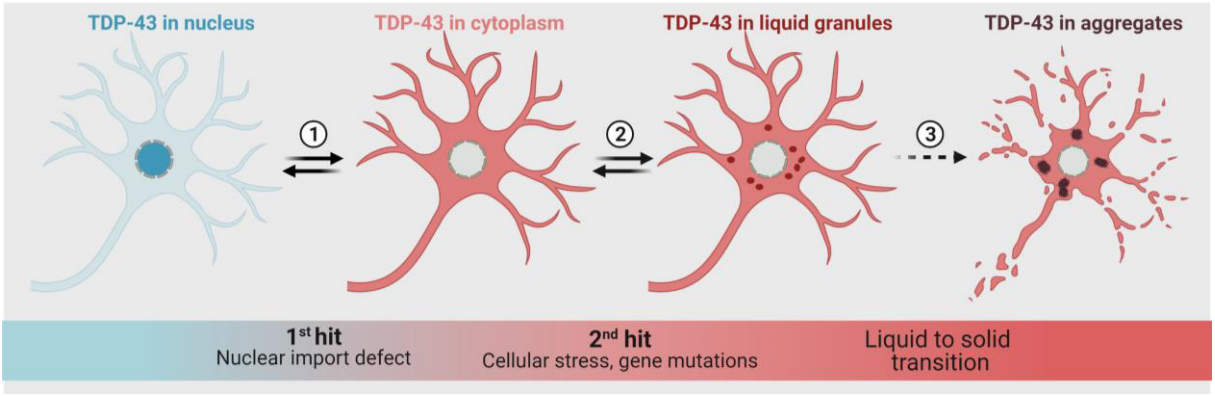

Figure 10. Two hit model of TDP-43 dysfunction in neurodegenerative diseases.
One hypothesis on how TDP-43 becomes dysfunctional in ALS and FTD is that TDP-43 mislocalization and aggregation arises via a ‘multiple hit’ process. First, a nuclear import defect, possibly through defects in the nuclear transport machinery, causes cytosolic mislocalization of TDP-43. Then additional stress (e.g. through external stressors, defects in protein quality control, additional mutations, etc.) can induce the recruitment of mislocalized TDP-43 into SGs or other ribonucleoprotein (RNP) granules. In case SGs are not reversible but undergo irreversible liquid-to-solid transitions, possibly favored by defects in chaperones or other defects in protein quality control, irreversible TDP-43 aggregates could rise. Figure adapted from (Sternburg *et al,* 2022) with journal author rights by *Elsevier*.

2.8.3 Disrupted Stress granule dynamics as potential contributor to neurodegeneration

How altered SG dynamics may contribute to cellular disturbances and neurodegeneration is still not clear, though several, mutually not exclusive, mechanisms have been proposed.

One possible mechanism is that solidification of SGs may lead to prolonged and irreversible suppression of translation of mRNAs essential for proper neuronal functions. Supporting this idea, some studies have shown that persistent oppression of translation by sequestration of phospho-eIF2α mRNA triggers synaptic loss and neurotoxicity (Moreno *et al,* 2013), as well as neuronal cell death following global brain ischemia (Jamison *et al,* 2008; Kayali *et al,* 2005).

Secondly, SG solidification, may cause toxic loss of function by trapping essential regulatory proteins, such as RBPs or translation factors, for a long period of time. For instance, prolonged sequestration of TDP-43 and FUS in solidified SGs might cause impairment of the proteins functions (e.g. regulation of transcription, splicing, mRNA localization and DNA damage repair) and consequently promote neurodegeneration (Bowden & Dormann, 2016).

Lastly, it has been proposed by Polymenidou and Cleveland that misfolded RBPs harboring prion-like domains may act as “seeds for neurodegeneration”, by inducing sequestration and

misfolding of their wild-type counterparts in SGs. Such a replication/transmissible mechanism has been reported for mutant FUS, with its ability to bind and recruit native endogenous FUS to SGs (Vance *et al,* 2013). Prion-like sequences allow the protein to assume a range of alternative structures (e.g. an intrinsically unfolded or an aggregated state) that are able of conformational self-replication by templating the conversion of other copies of the same protein (King *et al,* 2012). This effect is assumed to be boosted by high local concentration of proteins in SGs. Furthermore, such "seeds" may be transferred from cell to cell and induce templated misfolding and aggregation of RBPs in neighboring cells (Polymenidou & Cleveland, 2011). Supporting this hypothesis, some studies have showed that intracellular aggregation of TDP-43 can be initiated in cultured cells by transduction of *in vitro* prepared fibrillar aggregates (Furukawa *et al,* 2011; Gasset-Rosa *et al,* 2019), or exogenous application of conditioned medium comprising TDP-43 material derived from both cell cultured cells or ALS patient brain lysate (Feiler *et al,* 2015). Moreover, seeding of TDP-43 was also observed in vivo by intracerebral injections of active pathogenic seeds derived from FTD-TDP patients (Porta *et al,* 2018).

2.9 Stress granules and other membraneless compartments form through liquid-liquid phase separation (LLPS)

Cells are arranged into compartments called organelles. Classic organelles are well known for being delineated by a lipid bilayer membrane, which allows their physiochemical separation from the rest of the cell. Nevertheless, it is now clear that organelles can likewise exist without a membrane boundary. These are dubbed membraneless organelles (MLOs) or biomolecular condensates (Banani *et al,* 2017). MLOs are usually comprised of RNAs and RBPs and thus often called as RNP granules. Some examples of RNP granules are SGs, P bodies and germ granules in the cytoplasm, and paraspeckles, nucleoli and Cajal bodies in the nucleus (Courchaine *et al,* 2016; Banani *et al,* 2017; Gomes & Shorter, 2019) (Figure 11). Some MLOs occur in all cell types, whereas others are in fact specific for certain cell types. For instance, neurons show condensates that are exclusive to the axonal compartment (e.g. RNA transport granules) (Liao *et al,* 2019) and to the synapse (e.g. postsynaptic density) (Zeng *et al,* 2018). Another example of a cell-type specific MLO is the Balbiani body in oocytes. These are solid-like MLOs composed of an intrinsic disorder proteins (IDP) that forms solid-like condensates as well as membrane-bound organelles (mitochondria, ER and Golgi) and is essential for primordial germ cell formation in most non-mammalian vertebrate oocytes (Boke *et al,* 2016). RNP granules have important roles in RNA processing, such as RNA transport, storage, and degradation (Alberti *et al,* 2017). Together, membrane-less and membrane-bound organelles play crucial roles in biology allowing spatiotemporal control of biological reactions through the compartmentalization of macromolecules in the cell (Brangwynne *et al,* 2015).

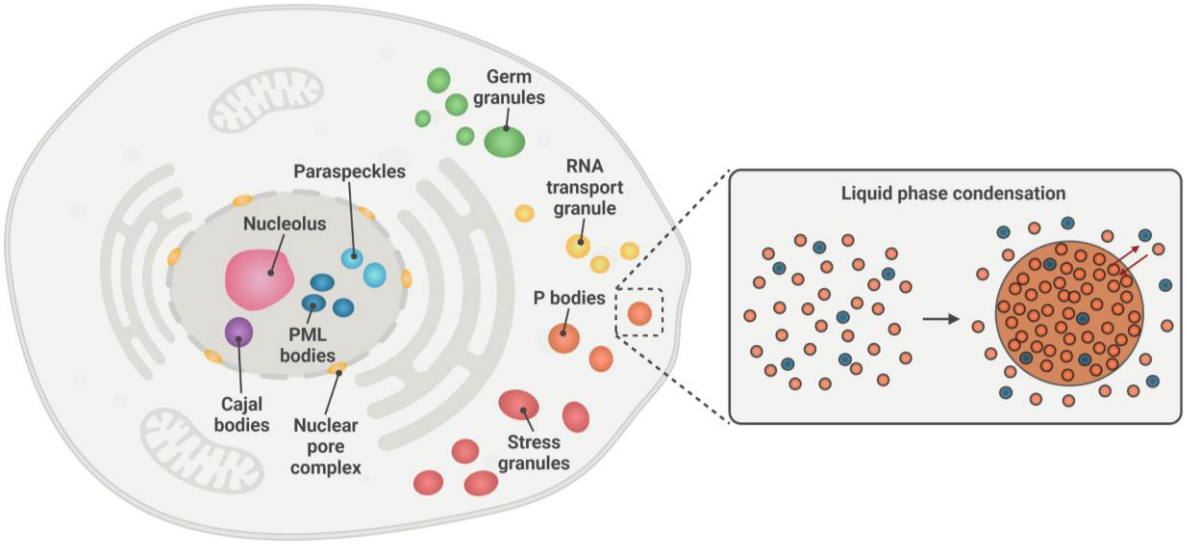

Figure 11. Cellular organization by membraneless organelles.

Illustrated here is a nonexhaustive list of different membraneless organelles (MLOs), also called biomolecular condensates, which can be detected in the nucleus, cytoplasm, and on membranes of eukaryotic cells (left). Each type of condensate is enriched in a distinct set of biomolecules that assemble through liquid-liquid phase separation into a dense phase (orange) featuring a high concentration of certain biomolecules, while excluding others (right).

2.9.1 Many membraneless organelles (MLOs) are liquid droplets

The mechanism how MLOs assemble specific biomolecular components into defined structures and provide a suitable environment for certain molecular reactions, has been suggested by studies of germline P granules in *C. elegans* (Brangwynne *et al,* 2009). In the early embryonic state, P granules asymmetrically localize to the posterior of the one-cell embryo, which are incorporated into the newborn germ cell upon cell division. This process was found to be mediated by a spatiotemporal transition from a soluble phase, where RNA and protein elements are diffuse in the cytoplasm, to a condensed phase, where these elements concentrate into P granules. Such P granules display features of liquid droplets, including drip off and wetting of cellular surfaces and fusion into larger droplets. Moreover, like any other liquids, these granules rapidly dissolve and condense (Brangwynne *et al,* 2009). This process suggests that formation and localization of P granules is regulated by classic liquid phase transition (Weber & Brangwynne, 2012). This behavior is not exclusive for P granules. Similarly, spontaneous phase separation has also been shown to drive the formation of other MLOs, such as nucleoli in *Xenopus* (Brangwynne *et al,* 2011) and SGs in mammalian cells (Patel *et al,* 2015) and yeast (Kroschwald *et al,* 2015). These findings suggested that liquid-liquid phase separation (LLPS) is a general biophysical process that triggers the assembly of membraneless organelles, such as RNP granules, in cells (Figure 11). LLPS is a type of phase transition that results from the spontaneous separation (“demixing”) of a homogenous solution of molecules into two coexisting liquid phases: a dense phase that concentrates the macromolecules and a dilute phase where they are depleted (Alberti, 2017).

2.9.2 Functional importance of intracellular phase separation

MLOs display distinct molecular composition, dimensionality, physical properties, cellular localization and function, nevertheless they all share common dynamicity, self-assembly and membraneless structure (Banani *et al,* 2017; Alberti *et al,* 2019). Biomolecular condensates can have an impact on innumerable biochemical processes within cells. For example, phase separation can stimulate biochemical interactions by bringing molecules into an optimally concentrated state that promotes their interactions (also known as crucible reactions) or can limit other reactions through the sequestration of certain macromolecules from the surrounding environment. Phase separation can also provide important spatial organization in the cell (e.g. organization of chromatin topology), or can be responsible for the packaging of cellular contents for intracellular transport (e.g. RNA transport granules in neurons) (Nedelsky & Taylor, 2019; Shin & Brangwynne, 2017). These mechanisms regulate a wide variety of biological functions, such as arrangement of DNA repair, sorting of molecules at the nuclear pore, regulation of mRNA fate, management of microRNAs and ribosome biogenesis, organization of chromatin topology, induction of membrane receptor clustering, and seeding of spindle assembly (Nedelsky & Taylor, 2019). The physicochemical properties of biomolecular condensates allow a tight spatiotemporal control of biochemical reactions suggesting a broad variety of potential cellular functionalities, like for example the vital cellular roles of cell differentiation (Liu *et al,* 2020), metabolic control (Prouteau & Loewith, 2018), and cytoskeletal regulation (Case *et al,* 2019). In comparison to membrane-bound organelles, the lack of membranes in biomolecular condensates not only provides the possibility to concentrate macromolecules in space but also a rapid assembly and disassembly, allowing rapid exchange of elements with the surrounding milieu (Nedelsky & Taylor, 2019).

2.9.3 Driving forces of Liquid-liquid Phase separation (LLPS)

As described before, assembly of biomolecular condensates (e.g. RNP granules) occurs when certain macromolecules (proteins and nucleic acids) that are in solution (i.e. dispersed in the cytoplasm or nucleoplasm) coalesce into a concentrated state (dense /condensed phase) distinct from the surrounding milieu (dilute/soluble phase). Unlike the irreversible pathological inclusions detected in neurodegenerative diseases, these physiological condensates mostly display liquid-like behaviors, such as classic surface dripping and wetting and fusion into larger compartments (Brangwynne *et al,* 2009).

Biomolecular condensates are complex cellular structures typically comprised of dozens of different types of proteins and RNAs. Nevertheless, by means of purified proteins and/or RNA it is possible to reconstitute such condensates or “droplets” that resemble to some extent the more complex intracellular condensates. Curiously, these reactions often require no more than one or two components, suggesting that the assembly of some intracellular condensates may sometimes only require a single protein (Brangwynne *et al,* 2015).

The main driving forces underlying the formation of RNP granules is based on various types of weak and adhesive interactions of multivalent proteins and RNAs (Alberti *et al,* 2019; Shin & Brangwynne, 2017). Multivalency is a key physical parameter that determines whether or

not a certain protein will undergo phase separation (Li *et al,* 2012). Multivalency refers to the number of different modules (domains or motifs) a single biomolecule species can simultaneously interact with (Alberti *et al,* 2019; Martin & Holehouse, 2020). Phase separation of multivalent proteins displays a critical threshold that depends on the amount of interacting modules and accessible ligands, and increasing the number of interacting modules promotes the formation of larger macroscopic phase-separated condensates (Alberti, 2017).

The forces underlying RNP granule formation can be distinguished into four types of multivalent interactions (Figure 12): weak and transient LCD-LCD interactions; standard protein-protein interactions between folded domains; protein-RNA interactions; and RNA-RNA interactions (Nedelsky & Taylor, 2019). Beyond controlling the assembly and disassembly of the condensates, these forces also work together to determine the material properties (e.g. surface tension, viscosity and internal diffusion rates) of biomolecular condensates (Nedelsky & Taylor, 2019). Tuning of these forces is of great importance because they allow the diffusion and dynamic exchange of different elements required for proper biological function. Therefore, each of these forces is subject to higher-order regulation, for instance by chaperones, PTMs on proteins, chemical modifications on RNA, or by charged molecules, such as adenosine triphosphate (ATP) (Note that this topic is described in more detail in section 2.9.5).

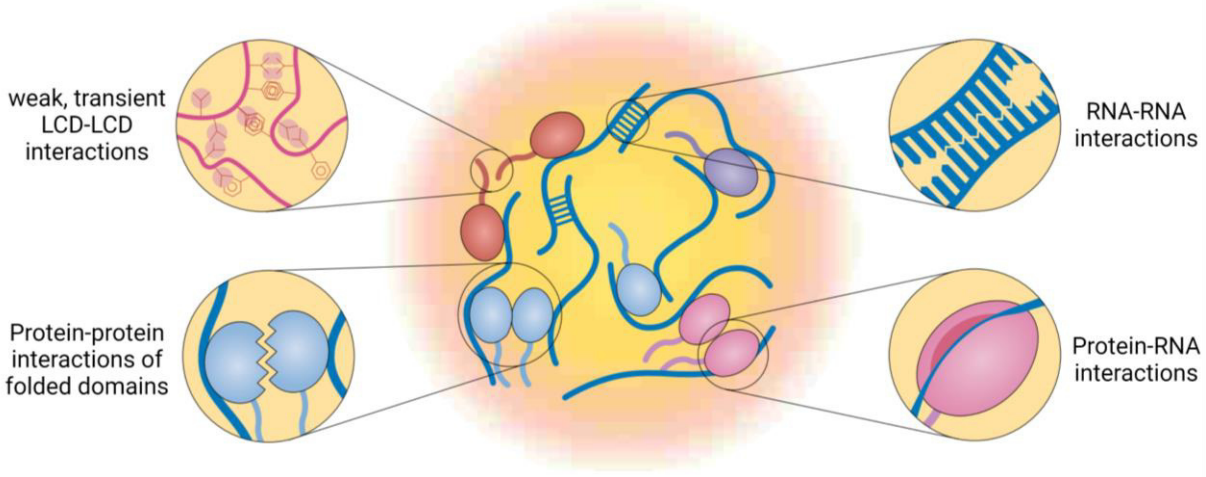

Figure 12. Forces governing the assembly of RNP granules.
Four different forces underly the phase separation of RBPs and RNA in ribonucleoprotein (RNP) granules, including weak and transient LCD-LCD interaction, protein-protein interactions of folded domains, RNA-RNA and protein-RNA interaction. Figure reproduced from (Nedelsky & Taylor, 2019) with permission from *Springer Nature*.

Among the key forces that cooperatively drive phase separation, LCD-LCD interactions have so far drawn the most attention in the experimental field (Nedelsky & Taylor, 2019). One of the reasons is that RNP granules are highly enriched in proteins harboring stretches of low sequence complexity (Shin & Brangwynne, 2017). Moreover, disease-causing mutations in RBPs, one of the main components of RNP granules, are frequently found within LCDs (Nedelsky & Taylor, 2019).

LCDs are protein stretches of low amino acid diversity when compared to the proteome as a whole. Often these sequences are enriched in polar amino acid residues, such as serine (S), threonine (T), glutamine (Q), or asparagine (N) (Alberti *et al,* 2019), but they can also be enriched in other amino acids, such as arginine (R) and glycine (G) in RGG/RG regions (Chong *et al,* 2018) or phenylalanine (F) and G in nucleoporins of the nuclear pore complex (Lemke, 2016). Although LCDs can harbor various amino acid combinations and therefore show different biochemical properties, they are often intrinsically disordered (Nedelsky & Taylor, 2019). Intrinsically disordered regions (IDRs) of proteins are protein segments that do not adopt any folded three-dimensional structure (Alberti *et al,* 2019). The category of LCDs largely overlaps with IDRs, but not all IDRs are LCDs, neither are all LCDs necessarily IDRs (Figure 13). A subgroup of low-complexity IDPs are prion-like proteins that contain certain amino acid sequences predicted to adopt cross-beta structures analogous to yeast prion proteins (Alberti *et al,* 2009; Mittag & Parker, 2018) (Figure 13).

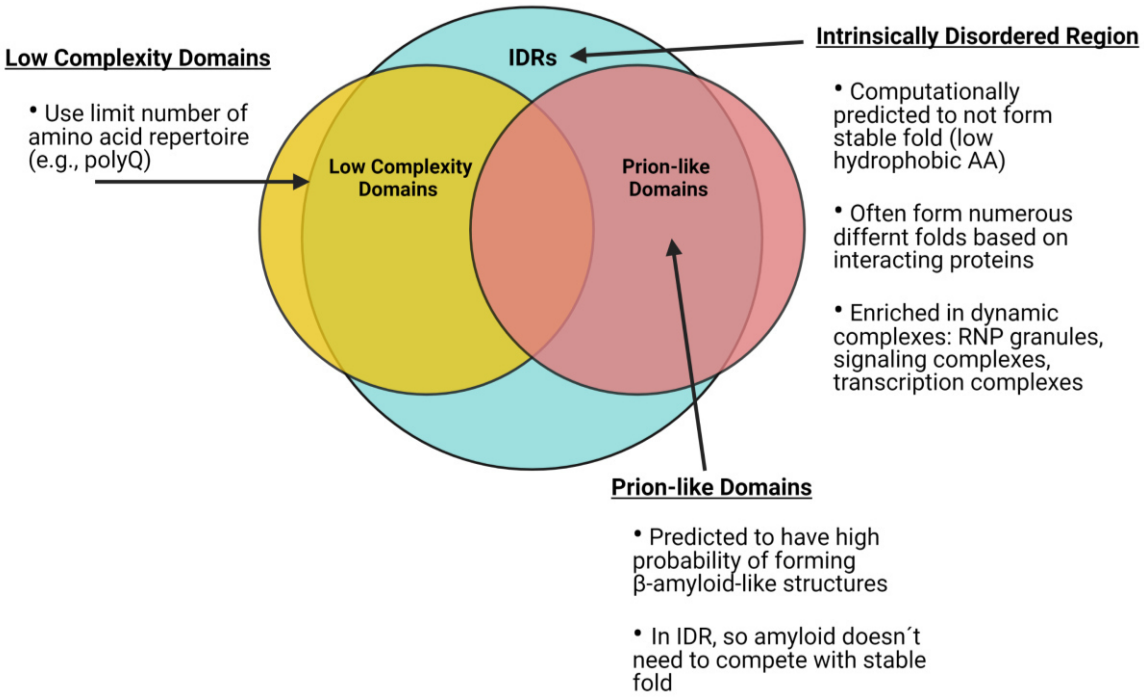

Figure 13. Schematic representation of overlapping types of intrinsically disordered proteins.

Low complexity domains are defined based on their amino acid composition, and prion-like domains based on their high ability to form cross β-sheet structures, similar to prion domains (Mittag & Parker, 2018). Note that the overlapping regions and the circle sizes do not correspond to the exact proportions. Figure adapted from (Mittag & Parker, 2018) with permission from *Elsevier*.

Prion-like domains (PrLD) are composed mostly of polar amino acids (S, Q, N) and glycine (G) with interspersed aromatic residues (F, Y). The absence of charges, intermittent aromatic residues and flexibility of the chain make these domains very prone to interact (Alberti, 2017; Alberti & Hyman, 2016). Interestingly, many LCDs in RBPs also meet the standards for PrLD, and several of the disease-causing mutations in these RBPs are located within these LCDs

(Nedelsky & Taylor, 2019; Kim *et al,* 2013). Another subset of low-complexity IDPs contain a high number of amino acids with acidic and/or basic (often R) side chains. These charged sequences often undergo electrostatic interactions highly sensitive to ionic strength and pH of the solution. One example are RGG domains that frequently occur in RBPs (Alberti & Hyman, 2016; Alberti, 2017; Chong *et al,* 2018). Most of the RBPs that participate in biomolecular condensate assembly, mainly RNP granules, are low complexity IDPs. Interestingly, a variety of IDR sequences present in such RBPs (e.g. hnRNP A1, FUS and TDP-43) have been shown to drive LLPS *in vitro* (Molliex *et al,* 2015; Patel *et al,* 2015; Conicella *et al,* 2016), strongly implying that short-lived multivalent interactions must be encoded within LCD sequences. A well-studied example of this types of IDPs is hnRNP A1, which is composed of >50% serine and glycine residues that are semi-regularly spaced by aromatic residues (F, Y) and some charged residues (R, E). This sequence arrangement can contribute to a variety of different weak multivalent interactions that can drive liquid droplet assembly. Indeed, LLPS of hnRNP A1 has been shown to be enhanced by decreasing salt concentration, underscoring the role of electrostatic/charge mediated interactions (Molliex *et al,* 2015). Moreover, the presence of aromatic residues (F, Y) sprinkled throughout the hnRNP A1 LCD sequence with a regular spacing, suggests that cation-π interactions may be another force for hnRNP A1 phase separation (Molliex *et al,* 2015). A good example of this type of interaction is Ddx4, another RBP localized in germ granules, to which cation-π interactions between RG and FG motifs have been cited as crucial driving forces for its LLPS (Nott *et al,* 2015). In addition, interactions between dipoles (S, G, N, Q) and π-π stacking interactions (aromatic residues interactions) have also been considered to drive phase separation (Brangwynne *et al,* 2015; Lee *et al,* 2016). Overall, weak multivalent interactions driving LLPS of IDPs appears to be a hierarchical interplay between long-range interactions (e.g. charge-charge/ electrostatic interactions) and different types of short-range, directional interactions (e.g. cation-π, π-π stacking and dipole-dipole interactions) (Brangwynne *et al,* 2015) (Figure 14). Besides weak multivalent interactions among low complexity IDRs, LLPS can also be driven by joined forces of modular binding domains (e.g. repeats of folded domains) and multivalent ligands (e.g. IDRs with repeats of short linear motifs (SLiMs)) (Li *et al,* 2012) (Figure 14). Moreover, IDRs can also induce LLPS over stronger specific interactions through short stretches of amino acids that form local structures that can self-interact. Some examples are steric zipper motifs, e.g. mediated by SLiMs in the LCD of hnRNP A1, or transient α-helix and low complexity, aromatic-rich, kinked segments (LARKS) as described for TDP-43 (note that this topic is explained in more detail in section 2.10) (Mittag & Parker, 2018) (Figure 14).

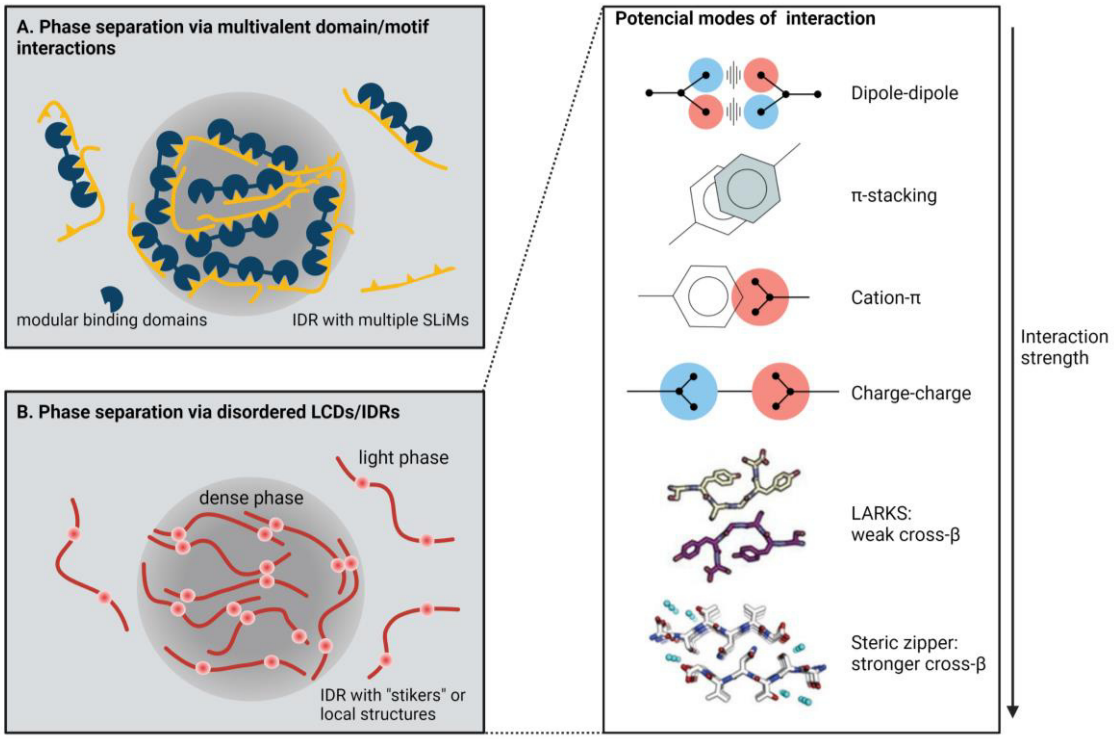

Figure 14. Archetypes of protein interaction modes mediating LLPS.

(A) One type of interactions that drives LLPS corresponds to multiple modular binding domains of one protein that interact with the intrinsically disordered region (IDR) of multiple short linear motifs (SLiMs) of another protein. (B) A second type refers to interactions between low complexity IDRs with several interaction motifs, or "stickers" that engage in transient and weak multivalent interactions such as dipole-dipole, π-stacking, cation-π and charge-charge interactions, as well as IDR-IDR interactions involving local structural modules, such as LARKS and steric zippers. Figure adapted from (Mittag & Parker, 2018) and (Nedelsky & Taylor, 2019) with permission from *Elsevier* and *Springer Nature*.

Importantly, the chemical nature of a macromolecule in solution is not the only key feature that determines whether it undergoes phase separation. Instead, formation of liquid-like condensates via spontaneous phase transitions depends strongly on the concentration (e.g. regulated by gene expression or degradation) and charge state (e.g. regulated by the presence or absence of PTMs and mutations) of the macromolecules (protein and RNA) and also on the environmental conditions, including salt/proton type and concentration, pH, osmotic pressure, and temperature (Brangwynne *et al,* 2015; Alberti *et al,* 2019). All of these factors together can influence the phase separation behavior of cellular macromolecules and determine the formation and material properties of MLOs.

2.9.4 Aberrant liquid to solid phase transitions

As mentioned before, proteins that undergo spontaneous LLPS do so under specific conditions (e.g. macromolecular concentration, temperature), therefore this process is extremely sensitive to changes in both environmental and protein status. Small perturbations of such conditions can, for instance, dysregulate the formation of LLPS-driven assemblies and induce their "metastability" through aberrant liquid-to-solid phase transitions (Alberti & Hyman, 2016; Shin & Brangwynne, 2017). Indeed, several lines of evidence indicate that associated RNP body

proteins (e.g. TDP-43, FUS, hnRNP A1 and others) initially undergo LLPS, but over time the emerging droplets can mature/convert into more solid-like structures, such as *in vitro* hydrogels and highly ordered fibrils due to high protein concentration and/or aged samples (Babinchak *et al,* 2019; Patel *et al,* 2015; Kato *et al,* 2012; Murakami *et al,* 2015; Molliex *et al,* 2015) (Figure 15).

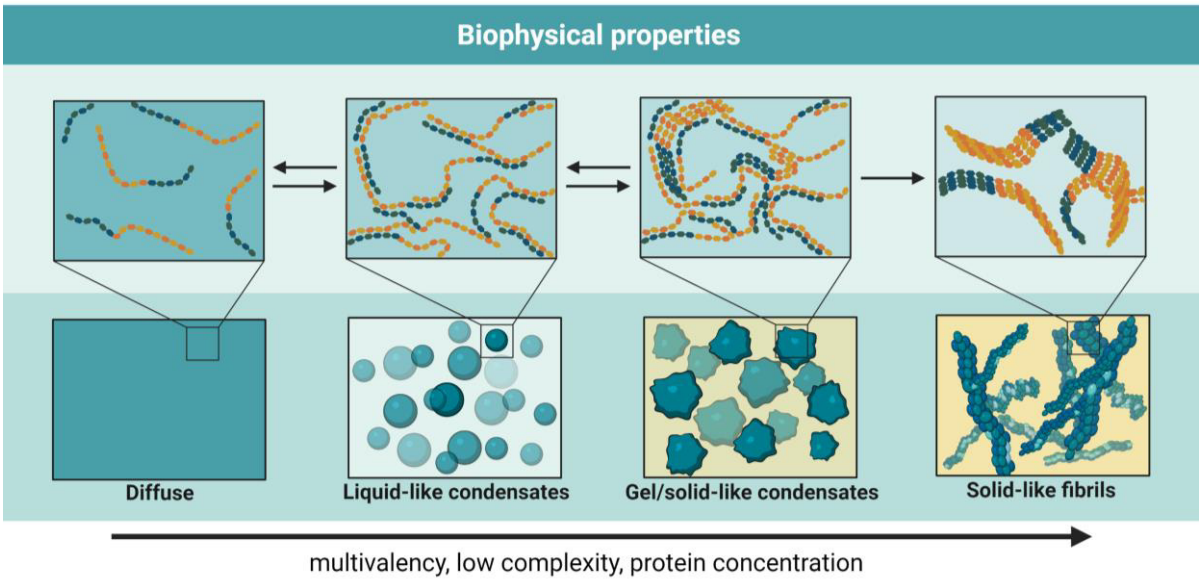

Figure 15. Aberrant liquid to solid phase transitions drive protein aggregation.
An IDP (shown in blue and orange) undergoes phase transition into a liquid droplet by spontaneous liquid-liquid demixing. This process is propelled by protein concentration and weak multivalent interactions among low-complexity domains or multivalent motifs. Liquid-liquid phase separation (LLPS) is initially reversible and the protein can go back to the diffuse phase. The formed droplet has higher protein concentrations when comparing to the surrounding solution and can "age" with time and assume distinct shapes and material properties. During aging different factors such as stress, pathogenic mutations and/or post-translational modifications (PTMs) can stimulate the conversion of this liquid-like droplet into a gel-like condensate. Such structures can persist and lead to the formation of solid-like and irreversible condensates composed of aggregated protein/ insoluble amyloid fibrils.

In contrast to their liquid-like precursors, that form through weak transient interactions, solid-like structures are characterized by more stable interactions, e.g. of short cross-β fibrils that are initially reversible (Kato *et al,* 2017) but ultimately change to irreversible, solid fibers (Murakami *et al,* 2015; Patel *et al,* 2015). This maturation process of a liquid droplet into a solid over time is often described as "molecular aging", and may underlie the pathological mechanisms that cause formation of aggregates in neurodegenerative diseases (Patel *et al,* 2015; Murakami *et al,* 2015). Supporting this idea, several studies have shown that disease-causing mutations in the LCDs of several RBPs, including TDP-43, FUS, hnRNP A1 and A2 promote a faster transition of the dynamic liquid droplet state to solid fibrillar aggregates, probably by enhanced multivalency and binding affinities of the interacting IDPs (Conicella *et al,* 2016; Molliex *et al,* 2015; Patel *et al,* 2015; Kim *et al,* 2013). Although most of these studies have been performed using purified proteins, this phenomenon of aberrant liquid-to-solid transition may also arise in RNP granules in living cells, where IDPs are highly concentrated. Indeed, a

recent study using a light-inducible (optogenetic based) system to induce chronic assembly of SGs in cells, has demonstrated that repetitive assembly of SGs is cytotoxic and leads ultimately to the evolution of initially liquid and reversible SGs into irreversible cytoplasmic aggregates (Zhang *et al,* 2019). Moreover, disease mutations in IDPs have been demonstrated to further promote their incorporation into SGs and to drive the development of cytoplasmic inclusions (Liu-Yesucevitz *et al,* 2010; Kim *et al,* 2013; Vance *et al,* 2013; Hackman *et al,* 2013; Mackenzie *et al,* 2017). Hence, dysregulation of RNP granule dynamics may lead to the formation of pathological inclusions as found in ALS, FTD and other neurodegenerative diseases (Figure 10).

2.9.5 Key regulatory mechanisms of biomolecular phase separation

Cells use several mechanisms in order to control and monitor the assembly, properties, dynamics and disassembly of biomolecular condensates (Alberti & Hyman, 2021). These mechanisms are of great importance so that functional condensates are built at the appropriate time and location, and therefore prevent the formation of pathological aggregates (Alberti *et al,* 2017; Snead & Gladfelter, 2019). Some of these key cellular mechanisms comprise of active processes mediated by e.g. adenosine triphosphate (ATP), molecular chaperones and PTMs.

2.9.5.1 Regulation of biomolecular condenses by adenosine triphosphate (ATP)

When phase separation happens, cells need to preserve and remodel biomolecular condensates to attain specific cellular requirements (Snead & Gladfelter, 2019). To actively maintain the function and identity of condensates, cells likely utilize energy sources that can prevent e.g. pathological fibril formation and gelation through aberrant phase transitions (Brangwynne *et al,* 2015). ATP, the canonical energy source for cellular reactions, has been shown to play a role in controlling the fluidity of intracellular compartments, such as SGs (Jain *et al,* 2016) and nucleoli (Brangwynne *et al,* 2011). Patel and coworkers found that ATP suppresses LLPS of RBPs and can dissolve preformed condensates of FUS, hnRNP A3, and TAF15. Therefore, besides being an energy source for the cell, ATP can also function as a biological hydrotrope at physiological concentrations between 5 to 10 millimolar. Interestingly, only micromolar concentrations of ATP are needed for ATP-dependent biological processes, suggesting that the millimolar concentrations observed in cells may act in order to maintain proteins soluble (Patel *et al,* 2017).

2.9.5.2 Regulation of biomolecular condensates by chaperones

Molecular chaperones are proteins that facilitate the folding or refolding of misfolded protein species, thereby preventing protein aggregation (Tyedmers *et al,* 2010; Morimoto *et al,* 2015). Besides their well-known role in protein quality control, chaperones can also regulate the material properties and functions of biomolecular condensates.

Previous studies on RNP granules in yeast have reported that absence of heat shock proteins (HSPs), such as HSP104, during heat shock conditions, induces mislocalization of P-body proteins (Lsm4 and Edc3) and its subsequent co-aggregation with misfolded proteins in SGs.

In contrast, enhanced expression of HSP104 decreases the recruitment and aggregation of these proteins in SGs, demonstrating that HSP104 may act as a chaperone through the inhibition of protein aggregation (Kroschwald *et al,* 2015).

Several studies have reported that molecular chaperones are components of SGs and that their presence is required to regulate SG material properties and disassembly during stress recovery (Cherkasov *et al,* 2013; Kroschwald *et al,* 2015; Wallace *et al,* 2015; Jain *et al,* 2016; Mateju *et al,* 2017). Molecular chaperones modify and restructure SGs in a way that upon stress recovery SG components remain active and functional (Cherkasov *et al,* 2013; Wallace *et al,* 2015). Molecular chaperones HSP70 and HSP27 were shown to be recruited to SGs positive for mutant RBPs (Ganassi *et al,* 2016; Mateju *et al,* 2017) and recruitment of HSP27 upon heat shock was shown to occur after polyubiquitination in SGs, suggesting that HSPs are particularly recruited into aberrant SGs containing mutant proteins and in reaction to aggregation of misfolded proteins (Mateju *et al,* 2017). Additionally, inhibition of HSP70 was reported to substantially increase misfolded SOD1 and poly-ubiquitinated proteins in SGs, indicating that HSP70 prevents the formation and recruitment of misfolded proteins into SGs (Mateju *et al,* 2017). Moreover, HSP70 inhibition along with aggregation of misfolded proteins drastically impairs SG dissolution, denoting that HSP70 facilitates rapid SG disassembly (Ganassi *et al,* 2016; Mateju *et al,* 2017).

Besides the traditional chaperones involved in protein quality control, other molecules such as importins can also act as physiological molecular chaperones. Indeed, several importins were shown to “chaperone” aggregation-prone proteins linked to the ALS/FTD spectrum, such as FUS, DPRs, hnRNP A1, TDP-43 and other hnRNPs (Guo *et al,* 2018a; Hofweber *et al,* 2018; Qamar *et al,* 2018; Hutten *et al,* 2020; Yoshizawa *et al,* 2018). For instance, Transportin was reported to act as chaperone by reducing FUS phase separation and subsequent aggregation (Guo *et al,* 2018a; Hofweber *et al,* 2018; Yoshizawa *et al,* 2018; Qamar *et al,* 2018).

These studies indicate that molecular chaperones provide a protective function by preventing aberrant phase transitions through the promotion of condensate dissolution.

2.9.5.3 Regulation of phase separation by post-translational modifications (PTMs)

PTMs are well-known key regulators of the dynamics and properties of biomolecular condensates (Bah & Forman-Kay, 2016; Hofweber & Dormann, 2019; Snead & Gladfelter, 2019). In particular, PTMs can adjust protein valency and interaction strength in order to promote or reduce phase separation under different conditions, this way they can tune the properties and general functions of molecular condensates (Brangwynne *et al,* 2015).

One of the most well characterized PTMs influencing phase separation of biomolecules is phosphorylation (Snead & Gladfelter, 2019). Phosphorylation is a rapid and reversible PTM that can act as a positive or negative regulator of LLPS in different contexts (Hofweber & Dormann, 2019). In line with this, the dynamics of RNP granules were found to be regulated by certain kinases. Kinases were shown to either modulate LLPS of specific RBPs, by inducing or reducing their condensation and therefore changing the dynamics of RNP condensates (Wippich *et al,* 2013; Rai *et al,* 2018), or to decrease the cellular concentration of certain RBPs

by inducing their degradation and therefore interfering with the assembly or disassembly of RNP granules (Krisenko *et al,* 2015; Carpenter *et al,* 2018). For instance, the kinase DYRK3 was shown to be present in SGs and to promote their dissolution (Wippich *et al,* 2013). The same kinase was also shown to act as a "dissolvase" preventing the assembly of multiple MLOs during mitosis (Rai *et al,* 2018). Another kinase that shows a suppressive effect on MLOs is Ime2 kinase. This kinase was shown to phosphorylate the yeast translational repressor Rim4, and induce dissolution of Rim4 amyloid-like condensates and their rapid degradation by the proteasome (Carpenter *et al,* 2018). This way yeast cells are released from translational repression, once mediated by amyloid-like structures during pre-miotic G1 phase, and can continue through meiosis (Berchowitz *et al,* 2015; Carpenter *et al,* 2018). As mentioned before, phosphorylation can also promote RNP granule formation. For example, AMP-activated protein kinase alpha 2(AMPK-α2) was found to localize to SGs upon stress conditions and to stimulate SG assembly in HeLa cells (Mahboubi *et al,* 2015; Mahboubi *et al,* 2016).

Moreover, phosphorylation was shown to suppress the phase separation of certain RBPs important for neuronal function, such as FUS (Monahan *et al,* 2017) and CPEB4 (Guillén-Boixet *et al,* 2016). In this case, phosphorylation disrupts electrostatic interactions within the low-complexity domains of FUS and CPEB4 (Guillén-Boixet *et al,* 2016; Monahan *et al,* 2017). On the other hand, phosphorylation of can also induce LLPS of certain proteins. One example is the microtube-binding protein Tau, which is found hyperphosphorylated in Tauopathies (Wang & Mandelkow, 2016). Several studies have found that Tau phosphorylation changes the global net charge and charge distribution to increase electrostatic interactions that promote Tau phase separation (Ambadipudi *et al,* 2017; Wegmann *et al,* 2018). This behavior could therefore be an explanation for the formation of Tau positive inclusions in disease through enhanced aberrant phase transitions.

Methylation is another essential PTM that regulates the phase separation of several proteins. While phosphorylation changes the net charge of target proteins by addition of negative charges in polar amino acids, methylation does not change the charge, but increases the bulkiness, hydrogen bonding and hydrophobicity of arginine residues (Fuhrmann *et al,* 2015). Arginine methylation was described to suppress phase separation of several RNPs, such as FUS, Ddx4 and hnRNPA2 through the disruption of cation-π interactions, known to drive the phase separation of these RBPs (Hofweber *et al,* 2018; Qamar *et al,* 2018; Nott *et al,* 2015; Ryan *et al,* 2018). It remains unclear whether methylation, besides suppressing phase separation, can also promote LLPS through other mechanisms (Hofweber & Dormann, 2019).

Arginines can also be converted into citrulline residues. Citrullination is a PTM mediated by peptidylarginine deiminases (PADs), which trigger the loss of a positive charge from arginine side chain and a conformational change (Vossenaar *et al,* 2003). Similar to methylation, citrullination of arginine residues was found to reduce phase separation of certain RBPs such as FUS, through the inhibition of cation-π interactions (Qamar *et al,* 2018). Moreover, PAD4-mediated citrullination was shown to reduce the aggregation of several ALS related proteins, including TAF-15, FUS, hnRNPA1 and other RBPs, suggesting a protective role of citrullination against pathological aggregation (Tanikawa *et al,* 2018).

Lysine acetylation was also found to reduce phase separation by neutralizing the positive charge of lysine and disrupting cation-π interactions (Saito *et al,* 2019). For instance, acetylation of lysine residues was reported to reduce phase separation and aggregation of Tau (Carlomagno *et al,* 2017; Ferreon *et al,* 2018), suggesting to be a protective PTM against pathological aggregation of Tau. Another study has found that acetylation at multiple lysine residues in the IDR of DDX3X, an important component of SGs, impairs the formation of liquid droplets *in vitro* (Saito *et al,* 2019).

2.10 Driving forces of TDP-43 phase transitions

As described previously, TDP-43 is a multidomain nuclear protein with a predicted low complexity IDR of PrLD nature (Figure 6), which is crucial for its reversible and irreversible self-association linked to LLPS. TDP-43 LCD region is largely devoid of charged amino acids but is enriched in scattered aromatic hydrophobic amino acids (Y, F) intercalated with rich hydrophilic segments of polar residues (Q, S, N) as well as glycines (G) (Figure 16). This amino acid composition largely suggests that LLPS of TDP-43 might be driven by aromatic residues involved in π-π interactions through its LCD. Indeed, three consecutive studies, have shown that regular-spaced hydrophobic sticker segments (composed of aromatic residues) adjacent to flexible, hydrophilic linkers (segments of polar residues) are a key factor for TDP-43 LLPS, by π-π intermolecular interactions of the low complexity region of the protein (Li *et al,* 2018b; Schmidt *et al,* 2019; Laurents *et al,* 2021) (Figure 16). Moreover, hydrophobic and arginine mediated LCD interactions have been shown to tune the properties of TDP-43 condensates (Schmidt *et al,* 2019) (Figure 16). However, the weak interactions mediating LLPS of TDP-43 are not solely dictated by the amino acid identity per se. In addition, a transient α-helix structure in the LCD of TDP-43 has been shown to drive TDP-43 LCD LLPS *in vitro* (Conicella *et al,* 2016; Conicella *et al,* 2020) (Figure 16). Accordingly, introduction of a single mutation (W334G) or ALS-associated TDP-43 mutations (A321G, Q331K and M337V) in the α-helix region disrupts multivalent interactions and consequently disturbs TDP-43 phase separation, demonstrating an essential role of this structure for TDP-43 LLPS (Li *et al,* 2018a; Conicella *et al,* 2016; Hallegger *et al,* 2021) (Figure 16). More recently, another structural and short motif dubbed LARKS (low-complexity, aromatic-rich, kinked segments) has also been described for TDP-43 (Guenther *et al,* 2018). LARKS are kinked β sheet segments that stack on top of each other, which unlike steric zippers and amyloid fibrils, interact weakly by means of polar atoms and aromatic side chains and have been found to be characteristic of proteins localized in MLOs (Hughes *et al,* 2018). Remarkably, familial ALS-causing mutations in TDP-43 were shown to convert such reversible β-sheet structures into irreversible aggregates, providing some insights into how some disease mutations might drive pathogenic aggregation (Guenther *et al,* 2018).

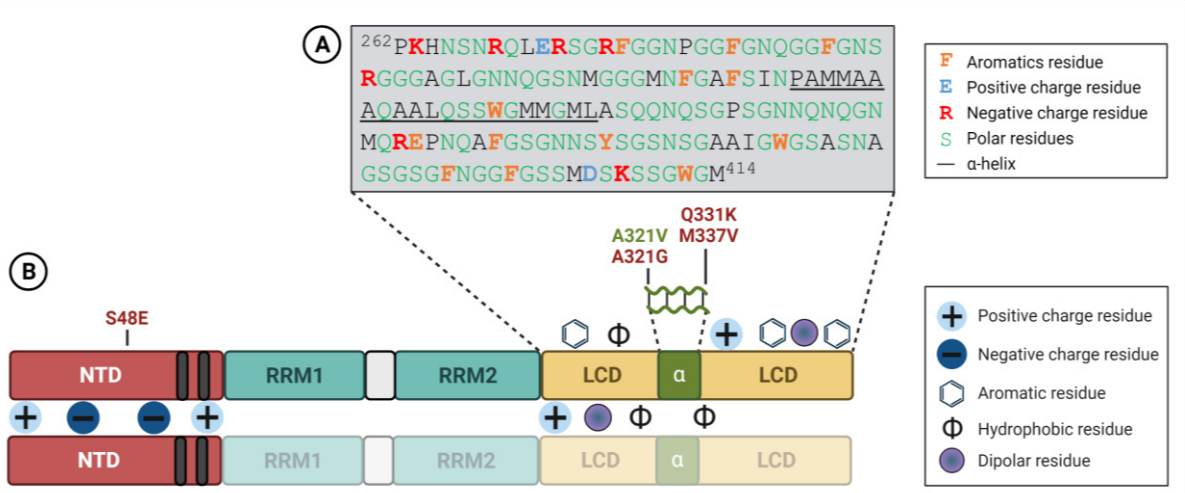

Figure 16. Schematic representation of protein intrinsic modulators of TDP-43 LLPS. (A) Schematic representation of the amino acid nature of TDP-43 LCD, which is rich in hydrophilic polar residues (Q, S, N) intercalated by aromatic hydrophobic amino acids (Y, F) and glycines (G) and largely devoid of charged amino acids. (B) The graphic depicts some of the primary sequence elements that modulate TDP-43 LLPS. Some of the elements that are known to enhance or decrease LLPS are shown in green or red, respectively. TDP-43 LLPS is mediated by aromatic, dipolar, hydrophobic, and positive residues (mainly arginine) present in the low complexity region of the protein (Schmidt *et al,* 2019; Laurents *et al,* 2021), as well as by the transient α-helix (Conicella *et al,* 2016). Some disease mutations in the helix impair TDP-43 LLPS (Conicella *et al,* 2016; Hallegger *et al,* 2021) with exception of A321V, that enhances it (Conicella *et al,* 2016). TDP-43 oligomerization mediated by the N-terminal domain (NTD) also contributes to LLPS, and disruption of the NTD-mediated oligomerization by the phosphomimetic S48E decreases TDP-43 LLPS (Wang *et al,* 2018a).

Even though the LCD is sufficient to drive LLPS of TDP-43 *in vitro* at high concentrations (Conicella *et al,* 2020), full-length TDP-43 has been shown to undergo phase separation at physiological concentrations *in vitro* and in cellular models (Schmidt *et al,* 2019; Wang *et al,* 2018a), indicating that additional structural components might play along with the LCD to control TDP-43 phase separation. As mentioned before, physiological TDP-43 undergoes self-oligomerization in the nucleus through its folded NTD, which is essential for TDP-43´s proper nuclear functions, e.g. in mRNA splicing regulation (Chang *et al,* 2012; Wang *et al,* 2018a; Afroz *et al,* 2017). Interestingly, TDP-43 oligomerization has been demonstrated to be crucial for *in vitro* and in cell phase separation, and an oligomerization-disrupting mimic of phosphorylation (S48E) was shown to reduce TDP-43 LLPS (Wang *et al,* 2018a) (Figure 16).

Furthermore, the phase separation behavior of TDP-43 has been shown to be modulated by RNA-binding. However, how TDP-43 phase transitions are regulated by specific and non-specific RNA-binding, remains still controversial and not well understood. On the one hand, in vitro and in cellular experiments, using constructs harboring the RRMs of TDP-43, showed that the presence of specific GU-rich target RNAs increases protein solubility preventing LLPS (Mann *et al,* 2019). Additionally, another study suggests that non-specific RNA sequences generally suppresses RBP phase separation, including that of TDP-43, and that reduced RNA levels leads to TDP-43's irreversible aggregation via liquid-solid phase separation (Maharana *et al,*

2018). On the other hand, increase of a specific target RNA (NEAT1) has been shown to promote TDP-43 LLPS *in vitro* (Wang *et al,* 2020). More recently, Grese and coworkers have shown that specific GU-rich target RNAs promote TDP-43 LLPS and enhance the liquidity properties of TDP-43 condensates, while non-specific RNAs do so but to a much lesser extent. The same study showed that RNA-driven condensation is mediated by both the NTD and the CTD of TDP-43 (Grese *et al,* 2021).

2.10.1 Regulation of TDP-43 LLPS by PTMs

As described before, PTMs have a key role in regulating the assembly and properties of biomolecular condensates, though their role in TDP-43 LLPS has so far not been extensively studied. A single phosphomimetic substitution at S48 (S48E) in the NTD of TDP-43 was found to drastically reduce TDP-43 LLPS *in vitro*. Moreover, expression of S48E in cells was shown to increase the liquidity of TDP-43 nuclear assemblies, and decrease splicing activity, suggesting that phase separation of TDP-43 may be required for proper splicing activity (Wang *et al,* 2018a). S48 is found constitutively phosphorylated in different cell types (Rigbolt *et al,* 2011; Hornbeck *et al,* 2012; Hornbeck *et al,* 2015; Wang *et al,* 2018a), however it is not clear whether this modification also occurs in disease. Additionally, acetylation of lysines within the RRM domains of TDP-43 was described to disrupt protein-RNA interactions and to promote TDP-43 phase separation and aggregation in cells (Cohen *et al,* 2015; Morato *et al,* 2020). Nevertheless, the influence of disease-linked PTMs, such as ubiquitination and C-terminal phosphorylation, on TDP-43 phase separation remains so far unclear.

2.11 Aims of the PhD

TDP-43 is known to be the main component of intracellular pathological inclusions in ALS and FTD patients (Neumann *et al,* 2006). A well-recognized feature of TDP-43 inclusions is the hyperphosphorylation of several serine residues in the C-terminal LCD of TDP-43 (Hasegawa *et al,* 2008; Inukai *et al,* 2008; Kametani *et al,* 2016; Neumann *et al,* 2009a). TDP-43 phosphorylation is considered to be one of the main pathological hallmarks and typically believed to promote TDP-43 aggregation (Buratti, 2018). Aggregation of TDP-43 is thought to arise via aberrant phase separation, which is believed to be largely dependent on the prion-like LCD of the protein (Nedelsky & Taylor, 2019), where hyperphosphorylation of TDP-43 is observed in disease. So far, the effects of this disease-linked PTM on TDP-43 LLPS and aggregation as well as molecular function is still poorly understood and no in vitro reconstitution approach has been taken so far.

Therefore, the overall aim of this project was to decipher how C-terminal hyperphosphorylation alters the phase separation and aggregation behavior of TDP-43 and to understand how this disease-linked PTM affects the cellular and functional properties of TDP-43. Specifically, I had the following three aims:

1st Aim: Establishment of methods to study the effect of PTMs on the phase separation of RBPs.

To study the phase separation behavior of TDP-43 in the presence or absence of phosphorylation, two sedimentation assays were established in order to analyze the solubility of TDP-43 *in vitro* and in cells as a read out for TDP-43 phase separation.

2nd Aim: Characterize the phase separation behavior of the disease-linked C-terminal hyperphosphorylation of TDP-43.

To understand the impact of C-terminal hyperphosphorylation on TDP-43 phase separation and aggregation, I used *in vitro* phase separation experiments to assess the effects of this disease-liked PTM in the context of full-length TDP-43, using *in vitro* phosphorylation with casein kinases and phosphomimetic mutants.

3rd Aim: Understand the functional consequences of the altered TDP-43 phase separation in cells.

Another aim of this thesis was to address how altered phase separation by TDP-43 hyperphosphorylation affects key physiological functions of TDP-43 and the recruitment of TDP-43 into MLOs in cells.

3 Publication I

Sedimentation assays to assess the impact of post-translational modifications on phase separation of RNA-binding proteins *in vitro* and in cells

In Press as

Lara A. Gruijs da Silva, Dorothee Dormann. Sedimentation assays to assess the impact of post-translational modifications on phase separation of RNA-binding proteins in vitro and in cells. Huan-Xiang Zhou, Jan-Hendrik Spille, Priya Banerjee, Phase-Separated Biomolecular Condensates. Springer Nature, Methods in Molecular Biology (MiMB) series.

Sedimentation assays to assess the impact of post-translational modifications on phase separation of RNA-binding proteins in vitro and in cells

Lara A. Gruijs da Silva[1,2], Dorothee Dormann[1,3*]

[1] Johannes Gutenberg-Universität (JGU), Biocenter, Institute of Molecular Physiology, 55128 Mainz, Germany

[2] Graduate School of Systemic Neurosciences (GSN), 82152 Planegg-Martinsried, Germany

[3] Institute of Molecular Biology (IMB), 55128 Mainz, Germany

*For correspondence: ddormann@uni-mainz.de

Abstract

In the last years RNA-binding proteins (RBPs) have been highlighted for their capacity to undergo liquid-liquid phase separation (LLPS). Aberrant phase transitions of RBPs from a liquid to a solid state are believed to underlie the formation of pathological RBP aggregates in several neurodegenerative diseases. Both in the physiological and the disease state, RBPs are often decorated with diverse post-translational modifications (PTMs) that can influence the phase separation behavior, the physiological function and the pathological behavior of the RBP. Here we describe two simple methods, sedimentation assays *in vitro* and in cells, that allow the analysis of RBP solubility as a measure of RBP phase separation in the absence or presence of a certain PTM.

Running Head: Sedimentation assays to study RBP phase separation

Key Words

RNA-binding proteins (RBPs), Neurodegeneration, liquid-liquid phase separation (LLPS), post-translational modifications (PTMs), TAR DNA-binding protein of 43 kDa (TDP-43), phosphorylation

1. Introduction

RNA-binding proteins (RBPs) play an important role in the control of cellular RNA metabolism, for example in RNA splicing, stability, translation or transport [1]. Together with RNA, they form so-called ribonucleoprotein (RNP) granules [2], dynamic membrane-less organelles that form through liquid-liquid phase separation (LLPS) [3]. LLPS results from weak, multivalent interactions between RBPs, RNAs or RBPs-RNAs and allows these molecules to physicochemically separate from other molecules and condense into droplet-like organelles or “biomolecular condensates” [4]. RBPs in RNP granules can also undergo liquid-to-solid phase transitions and transition from a liquid to a solid-like state [5–7]. These aberrant phase transitions are believed to underlie the formation of pathological protein aggregates observed for characteristic RBPs in neurodegenerative diseases, such as TDP-43 or FUS in amyotrophic lateral sclerosis (ALS) and frontotemporal dementia (FTD) [8]. Frequently, RBPs within such aggregates are characterized by a non-physiological pattern of post-translational modifications (PTMs) [9, 10]. PTMs are commonly located in intrinsically disordered regions (IDRs) of RBPs, such as low complexity domains (LCDs) or prion-like domains (PLDs), which often drive LLPS [11]. Therefore PTMs frequently have an impact on the RBP phase separation behavior [11–13]. Specifically, PTMs can modify the physicochemical properties of amino acids (e.g. charge, bulkiness or hydrophilicity/hydrophobicity), which can change the valency and strength of multivalent RBP or RBP-RNA interactions. This way, PTMs can enhance or reduce RBP phase separation and modulate material properties of RBP condensates [12, 13]. Hence, it is of great interest to understand how absence or presence of certain PTMs influences RBP phase separation behavior and consequently RBP-related pathology.

Here, we describe two methods to study the impact of specific PTMs on RBP solubility as a readout for RBP phase separation *in vitro* and in intact cells. For the *in vitro* approach, an unmodified versus *in vitro* modified protein-of-interest can be directly compared side-by-side under identical experimental conditions. LLPS of the protein-of-interest is induced, e.g. by protease-mediated removal of a solubility tag, and after a short incubation time the formed condensates (C) are separated from the cleared supernatant (S) by centrifugation. The amount of protein in condensates vs. supernatant is subsequently quantified by SDS-PAGE and Western Blot analysis (Figure 1). For studying the impact of the same PTM on protein solubility in cells, wild-type protein vs. protein variants with PTM-mimicking mutations can be expressed in cells and biochemical fractionation into a RIPA-soluble (S) and RIPA insoluble (I) fraction can be performed (Figure 2). Here, we describe these two assays using the neurodegeneration-linked RBP TAR DNA binding protein of 43 kDa (TDP-43) and phosphorylation as an example. More specifically, we show how TDP-43 solubility *in vitro* and in HeLa cells is influenced by C-terminal hyperphosphorylation (Figure 3), which is a well-known pathological hallmark of TDP-43 aggregates in ALS and FTD patients [14–17]. To introduce or mimic disease-associated C-terminal hyperphosphorylation, we *in vitro* phosphorylated TDP-43 using Casein Kinase 1 delta (CK1δ) or used a phosphomimetic protein harboring 12 serine-to-aspartate (S-to-D) mutations (12D) in disease-linked phosphorylation sites [16, 18].

The described assays can be adopted to measure and quantify phase separation of other post-translationally modified RBPs, for instance other RBPs linked to human diseases [19–21] and more broadly to other phase separating proteins that are modified by PTMs.

2. Materials

2.1. In vitro sedimentation assay

1. Recombinant RBP-of-interest. In order to avoid protein precipitation during purification, we use a fusion protein with a solubility tag (e.g. MBP) separated by a protease recognition cleavage site (e.g. TEV protease) to allow for controlled induction of phase separation (e.g. TDP-43-TEV-MBP-His_6 [22], see note 1).
2. CK1δ or other kinases that phosphorylate protein-of-interest (e.g. TDP-43)
3. ATP (Stock solution, e.g., 100 mM dissolved in phosphorylation buffer)
4. Phosphorylation buffer (50 mM Tris-HCl, pH 7.5, 100 mM NaCl, 10 mM $MgCl_2$, 1 mM DTT) (see note 2)
5. Amicon Ultra 0.5 mL Centrifugal Filters or Zeba Spin Desalting Columns, 7K MWCO, 0.5 mL
6. Nano drop
7. 1.5 mL low binding tubes (see note 3)
8. Optional: Protein-of-interest with PTM-mimicking mutations (e.g.TDP-43-12S-to-D) (see note 4)
9. Recombinant protease matching protease recognition cleavage site in recombinant RBP-of-interest (e.g. His_6-TEV protease, or any other commercially available TEV protease)
10. Reaction buffer (e.g. 20 mM Hepes, pH 7.5, 1 mM DTT) (see note 5)
11. Reaction buffer containing 1M NaCl (1M NaCl in 20 mM Hepes, pH 7.5,1 mM DTT)
12. 1.5 mL tubes
13. Pre-cooled bench centrifuge for Eppendorf tubes
14. 4x Lämmli buffer (250 mM Tris HCl, pH 6.8, 40% glycerol, 8% SDS, 0.1% bromophenol-blue, 4% β-mercaptoethanol)
15. 1x Lämmli buffer (62.5 mM Tris HCl, pH 6.8, 10% glycerol, 2% SDS, 0.025% bromophenol-blue, 1% β-mercaptoethanol)

2.2. In cell sedimentation assay

1. Adherent, easily transfectable cell line, e.g. HeLa or HEK
2. 6-well tissue culture plate
3. Dulbecco's Modified Eagle' Medium (DMEM) (or other suitable cell culture medium)
4. Fetal bovine serum (FBS)
5. Trypsin
6. PBS
7. Transfection reagent suitable for high transfection rates (60-70%) for chosen cell line, e.g Lipofectamine 2000 (Thermo)
8. Reduced serum medium, e.g. Opti-MEM I (Thermo)
9. Plasmids coding for the protein-of-interest (see note 6)
10. Cell scraper
11. bucket with ice
12. RIPA buffer (50 mM Tris-HCl, pH 8.0, 150 mM NaCl, 1% NP-40, 0.5% deoxycholate, 0.1% SDS)
13. Protease inhibitor cocktail (e.g. 100x stock solution, can be prepared from one solid tablet from Sigma)
14. Phosphatase inhibitors (250x stock solution: 2.5 M NaF, 250 mM β-glycerophosphate, 250 mM Na_3VO_4) (see note 7)
15. Benzonase (e.g. stock solution from Sigma: 250 units/µl)
16. Urea buffer (7 M urea, 2 M thiourea, 4% CHAPS, 30 mM Tris-HCl, pH 8.5)
17. 1.5 mL tubes
18. Sonication system (e.g. BioRuptorPico from Diagenode)
19. Pre-cooled bench centrifuge
20. 4x Lämmli buffer (250 mM Tris HCl, pH 6.8, 40% glycerol, 8% SDS, 0.1% bromophenol-blue, 4% β-mercaptoethanol)
21. Heating block at 95 °C

2.3. *In vitro* or in cell sedimentation assay analysis

1. Electrophoresis and blotting systems
2. Electrophoresis and blotting buffers
3. SDS-PAGE gel
4. Blotting membrane (e.g. nitrocellulose membrane, see note 8)
5. Imaging system for Western blot detection and visualization (e.g. Odyssey CLx from LI-COR)
6. Densitometry software for gel image analysis (e.g. Image Studio Lite, LI-COR)
7. Microsoft Excel
8. Optional: Graph Pad Prism

3. Methods

3.1. *In vitro* sedimentation assay

3.1.1. *In vitro* phosphorylation

1. Buffer exchange the stock containing recombinant protein (e.g. TDP-43-TEV-MBP-His_6) to phosphorylation buffer using Amicon Ultra Centrifugal Filters or Zeba Spin Desalting Columns.
2. Centrifuge protein at 21,000 g for 10 min at 4°C, to remove any precipitated/aggregated protein.
3. Re-determine protein concentration in supernatant by measuring absorbance at 280 nm at the Nano drop using the respective extinction coefficient (ε).
4. Calculate the amount of protein-of-interest, kinase and ATP for phosphorylation reaction. In order to phosphorylate TDP-43-TEV-MBP-His_6, we performed a 10 µl phosphorylation reaction with 2-fold molar excess of TDP-43 over CK1δ (e.g., 10 µM of TDP-43 and 5 µM CK1δ) and a final concentration of 200 µM ATP in phosphorylation reaction buffer (see note 9). As controls, prepare a reaction lacking both kinase and ATP and reactions lacking either the kinase (-CK1δ, +ATP) or ATP (+CK1δ, -ATP).

5. Mix all components (protein, CK1δ, ATP) according to the previous calculations in a 1.5 ml low binding tube (see note 3).
6. Incubate for 2 h at RT to allow protein phosphorylation (see note 9).
7. Confirm phosphorylation using phospho-specific antibodies (e.g. mouse anti-TDP-43-phospho Ser403/404 from Proteintech) and/or by analyzing the running behavior in SDS-PAGE.

3.1.2. Setup of experiment and LLPS induction

1. Pre-spin all proteins, including all controls, at 21,000 g for 10 min at 4°C, to remove any precipitated/aggregated protein, and use supernatant for following steps.
2. Re-determine protein concentration if necessary (see note 10).
3. Calculate the amount of TDP-43, protease, NaCl solution and cleavage buffer required to prepare a 50 µl reaction with a final concentration of 1 µM of TDP-43-MBP-His, 20 µg/ml of TEV protease and 150 mM NaCl in Hepes buffer (see example in table 1) (see notes 5 and 11). Importantly, consider the amount of NaCl brought into the reaction by the protein and protease stock solution (see table 1).
4. Mix all components according to the previous calculations in a 1.5 ml tube. Importantly, the protease must be added as last component, as its presence will induce TDP-43 phase separation (see notes 1 and 12).
5. Incubate reactions (here: 60 min at 30°C, see note 13).

3.1.2. Sedimentation and fraction collection

1. Centrifuge tubes for 15 min at 21,000 g at 4°C in order to pellet formed condensates.
2. Collect supernatant fraction (S) by transferring the entire supernatant (~50 µl) into a new 1.5 ml tube (see note 14).
3. Add 17 µl of 4x Lämmli buffer to (S).
4. Resuspend condensates fraction (C) by adding 67 µl 1x Lämmli buffer to the pellet.
5. Boil (S) and (C) samples at 95°C for 5 min.

6. For all the conditions, load side-by-side equal amounts of supernatant (S) and condensate (C) fraction (e.g. 5 µl) on a SDS-PAGE gel (e.g. 10%) and proceed to the analysis described in section 3.3.

3.2. In cell sedimentation assay

3.2.1. Cell culture and transfection

1. Seed cells in a 6-well tissue culture plate so that cell density is appropriate for transfection the next day and that cells can be kept in culture for 2-3 more days (see note 15).
2. The next day, transfect constructs coding for the RBP-of-interest using the transfection reagent of choice (see note 16). We recommend omitting antibiotics during and after transfection as this increases transfection efficiency and reduces cell stress. Additionally, changing medium 3 to 5 hours after transfection will help to reduce cellular stress.
3. Keep cells in culture for 24-48h to allow sufficient protein expression (see note 17).

3.2.2. Cell harvesting and lysis

1. Prepare a fresh master mix of RIPA-Benzonase buffer, by supplementing 1x RIPA buffer with 1x protease inhibitor cocktail, 1x phosphatase inhibitors and 0.05 unit/µl Benzonase (see note 18) and place it on ice. Per 6 well, 200 µl of RIPA buffer are required, prepare your total volume including some spare volume (e.g. extra 200 µl) (see note 19).
2. Aspirate cell culture medium and wash cells once with 1x PBS.
3. Add 1 mL of 1x PBS into each 6-well and detach cells using a cell scraper.
4. Transfer cell suspension into a 1.5 mL tube and centrifuge at 1100 g for 5 min to pellet cells.
5. Carefully remove supernatant and place cell pellets on ice.

6. Add 200 µl of ice-cold RIPA-Benzonase buffer to cell pellets and resuspend cell pellet by gently pipetting up and down 2 to 3 times. Incubate on ice for 15 min to achieve cell lysis.
7. Sonicate lysates (e.g. in BioRuptorPico for 45 secs) to shear remaining DNA and further reduce sample viscosity (see notes 20 and 21).

3.2.3. For subsequent analysis, take 10% of the total volume as an "input" sample (20 µl). Next, add 7 µl 4x Lämmli buffer to the input sample and boil it for 5 min at 95 °C. For the remaining 180 µl sample, continue with fractionation in RIPA-Benzonase buffer as described in section 3.2.4.

3.2.4. Fractionation into RIPA-soluble and -insoluble fractions in RIPA-Benzonase buffer

1. Centrifuge samples for 30 min at 13,000 g and 4°C.
2. During centrifugation, label 1.5 ml tubes for RIPA soluble fractions (S) and place them on ice.
3. After centrifugation, collect (S) by completely transferring the resulting supernatants (~ 180 µl) into the pre-cooled 1.5 ml tubes and store the remaining RIPA insoluble pellet on ice.
4. Add 60 µl 4X Lämmli buffer to (S), boil for 5 min at 95 °C in a heating block and then freeze at -20°C.
5. Proceed with RIPA-insoluble pellets stored on ice in step 3. First, wash pellets by resuspending them in 200 µl of RIPA-Benzonase buffer. Then, repeat sonication step (e.g. in BioRuptorPico for 45 secs) and pellet for 30 min at 13,000 g and 4°C.
6. After centrifugation, discard the supernatants from the washing step and dissolve the RIPA insoluble fractions (I) in 36 µl Urea buffer (see note 22). Solubilize (I) pellets by sonicating them (e.g. in BioRuptor Pico for 45 secs).
7. Add 12 µl 4x Lämmli buffer to (I) and freeze directly at -20 °C (see note 23).
8. Load 20 µl of each input, (S) and (I) samples on a SDS-PAGE gel (e.g. 12%) (see note 24) and proceed to the analysis described in section 3.3. For easier visualization, load

all input samples next to each other and corresponding (S) and (I) samples side by side (for an example, see Fig. 3C).

3.3. Analysis of *in vitro* or in cell sedimentation assay

3.3.1 Visualization of protein-of-interest

1. Proceed with standard SDS-PAGE and Western Blot protocols using samples from step 6 section 3.1 or step 8 section 3.2.
2. Visualize the protein-of-interest using an Imaging system (e.g. fluorescent Western blot detection using Odyssey CLx, LI-COR or alternative device).

3.3.2 Quantitative analysis

1. Upload image into the software of the Western blot detection device (e.g. Image Studio Lite by LI-COR) or Fiji/Image J.
2. Extract the optical densities of each band, by adding or drawing a rectangle around each band and subtract background. E.g. in the software Image Studio Lite (LI-COR), select the background option (e.g. average background, top and bottom) to obtain the signal value, in which local background is automatically subtracted. For analysis in Fiji/Image J, see note 25. Export obtained data into an Excel sheet.
3. Divide the background corrected signal values of corresponding (S) and (C) samples (S/C) or (S) and (I) samples (S/I), respectively. Alternatively, the background corrected signal values of (S) can be divided by the total (S+C) or (S+I) background corrected signal values, in order to obtain a S/(S+C) or S/(S+I) ratio.
3. S/C or S/I ratios can be plotted as mean ±SEM using Excel or Graph Pad Prism. It is recommended to be perform a minimum of 3 independent experimental replicates.

4. Notes

1. Other constructs and methods for recombinant protein purification can also be used. One possibility is to omit a solubility tag and purify the protein-of-interest using high salt (e.g. 1 M). In this case, phase separation can be induced by lowering the salt concentration [23].
2. Buffer conditions depend on kinase / enzyme and protein-of-interest being used. Therefore, different buffer conditions may be necessary when using another kinase / enzyme or protein-of-interest.
3. In case low binding tubes are not available, another way of preventing non-specific binding of proteins to plastic is to add 0.1 mg/ml BSA.
4. One disadvantage of *in vitro* protein modification is that one may not always be able to control the specific sites that get modified, unless the enzyme is highly specific for a certain motif. Modified sites need to be determined by modification-specific antibodies and/or mass spectrometric analysis. Alternatively, at least some PTMs can be mimicked by mutations, e.g. phosphomimetic serine-to-aspartate (S-to-D) or serine-to-glutamate (S-to-E) mutations, mimicking the negative charge of the phospho-group.
5. Pilot experiments should be performed to determine the best buffering system for the protein-of-interest, e.g. Tris vs. phosphate vs. Hepes based buffers.
6. Protein-of-interest can either be tagged (e.g. Myc-TDP-43, allowing subsequent detection with an anti-Myc antibody) or untagged (in case the protein-of-interest in not expressed in the chosen cell line, e.g. due to knockout or knockdown or cell type specificity, allowing for subsequent detection with an antibody specific to the protein-of-interest).
7. Phosphatase inhibitors can also be omitted when studying PTMs other than phosphorylation.
8. Nitrocellulose membrane can be used in most cases, but some proteins might require PVDF membrane.

9. Phosphorylation reaction might need to be optimized depending on protein-of-interest and kinase (e.g. buffer conditions, kinase-substrate ratio, temperature, incubation time).
10. If a pellet is observed after centrifugation, it is recommended to re-determine the protein concentration. If the protein stock only contains the purified recombinant protein, protein concentration can be determined by absorbance at 280 nm using the respective extinction coefficient (ε). Otherwise, if the stock contains a mixture of proteins (e.g. TDP-43 *in vitro* phosphorylated with CK1δ and ATP), the concentration of the protein-of-interest can be determined by SDS-PAGE and Coomassie staining and subsequent densiometric methods, in comparison to a protein of known concentration.
11. When studying other proteins or PTMs, it is recommended to optimize the experimental conditions [e.g. protein concentration and buffer conditions (e.g. NaCl concentration)] according to the question and protein-of-interest. For example, if one expects that a certain variant of the protein-of-interest (e.g. modified, PTM-mimetic or mutant protein) has an enhanced tendency to undergo LLPS in comparison to the unmodified or wild-type (Wt) protein, one would aim to use experimental conditions that result in only partial LLPS of the unmodified or Wt protein (e.g. by using higher NaCl concentrations).
12. It is recommended to confirm the induction of phase separation by analysis of condensates under the microscope (e.g. bright field or DIC microscopy). An example of what to expect when observing *in vitro* TDP-43 phase separation by bright field microscopy is shown in Figure 3E.
13. We chose 60 min incubation time at 30°C to allow for complete TEV protease-mediated cleavage of the solubility tag (MBP). However, different temperatures and incubation times can also be applied, depending on the protease and RBP used. These factors can also be used to optimize the experimental setup, for example when exploring the ideal time point for a comparison of different variants.

14. Be aware that the pellet can be invisible. Therefore, it is recommended to place the 1.5 ml tubes in a specific orientation into the rotor of the centrifuge. Subsequently, try to avoid touching the side of the tube where a pellet might form. Moreover, it is crucial to not pipet up and down after centrifugation, to avoid disturbing the pellet.
15. Optionally, cells can be split after transfection if they get too dense.
16. Transient transfection can be omitted if cell lines stably expressing the protein-of-interest are used.
17. Expression time varies depending on the protein-of-interest and should be optimized for the protein-of-interest. Before proceeding with the protocol, make sure that cells for the different conditions have the same confluency. If after transient transfection protein variants display different expression rates, try to optimize by adjusting the amount of transfected DNA. If a stable cell line is used, a BCA assay can be performed to determine the total protein concentration. This way, equal amounts of protein for each sample can be calculated and used for the next steps of the protocol.
18. Benzonase is added to degrade all nucleic acid that might still be bound to the RBP-of-interest. Studies focused on other classes of proteins may not require the use of Benzonase. However, the use of Benzonase can also help to reduce lysate viscosity.
19. The experiment can also be done in a smaller scale (e.g. 12-well). For doing so, lyse cells directly in the well in 80 to 100 µl of RIPA-Benzonase buffer and transfer cell lysates into 1.5 ml tubes by gently pipetting up and down. Subsequent buffer volumes will need to be scaled down accordingly.
20. The conditions for the sonication step (intensity, length…) need to be optimized depending on the sonicator used. If using a BioRuptorPico, choose the highest intensity for all steps where sonication is mentioned and sonicate the 200 µl lysate for 45 secs.
21. At this point samples are completely lysed and can be stored at -20 °C if necessary.
22. For reasons of detection sensitivity, we recommend the (I) fractions to be 5X more concentrated than the (S) fractions.

23. Do not boil urea-resuspended pellets, since urea modifications of proteins can occur.
24. As RIPA insoluble samples (I) are highly viscous, it is recommended to use yellow tips (20 µl - 200 µl pipette tips) instead of thin gel-well loading tips for sample loading. Additionally, for easier loading of the samples, it is recommended to use thick SDS-polyacrylamide gels (1.5 mm) and to load samples slowly to avoid sample leakage.
25. When using Fiji/imageJ software, the background corrected signal value is not obtained automatically. Here, manually draw the background area in a representative area of the blot and subtract (e.g. in Excel) the raw value from the total signal value to obtain the background corrected signal value.

Acknowledgements

We thank Dr. Saskia Hutten for critical reading and helpful suggestions on the manuscript. This work was supported by the Deutsche Forschungsgemeinschaft (DFG), in particular the priority programme SPP2191 - ID 402723784 (to D.D.), the Munich Cluster for Systems Neurology (EXC2145 SyNergy – ID 390857198 to D.D.), the Paul Ehrlich and Ludwig Darmstädter Award for Young Researchers 2019 (to D.D.) and the Fritz Thyssen Foundation (to D.D.). D.D. also acknowledges support by ReALity – Resilience, Adaptation and Longevity (Forschungsinitiative des Landes Rheinland-Pfalz) and the Gutenberg Forschungskolleg (GFK) of JGU Mainz.

5. References

1. Müller-McNicoll M, Neugebauer KM (2013) How cells get the message: dynamic assembly and function of mRNA-protein complexes. Nat Rev Genet 14:275–287. https://doi.org/10.1038/nrg3434
2. van Treeck B, Parker R (2018) Emerging Roles for Intermolecular RNA-RNA Interactions in RNP Assemblies. Cell 174:791–802. https://doi.org/10.1016/j.cell.2018.07.023
3. Shin Y, Brangwynne CP (2017) Liquid phase condensation in cell physiology and disease. Science 357. https://doi.org/10.1126/science.aaf4382
4. Salman F. Banani, Hyun O. Lee, Anthony A. Hyman et al. Biomolecular condensates: Organizers of cellular biochemistry
5. Franzmann TM, Alberti S (2019) Prion-like low-complexity sequences: Key regulators of protein solubility and phase behavior. J Biol Chem 294:7128–7136. https://doi.org/10.1074/jbc.TM118.001190
6. Patel A, Lee HO, Jawerth L et al. (2015) A Liquid-to-Solid Phase Transition of the ALS Protein FUS Accelerated by Disease Mutation. Cell 162:1066–1077. https://doi.org/10.1016/j.cell.2015.07.047
7. Nedelsky NB, Taylor JP (2019) Bridging biophysics and neurology: aberrant phase transitions in neurodegenerative disease. Nat Rev Neurol 15:272–286. https://doi.org/10.1038/s41582-019-0157-5
8. Alberti S, Dormann D (2019) Liquid-Liquid Phase Separation in Disease. Annu Rev Genet 53:171–194. https://doi.org/10.1146/annurev-genet-112618-043527
9. Schaffert L-N, Carter WG (2020) Do Post-Translational Modifications Influence Protein Aggregation in Neurodegenerative Diseases: A Systematic Review. Brain Sci 10. https://doi.org/10.3390/brainsci10040232
10. Basso M, Pennuto M (2015) Serine phosphorylation and arginine methylation at the crossroads to neurodegeneration. Exp Neurol 271:77–83. https://doi.org/10.1016/j.expneurol.2015.05.003

11. Bah A, Forman-Kay JD (2016) Modulation of Intrinsically Disordered Protein Function by Post-translational Modifications. J Biol Chem 291:6696–6705. https://doi.org/10.1074/jbc.R115.695056
12. Hofweber M, Dormann D (2019) Friend or foe - Post-translational modifications as regulators of phase separation and RNP granule dynamics. J Biol Chem 294:7137–7150. https://doi.org/10.1074/jbc.TM118.001189
13. Snead WT, Gladfelter AS (2019) The Control Centers of Biomolecular Phase Separation: How Membrane Surfaces, PTMs, and Active Processes Regulate Condensation. Mol Cell 76:295–305. https://doi.org/10.1016/j.molcel.2019.09.016
14. Hasegawa M, Arai T, Nonaka T et al. (2008) Phosphorylated TDP-43 in frontotemporal lobar degeneration and amyotrophic lateral sclerosis. Ann Neurol 64:60–70. https://doi.org/10.1002/ana.21425
15. Neumann M, Kwong LK, Lee EB et al. (2009) Phosphorylation of S409/410 of TDP-43 is a consistent feature in all sporadic and familial forms of TDP-43 proteinopathies. Acta Neuropathol 117:137–149. https://doi.org/10.1007/s00401-008-0477-9
16. Kametani F, Obi T, Shishido T et al. (2016) Mass spectrometric analysis of accumulated TDP-43 in amyotrophic lateral sclerosis brains. Sci Rep 6:23281. https://doi.org/10.1038/srep23281
17. Inukai Y, Nonaka T, Arai T et al. (2008) Abnormal phosphorylation of Ser409/410 of TDP-43 in FTLD-U and ALS. FEBS Lett 582:2899–2904. https://doi.org/10.1016/j.febslet.2008.07.027
18. da Silva LG, Simonetti F, Hutten S et al. (2021) Disease-linked TDP-43 hyperphosphorylation suppresses TDP-43 condensation and aggregation. https://doi.org/10.1101/2021.04.30.442163
19. Gebauer F, Schwarzl T, Valcárcel J et al. (2021) RNA-binding proteins in human genetic disease. Nat Rev Genet 22:185–198. https://doi.org/10.1038/s41576-020-00302-y

20. Nussbacher JK, Batra R, Lagier-Tourenne C et al. (2015) RNA-binding proteins in neurodegeneration: Seq and you shall receive. Trends Neurosci 38:226–236. https://doi.org/10.1016/j.tins.2015.02.003
21. Ling S-C, Polymenidou M, Cleveland DW (2013) Converging mechanisms in ALS and FTD: disrupted RNA and protein homeostasis. Neuron 79:416–438. https://doi.org/10.1016/j.neuron.2013.07.033
22. Wang A, Conicella AE, Schmidt HB et al. (2018) A single N-terminal phosphomimic disrupts TDP-43 polymerization, phase separation, and RNA splicing. EMBO J 37. https://doi.org/10.15252/embj.201797452
23. Alberti S, Saha S, Woodruff JB et al. (2018) A User's Guide for Phase Separation Assays with Purified Proteins. J Mol Biol 430:4806–4820. https://doi.org/10.1016/j.jmb.2018.06.038
24. Dormann D, Capell A, Carlson AM et al. (2009) Proteolytic processing of TAR DNA binding protein-43 by caspases produces C-terminal fragments with disease defining properties independent of progranulin. J Neurochem 110:1082–1094. https://doi.org/10.1111/j.1471-4159.2009.06211.x
25. Zhang Y-J, Xu Y-F, Dickey CA et al. (2007) Progranulin mediates caspase-dependent cleavage of TAR DNA binding protein-43. J Neurosci 27:10530–10534. https://doi.org/10.1523/JNEUROSCI.3421-07.2007

Figure Captions and Legends

Figure 1. Workflow for the *in vitro* sedimentation assay.

Figure 2. Workflow for the in cell sedimentation assay.

Figure 3. Solubility of unmodified vs. hyperphosphorylated or phosphomimetic TDP-43 determined by *in vitro* and in cell sedimentation assays.

A) *In vitro* sedimentation assay to quantify condensation of unmodified TDP-43 versus *in vitro* phosphorylated TDP-43 (+CK1δ, +ATP), controls (CK1δ only or ATP only) and phosphomimetic TDP-43 (with 12 phosphomimetic serine-to-aspartate substitutions (12D). TDP-43 is detected by Western blot using a rabbit anti-TDP-43 N-term antibody (Proteintech). Upper band corresponds to residual uncleaved TDP-43-MBP-His_6, lower band to free TDP-43. Note that the *in vitro* phosphorylated and phosphomimetic 12D protein show an altered running behavior (high molecular weight shift) compared to unmodified TDP-43.

B) Quantification of TDP-43 band intensities in the Supernatant (S) vs. Condensate (C) fraction, plotted as S/C ratio. Values represent means (3=n) ± SD. *p< 0.0332, ***p < 0.0002 by one-way ANOVA with Dunnett´s multiple comparison test to Wt.

C) In cell sedimentation assay to determine solubility of wild-type vs. phosphomimetic TDP-43 in HeLa cells. Biochemical fractionation into RIPA-soluble (S) and RIPA-insoluble (I) fractions to compare phase separation of myc-TDP-43 wild-type (Wt), phosphomimetic (12D) TDP-43 or the corresponding 12A control protein in cells. Myc-TDP-43 was detected by Western blot using a rabbit anti-TDP-43 C-term antibody (Proteintech). Note that the TDP-43 Western blot also detects endogenous TDP-43 and C-terminal fragments of TDP-43 that arise through caspase cleavage of TDP-43 [24, 25]. Myc-TDP-43 12D protein shows an altered running behavior (high molecular weight shift) compared to Myc-TDP-43 Wt.

D) Quantification of TDP-43 variants (Wt, 12D and 12A) in (S) versus (I) fractions, plotted as S/(S+P). Values represent means (4=n) ± SD. *p< 0.0332 by one-way ANOVA with Dunnett´s multiple comparison test to Wt.

E) Representative bright field microscopic images of TDP-43 condensates after addiction of Tev protease (+Tev) to TDP-43-TEV-MBP-His_6 (5 µM), scale bar, 20 µm. Picture was taken on a widefield microscope.

Table Captions

Table 1. Representative calculation table for the *in vitro* sedimentation assay.

Table 1.

	Stock concentration						
	Protein [µM]	NaCl [mM]	1	2	3	4	5
TDP-43-MBP-His_6 (-CK1, -ATP)	16	300	3				
Phospho TDP-43-MBP-His_6 (+CK1, +ATP)	5	95		10			
TDP-43-MBP-His_6 (+CK1, -ATP)	5	95			10		
TDP-43-MBP-His_6 (-CK1+ATP)	5	95				10	
12S to D TDP-43-MBP-His_6	8	300					6.3
His_6-Tev protease	~80 (2 mg/ml)	150	0.5	0.5	0.5	0.5	0.5
1 M NaCl in 20 mM Hepes, 1 mM DTT			6.5	6.5	6.5	6.5	5.5
Buffer (20 mM Hepes, pH 7.5, 1 mM DTT)			40	33	33	33	37.7

Final concentration of TDP-43 variants [µM]	*1*				
Final volume [µl]	*50*				
Final concentration of NaCl [mM]	*150*				
Final concentration of His_6-Tev protease [µg/ml]	*20*				
NaCl brought in by TDP-43 variants [mM]	18	19	19	19	37.8
NaCl brought in by His6-Tev [mM]	1.5	1.5	1.5	1.5	1.5

Figure 1.

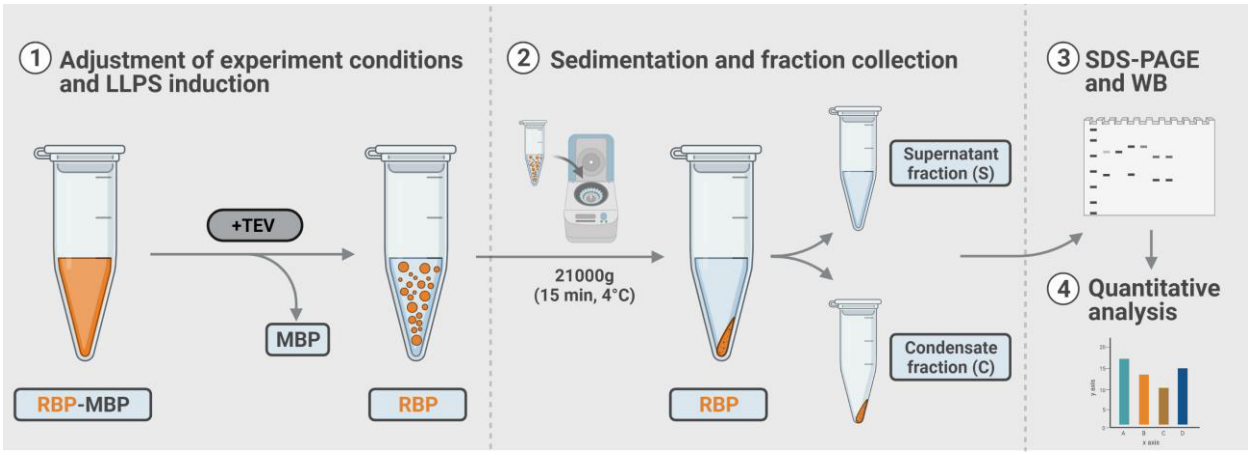
1 Adjustment of experiment conditions and LLPS induction
+TEV
MBP
RBP-MBP
RBP
2 Sedimentation and fraction collection
21000g
(15 min, 4°C)
RBP
Supernatant fraction (S)
Condensate fraction (C)
3 SDS-PAGE and WB
4 Quantitative analysis

Figure 2.

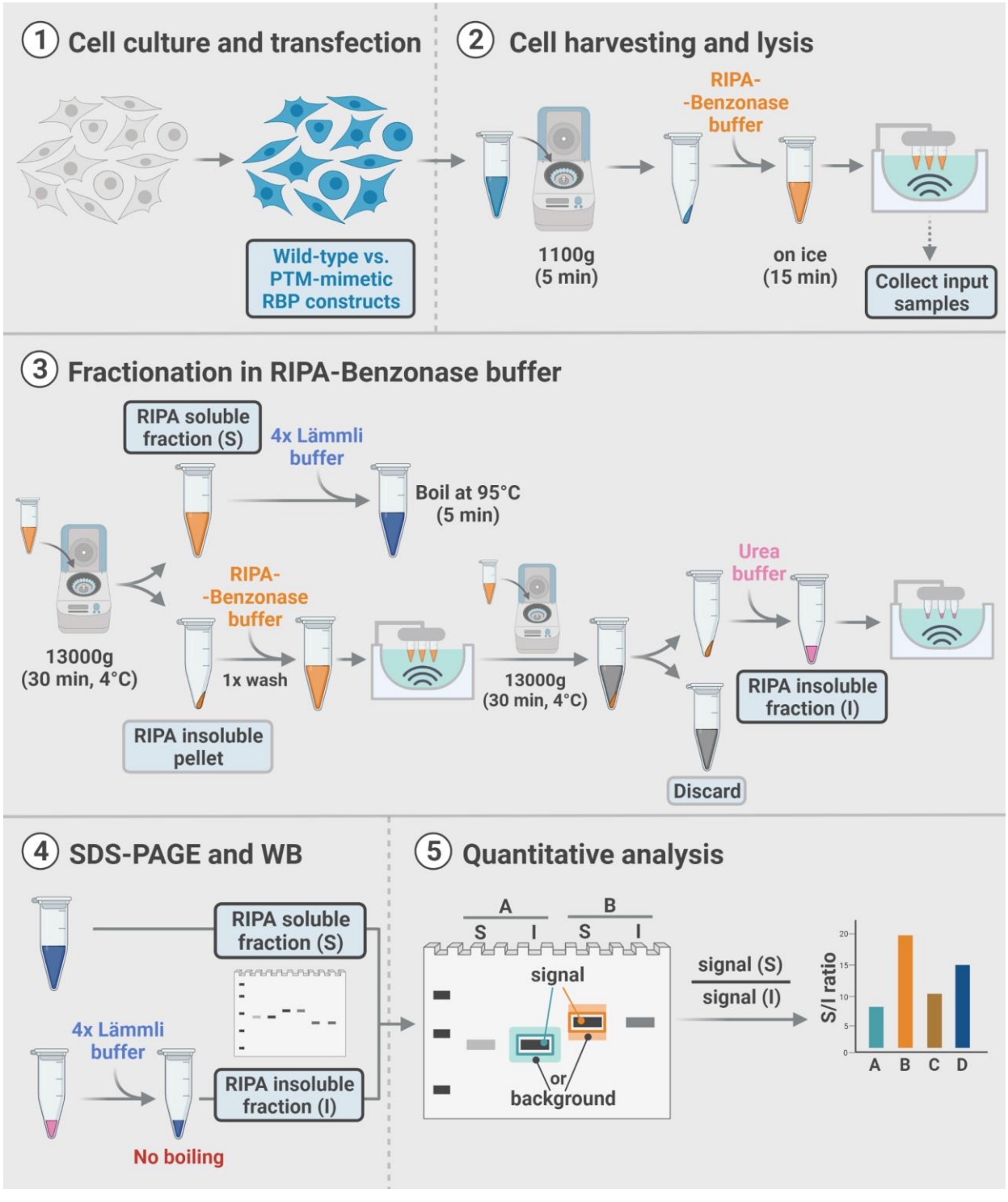
1 Cell culture and transfection
Wild-type vs. PTM-mimetic RBP constructs
2 Cell harvesting and lysis
1100g (5 min)
RIPA--Benzonase buffer
on ice (15 min)
Collect input samples
3 Fractionation in RIPA-Benzonase buffer
RIPA soluble fraction (S)
4x Lämmli buffer
Boil at 95°C (5 min)
13000g (30 min, 4°C)
RIPA--Benzonase buffer
1x wash
RIPA insoluble pellet
13000g (30 min, 4°C)
Urea buffer
RIPA insoluble fraction (I)
Discard
4 SDS-PAGE and WB
RIPA soluble fraction (S)
4x Lämmli buffer
RIPA insoluble fraction (I)
No boiling
5 Quantitative analysis
A
B
S
I
S
I
signal
or
background
signal (S)
signal (I)
S/I ratio
20
15
10
5
0
A
B
C
D

Figure 3.

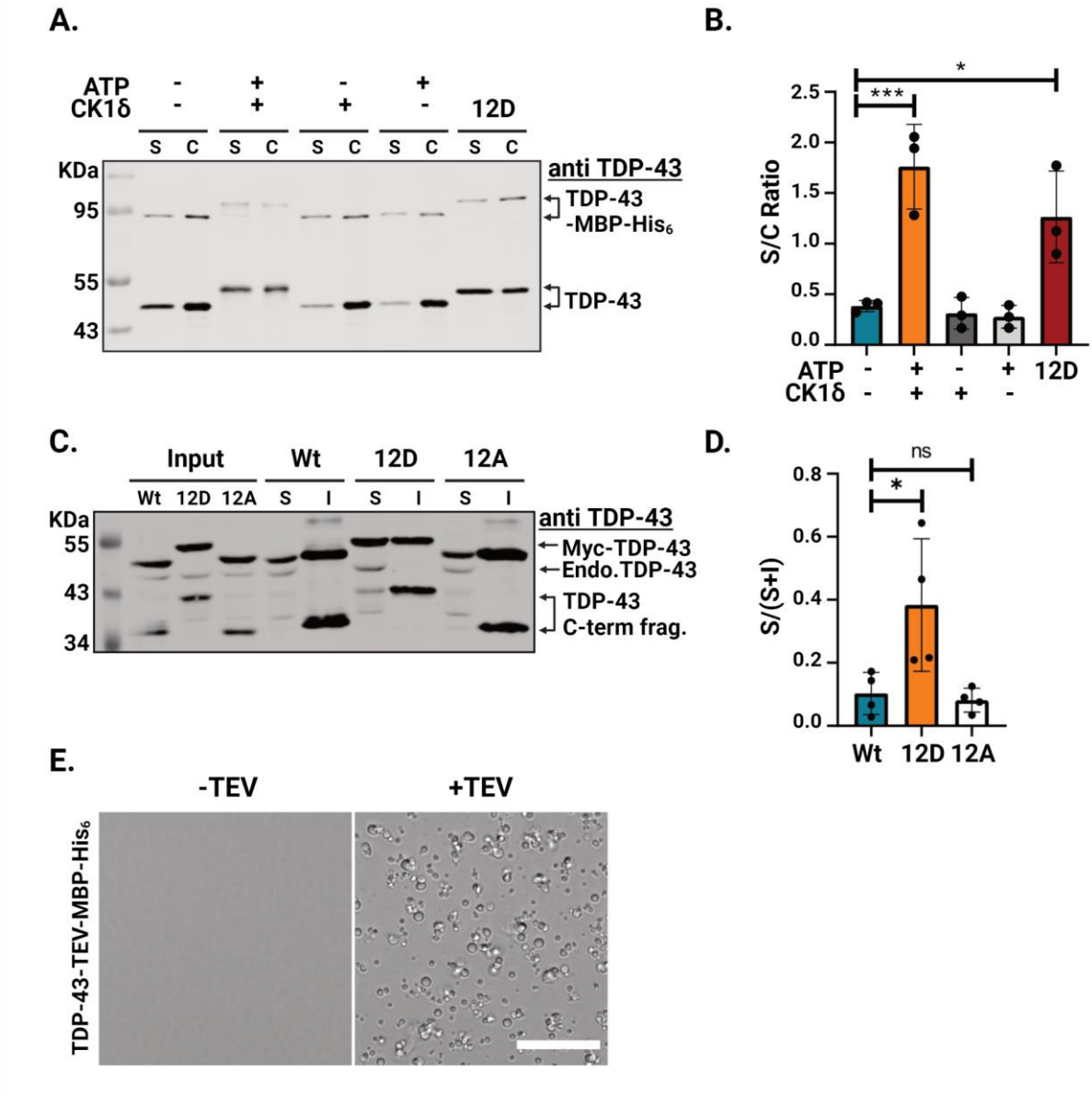
A.
ATP
CK1δ
12D
S C S C S C S C S C
KDa
95
55
43
anti TDP-43
TDP-43
-MBP-His6
TDP-43
B.
S/C Ratio
2.5
2.0
1.5
1.0
0.5
0.0
***
*
ATP - + - + 12D
CK1δ - + + -
C.
Input
Wt
12D
12A
Wt 12D 12A S I S I S I
KDa
55
43
34
anti TDP-43
Myc-TDP-43
Endo.TDP-43
TDP-43
C-term frag.
D.
S/(S+I)
0.8
0.6
0.4
0.2
0.0
ns
*
Wt 12D 12A
E.
-TEV
+TEV
TDP-43-TEV-MBP-His6

4 Publication II

Disease-linked TDP-43 hyperphosphorylation suppresses TDP-43 condensation and aggregation

Published as

Lara A. Gruijs da Silva, Francesca Simonetti, Saskia Hutten, Henrick Riemenschneider, Erin L. Sternburg, Lisa M. Pietrek, Jakob Gebel, Volker Dötsch, Dieter Edbauer, Gerhard Hummer, Lukas S. Stelzl, Dorothee Dormann. Disease-linked TDP-43 hyperphosphorylation suppresses TDP-43 condensation and aggregation. The EMBO Journal (2022) e108443. doi: 10.15252/embj.2021108443

Article

SOURCE DATA | TRANSPARENT PROCESS | OPEN ACCESS

THE EMBO JOURNAL

Disease-linked TDP-43 hyperphosphorylation suppresses TDP-43 condensation and aggregation

Lara A Gruijs da Silva[1,2], Francesca Simonetti[1,2,3], Saskia Hutten[1], Henrick Riemenschneider[3], Erin L Sternburg[1], Lisa M Pietrek[4], Jakob Gebel[5], Volker Dötsch[5], Dieter Edbauer[2,3,6], Gerhard Hummer[4,7], Lukas S Stelzl[1,4,8,9] & Dorothee Dormann[1,6,9,*]

Abstract

Post-translational modifications (PTMs) have emerged as key modulators of protein phase separation and have been linked to protein aggregation in neurodegenerative disorders. The major aggregating protein in amyotrophic lateral sclerosis and frontotemporal dementia, the RNA-binding protein TAR DNA-binding protein (TDP-43), is hyperphosphorylated in disease on several C-terminal serine residues, a process generally believed to promote TDP-43 aggregation. Here, we however find that Casein kinase 1δ-mediated TDP-43 hyperphosphorylation or C-terminal phosphomimetic mutations reduce TDP-43 phase separation and aggregation, and instead render TDP-43 condensates more liquid-like and dynamic. Multi-scale molecular dynamics simulations reveal reduced homotypic interactions of TDP-43 low-complexity domains through enhanced solvation of phosphomimetic residues. Cellular experiments show that phosphomimetic substitutions do not affect nuclear import or RNA regulatory functions of TDP-43, but suppress accumulation of TDP-43 in membrane-less organelles and promote its solubility in neurons. We speculate that TDP-43 hyperphosphorylation may be a protective cellular response to counteract TDP-43 aggregation.

Keywords neurodegeneration; phase separation; phosphorylation; RNA-binding protein; TDP-43

Subject Categories Neuroscience; RNA Biology

DOI 10.15252/embj.2021108443 | Received 15 April 2021 | Revised 23 December 2021 | Accepted 4 January 2022

The EMBO Journal (2022) e108443

Introduction

TAR DNA-binding protein (TDP-43) is the major aggregating protein in amyotrophic lateral sclerosis (ALS) and frontotemporal dementia (FTD) patients and also forms pathological aggregates in up to 50% of Alzheimer's disease patients (Neumann *et al*, 2006; Josephs *et al*, 2014). It is a ubiquitously expressed RNA-binding protein (RBP) with key functions in RNA processing, e.g., regulation of alternative splicing and polyadenylation, miRNA processing, mRNA stability and localization (Ratti & Buratti, 2016). In the affected brain regions of ALS and FTD patients, the physiological diffuse nuclear localization of TDP-43 is lost. Instead the protein forms cytoplasmic and occasionally nuclear inclusions in neurons and glial cells (Mackenzie *et al*, 2010). TDP-43 pathology closely correlates with neurodegeneration, and both loss-of-function mechanisms, e.g., misregulation of nuclear RNA targets, and gain-of-function mechanisms, e.g., aberrant interactions of the TDP-43 aggregates, are believed to contribute to neuronal dysfunction and eventually neurodegeneration (Ling *et al*, 2013; Tziortzouda *et al*, 2021).

Similar to other prion-like RBPs, TDP-43 is thought to aggregate through aberrant liquid–liquid phase separation (LLPS), i.e., the transition of liquid-like RBP condensates into a solid-like state (Nedelsky & Taylor, 2019). Aberrant phase transitions may occur in stress granules (SGs) or other membrane-less organelles (MLOs), where aggregation-prone RBPs are highly concentrated and exceed the critical concentration for LLPS (Alberti & Dormann, 2019; Alberti & Hyman, 2021). Subsequent liquid-to-solid phase transition, as demonstrated for various disease-linked RBPs *in vitro* (Molliex *et al*, 2015; Patel *et al*, 2015), may then cause formation of pathological RBP inclusions. LLPS is often driven by intrinsically disordered low complexity domains (LCDs), that tend to engage in weak multivalent interactions with other molecules (Alberti, 2017). TDP-43 harbors a long C-terminal LCD enriched in glycine, serine, asparagine and

1 Biocenter, Institute of Molecular Physiology, Johannes Gutenberg-Universität (JGU), Mainz, Germany
2 Graduate School of Systemic Neurosciences (GSN), Planegg-Martinsried, Germany
3 German Center for Neurodegenerative Diseases (DZNE), Munich, Germany
4 Department of Theoretical Biophysics, Max Planck Institute of Biophysics, Frankfurt am Main, Germany
5 Institute for Biophysical Chemistry, Goethe-Universität, Frankfurt am Main, Germany
6 Munich Cluster for Systems Neurology (SyNergy) Munich, Munich, Germany
7 Institute for Biophysics, Goethe-Universität, Frankfurt am Main, Germany
8 KOMET1, Institute of Physics, Johannes Gutenberg-Universität (JGU), Mainz, Germany
9 Institute of Molecular Biology (IMB), Mainz, Germany
*Corresponding author. Tel: +49 6131 39 36206; E-mail: ddormann@uni-mainz.de

glutamine residues, which drives intermolecular TDP-43 interactions and assembly by phase separation (Conicella *et al*, 2016; Babinchak *et al*, 2019). The LCD is also the region that harbors numerous ALS-linked point mutations (Buratti, 2015), suggesting that small chemical changes to the TDP-43 LCD can cause neurodegeneration.

Liquid–liquid phase separation and MLO dynamics are often regulated by post-translational modifications (PTMs) in LCDs, as the introduction of small chemical groups or proteins changes the chemical nature of amino acids, e.g., their charge or hydrophobicity, which can alter their molecular interactions and LLPS behavior (Bah & Forman-Kay, 2016; Hofweber & Dormann, 2019). A highly disease-specific PTM on deposited TDP-43 inclusions is hyperphosphorylation on C-terminal serine residues in the LCD (Hasegawa *et al*, 2008; Inukai *et al*, 2008; Neumann *et al*, 2009; Kametani *et al*, 2016). Antibodies specific for C-terminal TDP-43 phosphorylation sites (e.g., S409/S410 and S403/S404) detect inclusion pathology in patients, without cross-reactivity with physiological nuclear TDP-43. Therefore, C-terminal TDP-43 hyperphosphorylation is considered a pathological hallmark and is generally believed to promote TDP-43 aggregation (Buratti, 2018). This view is largely based on the observations that C-terminal TDP-43 phosphorylation correlates with inclusion pathology and that overexpression of kinases that can phosphorylate TDP-43 enhance TDP-43 aggregation and neurotoxicity (Choksi *et al*, 2014; Liachko *et al*, 2014; Nonaka *et al*, 2016; Taylor *et al*, 2018). Based on these studies, inhibition of TDP-43 phosphorylation by specific kinase inhibitors has even been proposed as a potential therapeutic strategy for ALS (Liachko *et al*, 2013; Salado *et al*, 2014; Martinez-Gonzalez *et al*, 2020). However, the molecular consequences of this disease-linked PTM are still poorly understood, and its effects on TDP-43 LLPS and aggregation are still unknown.

Using *in vitro*, *in silico* and cellular experiments, we now demonstrate that disease-linked C-terminal hyperphosphorylation of TDP-43 suppresses TDP-43 condensation and insolubility. We show this through (i) *in vitro* phase separation and aggregation assays with recombinant, full-length TDP-43; (ii) coarse-grained and atomistic molecular dynamics (MD) simulations of condensates of TDP-43 LCDs, elucidating molecular driving forces; and (iii) experiments in HeLa cells, stable inducible U2OS cells and primary rat neurons, where C-terminal phosphomimetic mutations do not disturb nuclear import or RNA processing functions of TDP-43, but abrogate TDP-43 condensation into MLOs and enhance its solubility. Based on our findings, we speculate that C-terminal TDP-43 hyperphosphorylation may be a protective cellular response to counteract TDP-43 solidification, rather than being a driver of TDP-43 pathology, as has so far been assumed.

Results

In vitro phosphorylation with Casein kinase 1δ reduces condensation of TDP-43

To examine how phosphorylation affects TDP-43 phase transitions, we expressed and purified unphosphorylated full-length TDP-43 with a solubilizing MBP tag and a His_6-tag in *Escherichia coli* (Wang *et al*, 2018) (Appendix Fig S1A–E). We then *in vitro* phosphorylated the purified protein with casein kinase 1 delta (CK1δ), a kinase previously reported to phosphorylate TDP-43 at disease-associated sites (Kametani *et al*, 2009), and confirmed phosphorylation of C-terminal serines (S403/S404; S409/S410) with phospho-specific antibodies (Fig EV1A). Mass spectrometric analysis detected phosphorylation on several additional serine/threonine sites (Fig EV1B), and the running behavior in SDS–PAGE suggests hyperphosphorylation on multiple sites (Figs 1B and EV1A). We then induced phase separation of the unphosphorylated vs *in vitro* phosphorylated TDP-43 by cleaving off the MBP tag with TEV protease (Wang *et al*, 2018) and used centrifugation to separate the condensates (C) from the cleared supernatant (S; Fig 1A). Cleaved TDP-43 was mostly in the condensate fraction (S/[S + C] ratio ~0.25), whereas *in vitro* phosphorylated TDP-43 was predominantly in the supernatant (S/[S + C] ratio > 0.6; Fig 1B and C). Reduced sedimentation of TDP-43 was not seen upon addition of adenosine triphosphate (ATP) or CK1δ alone, suggesting that it is indeed caused by the addition of phospho-groups to TDP-43.

C-terminal phosphomimetic substitutions mimicking disease-linked phosphorylation suppress TDP-43 phase separation

To study defined disease-linked phosphorylation sites, we generated phosphomimetic proteins harboring different numbers of

Figure 1. TDP-43 phosphorylation by CK1δ and C-terminal phosphomimetic substitutions reduce TDP-43 condensation *in vitro*.

A Scheme of sedimentation assay (created in BioRender.com): phase separation of TDP-43 was induced by TEV protease cleavage of TDP-43-MBP-His_6, and condensates were pelleted by centrifugation.

B Sedimentation assay to quantify condensation of unmodified TDP-43 versus *in vitro* phosphorylated TDP-43 (+CK1δ, +ATP) and controls (CK1δ or ATP only); TDP-43 detected by Western blot (rabbit anti-TDP-43 N-term). Due to incomplete TEV cleavage, some TDP-43-MBP-His_6 remains present and co-fractionates with cleaved TDP-43, due to TDP-43 self–self interaction.

C Quantification of band intensities of cleaved TDP-43 shown as mean of Supernatant/(Supernatant + Condensate) (S/[S + C]) ratio of three independent experimental replicates ($n = 3$) ± SD. ***$P < 0.0002$ by one-way ANOVA with Dunnett's multiple comparison test to Wt.

D Schematic diagram of TDP-43 and sequence of C-terminal region (aa. 370–414) for Wt, phosphomimetic (S-to-D) variants and control (S-to-A) variants. NTD, N-terminal domain; RRM, RNA recognition motif; LCD, low complexity domain with α-helical structure.

E Turbidity measurements (optical density [OD] at 600 nm) to quantify phase separation of the indicated TDP-43 variants at three different concentrations (in Hepes buffer). Values represent mean of three independent experimental replicates ($n = 3$) ± SD. *$P < 0.0332$, **$P < 0.0021$ and ***$P < 0.0002$ by one-way ANOVA with Dunnett's multiple comparison test to Wt, comparing the respective concentration condition (5, 10 and 20 μM).

F–I Representative bright field microscopic images of TDP-43 condensates (in Hepes buffer), Bar, 25 μm (F) and quantification of condensate number (G), size (H) and roundness (I). Box plots show the comparison of median and inter-quartile range (upper and lower quartiles) of all fields of view (FOV) from Min to Max (whiskers) of two replicates (≥ 22 FOV per condition). *$P < 0.0332$, **$P < 0.0021$ and ***$P < 0.0002$ by one-way ANOVA with Dunnett's multiple comparison test to Wt, comparing the respective concentration condition (5, 10 and 20 μM).

Source data are available online for this figure.

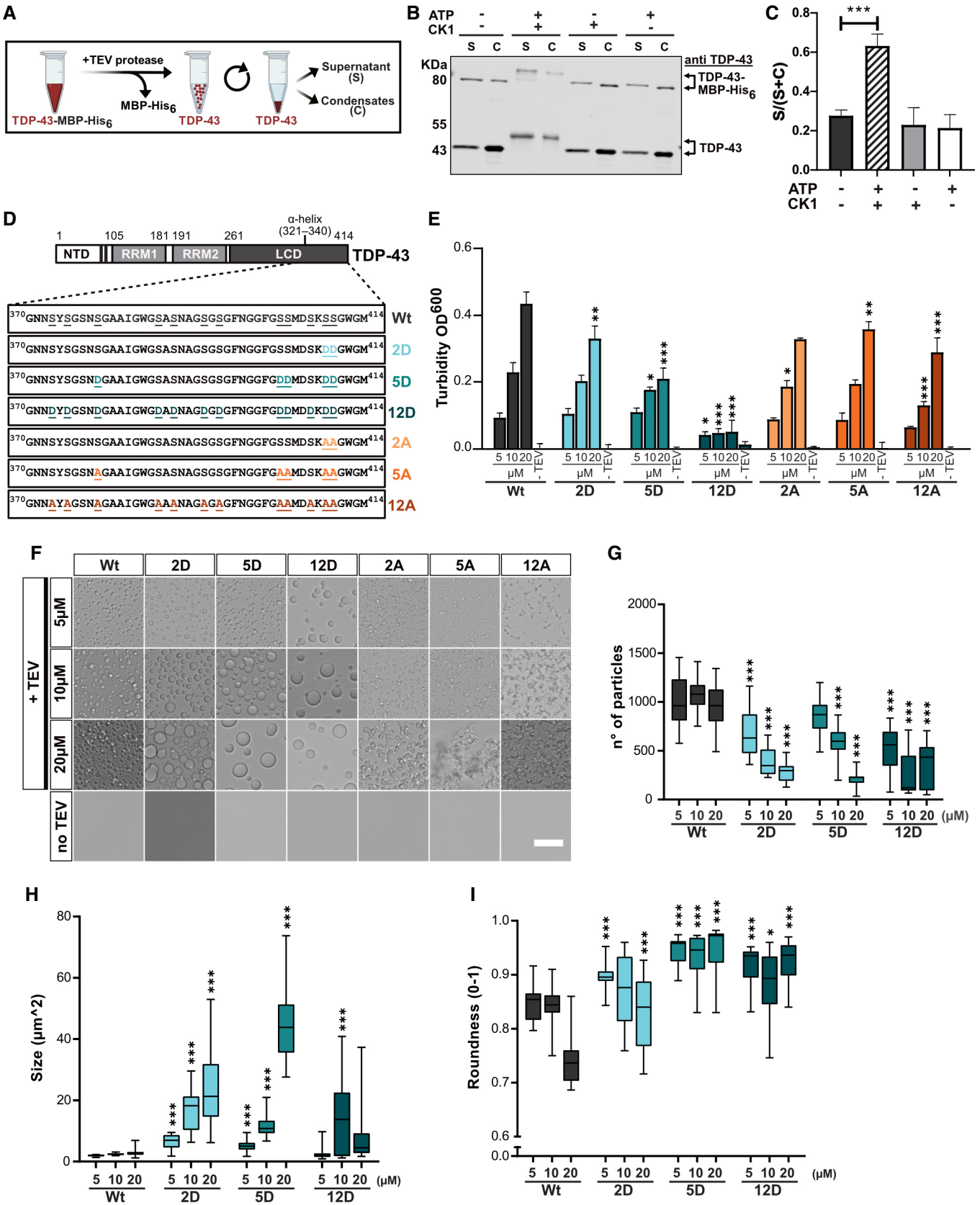
A
+TEV protease
MBP-His6
TDP-43-MBP-His6
TDP-43
TDP-43
Supernatant (S)
Condensates (C)
B
ATP
CK1
S C S C S C S C
KDa
80
55
43
anti TDP-43
TDP-43-MBP-His6
TDP-43
C
S/(S+C)
ATP
CK1
D
1 105 181 191 261 α-helix (321–340) 414
NTD RRM1 RRM2 LCD TDP-43
Wt
2D
5D
12D
2A
5A
12A
E
Turbidity OD600
5 10 20 μM -TEV
Wt 2D 5D 12D 2A 5A 12A
F
Wt 2D 5D 12D 2A 5A 12A
+ TEV
5μM
10μM
20μM
no TEV
G
n° of particles
5 10 20 (μM)
Wt 2D 5D 12D
H
Size (μm^2)
5 10 20 (μM)
Wt 2D 5D 12D
I
Roundness (0-1)
5 10 20 (μM)
Wt 2D 5D 12D

Figure 1.

phosphomimetic serine-to-aspartate (S-to-D) mutations or corresponding serine-to-alanine (S-to-A) mutations as control. Phosphomimetic substitutions rely on the replacement of a phosphorylated serine or threonine with a negatively charged amino acid (D or E), thus mimicking the negative charge of the phospho group. Even though they under-appreciate the charge change (net charge of aspartate = −1 instead of −2 for a phospho-group) and do not always accurately mimic the chemistry of a phospho group, phosphomimetics have been successfully used to probe the biological function of phosphorylated residues (Martin *et al*, 2014). Phosphorylation on S409/S410 is a highly specific and consistent feature of aggregated TDP-43 in all ALS/FTD subtypes (Inukai *et al*, 2008; Neumann *et al*, 2009), and five phosphorylation sites (S379, S403, S404, S409 and S410) were detected with phosphorylation site-specific antibodies in human post-mortem tissue (Hasegawa *et al*, 2008). Therefore, we mutated these serines to create "2D" and "5D" variants as well as the corresponding "2A" and "5A" controls (Fig 1 D). Based on a mass spectrometric study that found phosphorylation on 12 out of 14 serines in the C-terminal LCD of TDP-43 in ALS spinal cord (Kametani *et al*, 2016), we also mutated these 12 sites (S373, S375, S379, S387, S389, S393, S395, S403, S404, S407, S409 and S410) to create "12D" or "12A" variants (Fig 1D). Interestingly, the PLAAC web tool (http://plaac.wi.mit.edu/) that allows prediction of probable prion subsequences using a hidden-Markov model (HMM) algorithm (Lancaster *et al*, 2014), predicted a reduced prion-like character of the C-terminal region in the phosphomimetic 12D variant compared with the wild-type (Wt) and 12A protein (Appendix Fig S2).

To study phase separation experimentally, all variants were expressed and purified as TDP-43-MBP-His_6 fusion proteins (Appendix Fig S1A–E), and phase separation induced by TEV protease-mediated cleavage of the MBP tag was examined by turbidity, sedimentation or microscopic condensate assays. Turbidity measurements revealed a concentration-dependent increase in phase separation for TDP-43 Wt, as expected, whereas the increase was less pronounced for the 2D and 5D variants and no concentration-dependent increase was seen for the 12D mutant (Fig 1E). The gradual decrease in turbidity caused by the phosphomimetic mutations (Wt > 2D > 5D > 12D) was not seen to the same extent for the corresponding S-to-A control mutations (Fig 1E), hence suppression of phase separation is not due to the loss of serines at these positions, but can be attributed to the additional negative charges introduced by the D substitutions. Turbidity assays in phosphate buffer instead of Hepes buffer gave similar results (Fig EV2A), and sedimentation assays confirmed that TDP-43 condensation is gradually suppressed by increasing numbers of phosphomimetic mutations (Fig EV2B and C).

Phosphomimetic S-to-D substitutions lead to rounder TDP-43 condensates, whereas S-to-A mutations cause an amorphous, aggregate-like morphology

Interestingly, bright field microscopy revealed that TDP-43 Wt formed relatively small, amorphous condensates, suggestive of solid-like material properties (Fig 1F). In contrast, the phosphomimetic S-to-D proteins formed fewer, but much larger and rounder condensates (Fig 1F, see G–I for quantification), suggesting a more liquid-like behavior and therefore fusion of condensates into larger droplets. Again, the observed changes were correlated with the number of phosphomimetic mutations, i.e., they were most pronounced for the 12D mutant, which formed very few, but large and perfectly circular protein droplets. (Note that these few large condensates most likely escape detection in the turbidity assay due to rapid sedimentation during the assay.) In contrast, the S-to-A control variants formed numerous small, amorphous condensates and had a more irregular, aggregate-like appearance than TDP-43 Wt (Fig 1F). This phenotype suggests that the OH groups in the respective serines influence the material properties of TDP-43 and contribute to preventing its aggregation. Similar results were obtained when the assay was carried out in phosphate buffer instead of Hepes buffer, except that 12D formed only very few, small condensates in phosphate buffer (Fig EV2D), possibly because the ions in phosphate buffer may screen certain attractive interactions between TDP-43 molecules and disfavor phase separation. Together, these results demonstrate that phosphomimetic substitutions mimicking disease-linked C-terminal TDP-43 phosphorylation reduce the tendency of TDP-43 to phase separate into amorphous condensates and suggest a more dynamic, liquid-like behavior of C-terminally phosphorylated TDP-43.

C-terminal phosphomimetic substitutions yield more liquid-like, dynamic TDP-43 condensates

To test whether the phosphomimetic mutations indeed render TDP-43 more liquid-like, we performed live imaging of Alexa488-labeled Wt, 5D and 12D condensates by spinning disc confocal microcopy. For TDP-43 Wt, no fusion events were observed over a time course of several minutes. Instead the small condensates stuck to each other in a chain-like arrangement (Movie EV1, Fig 2A). In contrast, 5D condensates occasionally and slowly fused with each other, and 12D condensates readily fused upon contact and relaxed into perfectly round spheres, indicating a liquid droplet-like nature (Movies EV2 and EV3, Fig 2A). To assess the mobility of TDP-43 molecules in condensates, we performed half-bleaches of condensates and analyzed fluorescent recovery after photobleaching (FRAP) in the bleached half. In TDP-43 Wt condensates, fluorescence recovered very slowly, indicating a low mobility of TDP-43 molecules, whereas recovery was faster in 5D and even faster in 12D condensates (Fig 2B and C), in line with an increased mobility of phosphomimetic TDP-43 compared with "unmodified" TDP-43. Taken together, phosphomimetic S-to-D substitutions in the C-terminal region enhance the liquidity of TDP-43 condensates, suggesting that phosphorylation in this region might counteract TDP-43's tendency to form solid, irreversible aggregates.

C-terminal phosphomimetic substitutions reduce TDP-43 aggregation

To address whether phosphorylation indeed counteracts TDP-43 aggregation, we performed *in vitro* aggregation assays modified from published protocols (Halfmann & Lindquist, 2008; French *et al*, 2019). Under the assay conditions, TEV cleavage of fluorescently labeled TDP-43-MBP-His_6 yields amorphous TDP-43 aggregates that can be visualized by confocal microscopy. In contrast to Wt or 12A, the phosphomimetic 5D or 12D proteins formed much smaller and fewer aggregates, respectively (Fig 2D), suggesting that C-terminal

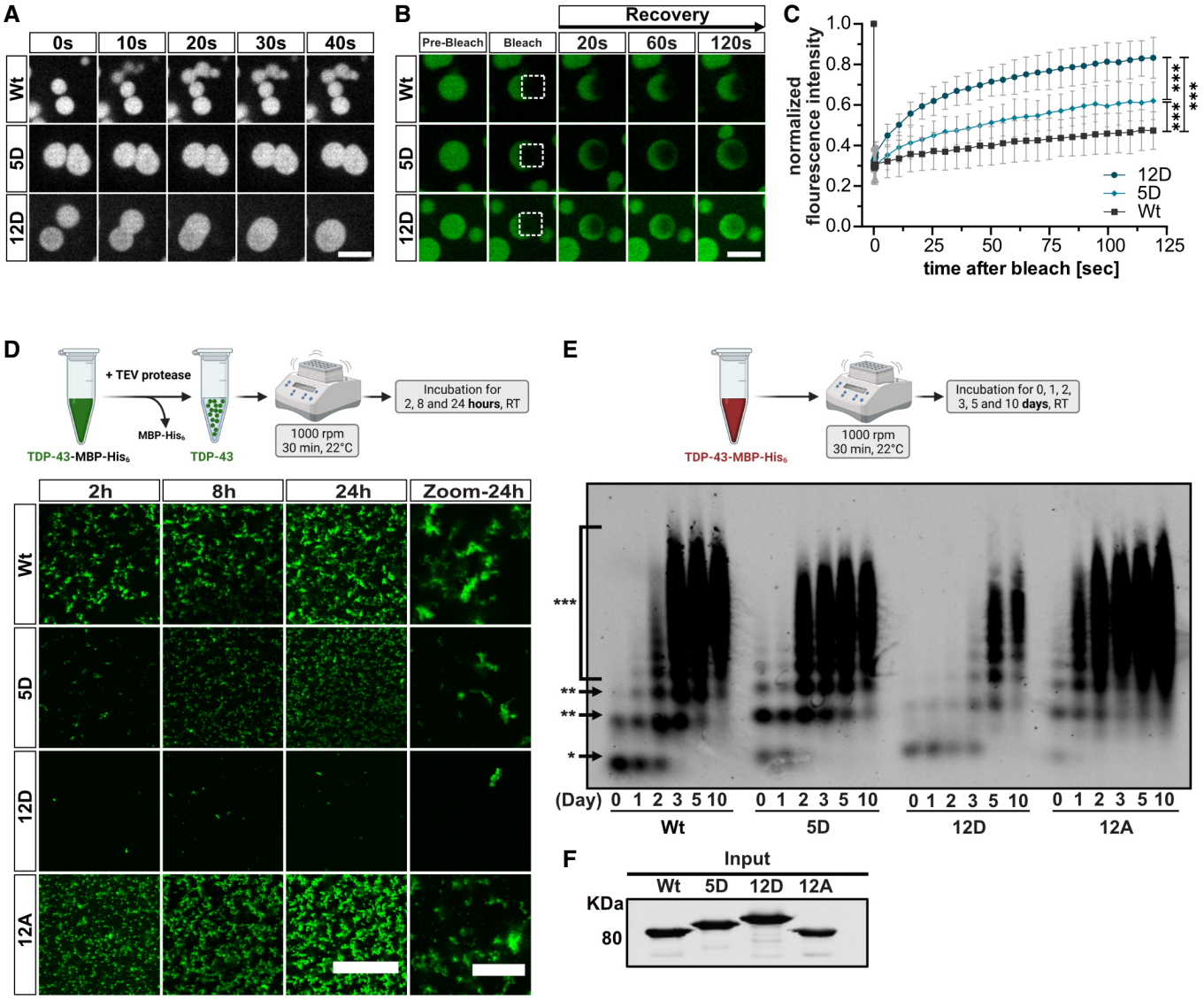

Figure 2. C-terminal phosphomimetic substitutions enhance liquidity of TDP-43 condensates and reduce TDP-43 aggregation *in vitro*.

A Representative still images of Alexa488-labeled TDP-43 condensates by spinning disc timelapse confocal microscopy. Wt condensates do not fuse, 5D condensates fuse slowly and 12D condensates readily fuse upon contact and relax into spherical droplets. Bar, 5 μm.

B Representative images of FRAP experiments at indicated time-points. Boxes indicate bleached area (half-bleach of condensate). Bar, 5 μm.

C FRAP curves after half-bleach of freshly formed Alexa488-labeled TDP-43 condensates. Values represent mean ± SD of three independent experimental replicates ($n = 3$) of ≥ 9 droplets analyzed per condition. ***$P < 0.0002$ by one-way ANOVA with Tukey's multiple comparison test for area under the curve (AUC) of individual droplets.

D Confocal images of Alexa488-labeled TDP-43 aggregates formed in an *in vitro* aggregation assay (with TEV protease cleavage). Bar, 100 μm. Zoom shows magnified view of aggregates at the 24 h time point. Bar, 20 μm.

E SDD-AGE followed by TDP-43 Western blot to visualize SDS-resistant oligomers/high-molecular-weight species of TDP-43-MBP-His_6 in an *in vitro* aggregation assay (without TEV protease cleavage). Asterisks represent monomeric (*), oligomeric (**) and polymeric (***) species.

F Input of TDP-43-MBP-His_6 variants used in the SDD-AGE assay, detected by Western blot (anti-TDP-43 N-term).

Source data are available online for this figure.

TDP-43 phosphorylation can efficiently suppress TDP-43 aggregation. For biochemical characterization of the formed aggregates, we performed semi-denaturing detergent-agarose gel electrophoresis (SDD-AGE) under the same assay conditions, just in the absence of TEV, as MBP-tagged TDP-43 aggregates slower than TDP-43 and distinct oligomeric/polymeric species resistant to 0.5% SDS can be visualized under these conditions (Appendix Fig S3). In comparison to TDP-43 Wt and 5D, 12D showed reduced and delayed oligomerization and formation of high-molecular-weight species (Fig 2E, equal protein input shown in Fig 2F). In contrast, 12A formed SDS-resistant oligomers/high-molecular-weight species at a higher rate, which together with our microscopic images of TDP-43 condensates

(Fig 1F), suggests that C-terminal alanine substitutions make TDP-43 more aggregation-prone. Taken together, C-terminal phosphomimetic substitutions that mimic the phosphorylation pattern in ALS patients reduce the formation of SDS-resistant high-molecular-weight oligomers and TDP-43 aggregates *in vitro*.

Multi-scale simulations of the TDP-43 LCD reveal reduced protein-protein interactions through enhanced solvation of phosphomimetic residues

To understand the effect of C-terminal TDP-43 phosphorylation on phase separation at the molecular level, we used coarse-grained and atomistic MD simulations of the disordered TDP-43 LCD (aa. 261–414) with and without phosphomimetic substitutions. In coarse-grained simulations, we can access the relevant long time and large length scales to characterize phase behavior, while in atomistic simulations we can resolve the interactions of condensates with high resolution and high accuracy (Dignon *et al*, 2018; Pietrek *et al*, 2020; Benayad *et al*, 2021). We found that phosphomimetic substitutions locally reduce protein–protein interactions (Fig EV3) and increase protein–solvent interactions (Fig 3). In the coarse-grained simulations, the LCD of both TDP-43 Wt and 12D phase separated spontaneously to form condensates (shown for Wt in Fig 3A and Movie EV4). Yet, phosphomimicking residues are less prone to interact with protein in the phase-separated condensates and are somewhat more solvated than the corresponding serine residues (Figs 3B and EV3A and B). The aspartate side chains in 12D LCDs engage in partially compensatory interactions with arginines, showing that introduction of charged side chains gives rise to both stabilizing and destabilizing interactions in condensates. Importantly, our simulations are in line with previous studies that have highlighted the importance of aromatic sticker–sticker interactions in driving phase separation of prion-like domains and the TDP-43 LCD (Li *et al*, 2018; Schmidt *et al*, 2019; Martin *et al*, 2020).

To characterize the interactions of TDP-43 LCDs further, we performed atomistic MD simulations of dense protein condensates (Fig 3C, Movie EV5) assembled with hierarchical chain growth (HCG; Pietrek *et al*, 2020) to enhance the sampling of polymeric degrees of freedom. In microsecond dynamics with explicit solvent and a highly accurate atomistic description of molecular interactions (Robustelli *et al*, 2018), we again found serine residues in the Wt protein to be more prone to interact with other protein residues than interacting with solvent (Fig 3D). By contrast, phosphomimicking aspartate side chains bind comparably more water molecules and show an overall reduced tendency for protein-protein interactions (Fig 3D and E, Appendix Fig S4A). Enhanced side chain solvation is consistent across the 12 phosphomimetic substitution sites (Appendix Fig S4B). The atomistic simulations are consistent with an increase in charge favoring solvated states and thus weakening TDP-43 condensates.

Effects of phosphomimicking mutations and phosphorylation on TDP-43 LCD phase behavior

To characterize possible differences between phosphomicking mutations and phosphorylation, we employed the highly efficient hydrophobicity scale (HPS) coarse-grained model (Dignon *et al*, 2018). The HPS implicit solvent model enabled us to quantify differences in the phase behavior of TDP-43 LCD variants. In line with experiments on full-length TDP-43 (Fig 1), 12D LCD phase-separated, but more protein remained in the dilute phase compared with Wt (Fig 3F–H). Indeed, computing the excess free energy of transfer $\Delta G_{\mathrm{trans}}$ from the density profile (Appendix Fig S5D), which reports how favorable it is to move one chain from dilute solution at the saturation density to the dense phase of the condensate, showed that 12D LCDs are less prone to interact with each other in a condensate than Wt LCDs (Appendix Table S1). Loss of local contacts in the C-terminal region due to phosphomimetic substitutions was only partially compensated by new protein–protein interactions with arginines (Appendix Fig S5A–C), in accordance with coarse-grained simulations with explicit solvent (Fig EV3C). The 12A substitutions stabilized the TDP-43 LCD condensates, as expected based on our experiments, with little protein remaining in the dilute phase (Fig 3F). Phosphorylation modulates the stability of LCD condensates in a dose-dependent way. Attaching five phospho groups (5pS) led to a somewhat less-dense LCD condensate, but overall the excess free energy of transfer is on par with Wt (Appendix Table S1, Appendix Fig S5D). By contrast, fully phosphorylating all twelve sites (12pS) dissolved the LCD condensate in our simulations, with no clear peak in the density profile (Fig 3F).

Figure 3. Atomistic and coarse-grained simulations of TDP-43 LCD: phosphomimicking residues form fewer protein–protein interactions and more protein–solvent interactions.

A TDP-43 LCD phase separates in coarse-grained simulations with explicit solvent. Condensate of TDP-43 Wt LCD is shown, protein colored according to chain identity. Water omitted for clarity. Ions shown in cyan.

B Normalized probability of protein-protein contacts by phosphomimicking aspartates in 12D and serines in Wt resolved by amino acid type from coarse-grained simulations. Error bars smaller than symbols. Inset: Distributions of the number of water molecules within 5 Å of side chains of phosphomimicking aspartates of 12D and corresponding serines in Wt from 15 μs of coarse-grained molecular dynamics simulations.

C Atomistic simulation setup of 32 TDP-43 LCDs. Different LCD chains shown in different colors in space-filling representation. For one chain (lower left), a transparent surface reveals its atomic structure as sticks.

D Normalized probability of protein–protein contacts by phosphomimicking aspartates in 12D and serines in Wt resolved by amino acid type from atomistic simulations. Two 1 μs simulations are distinguished by color intensity. Inset: distributions of the number of water molecules within 5 Å of the side chains of phosphomimicking aspartates of 12D and the corresponding serines in Wt from atomistic simulations.

E Representative snapshots of atomistic simulations showing water within 3 Å of (left) Wt S407, S409 and S410 with nearby LCDs in surface representation and (right) 12D D407, D409 and D410. Protein surfaces are colored according to chain identity.

F Density profiles in TDP-43 LCD condensates (peak at center) coexisting with dilute solutions for Wt, 12D, 5pS, 12pS and 12A from coarse-grained simulations with the implicit solvent coarse-grained HPS model.

G, H Snapshots of 12D condensate (G) and fragmented 12pS clusters (H) in simulations with the coarse-grained HPS model. Side view on elongated boxes (blue lines).

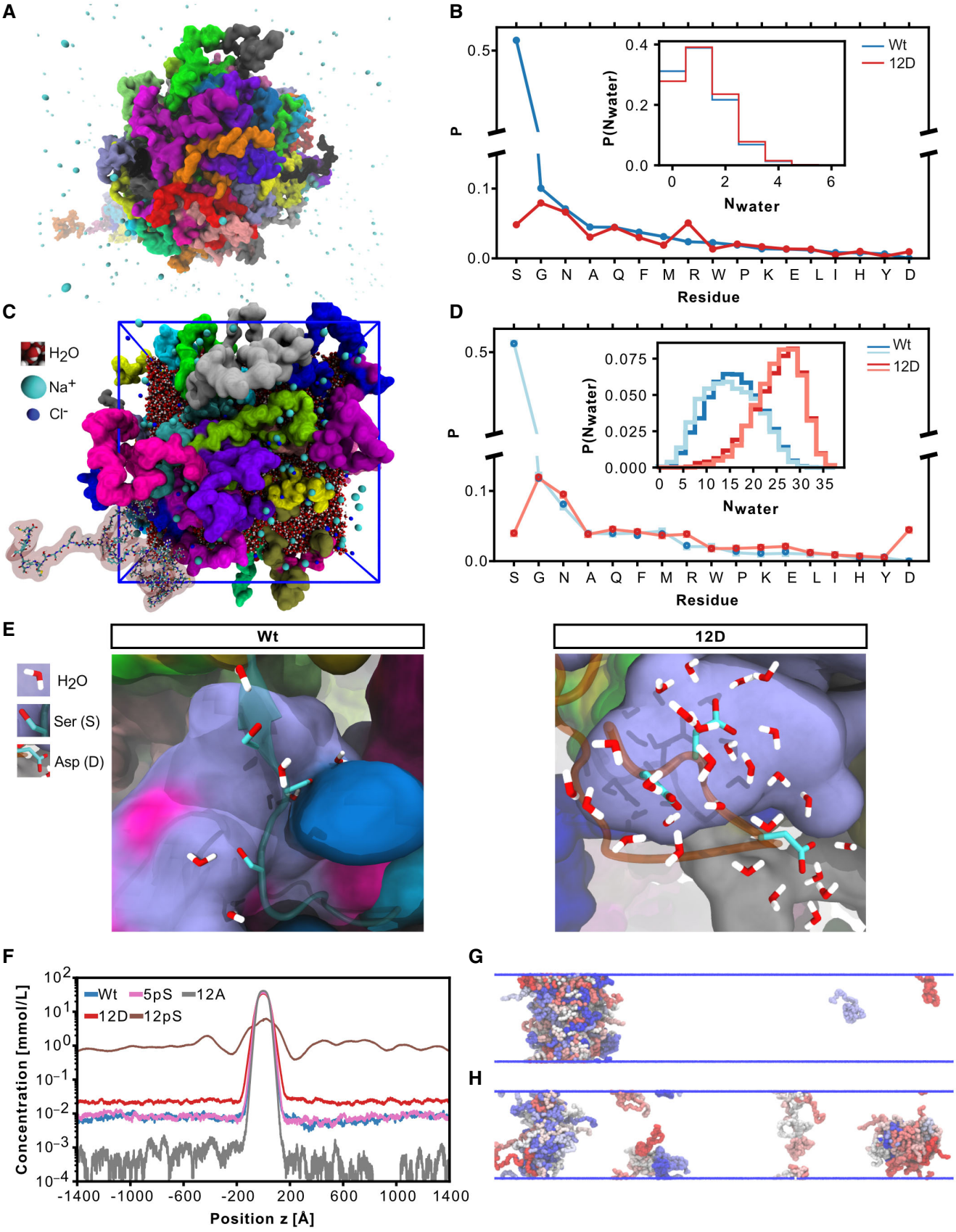
A
B
0.5
0.1
0.0
P
0.4
0.2
0.0
P(Nwater)
0 2 4 6
Nwater
Wt
12D
S G N A Q F M R W P K E L I H Y D
Residue
C
H2O
Na+
Cl-
D
0.5
0.1
0.0
P
0.075
0.050
0.025
0.000
P(Nwater)
0 5 10 15 20 25 30 35
Nwater
Wt
12D
S G N A Q F M R W P K E L I H Y D
Residue
E
Wt
12D
H2O
Ser (S)
Asp (D)
F
Wt 5pS 12A
12D 12pS
Concentration [mmol/L]
10^2
10^1
10^0
10^-1
10^-2
10^-3
10^-4
-1400 -1000 -600 -200 200 600 1000 1400
Position z [Å]
G
H

Figure 3.

Overall, the simulations with the HPS model rank the saturation density to form condensates as 12A ≫ Wt ~5pS > 12D ≫ 12pS. The calculations thus predict that (i) phosphorylation may indeed dissolve condensates, and (ii) that phosphorylation may have an even stronger effect than phosphomicking substitutions, due to the larger negative charge of phospho-serine compared with aspartate.

C-terminal phosphomimetic substitutions do not impair nuclear import and RNA regulatory functions of TDP-43

Next, we turned to cellular experiments to investigate how C-terminal TDP-43 phosphorylation affects the behavior and function of TDP-43 in cells. As TDP-43 hyperphosphorylation is found in the disease state, it seems possible that this PTM has detrimental effects on the protein and contributes to mislocalization and/or malfunction of TDP-43, thus driving neurodegeneration. To address this possibility, we transiently expressed different myc-tagged TDP-43 variants (Wt, 12D, 12A) in HeLa cells and analyzed their intracellular localization, nuclear import and RNA processing functions. All three TDP-43 variants showed a predominantly nuclear steady-state localization (Fig EV4A). We also compared their nuclear import rates in a hormone-inducible reporter assay by live cell imaging (Hutten *et al*, 2020). In this assay, a protein-of-interest harboring a nuclear localization signal (NLS) is fused to a tandem EGFP and two hormone binding domains of the glucocorticoid receptor (GCR), which retains the reporter protein in the cytoplasm. Upon addition of a steroid hormone (dexamethasone), the reporter protein is released from the cytoplasm and imported into the nucleus, by virtue of the NLS in the protein-of-interest. We examined reporters containing the different TDP-43 variants (Wt, 12D, 12A) and found that their import rates were indistinguishable (Fig 4A and B).

To assess whether hyperphosphorylated TDP-43 shows functional impairments in RNA processing, we first assessed its ability to autoregulate its own levels when transiently overexpressed in HeLa cells (Ayala *et al*, 2011; Avendano-Vazquez *et al*, 2012). However, endogenous TDP-43 was downregulated to the same degree by all three myc-TDP-43 variants (Fig 4C), indicating that hyperphosphorylated TDP-43 can normally bind to its own 3′UTR and autoregulate its own levels. In line with these findings, recombinant TDP-43 Wt, 12D and 12A showed comparable RNA binding in electrophoretic mobility shift assays (EMSAs) with *in vitro* transcribed RNA comprised of the autoregulatory TDP-43 binding site (Fig 4D) or synthetic $(UG)_{12}$ RNA (Fig EV4B). Second, we examined splicing of two known TDP-43 splice targets that get mis-spliced upon loss of TDP-43 (Tollervey *et al*, 2011; Fiesel *et al*, 2012). After siRNA-mediated silencing of endogenous TDP-43 expression and re-expression of siRNA-resistant myc-TDP-43 Wt, 12D or 12A (Appendix Fig S6A), splicing of *SKAR* and *Bim* exon 3 were fully restored by all three TDP-43 variants (Fig 4E), indicating normal function of phosphomimetic TDP-43 in splicing regulation. Normal nuclear localization and autoregulation of TDP-43 were also replicated in a cellular system that avoids high overexpression and has homogenous expression levels, namely stable inducible Flp-In U2OS cell lines that express the different myc-TDP-43 variants (Wt, 12D and 12A) after overnight doxycycline addition (Fig EV4C–E, in Fig EV4C endogenous TDP-43 was silenced with siRNAs, see Appendix Fig S6C). In conclusion, even though an effect on other RNA targets/RNA processing events or intracellular transport in other cell types cannot be excluded, our data suggest that C-terminal TDP-43 hyperphosphorylation is not primarily responsible for cytosolic mislocalization or impaired RNA regulatory functions of TDP-43 in disease.

Phosphorylation suppresses recruitment of TDP-43 into stress-induced MLOs

Finally, we investigated how C-terminal TDP-43 phosphorylation affects TDP-43 condensation in cellular MLOs. First, we used a quantitative assay to measure SG association of recombinant proteins under controlled conditions in semi-permeabilized HeLa cells (Hutten & Dormann, 2020) (Fig 5A). In line with our *in vitro* condensation experiments, increasing the number of phosphomimetic S-to-D substitutions caused a gradual decrease in SG association of TDP-43 (Fig EV5A and B). *In vitro* phosphorylated TDP-43 showed a similar or even stronger reduction in SG association as the 12D protein (Fig 5B and C), demonstrating that the phosphomimetic substitutions and phospho-groups introduced by a kinase have similar effects on SG association of TDP-43. Second, we expressed the different TDP-43 variants in intact HeLa cells to analyze their recruitment into stress-induced MLOs. To this end, we silenced endogenous TDP-43 expression using siRNA (Appendix Fig S6A and B) and then re-introduced siRNA-resistant myc-tagged TDP-43 Wt, 12D or 12A, thus avoiding oligomerization with endogenous TDP-43 via the N-terminal domain (Afroz *et al*, 2017). Short term oxidative stress treatment with H_2O_2 caused a partially cytosolic relocalization

Figure 4. Phosphomimetic substitutions do not alter the rate of TDP-43 nuclear import and do not impair TDP-43 autoregulation, RNA-binding or alternative splicing function.

A Hormone-inducible nuclear import assay, representative still images of GCR_2-$EGFP_2$-TDP-43 Wt, 12D and 12A before and during import triggered by addition of dexamethasone. Images were live recorded by spinning disc confocal microscopy. Bar, 20 μm.

B Quantification of the hormone-inducible nuclear import measured during a total time course of 50 min. Values represent the mean fluorescence intensity of GCR_2-$EGFP_2$-TDP-43 in the cytoplasm for three independent replicates ± SEM (≥ 42 cells per condition).

C Phosphomimetic 12D TDP-43 is competent in autoregulating TDP-43 expression. SDS–PAGE followed by TDP-43 Western blot showing downregulation of endogenous TDP-43 through autoregulation (*60*) after 48 h expression of Wt, 12D and 12A variants in HeLa cells. TDP-43 was detected using rabbit anti-TDP-43 C-term antibody (Proteintech), Histone H3 (rabbit anti-Histone H3 antibody, Abcam) was visualized as a loading control. * denotes an unspecific band.

D Electrophoretic mobility shift assays (EMSA) of TDP-43-MBP-His_6 variants (Wt, 12D and 12A) in a complex with TDP-43 autoregulatory RNA binding site (*60*). All TDP-43 variants form TDP-43-RNA complexes equally well.

E Splicing analysis by RT–PCR of known TDP-43 splice targets (*SKAR* exon 3 and *Bim* exon 3) in HeLa cells. Silencing of endogenous TDP-43 by siRNA leads to altered splice isoforms of *SKAR* and *Bim* (second vs first lane). These splicing alterations can be rescued by re-expression of TDP-43 Wt, but also 12D or 12A variants, demonstrating that phosphomimetic TDP-43 is fully competent in regulation splicing of these TDP-43 splice targets.

Source data are available online for this figure.

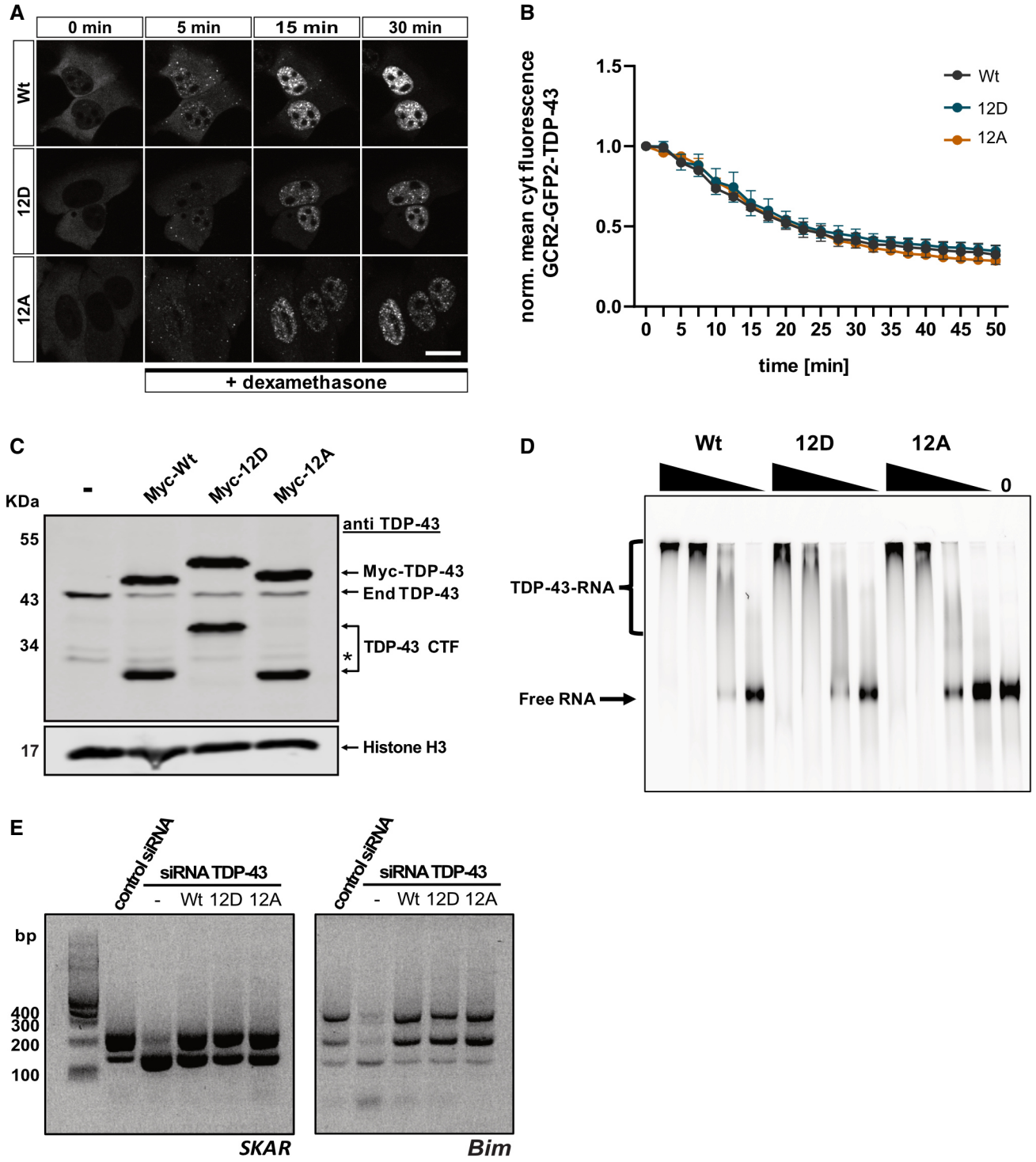

Figure 4.

of TDP-43 and led to recruitment of TDP-43 Wt and 12A, but significantly reduced recruitment of the 12D mutant into TIA-1-positive SGs (Fig 5D and E, see Appendix Fig S6D for control staining of untransfected cells). Similar results were obtained for nuclear import-deficient TDP-43 (Fig 5F and G) that was strongly mislocalized to the cytoplasm due to point mutations in the nuclear localization signal (NLSmut; Appendix Fig S7). Finally, we examined recruitment of TDP-43 into arsenite-induced nuclear bodies (NBs) (Wang *et al*, 2020) and found that TDP-43 Wt and 12A were readily recruited into stress-induced NBs, while the phosphomimetic 12D protein remained dispersed in the nucleoplasm (Fig 5H–J, see Appendix Fig S6E for control staining of untransfected cells). TDP-

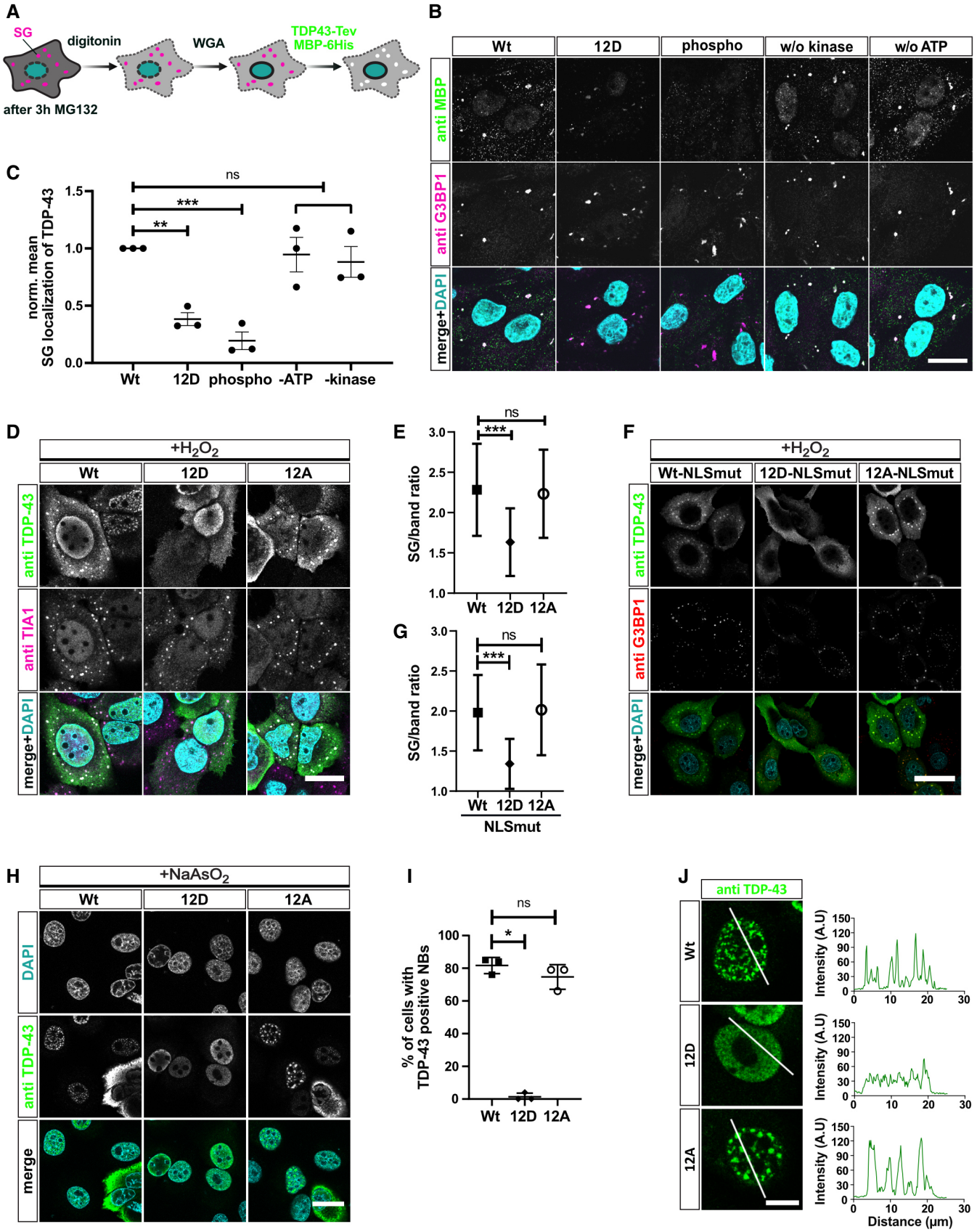

Figure 5.

Figure 5. Phosphorylation and phosphomimetic substitutions reduce recruitment of TDP-43 into stress-induced membrane-less organelles.

A Scheme of stress granule (SG) recruitment assay in semi-permeabilized cells.
B Reduced SG association of TDP-43 by 12D mutations or *in vitro* phosphorylation. Bar, 20 μm.
C Quantification of TDP-43-MBP-His_6 mean fluorescence intensity in SGs normalized to Wt ± SEM of three independent experimental replicates ($n = 3$; ≥ 10 cells; ≥ 46 SGs each). $^{**}P < 0.0021$ and $^{***}P < 0.0002$ by one-way ANOVA with Dunnett's multiple comparison test to Wt.
D SG recruitment of TDP-43 variants in intact HeLa cells in absence of endogenous TDP-43. After TDP-43 silencing and expression of myc-TDP-43 Wt, 12D and 12A variants, SGs were induced by H_2O_2 treatment and SG recruitment of TDP-43 was monitored by TDP-43 and TIA1 immunostaining. For clarity, signals were converted to grey values in the individual channels (upper two rows). In the merge (lower row), nuclei were stained in DAPI (turquoise), TDP-43 (green) and TIA-1 (magenta). Bar, 25 μm.
E Quantification of TDP-43 in SGs versus cytoplasm ± SD of two independent experimental replicates ($n = 2$; ≥ 62 cells; ≥ 234 SGs each). $^{***}P < 0.0002$ by Krustal–Wallis test with Dunn's multiple comparison test to Wt.
F SG recruitment of different TDP-43-NLSmut variants in intact HeLa cells in the absence of endogenous TDP-43. After TDP-43 silencing and expression of NLSmut Wt, 12D and 12A variants, SGs were induced by H_2O_2 treatment and SG recruitment of TDP-43 was monitored by TDP-43 and G3BP1 immunostaining. For clarity, signals were converted to grey values in the individual channels (upper two rows). In the merge (lower row), nuclei were stained in DAPI (turquoise), TDP-43 (green) and G3BP1 (red). Bar, 40 μm.
G Quantification of TDP-43-NLS mutants in SGs versus band around SGs of two independent replicates ± SD. $^{***}P < 0.0002$ by Kruskal–Wallis test with Dunn's multiple comparison test to Wt (≥ 56 cells; ≥ 315 SGs per condition).
H Recruitment of TDP-43 into arsenite-induced nuclear bodies (NBs) in HeLa cells. After TDP-43 silencing and expression myc-TDP-43 Wt, 12D and 12A, NBs were induced by sodium arsenite treatment and NB recruitment of TDP-43 was monitored by TDP-43 immunostaining. Bar, 20 μm.
I Percentage of cells with TDP-43 in NBs ± SD of three independent experimental replicates ($n = 3$). $^{*}P < 0.0332$ by Kruskal–Wallis test with Dunn's multiple comparison test to Wt.
J Intensity profiles (right) of TDP-43 Wt, 12D and 12A variants (green) along white lines (left). Bar, 10 μm.

43 12D also remained completely dispersed in the stable inducible U2OS cell lines treated with arsenite, whereas TDP-43 WT and 12A localized in NBs upon arsenite treatment (Fig EV5C and D). Taken together, phosphomimetic substitutions that mimic disease-linked phosphorylation of TDP-43 suppress the localization of TDP-43 in phase-separated MLOs that could be condensation sites for pathological TDP-43 aggregation.

Phosphomimetic substitutions enhance TDP-43 solubility and suppress SG recruitment in primary neurons

To further support the idea that phosphorylation enhances the solubility of TDP-43 and counteracts its aggregation propensity in cells, we expressed the different myc-tagged TDP-43 variants in HeLa cells and performed a biochemical fractionation into a RIPA-soluble (S) and RIPA-insoluble (I) fraction. Indeed, the 12D protein had a significantly higher S/(S + I) ratio compared with the Wt and 12A proteins (Fig 6A and B). We also expressed EGFP-tagged TDP-43 Wt, 12D, 12A or the corresponding NLS-mutant cytosolic versions in primary rat neurons (see Appendix Fig S8 and Fig 6D for subcellular localization, which was unaltered by the phosphomimetic mutations). We then probed for RIPA-insoluble high-molecular-weight material in a filter trap assay. Both the nuclear and the cytosolic 12D proteins showed a strong reduction in the amount of RIPA-insoluble TDP-43 in the transduced neurons (Fig 6C). Confocal microscopy of transduced neurons revealed a completely dispersed localization of the NLS-mutant 12D protein, whereas TDP-43 Wt and 12A showed a more granular, condensed pattern in the neuronal cytoplasm (Fig 6 D). Moreover, NLS mutant TDP-43 Wt and 12A were readily recruited into G3BP1-positive SGs induced by heat shock in primary rat neurons, whereas TDP-43 12D was not (Fig 6E). Thus, we conclude that phosphomimetic substitutions mimicking disease-linked C-terminal hyperphosphorylation reduce TDP-43's tendency to condense into MLOs and to become insoluble in neurons. Based on these findings, we speculate that TDP-43 phosphorylation might be a cellular response to counteract pathological TDP-43 aggregation.

Discussion

C-terminal TDP-43 phosphorylation is a long-recognized pathological hallmark in ALS and FTD (Hasegawa *et al*, 2008; Inukai *et al*,

Figure 6. Phosphomimetic substitutions enhance TDP-43 solubility in HeLa cells and primary neurons.

A Biochemical fractionation into RIPA-soluble (S) and RIPA-insoluble (I) fractions to analyze solubility of the different myc-TDP-43 variants (Wt, 12D and 12A) expressed in HeLa cells for 48 h. TDP-43 was detected by TDP-43 Western blot (upper blot, rabbit anti-TDP-43 C-term, Proteintech) and Myc Western blot (lower blot, mouse anti-Myc 9E10).
B Quantification of myc-TDP-43 variants (Wt, 12D and 12A) in (S) versus (I) fractions extracted from TDP-43 Western blots of four independent replicates ± SD, plotted as S/(S + I). $^{*}P < 0.0332$ by one way ANOVA with Dunnett's multiple comparison test to Wt.
C RIPA-insoluble material of the indicated EGFP-tagged TDP-43 variants (± NLS mutation) expressed in primary cortical neurons analyzed by filter-trap assay.
D Primary hippocampal neurons expressing EGFP-TDP-43 Wt, 12D or 12A with additional NLS mutation. Bar, 80 μm. Right: zoomed images of white squares (TDP-43 signal). Bar, 10 μm.
E SG recruitment of EGFP-TDP-43 NLS mutant variants (Wt, 12D, 12A) in primary hippocampal neurons. SG formation was induced by 1 h heat shock at 42°C. SGs and TDP-43 were monitored by G3BP1 antibody staining and EGFP fluorescence, respectively. For clarity, signals were converted to grey values in the individual channels (first two columns). In the merge (third column), EGFP-TDP-43 shown in green, G3BP1 in red and nuclei (DAPI staining) in turquoise. Bar, 20 μm.

Source data are available online for this figure.

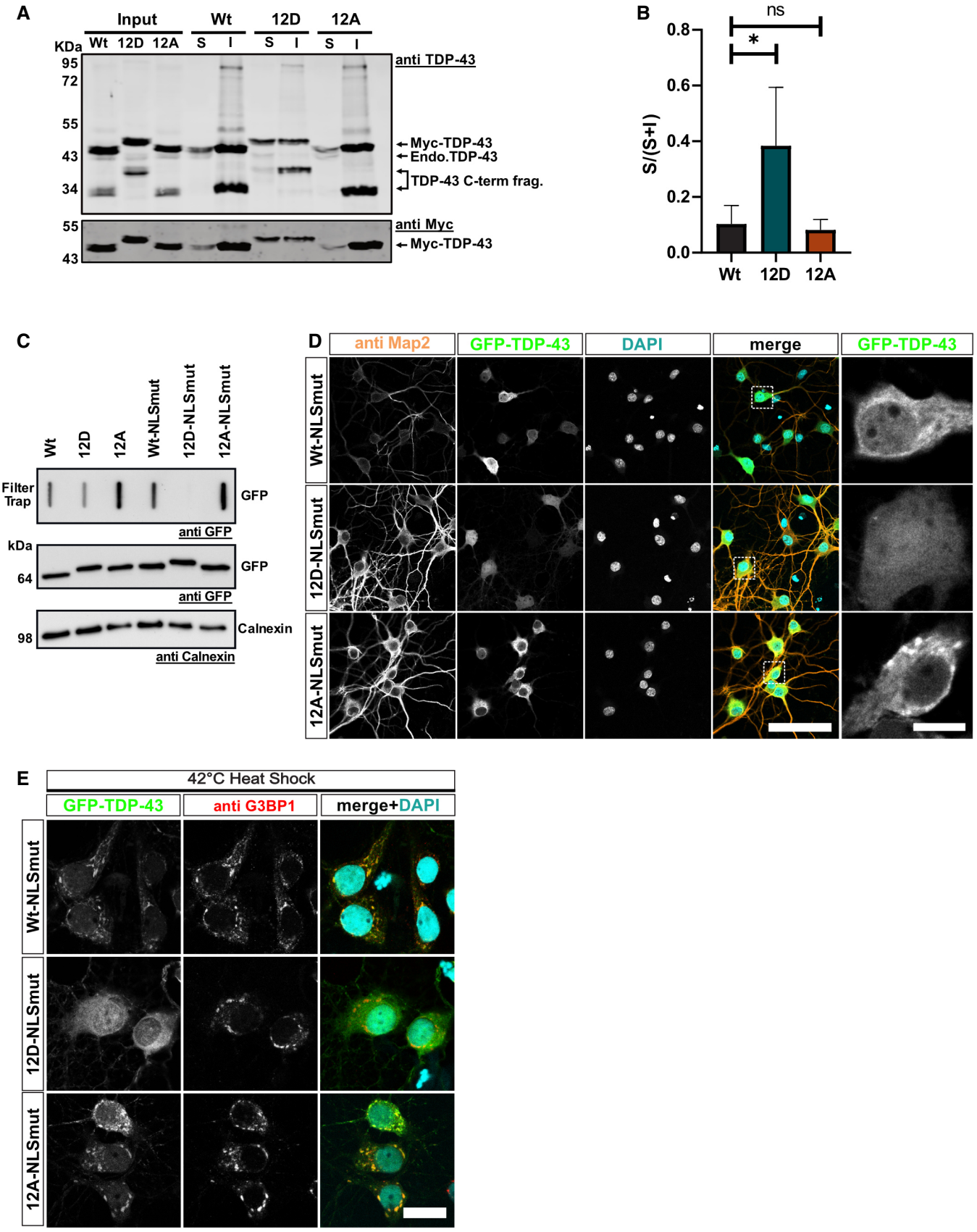

Figure 6.

2008; Neumann *et al*, 2009; Kametani *et al*, 2016). Against previous expectations, we now show that TDP-43 phosphorylation, and in particular phosphomimetic mutations mimicking the phosphorylation pattern in ALS/FTD (Hasegawa *et al*, 2008; Kametani *et al*, 2016), strongly suppress TDP-43 phase separation and aggregation both *in vitro* and in cells. Our data are in line with two previous studies that examined C-terminal fragments of TDP-43 with phosphomimetic 2D or 5D/E mutations and observed a reduced aggregation propensity and toxicity in cell lines and *Drosophila* (Brady *et al*, 2011; Li *et al*, 2011). Even though phosphomimetic mutations do not always recapitulate the effects of phosphorylation on protein-protein interactions (Yaffe *et al*, 1997; Durocher *et al*, 1999), our *in vitro* data with purified proteins show that the phosphomimetic 12D variant has a similar condensation behavior as CK1δ-phosphorylated TDP-43. We would like to point out that phosphomimetic mutations are an experimental under-appreciation of true charge, as aspartate has a net charge of −1, whereas phosphorylation has a net charge of −2. In line, our simulations show that 12S-p disrupts phase separation of the TDP-43 LCD more strongly than the phosphomimetic 12D mutations (Fig 3F–H). It seems possible that the number of phosphorylation sites, but not their exact position, is critical for the suppression of TDP-43 condensation, which would indicate that multisite phosphorylation may regulate TDP-43 phase separation through bulk electrostatics, as previously shown for other proteins (Serber & Ferrell, 2007; Strickfaden *et al*, 2007). Indeed, two recent studies showed that the net charge of IDR-containing RBPs tunes their driving force for assembly (preprint: Crabtree *et al*, 2020; preprint: Bremer *et al*, 2021). For instance, reducing the net charge of the disordered region of Ddx4 promotes its phase separation (preprint: Crabtree *et al*, 2020), and increasing the net charge of the low complexity region of hnRNP-A1 reduces its phase separation, likely due to repulsive electrostatic long-range interactions (preprint: Bremer *et al*, 2021). At physiological pH, TDP-43 has a net charge of −4.1, phosphomimetic 12D TDP-43 has a net charge of −16.1 and 12× phosphorylated TDP-43 has a net charge of −28.1. In line with the aforementioned studies, it seems likely that the strong increase in negative net charge in phosphomimetic/phosphorylated TDP-43 is responsible for the reduced propensity to self-assemble into condensates.

Various modes of TDP-43 assembly have been proposed, including homotypic interactions of an α-helical structure in the conserved region (CR) of the LCD (Conicella *et al*, 2016, 2020) and interactions between aromatic/aliphatic residues in the LCD (Li *et al*, 2018; Schmidt *et al*, 2019; Laurents *et al*, 2021). All phosphomimetic mutations examined in our study are outside of the α-helix/CR (aa. 321–360; Fig 1D), hence they are unlikely to interfere with helix-helix interactions. In line with this hypothesis, the contact maps extracted from the simulations of the TDP-43 LCD show that most interactions, including aromatic interactions, are not strongly affected by C-terminal phosphomimetics and that mainly interactions of serines with nearby residues are reduced. However, more work is required to understand how PTMs on TDP-43 affect aromatic "sticker"–"sticker" interactions on the molecular scale. C-terminal phosphorylation may also affect amyloid-like fibril formation: A recent cryo-EM structure of solid TDP-43 LCD fibrils showed that several C-terminal serines are buried inside the fibril structure (Li *et al*, 2021), hence phosphorylation could disrupt the amyloid fibril structure, in line with our experimental findings that TDP-43 aggregate formation is strongly reduced by phosphomimetic substitutions. We therefore speculate that TDP-43 phosphorylation might be a protective cellular mechanism that counteracts aberrant TDP-43 phase transitions and renders TDP-43 more dynamic and liquid-like by reducing C-terminal LCD-LCD interactions through negatively charged, highly hydrated phospho-groups.

Under what conditions C-terminal TDP-43 phosphorylation arises in cells and which form of TDP-43 (soluble, phase separated, aggregated) is phosphorylated is still unknown. Interestingly, we and others previously found that C-terminal TDP-43 phosphorylation follows TDP-43 insolubility, suggesting that phosphorylation arises downstream of TDP-43 aggregation (Dormann *et al*, 2009; Brady *et al*, 2011; Zhang *et al*, 2019). In line with these findings, treatment of neuron-like cells with amyloid-like particles triggers a solidification of initially liquid-like cytoplasmic TDP-43 droplets, along with C-terminal TDP-43 phosphorylation (Gasset-Rosa *et al*, 2019). Why phosphorylated TDP-43 aggregates nevertheless persist and are not readily disassembled after phosphorylation remains to be investigated. Further research into the functional consequences of C-terminal TDP-43 phosphorylation, e.g., how it affects global protein or RNA interactions, TDP-43 stability or the introduction of additional PTMs, is needed to understand the role of TDP-43 phosphorylation in physiology and pathology.

Several other studies on TDP-43 phosphorylation at first glance contrast our findings. Overexpression of various TDP-43 kinases in cell or animal models was shown to promote TDP-43 aggregation and neurotoxicity (Choksi *et al*, 2014; Liachko *et al*, 2014; Nonaka *et al*, 2016; Taylor *et al*, 2018). Based on these studies, inhibition of TDP-43 phosphorylation by kinase inhibitors has been proposed as a potential therapeutic strategy for ALS (Liachko *et al*, 2013; Salado *et al*, 2014; Martinez-Gonzalez *et al*, 2020). A possible explanation for the discrepant findings could be that kinase overexpression has pleiotropic effects that may cause TDP-43 aggregation and neurotoxicity independent of TDP-43 phosphorylation. Our data exclude such indirect effects, as they rely on experiments with purified components, MD simulations and defined phosphomimetic constructs rather than modulation of kinase levels/activity. Furthermore, our results suggest that beneficial effects seen with kinase inhibitors are likely not the direct consequence of reduced TDP-43 phosphorylation, but rather mediated by other mechanisms.

An alternative scenario that we cannot exclude is that reduced TDP-43 condensation due to hyperphosphorylation may have negative consequences by disturbing essential functions of TDP-43 that depend on its capacity to phase separate or solidify, e.g., certain DNA/RNA processing steps or recruitment of TDP-43 into cytoprotective NBs (Wang *et al*, 2020) or other MLOs. In support of this hypothesis, a deep mutagenesis study recently found that aggregating TDP-43 variants decrease toxicity in yeast, whereas dynamic, liquid-like variants enhance toxicity (Bolognesi *et al*, 2019), so further work is needed to investigate this possible scenario. However, our data clearly show that some essential RNA processing functions (autoregulation and regulation of certain splicing events), RNA-binding and nuclear localization/import of TDP-43 are not affected by C-terminal hyperphosphorylation, at least in HeLa and U2OS cells, and therefore do not depend on TDP-43's phase separation and solidification capacity. In line with our findings, an earlier study found that phase separation-deficient TDP-43 remains competent in splicing regulation (Schmidt *et al*, 2019).

Of note, abnormal PTMs are a common theme in neurodegenerative disorders, e.g., Tauopathies linked to pathological Tau aggregation (Morris *et al*, 2015; Alquezar *et al*, 2020). Interestingly, even though hyperphosphorylation is generally believed to trigger Tau aggregation, site-specific phosphorylation in the microtubule-binding region of Tau was recently shown to inhibit, rather than promote Tau fibrillization and seeding (Haj-Yahya *et al*, 2020). We now show that C-terminal TDP-43 phosphorylation as detected on ALS/FTD inclusions has a similar inhibitory effect on TDP-43 aggregation, underscoring the idea that aberrant PTMs detected on pathological inclusions may not necessarily all be drivers of protein aggregation, but could also have protective, anti-aggregation effects that are later-on overruled by other pathogenic mechanisms.

Materials and Methods

cDNA constructs

Bacterial expressing constructs

TDP-43 carrying mutations in serine 409 and 410, either to aspartate (2D) or to alanine (2A), were generated by site-directed mutagenesis using Q5 high fidelity DNA polymerase (NEB) using primers containing the mutations S409D/410D and S409A/410A and pJ4M TDP-43-TEV-MBP-His_6 vector as a template. Expression constructs with 5 or 12 serine substitutions (5D, 5A, 12D and 12A) were generated using synthetic double-stranded DNA fragments (gBlocks Gene Fragments, IDT) containing the respective mutations, cloned into PstI and XhoI sites of the pJ4M TDP-43-TEV-MBP-His_6-backbone.

Mammalian expressing constructs

To generate an expressing construct coding for Myc-hTDP-43, the coding sequence of hTDP-43 was PCR amplified from pEGFP-C1-hTDP-43 (Ederle *et al*, 2018), including a Myc coding sequence in the forward PCR primer, and cloned into a pcDNA5-FRT-TO-backbone using XhoI and BamHI restriction sites. Note, that the hTDP-43 template includes a resistance to TARDBPHSS118765 siRNA (Invitrogen) used to silence endogenous TDP-43 (see "siRNA-mediated knockdown of TDP-43"). For generation of the TDP-43 12D and 12A constructs, synthetic gBlocks (IDT) harboring the respective mutations were previously cloned into the NdeI and BamHI sites of the pEGFP-C1-hTDP-43 vector. In constructs carrying mutations in the NLS of TDP-43 (mNLS), amino acids 82–84 as well as 95, 97 and 98 were exchanged for alanine (pEGFP-hTDP-43 mNLS). Then, the mNLS region was transferred from the pEGFP-TDP-43 mNLS template to the pcDNA5-FRT-TO-Myc-hTDP-43, 12D and 12A vectors via the restriction enzymes XhoI and NdeI. To generate the GCR_2-$EGFP_2$-TDP-43 12D and 12A constructs, the respective coding sequences were PCR amplified and inserted into GCR_2-$EGFP_2$-backbone using EcoRV and BamHI. To allow for lentiviral packaging and subsequent neuronal transduction, coding sequences of TDP-43 Wt, 12D and 12A were subcloned into the FhSynW backbone in frame with mEGFP (May *et al*, 2014).

HeLa cell culture, transient transfection and stress treatment

HeLa cells were grown in DMEM high glucose GlutaMAX (Invitrogen) supplemented with 10% fetal bovine serum (FBS) and 10 μg/ml gentamicin and incubated in a humidified chamber with 5% CO_2 at 37°C. cDNA transfections were performed using Lipofectamine 2000 (Thermo) in culture medium without gentamicin and medium was exchanged after 4 to 6 h to avoid cellular stress by the transfection reagent. Note, that for equal transfection efficiency different amounts of DNA were transfected for the different constructs (for 12D: 100%; for Wt and 12A: 75% + 25% empty vector DNA). For immunostaining cells were fixed after ~24 h, hydrogen peroxide (H_2O_2; 1 mM) treatment was carried out for 2 h, MG132 (10 μM) treatment for 2.5–3 h and sodium arsenite (0.5 mM) treatment for 45 min.

Flp-In T-Rex U2OS cell culture and stress treatment

Inducible U2OS cell lines stably expressing myc-hTDP-43 variants (Wt, 12D and 12A) were generated using the Flp-In T-Rex system. Flp-In T-Rex U2OS cells (gift from A. Lamond lab) were cotransfected with pcDNA5-FRT-TO-hTDP-43 (Wt, 12D or 12A) and pOG44 Flp recombinase expression plasmids, followed by selection with Hygromycin (150 μg/ml) and Blasticidin (15 μl/ml). After expansion of surviving single cell colonies, myc-TDP-43 expression was induced by doxycycline (dox) addition for 24 h, using 0.005 μg/ml dox for myc-TDP-43 Wt and 0.25 μg/ml dox for TDP-43 12D and 12A, in order to yield similar protein expression levels. To induce nuclear stress bodies, cells were treated with sodium arsenite (0.5 mM) for 2 h.

Neuronal cell culture, lentiviral packaging and stress treatment

Primary hippocampal and cortical neuronal cultures were prepared from embryonic day 19 rats as described in detail previously (Guo *et al*, 2018). In brief, neocortex and hippocampus were dissected, followed by enzymatic dissociation and gentle trituration. For immunofluorescence experiments, hippocampal neurons (85,000 cells/ml) were plated on poly-D-lysine-coated glass coverslips (VWR) in 12-well plates (Thermo Fisher) and cultured in Neurobasal medium (Thermo Fisher) supplemented with 2% B27 (Thermo Fisher), 1% Penicillin–Streptomycin (Thermo Fisher), 0.5 mM L-glutamine (Thermo Fisher) and 12.5 μM glutamate (Thermo Fisher). Both, cortical and hippocampal neurons, were transduced on day *in vitro* (DIV) 5.

Cortical neurons (250,000 cells/ml) used for filter trap assays were plated on poly-D-lysine-coated six-well plates and cultured in Neurobasal medium containing 2% B27, 1% Penicillin–Streptomycin and 0.5 mM L-glutamine.

Lentiviral packaging was performed by seeding HEK293FT cells (Thermo Fisher) of low passage number into three 10 cm dishes per construct (5×10^6 cells/dish). Cells were plated in DMEM, high glucose, GlutaMAX (Thermo Fisher) supplemented with 10% FBS (Sigma), 1% Penicillin–Streptomycin (Thermo Fisher) and 1% non-essential amino acids (Thermo Fisher). On the following day, cells were co-transfected with 18.6 μg transfer vector (FhSynW-mEGFP-hTDP-43, FhSynW-mEGFP-hTDP-43 [12D], FhSynW-mEGFP-hTDP-43 [12A], FhSynW-mEGFP-hTDP-43-mNLS, FhSynW-mEGFP-hTDP-43-mNLS [12D] and FhSynW-mEGFP-hTDP-43-mNLS [12A]), 11 μg pSPAX2 and 6.4 μg pVSVG using Lipofectamine 2000 (Thermo Fisher). The transfection media was replaced by plating media supplemented with 13 mg/ml bovine serum albumin (BSA, Sigma)

on the next day. Lentivirus from the cell supernatant was collected 24 h later by ultracentrifugation with a Sw28 rotor (Beckman Coulter; 64,100 *g*, 2 h, 4°C). Finally, lentiviral particles were resuspended in Neurobasal media (Thermo Fisher), stored at −80°C and used for lentiviral transduction by adding to neuronal culture media upon thawing. Neurons were kept in culture for 4 additional days after transduction on DIV5 (DIV5 + 4). To induce SGs, heat shock was carried out by incubating neurons for 1 h at 42°C in a cell culture incubator.

Recombinant protein expression and purification

TDP-43-TEV-MBP-His$_6$

All TDP-43-MBP-His$_6$ variants were purified according to (Wang *et al*, 2018) with minor adaptations. First, expression of proteins was performed in *E. coli* BL21-DE3 Rosetta 2 using 0.5 mM IPTG and grown overnight at 16°C. Next, cells were resuspended in lysis buffer (20 mM Tris pH 8, 1 M NaCl, 10 mM imidazole, 10% (v/v) glycerol, 4 mM β-mercaptoethanol and 1 μg/ml each of aprotinin, leupeptin hemisulfate and pepstatin A) supplemented with 0.1 mg/ml RNase A, and lysed using lysozyme and sonication. Subsequently, the protein was purified by Ni-NTA agarose (Qiagen) and eluted with lysis buffer containing 300 mM imidazole. For all TDP-43-MBP-His$_6$ variants, a final size exclusion chromatography (SEC; Hiload 16/600 Superdex 200 pg, GE Healthcare) purification step was performed in purification buffer (20 mM Tris pH 8, 300 mM NaCl, 10% (v/v) glycerol supplemented with 2 mM TCEP), in order to separate TDP-43-MBP-His$_6$ from protein aggregates and contaminants. Purified monomeric TDP-43-MBP-His$_6$ was collected by pooling the fractions corresponding to peak B in the SEC profile (Appendix Fig S1D). All purified proteins were concentrated using Amicon ultra centrifugal filters and then flash frozen and stored at −80°C. To determine protein concentration, absorbance at 280 nm was measured using the respective extinction coefficient (ε) predicted by the ProtParam tool. Additionally, for all purified proteins, the A260/280 ratio was determined and found to be between 0.5 and 0.7.

CK1δ

The kinase domain of CSNK1D was expressed as an N-terminal MBP-tagged fusion in *E. coli* Rosetta 2 cells, co-expressing λ-phosphatase to guarantee a completely unphosphorylated protein. The cells were grown to an OD of 0.45 and subsequently the temperature was reduced to 18°C. Then the cells were induced (generally at OD 0.7–0.8) with 0.5 mM IPTG and expression was performed overnight. Cells were harvested and resuspended in AC-A buffer (25 mM Bis-Tris, 500 mM NaCl, 10 mM β-mercaptoethanol, pH 7.0), supplemented with DNAse, RNAse, lysozyme and protease inhibitor cocktail (selfmade) for cell disruption. Lysis was done by sonication on ice (5 × 30 s with breaks of 1 min between each pulse). Cell debris was pelleted by centrifugation (SS34 rotor, 34,541 *g*, 30 min). The supernatant was filtered and subsequently loaded on a Dextrin Sepharose column (cytiva), previously equilibrated with AC-A buffer. The column was washed for 5 column volumes with AC-A buffer. Elution was done with MBP-B buffer (25 mM Bis-Tris, 500 mM NaCl, 10 mM β-mercaptoethanol, 20 mM maltose, pH 7.0). The eluted protein was subject to TEV protease cleavage overnight at 4°C. On the next day the buffer was exchanged to IEX-A buffer (25 mM Bis-Tris, 50 mM NaCl, 10 mM. β-mercaptoethanol) by ultra-filtration (Amicon Ultra-15 30 kDa, Merck Millipore) and subject to cation-exchange chromatography by a linear to IEX-B buffer (25 mM Bis-Tris, 500 mM NaCl, 10 mM. β-mercaptoethanol). Eluted protein was concentrated and gel-filtered over a Superdex 75 (cytiva) into SEC buffer (25 mM Bis-Tris, 50 mM NaCl, 10 mM $MgCl_2$, 1 mM DTT). Fractions were collected, concentrated and aliquots of 200 μl were flash frozen and stored at −80°C until use.

His$_6$-TEV protease

His$_6$-TEV protease expression and purification was performed as described in Hutten *et al* (2020).

In vitro phosphorylation

TDP-43-MBP-His$_6$ was *in vitro* phosphorylated with CK1δ and 200 μM ATP in phosphorylation buffer (50 mM Tris–HCl, pH 7.5, 10 mM MgCl2, 1 mM DTT) for 2 h at RT, using a two-fold molar excess of TDP-43-MBP-His$_6$ over CK1δ. Subsequently, the reaction was used for sedimentation and SG association assays. As negative controls, either the kinase or the ATP was omitted and also included as controls in subsequent assays.

Enzymatic digestion, enrichment for phospho-peptides and mass spectrometric analysis

TDP-43-MBP-His$_6$ was *in vitro* phosphorylated as described above, separated on a 10% SDS–PAGE gel and visualized by Coomassie staining. The gel band corresponding to the phosphorylated TDP-43-MBP-His$_6$ was excised and destained twice for 30 min at 37°C with 50% acetonitrile in 50 mM Tris–HCl, pH 8. The gel piece was dehydrated with 100% acetonitrile, reduced and alkylated, and finally digested overnight at 37°C with 375 ng trypsin (Promega). The peptides were extracted from the gel twice using 100 μl of 50% acetonitrile and 0.25% TFA buffer. Both extractions were merged and evaporated in a vacuum evaporator. In order to enrich the phospho-peptides, 10 μl of 0.5 mg/μl TiO_2 beads (GL Sciences Cat. No.: 5010-21315) in loading buffer (80% ACN, 5% TFA and 1 M glycolic acid) were added to the dried samples in a ratio of 0.3 mg of beads to 5 pmol of protein. Samples were incubated for 10 min at RT on a shaker at 270 *g* and spun down at 100 *g* for 1 min. The supernatant was removed and kept for further analysis, while beads were sequentially washed with loading buffer, washing buffer 1 (80% ACN, 1% TFA) and washing buffer 2 (10% ACN, 0.2% TFA). Next, the beads were dried in the hood for 10 min and resuspended with 50 μl elution buffer (28% ammonia solution in H_2O). Finally, the samples were speed vacuum evaporated and resuspended with 15 μl 0.1% FA. For LC-MS purposes, desalted peptides were injected in an Ultimate 3000 RSLCnano system (Thermo) and separated in a 25-cm analytical column (75 μm ID, 1.6 μm C18, IonOpticks) with a 30-min gradient from 3 to 30% acetonitrile in 0.1% formic acid. The effluent from the HPLC was directly electrosprayed into a Qexactive HF (Thermo) operated in data-dependent mode to automatically switch between full scan MS and MS/MS acquisition. Survey full scan MS spectra (from m/z 300–1,600) were acquired with resolution $R = 60{,}000$ at m/z 400 (AGC target of 3×10^6). The 10 most intense peptide ions with charge states between 2 and 5 were

sequentially isolated to a target value of 1×10^5 with resolution $R = 15{,}000$ and isolation window 1.6 Th and fragmented at 27% normalized collision energy. Typical mass spectrometric conditions were: spray voltage, 1.5 kV; no sheath and auxiliary gas flow; heated capillary temperature, 250°C; ion selection threshold, 33.000 counts.

Fluorescent labeling of purified TDP-43

TDP-43-MBP-His_6 variants were labeled with Alexa Fluor 488 C5 maleimide (Thermo Fisher) at a low (~0.01–0.05) labeling efficiency in order to avoid interference with condensate formation. Labeling was performed according to the manufacture's protocol using a 1:100 or 1:20 protein:fluorescent dye mole ratio. Briefly, the Alexa Fluor reagent, previously dissolved in DMSO, was mixed with the protein and kept in the dark for 2 h at RT. Excess dye was removed by consecutive washes with TDP-43 purification buffer using Amicon ultra centrifugal filters. Subsequently, labeled protein was used for spinning disc confocal microscopy, FRAP and aggregation assays, respectively.

In vitro phase separation and aggregation assays

Sedimentation assay

For sedimentation analysis, 1 μM TDP-43-TEV-MBP-His_6 variants or *in vitro* phosphorylated TDP-43-TEV-MBP-His_6 was cleaved by addition of 20 μg/ml His_6-TEV protease in 50 or 25 μl Hepes buffer (20 mM Hepes, pH 7.5, 150 mM NaCl, 1 mM DTT), respectively, to remove the MBP-His_6 tag and induce phase separation. Samples were incubated for 60 min at 30°C, followed by centrifugation for 15 min at 21,000 g at 4°C to pellet the formed condensates. Equal amounts of supernatant (S) and condensate (C) fractions were loaded onto an SDS–PAGE gel and TDP-43 was detected by Western Blot (rabbit TDP-43 N-term, Proteintech, Cat. No.: 10782-2-AP).

Microscopic condensate assay

For all microscopic condensate assays, uncoated μ-Slide 18 Well-Flat chambers (Cat. No.: 81821, Ibidi) were pretreated with 10% Pluronics F-127 solution for 1 h and 5 times washed with MilliQ water. The water remained in the chamber until just before the experiment, as described in Ceballos *et al* (2018).

Purified TDP-43-TEV-MBP-His_6 variants were buffer exchange to Hepes buffer or phosphate buffer (20 mM Na_2HPO_4/NaH_2PO_4, pH 7.5, 150 mM NaCl, 2.5% glycerol, 1 mM DTT). Proteins were then centrifuged at 21,000 *g* for 10 min at 4°C to remove any preformed protein precipitates. For condensates formation, the reaction was setup directly in Pluronics-coated μ-Slide 18 Well-Flat chambers, where proteins were diluted to the indicated concentrations and phase separation was induced by addition of 100 μg/ml His_6-TEV protease at RT. After ~20 min, imaging was performed by bright field microscopy using a widefield microscope.

For fusion events and FRAP analysis, condensates were formed directly in Pluronics-coated μ-Slide 18 Well - Flat chambers as described above using 20 μM of each Al.488-labeled TDP-43 protein variants (Wt, 5D and 12D) in Hepes buffer and incubated for 10 min at RT before imaging. Note that experiments were performed until maximally 1 h after adding the TEV protease, in order to avoid *in vitro* aging of condensates.

Turbidity assay

Phase separation of TDP-43-TEV-MBP-His_6 variants was induced as described earlier for the microscopic condensate assay. Reactions of 20 μl samples were prepared at the indicated concentrations in 384-well plates and incubated for 30 min at RT after adding TEV protease. Subsequently, a BioTek Power Wave HT plate reader was used to measure turbidity at 600 nm. Turbidity measurements were performed in triplicates.

Semi-denaturing detergent agarose gel electrophoresis

SDD-AGE experiments were performed based on protocols published by French *et al* (2019) and Halfmann and Lindquist (2008). First, 2 μM purified TDP-43-MBP-His_6 variants (WT, 5D, 12D and 12A) were set up in low binding tubes (Eppendorf) in 35 μl aggregation buffer (50 mM Tris pH 8.0, 250 mM NaCl, 5% glycerol, 5% sucrose, 150 mM imidazole pH 8.0) and supplemented with 1× protease inhibitor (Sigma). Samples were shaken for 30 min on a thermomixer at 1,000 rpm at RT (~22°C) and then incubated at RT for the indicated time period. 5 μl of each sample was collected and diluted in SDD-AGE buffer (40 mM Tris–HCl pH 6.8, 5% glycerol, 0.5% SDS, 0.1% bromphenol-blue) and analyzed by SDD-AGE by horizontal 1.5% agarose gel electrophoresis (gel: 1.5% agarose in 20 mM Tris, 200 mM glycine and 0.1% SDS) in running buffer (60 mM Tris, 20 mM acetate, 200 mM glycine, 1 mM EDTA and 0.1% SDS) for ~6 h at 60 V. Detection of TDP-43 monomers, oligomers and high-molecular-weight species was performed after overnight capillary transfer in TBS (50 mM Tris pH 7.6, 150 mM NaCl) to a nitrocellulose membrane and by standard Western Blot using rabbit anti TDP-43 N-term antibody (Proteintech, Cat. No.: 10782-2-AP).

Formation of Alexa 488-labeled TDP-43 aggregates

In order to visualize TDP-43 (wt, 5D, 12D and 12A) aggregates formed under the above described assay conditions, 10 μM Al.488-labeled TDP-43-MBP-His_6 was set up in low binding tubes (Eppendorf) in aggregation buffer and incubated with or without 100 μg/ml His_6-TEV protease. Samples were shaken at 1,000 rpm at RT for 30 min and then transferred into a 384-well black plate (Greiner Bio-One), incubated at RT and imaged by confocal microscopy after 2, 8 and 24 h.

Cellular TDP-43 solubility assays

Fractionation in RIPA-Benzonase buffer

HeLa cells (~1×10^6) were washed twice in PBS, harvested by scraping and pelleted at 1,100 *g* for 5 min. Cell pellets were incubated on ice for 15 min in 200 μl RIPA buffer (50 mM Tris–HCl, pH 8.0, 150 mM NaCl, 1% NP-40, 0.5% deoxycholate, 0.1% SDS) with freshly added 1× protease inhibitor cocktail (Sigma), 1× phosphatase inhibitors (final concentration: 10 mM NaF, 1 mM β-glycerophosphate, 1 mM Na_3VO_4) and 0.05 unit/μl Benzonase (Sigma). Samples were sonicated in a BioRuptorPico (Diagenode) for 45 sec and 20 μl of sample was collected as "Input". The remaining sample was then centrifuged at 13,000 *g* for 30 min at 4°C. The resulting supernatants (S) were collected and the remaining pellets were washed in RIPA buffer with inhibitors, resonicated for 45 sec and recentrifuged for 30 min at 4°C at 13,000 *g*. Finally, the RIPA

insoluble pellets (I) were resuspended in 36 µl urea buffer (7 M urea, 2 M thiourea, 4% CHAPS, 30 mM Tris–HCl, pH 8.5) and sonicated. All samples were supplemented with 4× Lämmli buffer (250 mM Tris–HCl, pH 6,8, 40% glycerol, 8% SDS, 0.1% bromphenol-blue, 4% β-mercaptoethanol) and input and supernatant (S) samples were boiled prior to SDS–PAGE and Western Blot against TDP-43 (rabbit anti TDP-43 C-term, Proteintech, Cat. No.: 12892-1-AP) and Myc (mouse anti-myc 9E10 antibody, Helmholtz Center Munich). Note that for detection reasons, the (I) fractions were 4× more concentrated than the (S) fractions, so they are represented in a 1:5 ratio.

Filter trap assay

Cortical neurons expressing the indicated EGFP-tagged TDP-43 variants (DIV5 + 4 days expression) were washed two times with PBS and lysed on ice in RIPA buffer (50 mM Tris–HCl, pH 8.0, 150 mM NaCl, 1% NP-40, 0.5% deoxycholate, 0.1% SDS) freshly supplemented with 1× protease inhibitor cocktail (Sigma), 1× phosphatase inhibitor cocktail (Sigma) and 0.125 Units/µl benzonase (Sigma) for 20 min. Cell lysates were collected and centrifuged at 1,000 *g*, 4°C for 30 min. Two-third of the resulting supernatant (RIPA-insoluble fraction) was filtered through a nitrocellulose membrane (0.2 µM pore size, Merck) using a filter trap slot blot (Hoefer Scientific Instruments). After washing with PBS for three times, membranes were blocked for 1 h with 2% I-Block (Thermo Fisher) prior to immuno-detection with mouse anti-GFP (UC Davis/NIH Neuromab Facility, Cat. No.: N86/8) and rabbit anti Calnexin antibody (Enzo Life Sciences, Cat. No.: ADI-SPA-860). The remaining 1/3 of the lysates was diluted with 3× loading buffer (200 mM Tris–HCl pH 6.8, 6% SDS, 20% glycerol, 0.1 g/ml DTT, 0.1 mg bromophenol blue), boiled at 95°C and used for subsequent standard Western Blot analysis.

Multi-scale MD simulations

Explicit solvent coarse-grained MD simulations

Coarse-grained MD simulations with explicit solvent to investigate protein phase separation and phase-separated protein condensates were run with a rescaled version of the Martini forcefield (Marrink *et al*, 2007; Monticelli *et al*, 2008) as described by Benayad *et al* (2021). A similar approach was shown to describe the conformational ensembles of proteins with disordered domains very well (Larsen *et al*, 2020; Martin *et al*, 2021), and we recently showed that such approaches can be extended to simulations of LLPS of disordered proteins (Benayad *et al*, 2021). Protein–protein interactions were thus scaled to 0.8 of the default value. Chloride and sodium ions were added to neutralize the system in simulations of Wt and 12D proteins. 10% of the water beads were replaced by WF anti-freeze beads. Coarse-grained simulations were run with GROMACS 2018 (Abraham *et al*, 2015). Simulations boxes measured 450 × 450 × 600 Å. Simulations systems were energy minimized and equilibrated in MD simulations with and without position restraints. 118 Wt and 12D C-terminal LCDs (aa. 261–414) were simulated for 20 µs each. The coarse-grained simulations systems consist of roughly one million particles. Equations of motions were integrated with a 20-fs time step. Simulations were conducted in the NPT ensemble at 1 bar and 300 K using the Parrinello-Rahman barostat (Parrinello & Rahman, 1981) and the Bussi–Donadio–Parrinello velocity-rescaling thermostat (Bussi *et al*, 2007).

Note that in the coarse-grained approach we employed, four atoms are typically grouped together to a coarse-grained particle. For example, a coarse-grained water molecule would correspond to four water molecules in an atomistic simulation.

Implicit solvent coarse-grained MD simulations

The HPS coarse-grained model provides a coarser and thus computationally very efficient description of disordered proteins and their phase behavior (Dignon *et al*, 2018). Parameters for PTMs, such a phosphorylation, are available (Perdikari *et al*, 2021). Solvent is treated implicitly and electrostatics is described by Debye–Hückel theory. We simulated 100 C-terminal LCDs (aa. 261–414) in slab geometry (212 Å × 212 Å × 2800 Å) following the protocol of Mittal and co-workers (https://bitbucket.org/jeetain/hoomd_slab_builder/src/master/) (Dignon *et al*, 2018; Regy *et al*, 2020). Simulations were started with all proteins concentrated and equilibrated in a small sub volume so that the proteins formed an initial condensate. We studied the phase behavior of Wt, 12D, 12A, 5pS and 12pS TDP-43 LCDs. Production simulations (T = 310 K) were run for at least 5.8 µs and up to 6.5 µs for each LCD variant.

Atomistic MD simulations

HCG (Pietrek *et al*, 2020) enables us to generate statistically independent and chemically-meaningful conformations of a biomolecular condensate with atomic resolution, which serve as starting points for atomistic MD simulations. Atomic-resolution models of clusters of the C-terminal disordered domain of TDP-43 (aa. 261–414) were generated for both Wt protein and the 12D mutant. To assemble the disordered proteins into a condensate, we first assemble pairs of disordered domains, then pairs of pairs, pairs of quadruplets, and so forth, following the logic set out in (Pietrek *et al*, 2020). HCG Monte Carlo manifestly satisfies detailed balance and thus we generate representative ensembles. Finally, we arrive at densely packed disordered domains, while retaining atomic resolution at each modeling step. Periodic boundary conditions were employed during the assembly.

Clusters of Wt and 12D LCDs were solvated in a 150 Å × 150 Å × 150 Å simulation box, the system charge was neutralized and 150 mM NaCl was added. We employed the Amber-disp protein force field developed by Robustelli *et al* (2018), including the modified TPIP4P-D water model (Piana *et al*, 2015) that accompanies the Amber-disp protein force field. Temperature was maintained at 300 K by the Bussi–Donadio–Parrinello velocity-rescaling thermostat (Bussi *et al*, 2007). We employed the Parrinello–Rahman barostat (Robustelli *et al*, 2018) to set the pressure to 1 bar. Equations of motions were integrated with a 2-fs time step. Production simulations were prepared by energy minimization with and without soft-core potentials. To start production simulations, we equilibrated the atomistic simulations systems, running at least 5,000 steps with a 1-fs time step and position restraints and for 1.5 ns with a 2-fs time step also with position restraints. Equilibrium simulations of the clusters of the disordered domains were conducted with GROMACS 2019 (Abraham *et al*, 2015). For both wild-type and 12D, clusters of 32 chains with 154 residues were simulated for just over 1 µs, with two repeats each started from independently generated HCG structures.

Simulations were analyzed with the MDAnalysis (Michaud-Agrawal *et al*, 2011; Gowers *et al*, 2016) and the MDtraj Python libraries (McGibbon *et al*, 2015). Contact analysis was performed with the Contact Map Explorer Python library (https://github.com/dwhswenson/contact_map).

Analysis of MD simulations

Simulations were analyzed with the MDAnalysis (Michaud-Agrawal *et al*, 2011; Gowers *et al*, 2016) and the MDtraj Python libraries (McGibbon *et al*, 2015). Contact analysis of the coarse-grained simulations with the explicit solvent Martini model was performed with the Contact Map Explorer Python library (https://github.com/dwhswenson/contact_map). For simulations with the HPS implicit solvent coarse-grained model, contacts were computed with MDAnalysis. Two amino acids were deemed in contact in the simulations with the HPS model when their inter-bead distance was $< 2^{1/6}\sigma_{ij}$ where $\sigma_{ij} = \frac{1}{2}(\sigma_i + \sigma_j)$ is the average of bead diameter of the respective amino acids i and j. The concentrations c_{dilute} and c_{dense} of dilute and dense phases, respectively, were determined by adapting the workflow of Tesei *et al* (https://github.com/KULL-Centre/papers/tree/main/2021/CG-IDPs-Tesei-et-al) from the simulations of the HPS model (preprint: Tesei *et al*, 2021). The excess free energy of transfer from the dilute to the dense phase was then computed as $\Delta G_{\text{trans}} = -RT \ln (c_{\text{dense}}/c_{\text{dilute}})$, where R is the gas constant and T is the absolute temperature.

Nuclear transport assay

To analyze import of GCR_2-$EGFP_2$ tagged TDP-43 reporters, HeLa cells were grown for at least two passages in DMEM supplemented with 10% dialyzed FBS and were transiently transfected with the different GCR_2-$EGFP_2$-TDP-43 variants as described earlier. Import of the GCR_2-$EGFP_2$-TDP-43 reporters was induced by adding dexamethasone (5 μM final concentration) in imaging medium (fluorobrite) and followed by live cell imaging using a spinning disk confocal microscope (see below).

SG association assay

HeLa cells were grown on high precision (No. 1.5) poly-L-lysine coated 12 mm coverslips, and after SG induction with MG132 (10 μM for 2.5–3 h), cells were permeabilized for 2× 2 min with 0.004–0.005% digitonin in KPB (20 mM potassium phosphate pH 7.4, 5 mM $Mg(OAc)_2$, 200 mM KOAc, 1 mM EGTA, 2 mM DTT and 1 mg/ml each aprotinin, pepstatin and leupeptin). Soluble proteins were removed by several, stringent washes (4× 4 min in KPB on ice) before blocking nuclear pores by 15 min incubation with 200 mg/ml wheat germ agglutinin (WGA) on ice. Cells were then incubated for 30 min at RT with 100 nM TDP-43-MBP-His_6. For comparison of *in vitro* phosphorylated TDP-43 with controls, proteins were either subjected to the *in vitro* phosphorylation reaction or mock treated (Wt, 12D) in absence of kinase or ATP before exchanging the buffer to KPB using 40K Zeba spin desalting columns (Thermo). Subsequently, cells were washed (3× 5 min in KPB on ice) to remove unbound TDP-43-MBP-His_6 and processed by immunostaining to visualize SGs. SGs and TDP-43-MBP-His_6 were visualized by G3BP1 immunostaining (rabbit anti G3BP1antibody, Proteintech, Cat. No.: 13057-2-AP) and MBP immunostaining (by mouse anti MBP antibody, Proteintech, Cat. No.: 66003-1-Ig), respectively. On Fig 4B for clarity, signals were converted to grey values in the individual channels (upper two rows). In the merge (lower row), G3BP1 is shown in magenta, TDP-43-MBP-His_6 in green, white pixels indicate colocalization. Nuclei were counterstained with DAPI (turquoise).

siRNA-mediated knockdown of TDP-43

TDP-43 knockdown was achieved using the pre-designed TARDBPHSS118765 siRNA (Invitrogen) as described in Dormann *et al* (2009). Briefly, 20 nM siRNA was transfected into HeLa or U2OS cells using RNAimax (Thermo) transfection reagent. Knockdown was analyzed 48 h post transfection by immunohistochemistry using mouse anti TDP-43 antibody (Proteintech, Cat. No.: 60019-2-Ig) and immunoblotting using rabbit anti TDP-43 C-Term antibody (Proteintech, Cat. No.: 12892-1-AP) to detect TDP-43 and mouse anti alpha-Tubulin antibody (Proteintech, Cat. No.: 66031-1-Ig) for detection of α-Tubulin as a control.

RNA extraction and RT–PCR to analyze TDP-43 splice targets

TDP-43 expression was silenced in HeLa cells by siRNA as described earlier and 24 h later cells were transfected with siRNA-resistant pcDNA5-FRT-TO-Myc-hTDP43 constructs (Wt, 12D and 12A). 48 h after transfection, cells were harvested and total RNA was extracted using an RNeasy mini kit from Qiagen. cDNA was synthesized using 500 ng of total RNA, M-MLV reverse transcriptase polymerase (Invitrogen), and 6 μM of random hexamer primer (NEB). cDNA was amplified with Taq DNA polymerase (NEB) using the forward (FW) and reverse (RV) primers targeting the *SKAR* gene (FW—5′CCTTCATAAACCCACCCATTGGGACAG3′; RV—5′GTGGTGGAGA AAGCCGCCTGAG3′) (Fiesel *et al*, 2012) and the *BIM* gene (FW—5′TCTGAGTGTGACCGAGAAGG3′; RV—5′TCTTGGGCGATCCATAT CTC 3′) (Tollervey *et al*, 2011). PCR products were separated by electrophoresis on a 2.5% agarose gel containing GelRed (Sigma).

Electrophoretic mobility shift assays

The TDP-43 autoregulatory RNA site (Ayala *et al*, 2011) located in the *TARDBP* 3′UTR (5′UCACAGGCCGCGUCUUUGACGGUGGGUGU CCCAUUUUUAUCCGCUACUCUUUAUUUCAUGGAGUCGUAUCAAC GCUAUGAACGCAAGGCUGUGAUAUGGAACCAGAAGGCUGUCUGA ACUUUUGAAACCUUGUGUGGGAUUGAUGGUGGUGCCGAGGCAUG AAAGGCUAGUAUGAGCGAGAAAAGGAGAGAGCGCGUGCAGAGAC UUGGUGGUGCAUAAUGGAUAUUUUUUAACUUGGCGAGAUGUGU CUCUCAAUCCUGUGGCUUUGGUGAGAGAGUGUGCAGAGAGCAAU GAUAGCAAAUAAUGUACGAAUGUUUUUUGCAUUCAAAGGACAUC CACAUCUGUUGGAAGACUUUUAAGUGAGUUUUUGUUCUUAGAUA ACCCACAUUAGAUGAAUGUGUUAAGUGAAAUGAUACUUGUACUC CCCCUACCCCUUUGUCAACUGCUGUG) was *in vitro* transcribed from double-stranded DNA templates and Cy5-labeled using the HyperScribe™ T7 High Yield Cy5 RNA Labeling Kit (APExBIO, Cat. No.: K1062) per manufacturer's instructions. $(UG)_{12}$ RNA (5′ UGU GUGUGUGUGUGUGUGUGUG) was chemically synthesized with the addition of a 5′ Cy5-label (Metabion). 16 nM of Cy5-labeled RNA was mixed with varying amounts of TDP-43 Wt, 12A, and 12D (0–1.6 μM). Binding reactions (20 μl) were incubated in binding

buffer (20 mM $NaPO_4$ [pH 8], 150 mM NaCl, 1 mM DTT, 5 mM $MgCl_2$, 0.5 mg/ml BSA, 0.1 mg/ml yeast tRNA, 5% glycerol and 1 U/μl RNase inhibitor [NEB]) for 20 min at RT before loading onto a 1-mm thick non-denaturing polyacrylamide gel (6%) in 0.5× TBE. Gels were run at 100 V for 1 h at RT. Gels were imaged with a Typhoon™ FLA 9500 laser scanner.

Immunostaining

All steps were performed at RT. HeLa and Flp-In T-Rex U2OS cells were fixed in 4% formaldehyde in PBS for 10 min, permeabilized for 5 min using 0.2% (v/v) Triton X-100 in PBS and subsequently blocked in blocking buffer (5% goat or donkey serum in 0.1% saponine in PBS) for 30 min. Primary and secondary antibodies were diluted in blocking buffer and applied each for 1 h and washed three times using 0.1% saponine in PBS. Myc-TDP-43 was stained using mouse anti TDP-43 antibody (Proteintech) or mouse anti-myc 9E10 antibody (IMB protein production core facility), SGs were stained using goat anti TIA1 antibody (Santa Cruz, Cat. No.: sc-48371) or rabbit anti G3BP1 antibody (Proteintech) and DNA was stained with DAPI at 0.5 μg/ml in PBS for 5 min. Coverslips were then mounted on glass slides with ProLong™ Diamond Antifade reagent (Life Technologies) and dried overnight at RT.

Hippocampal neurons cultured on glass coverslips were washed twice with PBS and fixed for 10 min at RT using 4% paraformaldehyde and 4% sucrose in PBS. Primary antibody as well as secondary antibody (1:400) were diluted in GDB buffer (0.1% gelatin, 0.3% Triton X-100, 450 mM NaCl, 16 mM sodium phosphate pH 7.4). Primary antibodies (Mouse anti Map2, Sigma, Cat. No.: M1406; Rabbit anti G3BP1, Abam, Cat. No.: ab181150) were incubated overnight at 4°C while secondary antibodies was applied for 1 h at RT, each followed by three times washing with PBS. Coverslips were mounted using Vectashield Vibrance with DAPI (Biozol) to counterstain nuclei.

Microscopy

Bright and wide-field microscopy

Imaging of unlabeled TDP-43 condensates was done by bright-field microscopy on an Axio Oberver.Z1 wide-field fluorescence microscope, using a 63×/1.40 Oil objective and an AxioCam 506 (Zeiss, Oberkochen, Germany).

Confocal microscopy

Confocal microscopy of TDP-43 aggregates and HeLa cells was performed using an inverted Leica SP8 microscope and the LAS X imaging program (Leica), provided by the Bioimaging core facility of the Biomedical Center (LMU Munich), which included the excitation lasers for 405, 488, 552 and 638 nm. Images were acquired using two-fold frame averaging with a 63×1.4 oil objective, with an image pixel size of 180 nm for Al.488-TDP-43 aggregates and fixed cells, and 59 nm for images of cells subjected to the SG association assay. Confocal images of U2OS cells were obtained using an inverted Leica SP5 microscope and the LASAF imaging program (Leica), provided by the Light Microscopy core facility of the Biocenter (JGU Mainz). Images were acquired using two-fold frame averaging with a 100× 1.4 oil objective, with an image pixel size of 151 nm.

The following fluorescence settings were used for detection: DAPI: 419–442 nm, GFP: 498–533 nm, Alexa 555: 562–598 nm and Alexa 647: 650–700 nm. Recording was performed sequentially using a conventional photomultiplier tube to avoid bleed-through.

Spinning disc confocal microscopy

a Nuclear transport assay imaging:Images were acquired for a duration of 50 min in 2.5 min intervals at 36.5°C and 5% CO_2 (EMBLEM environmental chamber) using an inverted microscope (Axio Observer.Z1; Carl Zeiss, Oberkochen, Germany) equipped with a confocal spinning disc (CSU-X1; Yokogawa, Tokyo, Japan) and a 63×/1.4 oil immersion lens. Images were acquired using the 488 nm SD laser line and an EM-CCD camera (EvolveDelta; Photomoetrics) at bin 1 × 1.

b Fusion events and FRAP:Experiments were performed on an inverted microscope (Axio Observer.Z1; Carl Zeiss, Oberkochen, Germany) equipped with a confocal spinning disk unit (CSU-X1; Yokogawa, Tokyo, Japan) and an oil immersion lens of 100×/1.46 Oil Ph3. Images recording the dynamics of TDP-43 condensates were obtained using a EM-CCD camera (EvolveDelta; Photomoetrics), with a bin 1 × 1 in a recording mode of 5 s intervals in a block of 3 min. Images of TDP-43 condensates after bleaching were acquired with bin 1 × 1 in streaming mode for 1.5 s followed by a block of 2 min where images were recorded in intervals of 5 sec. Experiments were performed at RT and ≥ 11 condensates were analyzed per condition in three independent experiments. Localized photobleaching ("half-bleach") was obtained using a laser scanning device (UGA-42 Geo; Rapp OptoElectronic, Hamburg, Germany). The "Geo" module allowed for simultaneous laser illumination within hardware-defined shapes of different sizes. For this experiment, an illumination size of ~4 μm in a square-like shape was used. The targeting structure was half bleached to approximately 70% of the initial intensity using a 473-nm diode laser (DL-473/75; Rapp OptoElectronic, Hamburg, Germany).

Quantification and analysis

Droplet quantification

Wide-field images of droplets were processed and quantified and measured using Image J/Fiji software. First, a bandpass filter of 20 pixels was applied to all images in order to reveal some details and thresholds were adjusted to optimally include all droplets. Finally, droplets were counted and measured by their size and roundness [4*area/(π*major_axis^2), or the inverse of the aspect ratio] using the command Analyze Particles, excluding the detection of particles with a circularity below 0.3 and/or an area smaller than 3 pixels. Statistical analyses were performed using GraphPad Prism 8.

Analysis of cellular images

Analysis of the nuclear transport assay was performed using Image J/Fiji software by measuring loss in cytoplasmic fluorescence over time and normalizing $t = 0$ min to 1.

Images of cells from the SG association assay (Hutten & Dormann, 2020) were processed and analyzed using Image J/Fiji software, applying linear enhancement for brightness and contrast and implemented plugins for measurement of pixel intensities in SGs.

Quantification of Myc-hTDP-43 recruitment into SGs was performed using Image J/Fiji software. First, SGs from TDP-43-positive cells were selected using the Wand tracing tool and a band of 1 μm representing a proxy for the cytosol was drawn around all selected SGs using the "Make Band" command. Then, all pixel intensities for both SG and band selections was extracted for the TDP-43 channel. After subtraction of the background signal from all measured values, calculation of the SG/band ratio was performed for each SG.

Analysis of Myc-hTDP-43 recruitment into NBs was performed by counting the number of cells with positive TDP-43 nuclear condensates, excluding cells expressing TDP-43 staining only in the cytoplasm. Profile of TDP-43 nuclear staining was performed using Image J/Fiji software by using the "Plot Profile" command, which quantifies the gray values along the indicated lines.

All statistical analyses were performed using GraphPad Prism 8.

WB analysis

WB analysis was performed by extracting the optical densities of each band using the software Image Studio Lite (LI-COR), using the top and bottom average background option, to obtain the signal value, in which local background is automatically subtracted.

Analysis of Sedimentation assays and Fractionation in RIPA-Benzonase buffer experiments was performed by dividing the signal values of (S) by the total (S + C) or (S + I) signal values, to obtain a S/(S + C) or S/(S + I) ratio, respectively.

Analysis of TDP-43 autoregulation levels in the Flp-In T-Rex U2OS cell line was performed by comparing the signal values of endogenous TDP-43 protein between induced (+Dox) and non-induced (−Dox) expression conditions of myc-hTDP-43 variants. After housekeeping protein normalization using Histone H3, endogenous TDP-43 protein expression levels were normalized to 1 in the myc-TDP-43 Wt (−Dox) condition.

All statistical analyses were performed using GraphPad Prism 8.

FRAP analysis

FRAP analysis were performed using Image J/Fiji software by calculating the fluorescence intensity over time ($I(t)$) using the macro Time Series Analyzer command and the following formula:

$$I(t) = \frac{[\mathrm{ROI1}(t) - \mathrm{ROI3}(t)]}{[\mathrm{ROI2}(t) - \mathrm{ROI3}(t)]}.$$

ROI1 corresponds to the averaged gray values of the bleached area, and ROI2 to the averaged gray values of the total droplet. ROI3 corresponds to the averaged background values. Values were further normalized to the initial fluorescence by dividing $I(t)$ by the mean gray value of the initial 1 time step before bleaching $<I(1)>$. This way bleached areas were corrected for background noise and bleaching due to imaging over time. Statistical analyses were performed using GraphPad Prism 8.

Data availability

This study includes no data deposited in external repositories.

Expanded View for this article is available online.

Acknowledgements

We thank Bettina Schmid, Magdalini Polymenidou, Sören von Bülow, Kumar Gaurav and Zakarya Benayad for insightful discussions and Ignasi Forné, Tobias Straub, Fridolin Kielisch and Arya Changiarath Sivadasan for technical support and discussion. We thank Angus Lamond for gift of the Flp-In U2OS cell line. We acknowledge support by the Core Facilities Proteomics, Bioimaging and Bioinformatics of the BioMedical Center, LMU Munich, the Light Microscopy Core Facility of the Biocenter, JGU Mainz and the Bioinformatics Core Facility of IMB Mainz. We thank Peter Becker and Michael Kiebler for infrastructure and access to the spinning disc confocal microscope (DFG, INST 86/1581-1 FUGG) and are grateful to Edward Lemke for generously sharing lab space and infrastructure. The authors gratefully acknowledge the computing time granted on the supercomputer Mogon II at Johannes Gutenberg University Mainz (hpc.uni-mainz.de). This work was supported by the Deutsche Forschungsgemeinschaft (DFG, German Research Foundation), specifically by project DO1804/4-1 within the Priority Programme SPP2191 - ID 402723784 (to D.D.), projects DO1804/1-1 and DO1804/1-2 within the Emmy Noether Programme (to D.D.), project DO1804/5-1 within the Heisenberg Programme (to D.D.), the Paul Ehrlich and Ludwig Darmstädter Award for Young Researchers 2019 (to D.D.), the Munich Cluster for Systems Neurology (EXC2145 SyNergy—ID 390857198 to D.D. and D.E.) and the NOMIS foundation (D.E.). G.H. acknowledges financial support from the German Research Foundation (CRC 902: Molecular Principles of RNA Based Regulation) and the Max Planck Society. L.S.S. acknowledges support by ReALity (Resilience, Adaptation and Longevity), M^{3}ODEL and Forschungsinitiative des Landes Rheinland-Pfalz, and D.D. acknowledges support by ReALity and the Gutenberg Forschungskolleg (GFK). Open access funding enabled and organized by ProjektDEAL.

Author contributions

Lara A Gruijs da Silva: Investigation; Visualization; Methodology; Writing—original draft; Writing—review and editing. **Francesca Simonetti:** Investigation; Visualization; Methodology; Writing—review and editing. **Saskia Hutten:** Investigation; Visualization; Methodology; Writing—review and editing. **Henrick Riemenschneider:** Investigation; Visualization; Methodology; Writing—review and editing. **Erin L Sternburg:** Investigation; Visualization; Methodology; Writing—review and editing. **Lisa M Pietrek:** Methodology. **Jakob Gebel:** Resources; Investigation; Methodology. **Volker Dötsch:** Resources. **Dieter Edbauer:** Resources; Supervision; Methodology; Writing—review and editing. **Gerhard Hummer:** Resources; Methodology; Writing—review and editing. **Lukas D Stelzl:** Investigation; Visualization; Methodology; Writing—original draft; Writing—review and editing. **Dorothee Dormann:** Conceptualization; Supervision; Funding acquisition; Writing—original draft; Writing—review and editing.

In addition to the CRediT author contributions listed above, the contributions in detail are:

Conceptualization: DD, LAGS; Methodology: all authors; Investigation: LAGS, FS, SH, HR, ELS, LMP, JG, LSS; Resources: DD, GH, LSS, DE, VD; Writing–original draft: DD, LAGS; Writing–review and editing: all authors; Visualization: LAGS, FS, SH, HR, ELS, JG, LSS; Supervision: DD, GH, DE, VD, LSS; Project administration: DD; Funding acquisition: DD, DE, GH, LSS, VD.

Disclosure and competing interests statement

The authors declare that they have no conflict of interest.

References

Abraham MJ, Murtola T, Schulz R, Páll S, Smith JC, Hess B, Lindahl E (2015) GROMACS: high performance molecular simulations through multi-level parallelism from laptops to supercomputers. *SoftwareX* 1–2: 19–25

Afroz T, Hock E-M, Ernst P, Foglieni C, Jambeau M, Gilhespy LAB, Laferriere F, Maniecka Z, Plückthun A, Mittl P *et al* (2017) Functional and dynamic polymerization of the ALS-linked protein TDP-43 antagonizes its pathologic aggregation. *Nat Commun* 8: 45

Alberti S (2017) Phase separation in biology. *Curr Biol* 27: R1097–R1102

Alberti S, Dormann D (2019) Liquid-liquid phase separation in disease. *Annu Rev Genet* 53: 171–194

Alberti S, Hyman AA (2021) Biomolecular condensates at the nexus of cellular stress, protein aggregation disease and ageing. *Nat Rev Mol Cell Biol* 22: 196–213

Alquezar C, Arya S, Kao AW (2020) Tau post-translational modifications: dynamic transformers of tau function, degradation, and aggregation. *Front Neurol* 11: 595532

Avendano-Vazquez SE, Dhir A, Bembich S, Buratti E, Proudfoot N, Baralle FE (2012) Autoregulation of TDP-43 mRNA levels involves interplay between transcription, splicing, and alternative polyA site selection. *Genes Dev* 26: 1679–1684

Ayala YM, De Conti L, Avendaño-Vázquez SE, Dhir A, Romano M, D'Ambrogio A, Tollervey J, Ule J, Baralle M, Buratti E *et al* (2011) TDP-43 regulates its mRNA levels through a negative feedback loop. *EMBO J* 30: 277–288

Babinchak WM, Haider R, Dumm BK, Sarkar P, Surewicz K, Choi JK, Surewicz WK (2019) The role of liquid-liquid phase separation in aggregation of the TDP-43 low-complexity domain. *J Biol Chem* 294: 6306–6317

Bah A, Forman-Kay JD (2016) Modulation of intrinsically disordered protein function by post-translational modifications. *J Biol Chem* 291: 6696–6705

Benayad Z, von Bulow S, Stelzl LS, Hummer G (2021) Simulation of FUS protein condensates with an adapted coarse-grained model. *J Chem Theory Comput* 17: 525–537

Bolognesi B, Faure AJ, Seuma M, Schmiedel JM, Tartaglia GG, Lehner B (2019) The mutational landscape of a prion-like domain. *Nat Commun* 10: 4162

Brady OA, Meng P, Zheng Y, Mao Y, Hu F (2011) Regulation of TDP-43 aggregation by phosphorylation and p62/SQSTM1. *J Neurochem* 116: 248–259

Bremer A, Farag M, Borcherds WM, Peran I, Martin EW, Pappu RV, Mittag T (2021) Deciphering how naturally occurring sequence features impact the phase behaviors of disordered prion-like domains. *bioRxiv* https://doi.org/10.1101/2021.01.01.425046 [PREPRINT]

Buratti E (2015) Functional significance of TDP-43 mutations in disease. *Adv Genet* 91: 1–53

Buratti E (2018) TDP-43 post-translational modifications in health and disease. *Expert Opin Ther Targets* 22: 279–293

Bussi G, Donadio D, Parrinello M (2007) Canonical sampling through velocity rescaling. *J Chem Phys* 126: 014101

Ceballos AV, McDonald CJ, Elbaum-Garfinkle S (2018) Methods and strategies to quantify phase separation of disordered proteins. *Methods Enzymol* 611: 31–50

Choksi DK, Roy B, Chatterjee S, Yusuff T, Bakhoum MF, Sengupta U, Ambegaokar S, Kayed R, Jackson GR (2014) TDP-43 Phosphorylation by casein kinase Iepsilon promotes oligomerization and enhances toxicity *in vivo*. *Hum Mol Genet* 23: 1025–1035

Conicella AE, Zerze GH, Mittal J, Fawzi NL (2016) ALS mutations disrupt phase separation mediated by alpha-helical structure in the TDP-43 low-complexity C-terminal domain. *Structure* 24: 1537–1549

Conicella AE, Dignon GL, Zerze GH, Schmidt HB, D'Ordine AM, Kim YC, Rohatgi R, Ayala YM, Mittal J, Fawzi NL (2020) TDP-43 alpha-helical structure tunes liquid-liquid phase separation and function. *Proc Natl Acad Sci USA* 117: 5883–5894

Crabtree MD, Holland J, Kompella P, Babl L, Turner N, Baldwin AJ (2020) Repulsive electrostatic interactions modulate dense and dilute phase properties of biomolecular condensates. *bioRxiv* https://doi.org/10.1101/2020.10.29.357863 [PREPRINT]

Dignon GL, Zheng W, Kim YC, Best RB, Mittal J (2018) Sequence determinants of protein phase behavior from a coarse-grained model. *PLoS Comput Biol* 14: e1005941

Dormann D, Capell A, Carlson AM, Shankaran SS, Rodde R, Neumann M, Kremmer E, Matsuwaki T, Yamanouchi K, Nishihara M *et al* (2009) Proteolytic processing of TAR DNA binding protein-43 by caspases produces C-terminal fragments with disease defining properties independent of progranulin. *J Neurochem* 110: 1082–1094

Durocher D, Henckel J, Fersht AR, Jackson SP (1999) The FHA domain is a modular phosphopeptide recognition motif. *Mol Cell* 4: 387–394

Ederle H, Funk C, Abou-Ajram C, Hutten S, Funk EBE, Kehlenbach RH, Bailer SM, Dormann D (2018) Nuclear egress of TDP-43 and FUS occurs independently of Exportin-1/CRM1. *Sci Rep* 8: 7084

Fiesel FC, Weber SS, Supper J, Zell A, Kahle PJ (2012) TDP-43 regulates global translational yield by splicing of exon junction complex component SKAR. *Nucleic Acids Res* 40: 2668–2682

French RL, Grese ZR, Aligireddy H, Dhavale DD, Reeb AN, Kedia N, Kotzbauer PT, Bieschke J, Ayala YM (2019) Detection of TAR DNA-binding protein 43 (TDP-43) oligomers as initial intermediate species during aggregate formation. *J Biol Chem* 294: 6696–6709

Gasset-Rosa F, Lu S, Yu H, Chen C, Melamed Z, Guo L, Shorter J, Da Cruz S, Cleveland DW (2019) Cytoplasmic TDP-43 de-mixing independent of stress granules drives inhibition of nuclear import, loss of nuclear TDP-43, and cell death. *Neuron* 102: 339–357.e7

Gowers RJ, Linke M, Barnoud J, Reddy TJE, Melo MN, Seyler SL, Domański J, Dotson DL, Buchoux S, Kenney IM *et al* (2016) MDAnalysis: a python package for the rapid analysis of molecular dynamics simulations. In *Proceedings of the 15th Python in Science Conference*, pp 98–105. Austin, TX: SciPy 2016

Guo Q, Lehmer C, Martínez-Sánchez A, Rudack T, Beck F, Hartmann H, Pérez-Berlanga M, Frottin F, Hipp MS, Hartl FU *et al* (2018) *In situ* structure of neuronal C9orf72 Poly-GA aggregates reveals proteasome recruitment. *Cell* 172: 696–705.e12

Haj-Yahya M, Gopinath P, Rajasekhar K, Mirbaha H, Diamond MI, Lashuel HA (2020) Site-specific hyperphosphorylation inhibits, rather than promotes, tau fibrillization, seeding capacity, and its microtubule binding. *Angew Chem Int Ed Engl* 59: 4059–4067

Halfmann R, Lindquist S (2008) Screening for amyloid aggregation by semi-denaturing detergent-agarose gel electrophoresis. *J Vis Exp* 17. https://doi.org/10.3791/838

Hasegawa M, Arai T, Nonaka T, Kametani F, Yoshida M, Hashizume Y, Beach TG, Buratti E, Baralle F, Morita M *et al* (2008) Phosphorylated TDP-43 in frontotemporal lobar degeneration and amyotrophic lateral sclerosis. *Ann Neurol* 64: 60–70

Hofweber M, Dormann D (2019) Friend or foe-Post-translational modifications as regulators of phase separation and RNP granule dynamics. *J Biol Chem* 294: 7137–7150

Hutten S, Dormann D (2020) A quantitative assay to measure stress granule association of proteins and peptides in semi-permeabilized human cells. *Bio-protocol* 10: e3846

Hutten S, Usluer S, Bourgeois B, Simonetti F, Odeh HM, Fare CM, Czuppa M, Hruska-Plochan M, Hofweber M, Polymenidou M *et al* (2020) Nuclear import receptors directly bind to arginine-rich dipeptide repeat proteins and suppress their pathological interactions. *Cell Rep* 33: 108538

Inukai Y, Nonaka T, Arai T, Yoshida M, Hashizume Y, Beach TG, Buratti E, Baralle FE, Akiyama H, Hisanaga S-I *et al* (2008) Abnormal

phosphorylation of Ser409/410 of TDP-43 in FTLD-U and ALS. *FEBS Lett* 582: 2899–2904

Josephs KA, Whitwell JL, Weigand SD, Murray ME, Tosakulwong N, Liesinger AM, Petrucelli L, Senjem ML, Knopman DS, Boeve BF *et al* (2014) TDP-43 is a key player in the clinical features associated with Alzheimer's disease. *Acta Neuropathol* 127: 811–824

Kametani F, Nonaka T, Suzuki T, Arai T, Dohmae N, Akiyama H, Hasegawa M (2009) Identification of casein kinase-1 phosphorylation sites on TDP-43. *Biochem Biophys Res Commun* 382: 405–409

Kametani F, Obi T, Shishido T, Akatsu H, Murayama S, Saito Y, Yoshida M, Hasegawa M (2016) Mass spectrometric analysis of accumulated TDP-43 in amyotrophic lateral sclerosis brains. *Sci Rep* 6: 23281

Lancaster AK, Nutter-Upham A, Lindquist S, King OD (2014) PLAAC: a web and command-line application to identify proteins with prion-like amino acid composition. *Bioinformatics* 30: 2501–2502

Larsen AH, Wang Y, Bottaro S, Grudinin S, Arleth L, Lindorff-Larsen K (2020) Combining molecular dynamics simulations with small-angle X-ray and neutron scattering data to study multi-domain proteins in solution. *PLoS Comput Biol* 16: e1007870

Laurents DV, Stuani C, Pantoja-Uceda D, Buratti E, Mompean M (2021) Aromatic and aliphatic residues of the disordered region of TDP-43 are on a fast track for self-assembly. *Biochem Biophys Res Commun* 578: 110–114

Li HR, Chiang WC, Chou PC, Wang WJ, Huang JR (2018) TAR DNA-binding protein 43 (TDP-43) liquid-liquid phase separation is mediated by just a few aromatic residues. *J Biol Chem* 293: 6090–6098

Li HY, Yeh PA, Chiu HC, Tang CY, Tu BP (2011) Hyperphosphorylation as a defense mechanism to reduce TDP-43 aggregation. *PLoS One* 6: e23075

Li Q, Babinchak WM, Surewicz WK (2021) Cryo-EM structure of amyloid fibrils formed by the entire low complexity domain of TDP-43. *Nat Commun* 12: 1620

Liachko NF, McMillan PJ, Guthrie CR, Bird TD, Leverenz JB, Kraemer BC (2013) CDC7 inhibition blocks pathological TDP-43 phosphorylation and neurodegeneration. *Ann Neurol* 74: 39–52

Liachko NF, McMillan PJ, Strovas TJ, Loomis E, Greenup L, Murrell JR, Ghetti B, Raskind MA, Montine TJ, Bird TD *et al* (2014) The tau tubulin kinases TTBK1/2 promote accumulation of pathological TDP-43. *PLoS Genet* 10: e1004803

Ling SC, Polymenidou M, Cleveland DW (2013) Converging mechanisms in ALS and FTD: disrupted RNA and protein homeostasis. *Neuron* 79: 416–438

Mackenzie IR, Rademakers R, Neumann M (2010) TDP-43 and FUS in amyotrophic lateral sclerosis and frontotemporal dementia. *Lancet Neurol* 9: 995–1007

Marrink SJ, Risselada HJ, Yefimov S, Tieleman DP, de Vries AH (2007) The MARTINI force field: coarse grained model for biomolecular simulations. *J Phys Chem B* 111: 7812–7824

Martin I, Kim J, Lee B, Kang H, Xu J-C, Jia H, Stankowski J, Kim M-S, Zhong J, Kumar M *et al* (2014) Ribosomal protein s15 phosphorylation mediates LRRK2 neurodegeneration in Parkinson's disease. *Cell* 157: 472–485

Martin EW, Holehouse AS, Peran I, Farag M, Incicco JJ, Bremer A, Grace CR, Soranno A, Pappu RV, Mittag T (2020) Valence and patterning of aromatic residues determine the phase behavior of prion-like domains. *Science* 367: 694–699

Martin EW, Thomasen FE, Milkovic NM, Cuneo MJ, Grace CR, Nourse A, Lindorff-Larsen K, Mittag T (2021) Interplay of folded domains and the disordered low-complexity domain in mediating hnRNPA1 phase separation. *Nucleic Acids Res* 49: 2931–2945

Martinez-Gonzalez L, Rodriguez-Cueto C, Cabezudo D, Bartolome F, Andres-Benito P, Ferrer I, Gil C, Martin-Requero A, Fernandez-Ruiz J, Martinez A *et al* (2020) Motor neuron preservation and decrease of *in vivo* TDP-43 phosphorylation by protein CK-1delta kinase inhibitor treatment. *Sci Rep* 10: 4449

May S, Hornburg D, Schludi MH, Arzberger T, Rentzsch K, Schwenk BM, Grässer FA, Mori K, Kremmer E, Banzhaf-Strathmann J *et al* (2014) C9orf72 FTLD/ALS-associated Gly-Ala dipeptide repeat proteins cause neuronal toxicity and Unc119 sequestration. *Acta Neuropathol* 128: 485–503

McGibbon RT, Beauchamp KA, Harrigan MP, Klein C, Swails JM, Hernandez CX, Schwantes CR, Wang LP, Lane TJ, Pande VS (2015) MDTraj: a modern open library for the analysis of molecular dynamics trajectories. *Biophys J* 109: 1528–1532

Michaud-Agrawal N, Denning EJ, Woolf TB, Beckstein O (2011) MDAnalysis: a toolkit for the analysis of molecular dynamics simulations. *J Comput Chem* 32: 2319–2327

Molliex A, Temirov J, Lee J, Coughlin M, Kanagaraj AP, Kim HJ, Mittag T, Taylor JP (2015) Phase separation by low complexity domains promotes stress granule assembly and drives pathological fibrillization. *Cell* 163: 123–133

Monticelli L, Kandasamy SK, Periole X, Larson RG, Tieleman DP, Marrink SJ (2008) The MARTINI coarse-grained force field: extension to proteins. *J Chem Theory Comput* 4: 819–834

Morris M, Knudsen GM, Maeda S, Trinidad JC, Ioanoviciu A, Burlingame AL, Mucke L (2015) Tau post-translational modifications in wild-type and human amyloid precursor protein transgenic mice. *Nat Neurosci* 18: 1183–1189

Nedelsky NB, Taylor JP (2019) Bridging biophysics and neurology: aberrant phase transitions in neurodegenerative disease. *Nat Rev Neurol* 15: 272–286

Neumann M, Sampathu DM, Kwong LK, Truax AC, Micsenyi MC, Chou TT, Bruce J, Schuck T, Grossman M, Clark CM *et al* (2006) Ubiquitinated TDP-43 in frontotemporal lobar degeneration and amyotrophic lateral sclerosis. *Science* 314: 130–133

Neumann M, Kwong LK, Lee EB, Kremmer E, Flatley A, Xu Y, Forman MS, Troost D, Kretzschmar HA, Trojanowski JQ *et al* (2009) Phosphorylation of S409/410 of TDP-43 is a consistent feature in all sporadic and familial forms of TDP-43 proteinopathies. *Acta Neuropathol* 117: 137–149

Nonaka T, Suzuki G, Tanaka Y, Kametani F, Hirai S, Okado H, Miyashita T, Saitoe M, Akiyama H, Masai H *et al* (2016) Phosphorylation of TAR DNA-binding protein of 43 kDa (TDP-43) by truncated casein kinase 1delta triggers mislocalization and accumulation of TDP-43. *J Biol Chem* 291: 5473–5483

Parrinello M, Rahman A (1981) Polymorphic transitions in single crystals: a new molecular dynamics method. *J Appl Phys* 52: 7182–7190

Patel A, Lee H, Jawerth L, Maharana S, Jahnel M, Hein M, Stoynov S, Mahamid J, Saha S, Franzmann T *et al* (2015) A liquid-to-solid phase transition of the ALS protein FUS accelerated by disease mutation. *Cell* 162: 1066–1077

Perdikari TM, Jovic N, Dignon GL, Kim YC, Fawzi NL, Mittal J (2021) A predictive coarse-grained model for position-specific effects of post-translational modifications. *Biophys J* 120: 1187–1197

Piana S, Donchev AG, Robustelli P, Shaw DE (2015) Water dispersion interactions strongly influence simulated structural properties of disordered protein states. *J Phys Chem B* 119: 5113–5123

Pietrek LM, Stelzl LS, Hummer G (2020) Hierarchical ensembles of intrinsically disordered proteins at atomic resolution in molecular dynamics simulations. *J Chem Theory Comput* 16: 725–737

Ratti A, Buratti E (2016) Physiological functions and pathobiology of TDP-43 and FUS/TLS proteins. *J Neurochem* 138(Suppl 1): 95–111

Regy RM, Dignon GL, Zheng W, Kim YC, Mittal J (2020) Sequence dependent phase separation of protein-polynucleotide mixtures elucidated using molecular simulations. *Nucleic Acids Res* 48: 12593–12603

Robustelli P, Piana S, Shaw DE (2018) Developing a molecular dynamics force field for both folded and disordered protein states. *Proc Natl Acad Sci USA* 115: E4758 – E4766

Salado IG, Redondo M, Bello ML, Perez C, Liachko NF, Kraemer BC, Miguel L, Lecourtois M, Gil C, Martinez A *et al* (2014) Protein kinase CK-1 inhibitors as new potential drugs for amyotrophic lateral sclerosis. *J Med Chem* 57: 2755 – 2772

Schmidt HB, Barreau A, Rohatgi R (2019) Phase separation-deficient TDP43 remains functional in splicing. *Nat Commun* 10: 4890

Serber Z, Ferrell Jr JE (2007) Tuning bulk electrostatics to regulate protein function. *Cell* 128: 441 – 444

Strickfaden SC, Winters MJ, Ben-Ari G, Lamson RE, Tyers M, Pryciak PM (2007) A mechanism for cell-cycle regulation of MAP kinase signaling in a yeast differentiation pathway. *Cell* 128: 519 – 531

Taylor LM, McMillan PJ, Liachko NF, Strovas TJ, Ghetti B, Bird TD, Keene CD, Kraemer BC (2018) Pathological phosphorylation of tau and TDP-43 by TTBK1 and TTBK2 drives neurodegeneration. *Mol Neurodegener* 13: 7

Tesei G, Schulze TK, Crehuet R, Lindorff-Larsen K (2021) Accurate model of liquid-liquid phase behaviour of intrinsically-disordered proteins from optimization of single-chain properties. *bioRxiv* https://doi.org/10.1101/2021.06.23.449550 [PREPRINT]

Tollervey JR, Curk T, Rogelj B, Briese M, Cereda M, Kayikci M, König J, Hortobágyi T, Nishimura AL, Župunski V *et al* (2011) Characterizing the RNA targets and position-dependent splicing regulation by TDP-43. *Nat Neurosci* 14: 452 – 458

Tziortzouda P, Van Den Bosch L, Hirth F (2021) Triad of TDP43 control in neurodegeneration: autoregulation, localization and aggregation. *Nat Rev Neurosci* 22: 197 – 208

Wang A, Conicella AE, Schmidt HB, Martin EW, Rhoads SN, Reeb AN, Nourse A, Ramirez Montero D, Ryan VH, Rohatgi R *et al* (2018) A single N-terminal phosphomimic disrupts TDP-43 polymerization, phase separation, and RNA splicing. *EMBO J* 37: e97452

Wang C, Duan Y, Duan G, Wang Q, Zhang K, Deng X, Qian B, Gu J, Ma Z, Zhang S *et al* (2020) Stress induces dynamic, cytotoxicity-antagonizing TDP-43 nuclear bodies via paraspeckle LncRNA NEAT1-mediated liquid-liquid phase separation. *Mol Cell* 79: 443 – 458.e7

Yaffe MB, Rittinger K, Volinia S, Caron PR, Aitken A, Leffers H, Gamblin SJ, Smerdon SJ, Cantley LC (1997) The structural basis for 14-3-3: phosphopeptide binding specificity. *Cell* 91: 961 – 971

Zhang P, Fan B, Yang P, Temirov J, Messing J, Kim HJ, Taylor JP (2019) Chronic optogenetic induction of stress granules is cytotoxic and reveals the evolution of ALS-FTD pathology. *Elife* 8: e39578

Expanded View Figures

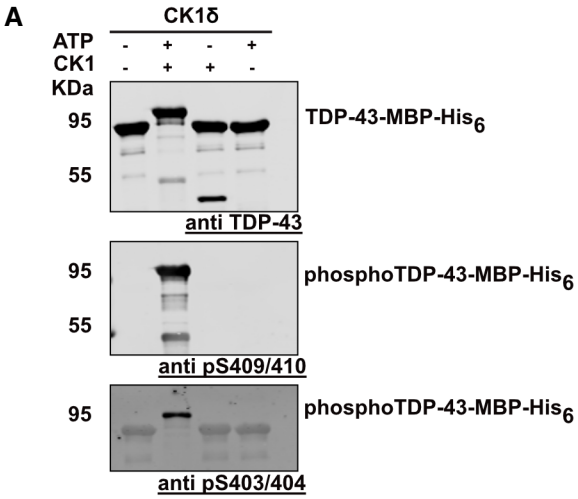

B

Trypsin digestion

MSEYIRVTEDENDEPIEIPSEDDGTVLLSTVTAQFPGACGLRYRNPVSQCMRGVRLVEGI
LHAPDAGWGNLVYVVNYPKDNKRKMDETDASSAVKVKRAVQKTSDLIVLGLPWKTTEQDL
KEYFSTFGEVLMVQVKKDLKTGHSKGFGFVRFTEYETQVKVMSQRHMIDGRWCDCKLPNS
KQSQDEPLRSRKVFVGRCTEDMTEDELREFFSQYGDVMDVFIPKPFRAFAFVTFADDQIA
QSLCGEDLIIKGISVHISNAEPKHNSNRQLERSGRFGGNPGGFGNQGGFGNSRGGGAGLG
NNQGSNMGGGMNFGAFSINPAMMAAAQAALQSSWGMMGMLASQQNQSGPSGNNQNQGNMQ
REPNQAFGSGNNSYSGSNSGAAIGWGSASNAGSGSGFNGGFGSSMDSKSSGWGM

Figure EV1. Identification of TDP-43-MBP-His$_6$ phospho-sites after *in vitro* phosphorylation with CK1δ.

A Identification of TDP-43 phospho-sites on *in vitro* phosphorylated TDP-43 (+CK1δ, +ATP) in comparison to controls (−CK1δ −ATP; CK1δ only; ATP only) by Western blot. Samples were analyzed by SDS–PAGE and Western blot using a rabbit anti-TDP-43 N-term antibody (Proteintech) to detect total TDP-43, rat anti-TDP-43-phospho Ser409/410 (clone 1D3, Helmholtz Center Munich) and mouse anti-TDP-43-phospho Ser403/404 (Proteintech, Cat. No.: 66079-1-Ig) antibodies.

B Schematic diagrams showing sequence coverage in mass spectrometry after trypsin digest (underlined) and phosphorylated serine/threonine residues (orange) of *in vitro* phosphorylated TDP-43-MBP-His$_6$ with CK1δ + ATP (one out of two representative experiments is shown).

Source data are available online for this figure.

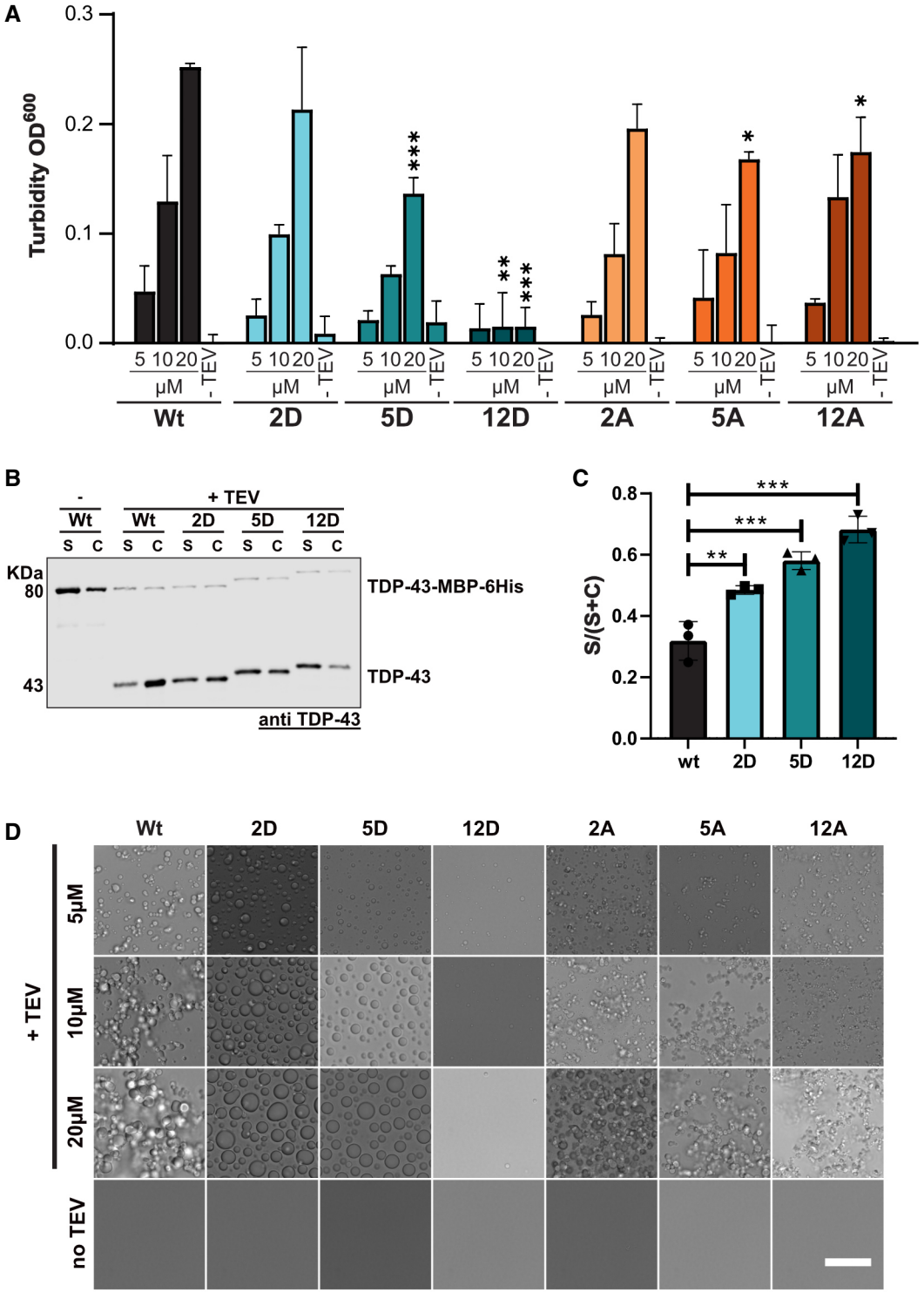
A
Turbidity OD600
0.3
0.2
0.1
0.0
5 10 20 - TEV
μM
Wt
2D
5D
12D
2A
5A
12A
B
-
+ TEV
Wt
Wt
2D
5D
12D
S C S C S C S C S C
KDa
80
43
TDP-43-MBP-6His
TDP-43
anti TDP-43
C
S/(S+C)
0.8
0.6
0.4
0.2
0.0
wt
2D
5D
12D
D
Wt
2D
5D
12D
2A
5A
12A
+ TEV
5μM
10μM
20μM
no TEV

Figure EV2.

Figure EV2. C-terminal phosphomimetic substitutions reduce TDP-43 condensation *in vitro*.

A Turbidity measurements (optical density [OD] at 600 nm) to quantify phase separation of different S-to-D and S-to-A mutants in comparison to TDP-43 Wt using phosphate buffer. Values represent mean of three independent experimental replicates ($n = 3$) ± SD. *$P < 0.0332$, **$P < 0.0021$ and ***$P < 0.0002$ by one-way ANOVA with Dunnett's multiple comparison test to Wt, comparing the respective concentration condition (5, 10, 20 μM).

B Sedimentation assay to quantify condensation of different S-to-D mutants in comparison to TDP-43 Wt (in Hepes buffer). TDP-43 was detected by TDP-43 Western blot (rabbit anti-TDP-43 N-term).

C Quantification of band intensities of cleaved TDP-43 corresponding to supernatant (S) and condensates (C) fractions is shown as mean of S/(S + C) ratio of three independent experimental replicates ($n = 3$) ± SD. **$P < 0.0021$ and ***$P < 0.0002$ by one-way ANOVA with Dunnett's multiple comparison test to Wt.

D Representative bright field microscopic images of TDP-43 condensates formed from TDP-43 Wt vs different S-to-D or S-to-A variants in phosphate buffer (Bar, 25 μm).

Source data are available online for this figure.

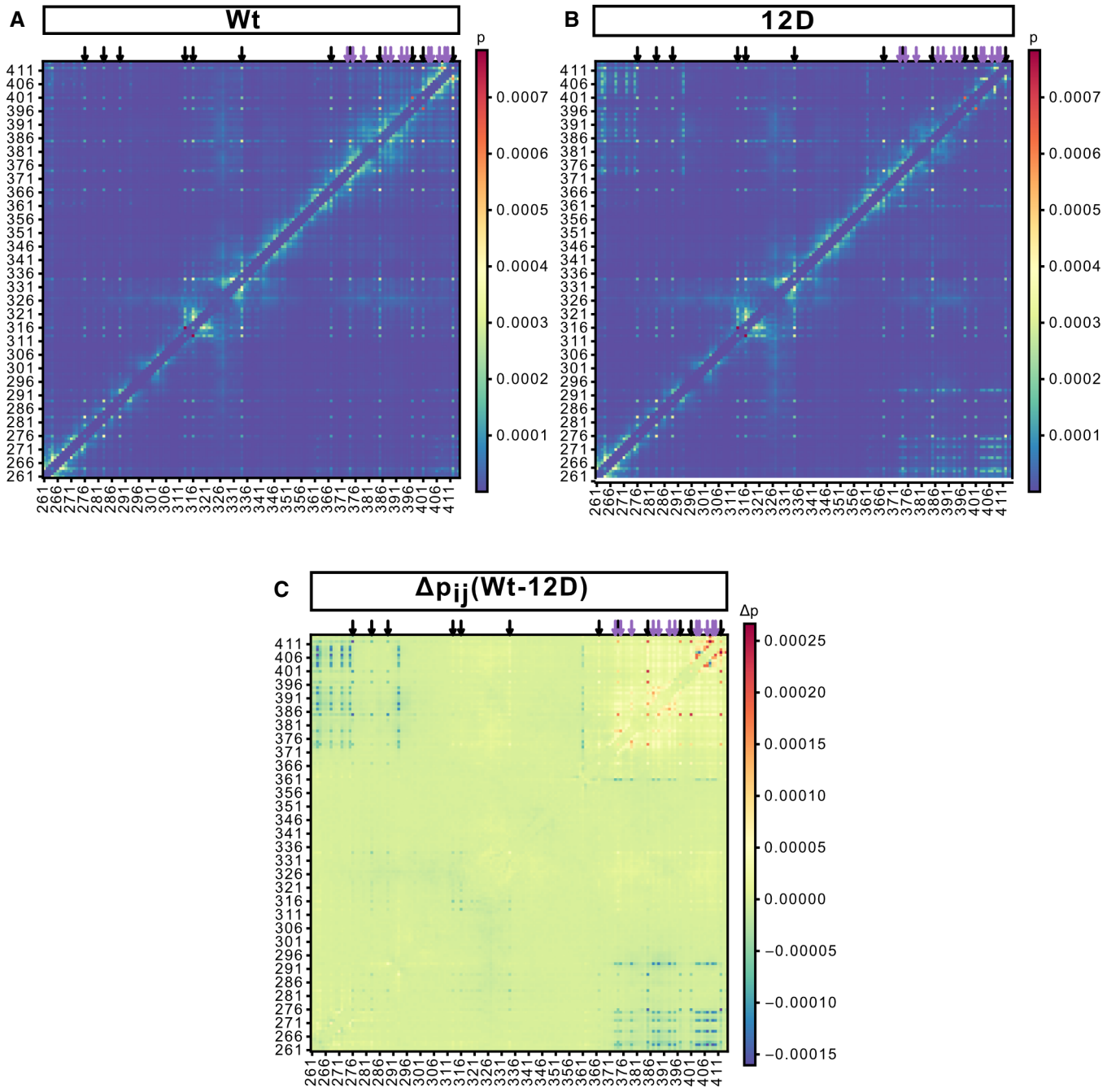

Figure EV3. Analysis of contacts in biomolecular condensates formed by the TDP-43 LCD in coarse-grained simulations.

A, B Contact maps for Wt (A) and 12D (B) TDP-43 LCD from simulations with the explicit solvent Martini coarse-grained model. Residue i and residue j are defined to be in contact if any of the coarse-grained beads are within 4.5 Å. The relative contact probability is calculated by averaging over all 118 protein chains and the last 5 of 20 μs simulations each. Intra-chain contacts with the two preceding and following residues are excluded from the analysis. Aromatic residues form prominent contacts and are highlighted by black arrows. For example, looking at the column for F276 and following it upwards one can see that F276 interacts with F276 in other chains and irrespective of the chain, with F283, F289, F313, F316, W334, F367, Y347, W385, F401, and W412. The sites of the phosphomicking S-to-D mutations are highlighted by purple arrows. At these sites differences between Wt and 12D LCD can be seen, with Wt forming more contacts close in protein sequence and 12D instead interacting with R268, R272, R275, R293, and R361 further away in the sequence.

C Differences in contact probability $P_{i,j} = P_{i,j}(\mathrm{Wt}) - P_{i,j}(12D)$ from simulations with the explicit-solvent Martini coarse-grained model. Differences highlight that wild-type S residues, unlike phosphomicking D residues, favor interactions with residues close in sequence, while demonstrating that most contacts are not affected by the phosphomicking S-to-D mutations. Black and purple arrows correspond to aromatic residues and phosphomicking S-to-D mutations, respectively.

Figure EV4. Phosphomimetic substitutions do not alter nuclear localization, UG-rich RNA binding and autoregulation of TDP-43.

A Immunostainings showing nuclear localization of myc-TDP-43 Wt, 12D and 12A in HeLa cells. Endogenous TDP-43 expression was silenced by siRNAs, followed by transient transfection of the indicated siRNA-resistant myc-TDP-43 constructs. After 24 h, localization of TDP-43 Wt, 12D and 12A variants was visualized by TDP-43 immunostaining (mouse anti-TDP-43 antibody, Proteintech). G3BP1 (rabbit anti-G3BP1 antibody, Proteintech) and DAPI signal is shown to visualize the cytoplasm and nuclei, respectively. In the merge (right column), DAPI is show in turquoise, TDP-43 in green, and G3BP1 in magenta. Bar, 30 μm.

B Electrophoretic mobility shift assay (EMSA) of TDP-43-MBP-His_6 variants (Wt, 12D and 12A) in a complex with $(UG)_{12}$ RNA.

C Representative confocal images of U2OS cells stably expressing the indicated myc-TDP-43 variants (Wt, 12D and 12A) after siRNA KD of endogenous TDP-43 and induction of myc-TDP-43 expression with doxycycline. Cells were stained with mouse monoclonal anti-myc 9E10 antibody (IMB protein production facility) and DAPI. For clarity, signals were converted to grey values in the individual channels (upper two rows). In the merge (lower row), DAPI is shown in turquoise) and myc-TDP-43 is shown in green. Bar, 20 μm.

D Western Blot showing the expression levels of myc-TDP-43 variants in stable inducible Flp-In T-Rex U2OS cell lines before and after addition of doxycycline (dox). Samples were analyzed by SDS–PAGE and Western blot using a rabbit anti-TDP-43 N-term antibody (Proteintech, upper blot), mouse anti-myc 9E10 antibody (IMB protein production core facility), and rabbit anti-Histone H3 antibody (Abcam) to detect the loading control Histone H3.

E Quantification of TDP-43 autoregulation after dox-induced expression of myc-TDP-43 variants in U2OS cell lines. Values represent the mean ± SD of four independent experimental replicates ($n = 4$) of endogenous TDP-43 expression levels normalized to Wt (−Dox) condition. *$P < 0.0332$ and ***$P < 0.0002$ by one-way ANOVA with Šídák's multiple comparisons test of TDP-43 endogenous expression levels, comparing the respective non-induced (−Dox) and induced (+Dox) lines.

Source data are available online for this figure.

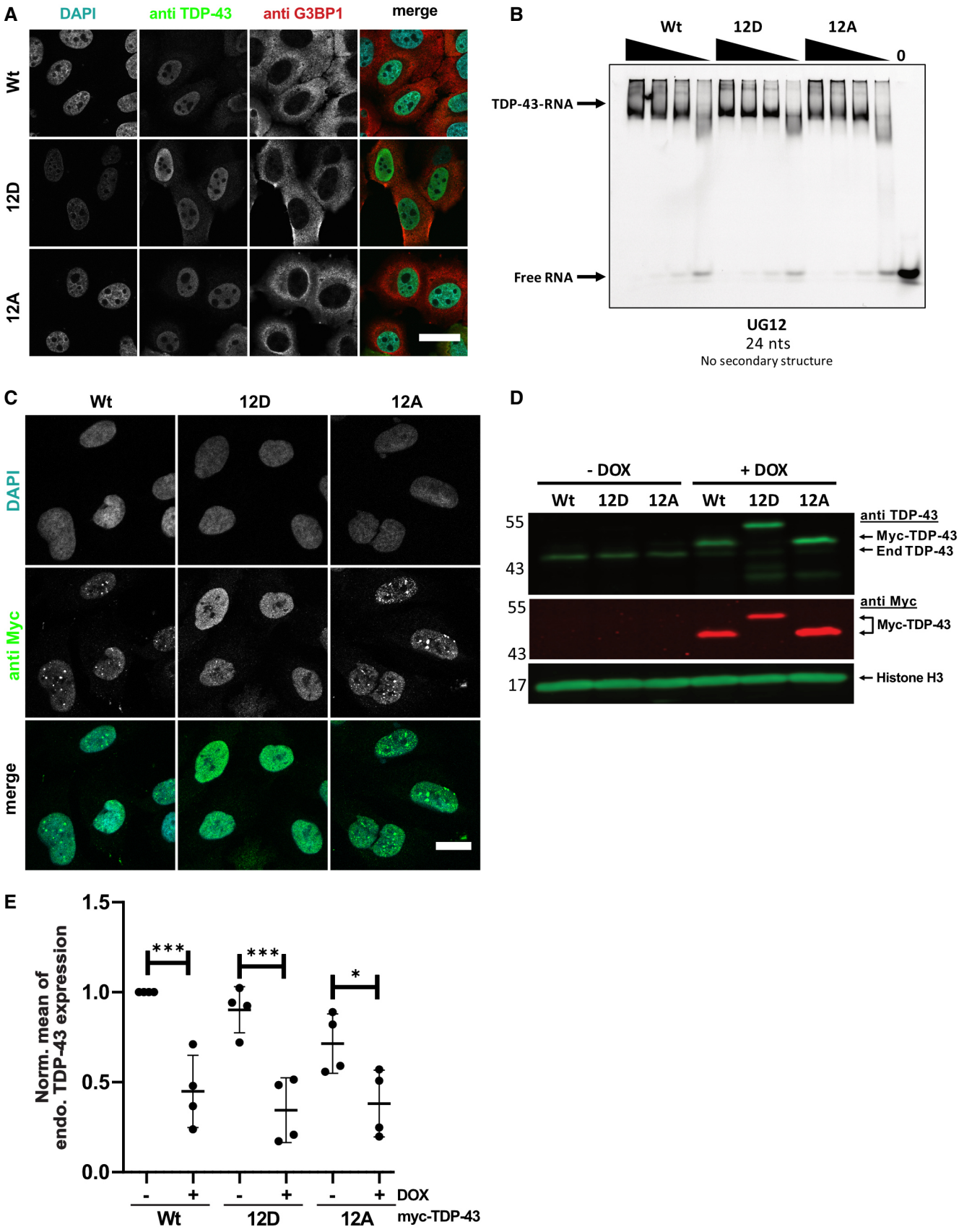

Figure EV4.

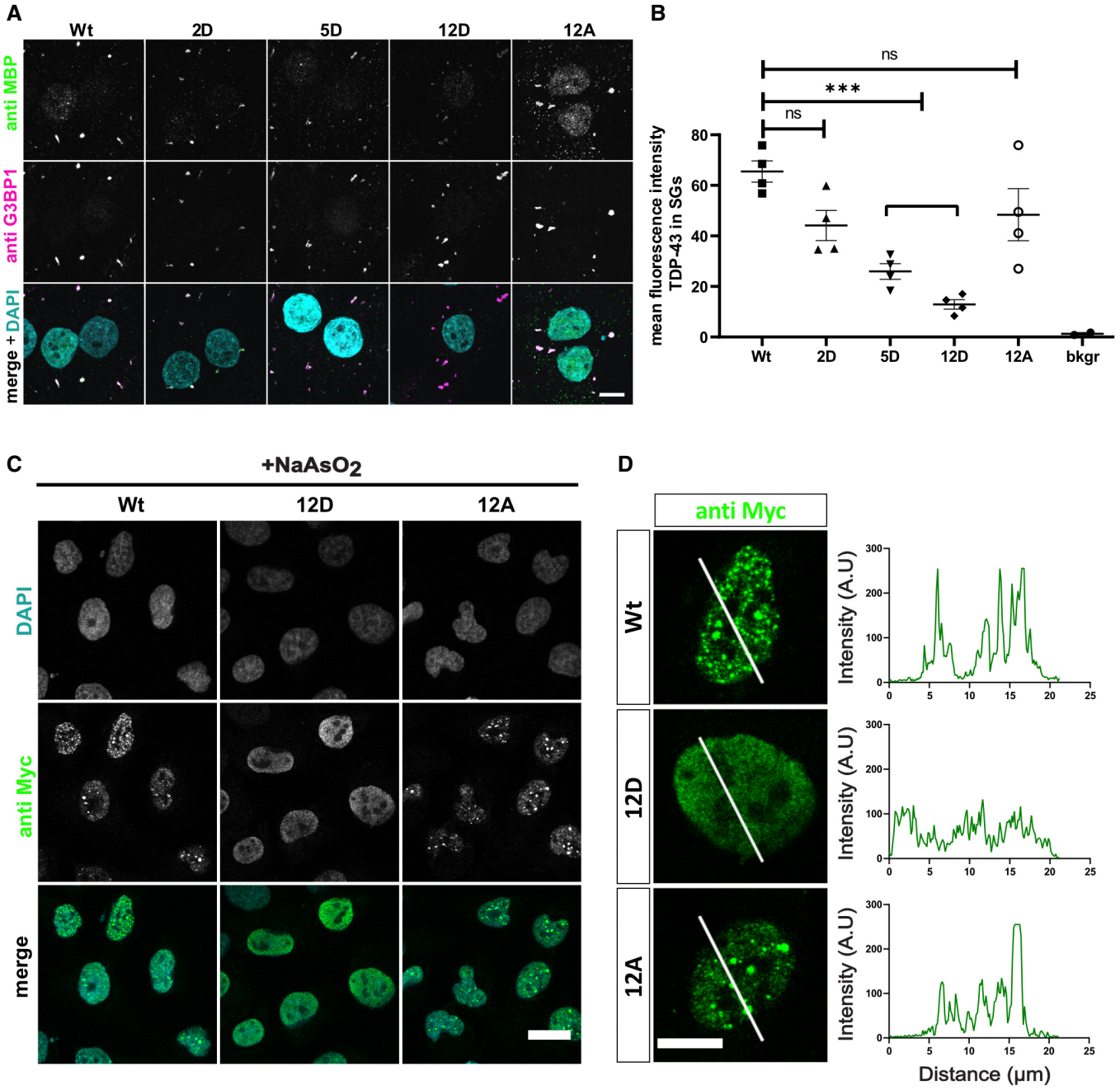

Figure EV5. Phosphomimetic S-to-D substitutions reduce association of TDP-43 with stress granules and nuclear stress bodies.

A Association of TDP-43 with stress granules (SGs) in semi-permeabilized HeLa cells is suppressed by phosphomimetic (2D, 5D and 12D) mutations in comparison to TDP-43 Wt and 12A. SGs and TDP-43-MBP-His_6 were visualized by G3BP1 and MBP immunostaining, respectively. For clarity, signals were converted to grey values in the individual channels (upper two rows). In the merge (lower row), G3BP1 is shown in magenta, TDP-43-MBP-His_6 in green, white pixels indicate colocalization. Nuclei were counterstained with DAPI (turquoise). Bar, 10 µm.

B Quantification of the mean fluorescence intensity of TDP-43-MBP-His_6 in SGs normalized to Wt for four independent replicates ± SEM, ***$P < 0.0002$ defined by 1-way ANOVA with Dunnett's multiple comparison test (≥ 10 cells; ≥ 46SGs per condition). Bkgr = background fluorescence in the green channel.

C Representative confocal images of U2OS cells stably expressing the indicated myc-TDP-43 variants (Wt, 12D and 12A) after siRNA KD of endogenous TDP-43 and induction of myc-TDP-43 expression with doxycycline, followed by sodium arsenite stress (2 h) to induce nuclear stress bodies (NBs). Cells were stained with mouse monoclonal anti-myc 9E10 antibody (IMB protein production facility) and DAPI. For clarity, signals were converted to grey values in the individual channels (upper two rows). In the merge (lower row), DAPI is shown in turquoise and myc-TDP-is shown in green. Bar, 20 µm.

D Intensity profiles (right) of myc-TDP-43 Wt, 12D and 12A variants (green), expressed in Flp-In T-Rex U2OS stable cell lines, along white lines (left). Bar, 10 µm.

Appendix

Disease-linked TDP-43 hyperphosphorylation suppresses TDP-43 condensation and aggregation

Table of content

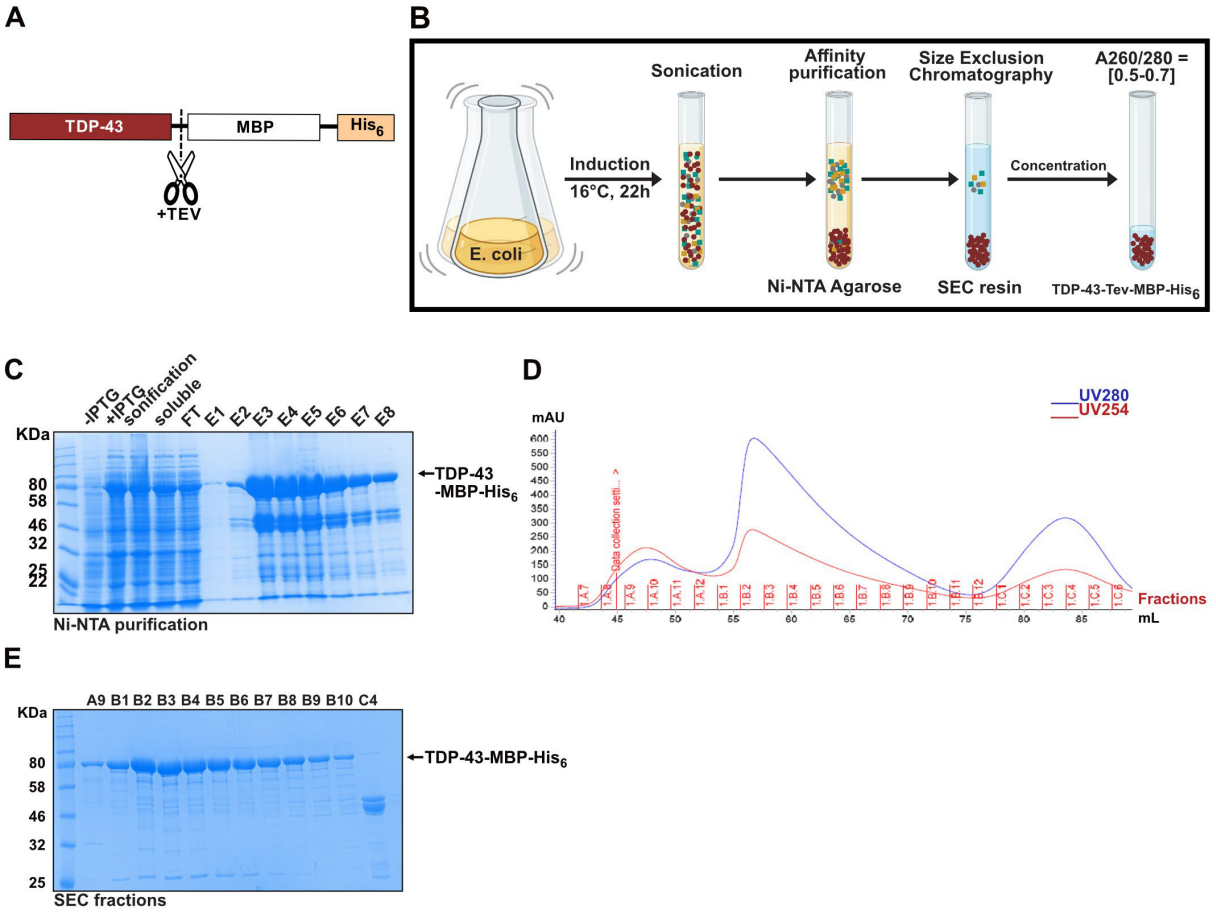

Appendix Figure S1. TDP-43-MBP-His$_6$ purification.

A Schematic representation of purified full-length TDP-43 containing a solubilizing maltose binding protein (MBP) tag, a His$_6$-tag and a TEV protease recognition site upstream of the MBP tag.

B Schematic diagram of TDP-43-MBP-His$_6$ expression and purification (created in BioRender.com). The protein is expressed in *E. coli* for 22 h at 16 °C and bacteria are lysed by sonication. Then the protein is purified under high salt conditions via Ni-NTA affinity purification and size exclusion chromatography (SEC) to obtain clean soluble TDP-43-MBP-His$_6$ (red circles), which is largely devoid of nucleic acids, as judged from the A260/280 ratio.

C Representative Coomassie-stained SDS-PAGE gel of the different steps from protein expression to Ni-NTA affinity purification. First and second lines correspond to samples before (-IPTG) and after (+IPTG) induction of TDP-43-MBP-His$_6$ expression. Third, fourth and fifth line correspond to samples after sonication, supernatant collection after spin down (soluble) and flow through (FT) after first wash with lysis buffer. The last 8 lines correspond to the consecutive elution steps (E1-E8) from the Ni-NTA agarose beads, fractions E2-E6 were pooled and used for SEC. ~89 kDa bands correspond to TDP-43-MBP-His$_6$.

D Representative SEC profile showing the absorption (mAU) of protein (UV280) and nucleic acids (UV254) on the y-axis, versus the volume (mL) of the different fractions on the x-axis.

E Coomassie-stained SDS-PAGE gel showing the indicated fractions (A9-C4) of the SEC run displayed in (D). A9, B1-B10 and C4 are fraction samples from peaks A, B and C in the SEC profile (D) and represent TDP-43-MBP-His$_6$ oligomeric, monomeric and cleaved species, respectively.

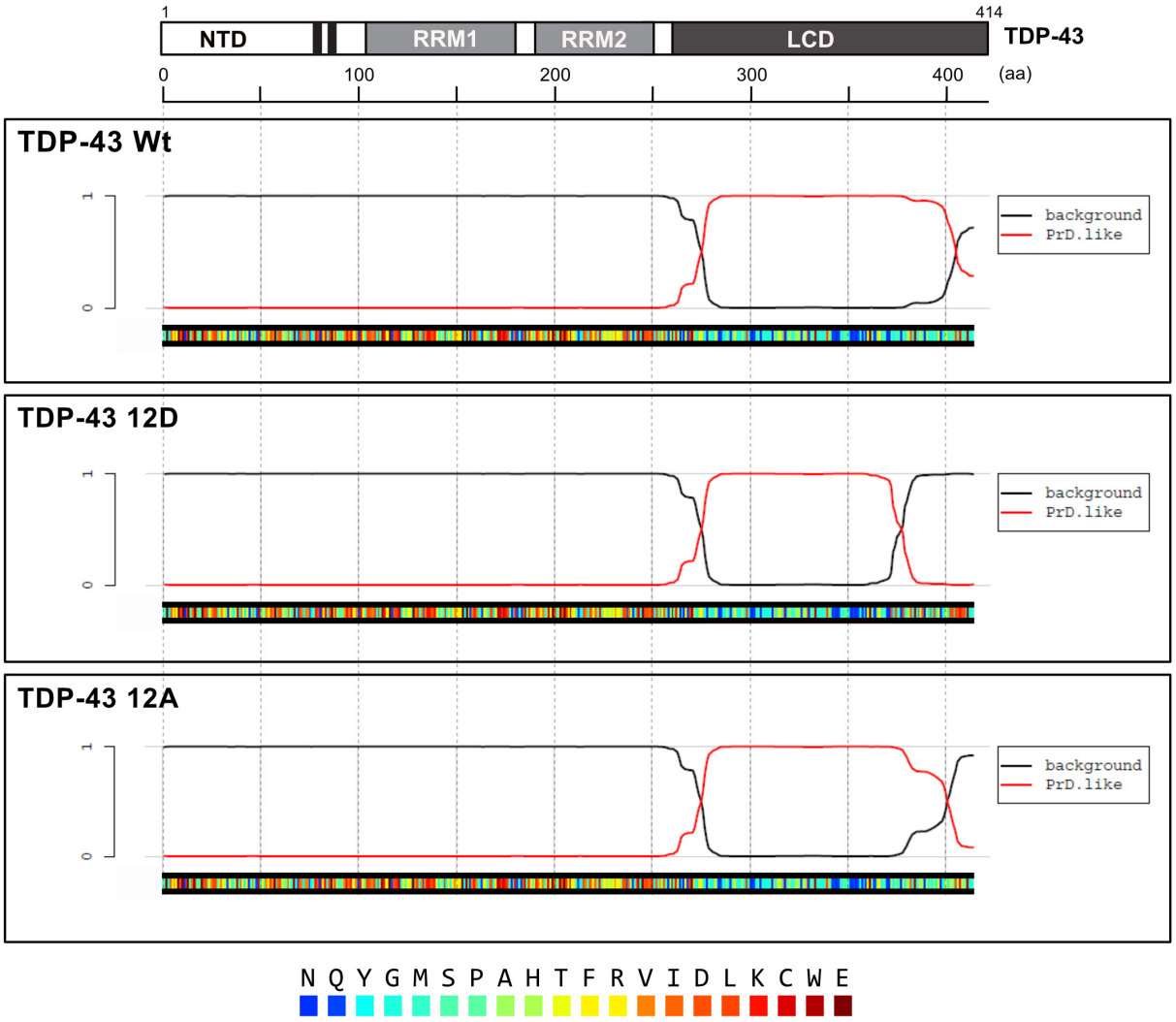

Appendix Figure S2. PLAAC predicts a reduced prion-like character of phosphomimetic TDP-43 12D.

Visualization outputs from PLAAC, a web application that scans protein sequences for domains with **p**rion-**l**ike **a**mino **a**cid **c**omposition (Lancaster et al., 2014). Each box shows a detailed visualization of different TDP-43 full-length variants (TDP-43 Wt, 12D and 12A) and respective Hidden Markov Model (HMM) prion-prediction score (probability scale from 0 to 1, shown on the y-axis), predicting prion domain-like (PrD. like, red) and non-prion domain-like (background, black) regions. The prediction reveals that the prion-like character of the C-terminal TDP-43 low complexity domain (LCD) is reduced by the 12 phosphomimetic S-to-D mutations. Bars below each diagram show amino acids (color-coded as in the legend).

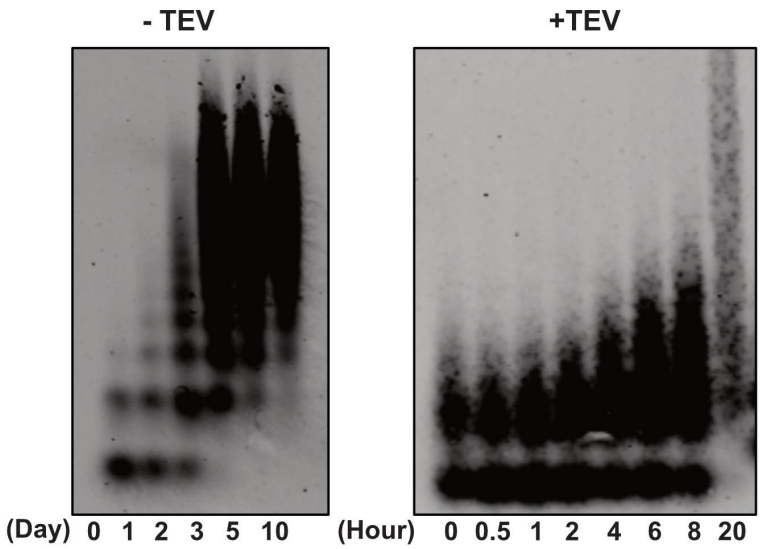

Appendix Figure S3. SDD-AGE analysis of TDP-43-MBP-His_6 with and without TEV protease-mediated cleavage.

Left: *In vitro* aggregation assay of TDP-43-MBP-His_6 in the absence of TEV protease (-TEV) leads to the appearance of SDS-resistant oligomers / high molecular weight species after several days of incubation. Distinct bands representing TDP-43-MBP-His_2 monomers, dimers, oligomers can be distinguished for the early timepoints (day 0 - 2). Note that the blot is the same as in Fig. 2E WT.

Right: *In vitro* aggregation assay of TDP-43-MBP-His_6 in the presence of TEV protease (+TEV), i.e. the MBP-His_6 tag is cleaved off with TEV protease. SDS-resistant oligomers / high molecular weight species already can be detected after several hours, but no distinct bands can be distinguished.

Detection was performed after SDD-AGE analysis by anti-TDP-43 Western blot (rabbit anti-TDP-43 N-term).

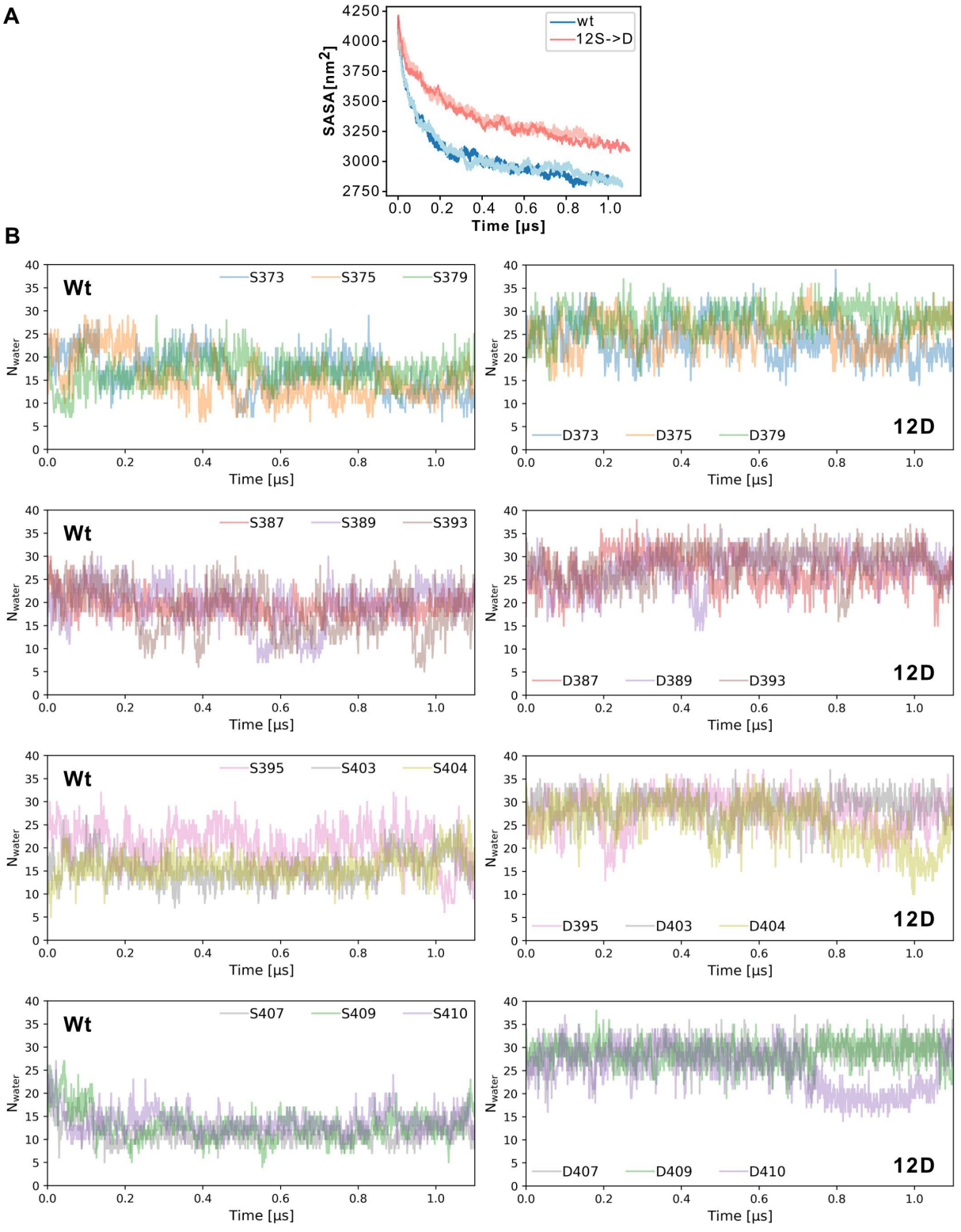

Appendix Figure S4. Differences in protein-protein and protein-water interactions in atomistic simulations of dense clusters of Wt and 12D TDP-43 LCDs.

A Solvent-accessible surface area (SASA) of the LCDs of Wt (blue and light blue) and 12D mutant (red and salmon) in atomistic simulations of dense protein solution. 12D mutant LCDs are more solvent-exposed than Wt LCDs, which is in line with the Wt LCDs forming stronger homotypic interactions.

B Dynamics of sidechain-water interactions at the sites of phosphomimicking S-to-D substitutions in atomistic simulations of Wt and 12D LCD clusters. Numbers of waters bound to sites of phosphomimicking S-to-D mutations (within 5 Å of the sidechain) are tracked over time for Wt (left) and 12D LCDs (right). While interactions are dynamic, there is a consistent trend that the phosphomimicking Asp residues bind more water molecules than the Ser residues in Wt LCDs.

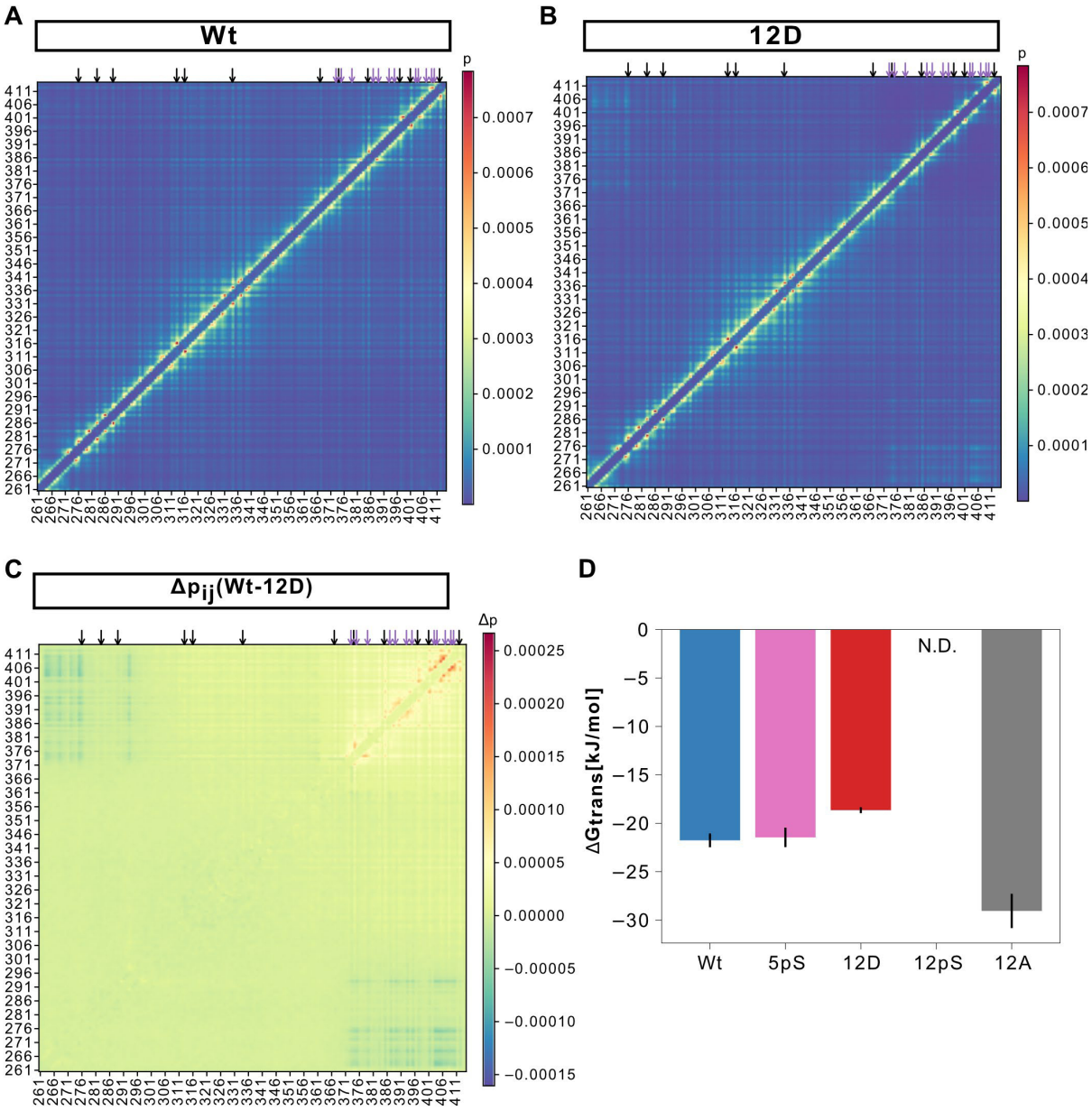

Appendix Figure S5. Analysis of coarse-grained simulations with the implicit-solvent HPS model.

A, B Contact maps for Wt (A) and 12D (B) TDP-43 LCD from simulations with the implicit solvent HPS coarse-grained model. Aromatic residues form prominent contacts and are highlighted by black arrows. The sites of the phosphomicking S-to-D mutations are highlighted by purple arrows.

C Differences in contact probability $\Delta p_{i,j} = p_{i,j}(\text{Wt}) - p_{i,j}(\text{12D})$ from simulations with implicit solvent HPS coarse-grained model. Black and purple arrows indicate positions of aromatic residues and sites of S-to-D substitutions respectively.

D Excess free energy of transfer ΔG_{trans} from the dilute phase to the condensate computed from the saturation and condensate densities of coexisting phases in simulations with the HPS coarse-grained model for different TDP-43 LDC variants. ΔG_{trans} could not be determined reliably for the 12pS LCD (N.D. = not determined).

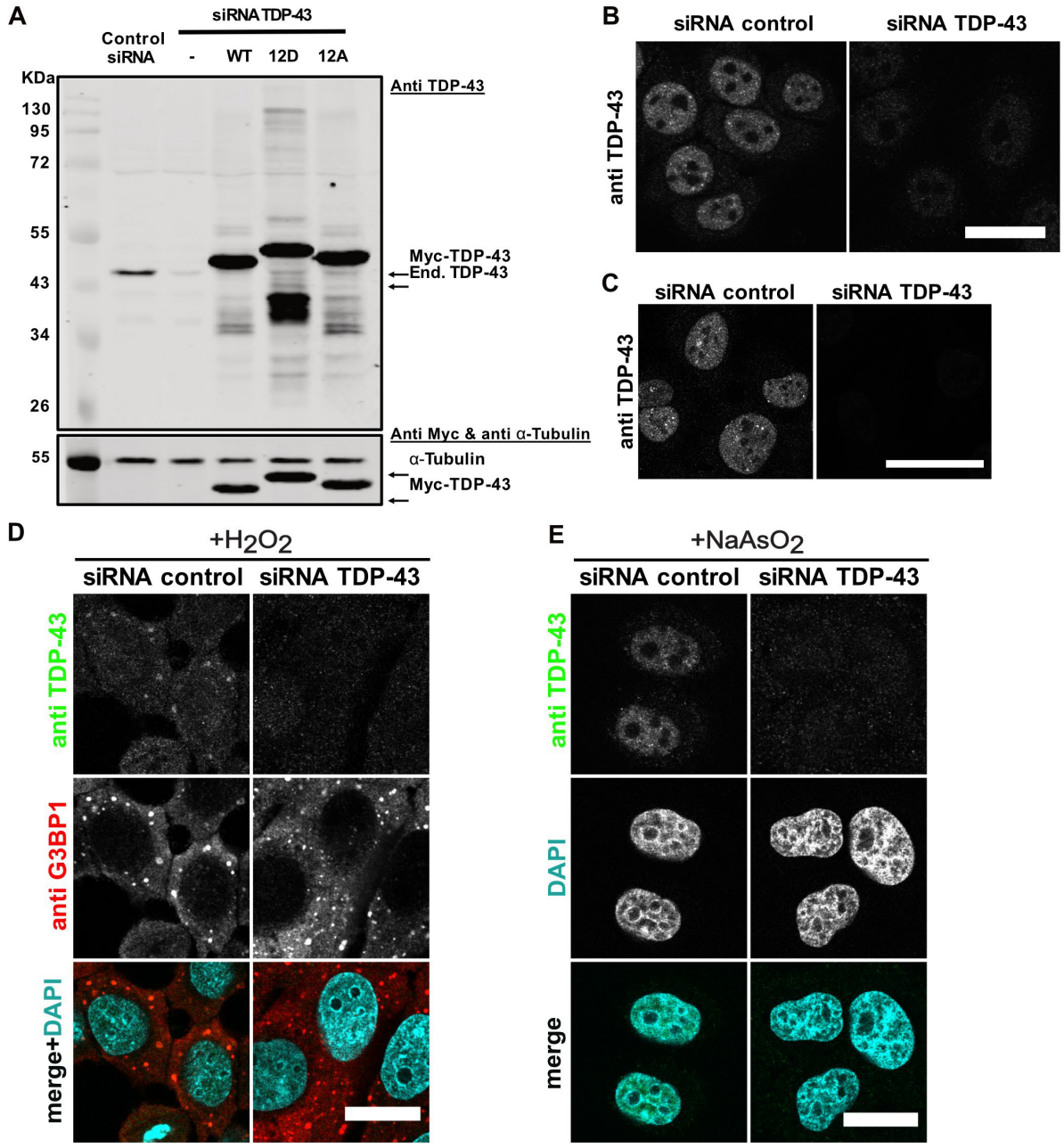

Appendix Figure S6. Controls showing endogenous TDP-43 levels after siRNA-mediated knockdown.

A SDS-PAGE followed by Western blot showing efficient siRNA-mediated knockdown of endogenous TDP-43 (running at ~43 kDa) and re-expression of myc-tagged TDP-43 Wt, 12D and 12A in Hela cells. Equal loading is demonstrated by α-Tubulin Western blot (bottom). TDP-43 was detected using rabbit anti-TDP-43 C-term antibody (Proteintech), α-Tubulin using mouse anti-alpha Tubulin antibody (Proteintech) and Myc-TDP-43 using mouse-anti Myc antibody (9E10, Helmholtz Center Munich).

B Representative confocal images of HeLa cells showing efficient siRNA-mediated knockdown of endogenous TDP-43 versus control siRNA transfection (control for experiment shown in Fig. 5D). TDP-43 (grey) was detected using a mouse anti-TDP-43 antibody (Proteintech). Bar, 25 µm.

C Representative confocal images of a Flp-In T-Rex U2OS stable cell line showing efficient siRNA-mediated knockdown of endogenous TDP-43 versus control siRNA transfection

(control for experiment shown in Fig. EV4C). TDP-43 (grey) was detected using a mouse anti-TDP-43 antibody (Proteintech). Bar, 40 µm.

D, E Representative confocal images of HeLa cells showing endogenous TDP-43 (grey, upper rows) in control siRNA-treated (left column) or TDP-43 siRNA-treated cells (right column) after H_2O_2 (C) or arsenite (D) stress (control for experiment shown in Fig. 5D and 5H). TDP-43 was detected using mouse anti-TDP-43 antibody (Proteintech), SGs using rabbit anti G3BP1 antibody (Proteintech) and nuclei were stained with DAPI. For clarity, signals were converted to grey values in the individual channels (upper two rows). In the merge (lower row), DAPI is shown in turquoise, TDP-43 in green and G3BP1 in red. Bar, 20 µm.

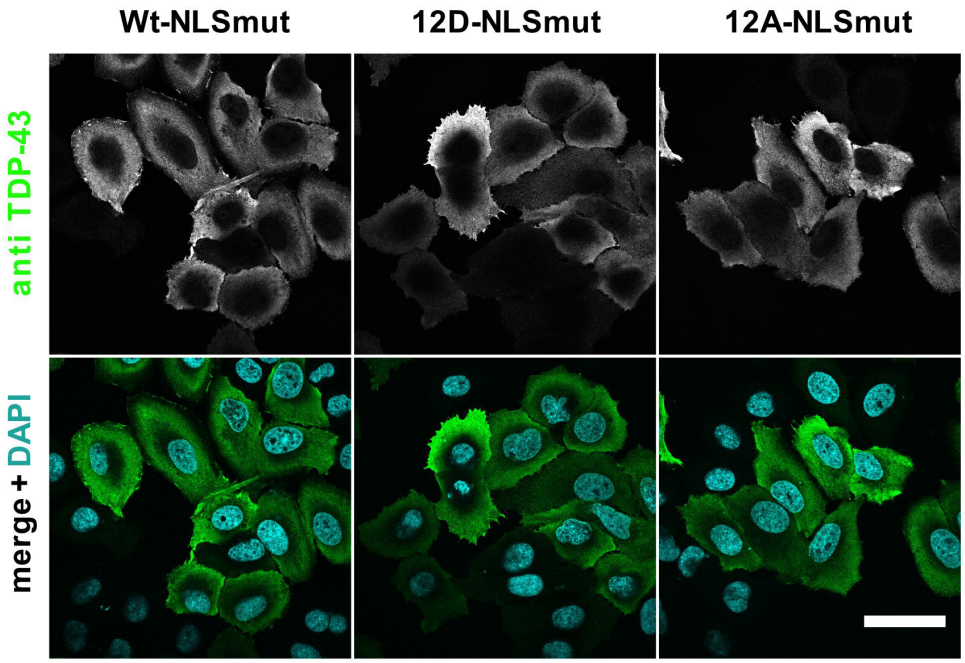

Appendix Figure S7. Control experiment for localization of NLS mutant TDP-43 variants in HeLa cells.

Representative confocal images of HeLa cells demonstrating equal cytoplasmic localization of all TDP-43-NLS mutant variants (Wt, 12D and 12A), 24 h after transfection and 48 h after endogenous TDP-43 silencing. Staining was carried out with a mouse anti-TDP-43 antibody (Proteintech), TDP-43 signal is shown in grey (upper row) or green (lower row); DAPI is shown in turquoise. Bar, 40 µm.

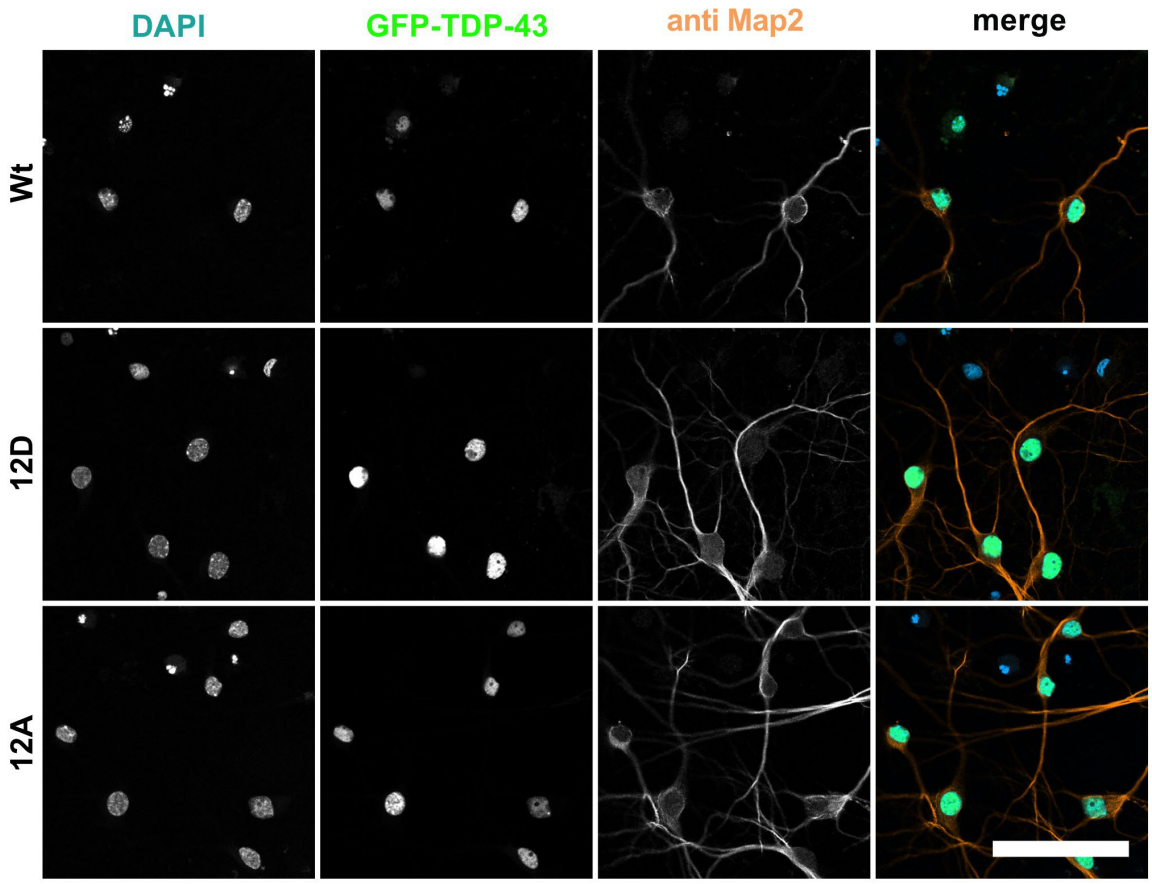

Appendix Figure S8. Control experiment for localization of EGFP-TDP-43 variants in primary hippocampal neurons.

Representative confocal images displaying nuclear localization of all EGFP-TDP-43 variants (Wt, 12D and 12A) in primary rat hippocampal neurons. Neurons were transduced on DIV 5 and stained on DIV5+4, with mouse anti-Map2 antibody and nuclei with DAPI. For clarity, signals were converted to grey values in the individual channels (first three columns). In the merge (fourth column), nuclei are shown in turquoise, EGFP-TDP-43 in green and Map2 (marker for neuronal cell body and dendrites) in orange. Bar, 80 µm.

Appendix Table S1. Concentrations of dense and dilute phases in simulations with the HPS coarse-grained model.

Uncertainties were estimated from block averaging. For 12pS the concentrations were not determined (N.D.), as it forms multiple clusters rather than a single dense-phase condensate.

	c_{dense} [mM]	c_{dilute} [mM]
Wt	34.546 +/- 0.026	0.007 +/- 0.002
12D	31.498 +/- 0.031	0.023 +/- 0.002
5pS	33.340 +/- 0.029	0.008 +/- 0.002
12pS (not a condensate)	N.D.	N.D.
12A	38.255 +/- 0.021	0.0005 +/- 0.0001

5 Publication III

Post-translational modifications on RNA-binding proteins: accelerators, brakes, or passengers in neurodegeneration?

Published as

Erin L. Sternburg, **Lara A. Gruijs da Silva**, Dorothee Dormann. Post-translational modifications on RNA-binding proteins: accelerators, brakes, or passengers in neurodegeneration? Review in Trends in biochemical sciences (2022) volume 47, doi: 10.1016/j.tibs.2021.07.004.

CellPress

Trends in Biochemical Sciences

Review

Post-translational modifications on RNA-binding proteins: accelerators, brakes, or passengers in neurodegeneration?

Erin L. Sternburg [1], Lara A. Gruijs da Silva [1,2] and Dorothee Dormann [1,3,*]

RNA-binding proteins (RBPs) are critical players in RNA expression and metabolism, thus, the proper regulation of this class of proteins is critical for cellular health. Regulation of RBPs often occurs through post-translational modifications (PTMs), which allow the cell to quickly and efficiently respond to cellular and environmental stimuli. PTMs have recently emerged as important regulators of RBPs implicated in neurodegenerative disorders, in particular amyotrophic lateral sclerosis (ALS) and frontotemporal dementia (FTD). Here, we summarize how disease-associated PTMs influence the biophysical properties, molecular interactions, subcellular localization, and function of ALS/FTD-linked RBPs, such as FUS and TDP-43. We will discuss how PTMs are believed to play pathological, protective, or ambiguous roles in these neurodegenerative disorders.

Highlights

Research in recent years has begun to tackle the impact of post-translational modifications (PTMs) on neurodegenerative disease-associated RNA binding proteins, such as FUS and TDP-43.

Alterations in arginine methylation of FUS and abnormal phosphorylation, acetylation, oxidation, nitrosylation, ubiquitination, and proteolytic cleavage of TDP-43 are observed in postmortem brains of amyotrophic lateral sclerosis (ALS) and frontotemporal dementia (FTD) patients.

Changes in the PTM landscape of FUS and TDP-43 seen in ALS and FTD alter the biophysical properties, molecular interactions, subcellular localization, and function of FUS and TDP-43.

Some disease-linked PTMs may accelerate the disease process (e.g., by promoting mislocalization or aberrant phase separation), whereas others may act as 'brakes', attempting to correct other primary cellular issues that occur earlier in disease.

RBPs and abnormal PTMs in neurodegeneration

RBPs are a diverse group of almost 2000 proteins [1] that are essential for the proper regulation of RNA throughout its lifecycle. Starting at transcription, RNAs are decorated with many RBPs that are responsible for their splicing, transport, translation, and stability [2]. Proper function of RBPs is thus vital for maintaining cellular health. It is therefore no surprise that dysregulation of RBPs has been implicated in a variety of diseases, including cancer and neurological disorders [3,4]. Prime examples are the neurodegenerative diseases **amyotrophic lateral sclerosis (ALS)** (see Glossary) and **frontotemporal dementia (FTD)**, where specific RBPs become mislocalized from the nucleus into cytoplasmic inclusions and drive disease through loss- and gain-of-function mechanisms [5].

The most prominent RBPs affected in ALS and FTD are **TAR DNA-binding protein of 43 kDa (TDP-43)**, [6] and **Fused in sarcoma (FUS)** [7–10]. Mutations in the genes encoding for TDP-43 and FUS cause familial ALS and insoluble inclusions containing TDP-43 or FUS occur specifically in the degenerating brain regions, but not in unaffected regions of ALS and FTD patients [11], supporting a causative role for the dysfunctional RBPs in these diseases. What triggers TDP-43 and FUS to become mislocalized and dysfunctional in ALS and FTD is still not fully understood. One hypothesis is that defects in nuclear transport lead to increased cytoplasmic concentrations of nuclear RBPs [12,13]. This, along with persistent **stress granule (SG)** recruitment, leads to aberrant phase separation and, ultimately, aggregation of these proteins [14,15] (Figure 1).

Another factor that might play an important role in the dysfunction of these RBPs are PTMs (Box 1), which can alter protein folding or molecular interactions with other proteins or nucleic acids and thereby affect protein activity, stability, and localization. Because of their accessibility, PTMs often

[1]Johannes Gutenberg-Universität (JGU) Mainz, Faculty of Biology, Mainz, Germany
[2]Graduate School of Systemic Neurosciences (GSN), Munich, Germany
[3]Institute of Molecular Biology (IMB), Mainz, Germany

*Correspondence:
ddormann@uni-mainz.de (D. Dormann).

occur in **intrinsically disordered regions (IDRs)** [16], which are commonly found in RBPs. IDRs can engage in weak multivalent interactions and thereby drive **liquid–liquid phase separation (LLPS)** and regulate RBP solubility and function [17]. PTMs occurring in IDRs often affect the process of LLPS and the dynamics of **membraneless organelles (MLOs)** in cells. Prominent examples of MLOs include nucleoli, SGs, P bodies, or other ribonucleoprotein (RNP) granules enriched in numerous RBPs and RNAs. As neurodegeneration-linked RBPs, including TDP-43 and FUS, are thought to become dysfunctional and solidify through aberrant LLPS and dysregulated RNP granule dynamics [14,15] (Figure 1), PTMs that alter phase separation of these RBPs might play an important role in the formation of pathological RBP inclusions in neurodegenerative diseases, as will be discussed in more detail later.

PTMs have generally emerged as important regulators of proteins implicated in neurodegenerative disorders; for example, modifications of the disease-associated proteins Tau (Alzheimer's disease), α-synuclein (Parkinson's disease), and Huntingtin (Huntington's disease) influence their aggregation propensity and impact neurodegeneration in various model systems [18]. Of particular interest are PTMs that are found exclusively in the pathological state (i.e., on the deposited protein) but not under physiological conditions. These so-called disease-linked PTMs have been particularly intensely studied and often have been found to drive the process of protein aggregation [18–20]. Of note, there are also examples of disease-associated PTMs (e.g., on Tau) that suppress or delay the aggregation and seeding process [21,22]. Hence, disease-linked PTMs observed in the pathological stage may not always be drivers or accelerators of the disease process, but could also have the opposite effect and might arise as compensatory mechanisms or 'brakes' to counteract or slow down certain pathological processes, such as protein aggregation. Alternatively, disease-linked PTMs may simply be innocuous bystanders or 'passengers' that arise as a byproduct of certain enzymes becoming dysfunctional during the disease process, but without having functional consequences.

Here, we will discuss how disease-associated PTMs influence the behavior of RBPs that are key players in neurodegenerative disorders, in particular FUS and TDP-43. We will summarize how disease-linked modifications affect the biophysical properties, aggregation, subcellular localization, and function of these RBPs and how they are believed to influence the process of neurodegeneration. We will also briefly discuss the role of PTMs on other neurodegeneration-associated RBPs, including hnRNPA1, hnRNPA2, EWS, and TAF15. We will focus on PTMs found in the disease states and discuss whether they have a pathological, protective, or ambiguous role in the process of neurodegeneration.

FUS pathology in neurodegeneration and disease-linked FUS PTMs

FUS (also known as TLS) is a ubiquitously expressed RBP which has crucial functions in many steps of RNA processing, including transcription, splicing, and translational control [23], as well as DNA damage repair [24]. FUS harbors an N-terminal **low complexity domain (LCD)** rich in SYGQ residues, two canonical RNA-binding domains (RRM and ZnF) flanked by arginine-glycine-rich **RGG/RG motifs**, and a C-terminal nuclear localization signal (NLS) (Figure 2A). FUS is predominantly nuclear under physiological conditions, in line with its major functions in transcription, splicing, and DNA repair. By contrast, FUS presents pathological cytoplasmic redistribution and aggregation in the degenerating brain regions of patients with ALS (ALS-FUS) and FTD (FTD-FUS), and mutations in *FUS* are a known genetic cause for ALS [7–10]. These disease-associated mutations are found throughout the protein, but many alter or truncate the C-terminal NLS (Figure 2A), causing cytoplasmic mislocalization and enhanced accumulation of FUS in SGs [25–27]. It is believed that abnormal cytoplasmic localization and a persistent recruitment of FUS into SGs may promote an aberrant liquid-to solid state transition, leading to the

Glossary

Amyotrophic lateral sclerosis (ALS): a neurodegenerative disease that affects motor neurons in the brain and spinal cord, leading to progressive muscle weakness and paralysis.
FET protein family: a family of three closely related proteins, FUS, EWS, and TAF15. All three proteins play a role in RNA processing and are implicated in neurodegenerative disorders.
Frontotemporal dementia (FTD): a neurodegenerative disease affecting neurons in the frontal and temporal lobes of the brain, leading to severe changes in personal and social conduct or language.
Fused in sarcoma (FUS): DNA/RNA-binding protein that plays a role in transcription, splicing, RNA transport, and the DNA damage response. Associates with the U1 snRNP.
Heterogeneous nuclear ribonucleoproteins (hnRNPs): a broad class of RBPs involved in nucleic acid metabolism.
Intrinsically disordered regions (IDRs): highly dynamic protein regions that do not adopt a stable three-dimensional folded structure and often have a biased amino acid composition (low amino acid complexity).
Liquid–liquid phase separation (LLPS): the demixing of a homogenous solution of molecules into two coexisting liquid phases, a dense phase enriched in certain molecules and a light phase depleted of these molecules [139].
Low complexity domain (LCD): a region of a protein that contains little diversity in its amino acid composition.
Membraneless organelles (MLOs): distinct compartments within a cell that are not enclosed by a lipid membrane but form through LLPS.
Phosphomimetic: an amino acid substitution that mimics phosphorylation.
RGG/RG motif: disordered protein regions containing multiple arginine-glycine-glycine and/or arginine-glycine motifs that can participate in weak interactions with RNA, DNA, and other proteins. Arginines in RGG/RG motifs are often subject to post-translational arginine methylation [140].
Stress granules (SGs): cytosolic MLOs composed of proteins and mRNAs that form in response to cellular stress. Their formation is triggered by stalled translation initiation complexes.

pathological FUS aggregation seen in disease [15,25,28,29] (Figure 1). Most likely, neurodegeneration is then driven by both loss- and gain-of function mechanisms; for example, reduced nuclear FUS leading to disturbed RNA processing, plus aberrant interactions in the cytoplasm, disturbing, for instance, translation or mitochondrial function [5,30–33].

TAR DNA-binding protein of 43 kDa (TDP-43): RNA binding protein involved in RNA biogenesis and processing. Regulates the splicing of cryptic exons.

What causes cytoplasmic mislocalization of FUS in patients who do not carry genetic mutations in *FUS* is not entirely clear. Possible mechanisms leading to FUS mislocalization include certain forms of cellular stress [34,35], pathological alterations to the nuclear import receptor Transportin [36–38], but also aberrant PTMs. Therefore, it is worth having a closer look at the PTMs found on FUS in the physiological and the disease state (Figure 2A), in particular in patients that lack *FUS* mutations.

A PTM alteration that is specific to FTD-FUS is hypomethylation of arginines [39,40] (Figure 2B). FUS is normally asymmetrically dimethylated on arginines in all three RGG/RG motifs. FUS is also dimethylated in ALS-FUS patients; however, FTD-FUS patients instead feature monomethylated and unmethylated FUS in pathological inclusions in the cortex [39,40]. Moreover, phosphorylation of serines/threonines in the LCD occurs upon DNA damage, which is believed to arise in FTD-FUS based on elevated γ-H2AX levels, even though phosphorylated FUS has so far not been detected in FTD-FUS patients [41,42]. Finally, both ALS and FTD patients with FUS pathology feature ubiquitin-positive aggregates [7], suggesting that deposited FUS may be (mono or poly) ubiquitinated. But what are the effects of these disease-associated modifications on FUS behavior and function?

FUS-PTMs as regulators of LLPS and aggregation

FUS is known to readily phase separate into liquid-like droplets [28], which is driven through cation–π interactions between tyrosines in the N-terminal LCD and arginines in the C-terminal RGG/RG motifs [43–45], as well as through additional π–π , hydrogen bonding, and hydrophobic interactions [46,47]. In addition, a region within the FUS LCD can adopt a cross-β amyloid-like structure, which may play a role in its fibrillization [29]. Disease-associated mutations are

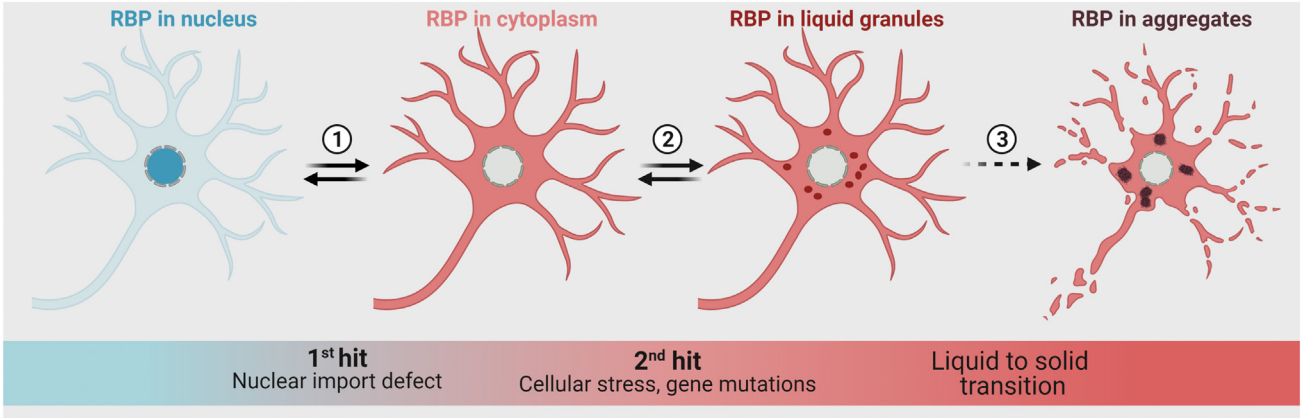

Figure 1. A multi-hit model of RNA-binding protein (RBP) dysfunction in neurodegenerative diseases. Although the exact mechanisms of how RBPs become dysfunctional in amyotrophic lateral sclerosis (ALS) and frontotemporal dementia (FTD) are not understood, one hypothesis is that RBP mislocalization and aggregation arises via a 'multi-hit' process [13]. First, a nuclear import defect causes cytosolic mislocalization of the disease-relevant nuclear RBP. This can arise through genetic mutations that alter the nuclear localization signal [25], or through broader defects in the nuclear transport machinery [12]. Additional stress (e.g., through defects in protein quality control, external stressors, additional mutations, etc.) may lead to the recruitment of the mislocalized RBP into stress granules or other phase-separated RNP granules. Over time, possibly favored by defects in chaperones or altered stress granule dynamics [15], the protein then undergoes a liquid-to-solid transition, leading to pathological aggregation.

Box 1. Different PTMs arising on RBPs

PTMs alter amino acids through the covalent linkage of functional groups, polymeric chains, small proteins, or through proteolytic cleavage (Figure I). Modifications can be added and/or removed in response to various signals and thus allow the cell to alter the biophysical properties and/or activity of an RBP based on cellular conditions. PTMs can change the charge, hydrophobicity, or bulkiness of certain amino acid side chains, enriching the chemical repertoire of the 20 natural amino acids and expanding the functional diversity of the protein. These chemical changes can alter protein folding or molecular interactions with other proteins or nucleic acids and thereby affect protein activity, stability, and localization. PTMs can occur in the RNA-binding domains of RBPs and thus tune RNA interactions. Most PTMs are added and removed by specialized enzymes (including kinases, phosphatases, ligases, transferases, polymerases, and proteases), which are often specific to distinct sets of amino acids. Some types of PTMs occur nonenzymatically, for example as a consequence of oxidative stress (oxidation and nitrosylation). Figure I shows PTMs that are often found on RBPs, including the neurodegeneration-linked proteins TDP-43 and FUS.

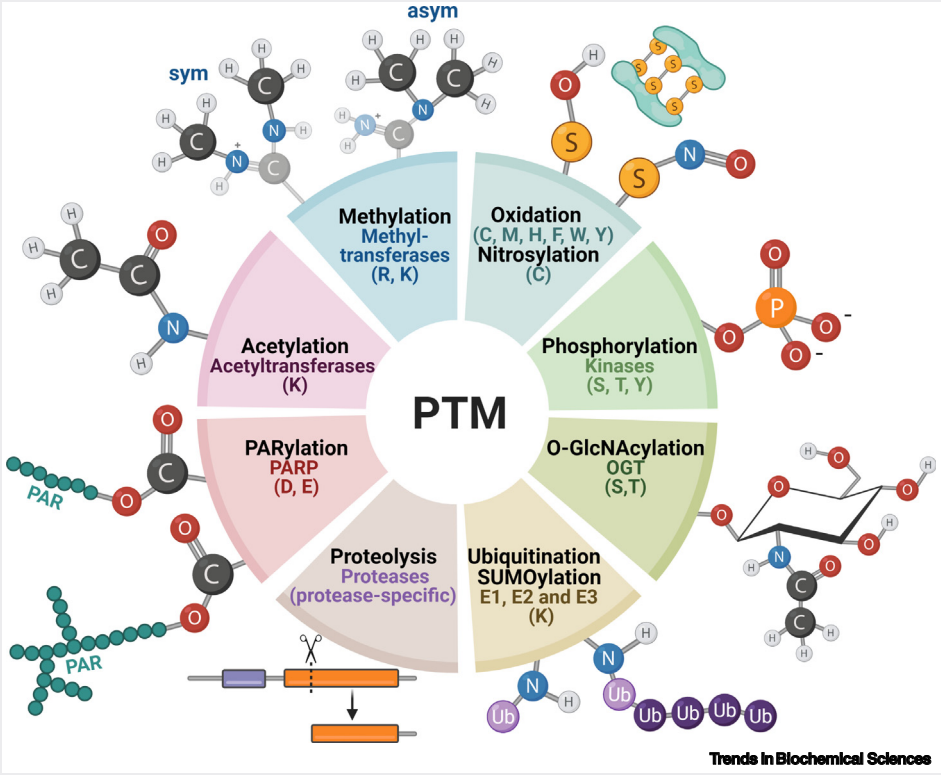

Figure I. Diagram showing the chemical nature of post-translational modifications (PTMs), enzymes that introduce them, and modified amino acids (single letter code). Methylation can come in different flavors, including monomethylation (not shown), symmetric and asymmetric dimethylation of R residues, and mono-, di-, or trimethylation of K residues (not shown). Oxidation refers to the addition of one or more oxygen atoms to a susceptible side chain or the formation of disulfide bonds between Cys residues. Nitrosylation is the covalent attachment of a nitric oxide group (-NO) to a cysteine thiol. Phosphorylation results from the addition of a phosphoryl group to a Ser, Thr, or Tyr residue by different kinases and thus imparts a negative charge onto the modified residue. O-GlcNAcylation adds a monosaccharide (N-acetylglucosamine, GlcNAc) to Ser/Thr residues via an O-linked glycosidic bond, catalyzed by OGT (O-linked N-acetylglucosamine transferase). During SUMOylation and ubiquitination, small, folded proteins of the small ubiquitin-related modifier (SUMO) family and ubiquitin, respectively, are covalently linked to K residues with the help of E1, E2, and E3 ligases, either as a monomer or as polymeric chains. Proteolysis can be mediated by different types of proteases on protease-specific cleavage sites and is an example of an irreversible PTM. PARylation refers to the addition of linear or branched Poly-(ADP-ribose) (PAR) polymers, catalyzed by Poly (ADP-ribose) polymerases (PARPs). Acetylation is a reaction catalyzed by acetyltransferases that transfer an acetyl group onto a Lys residue.

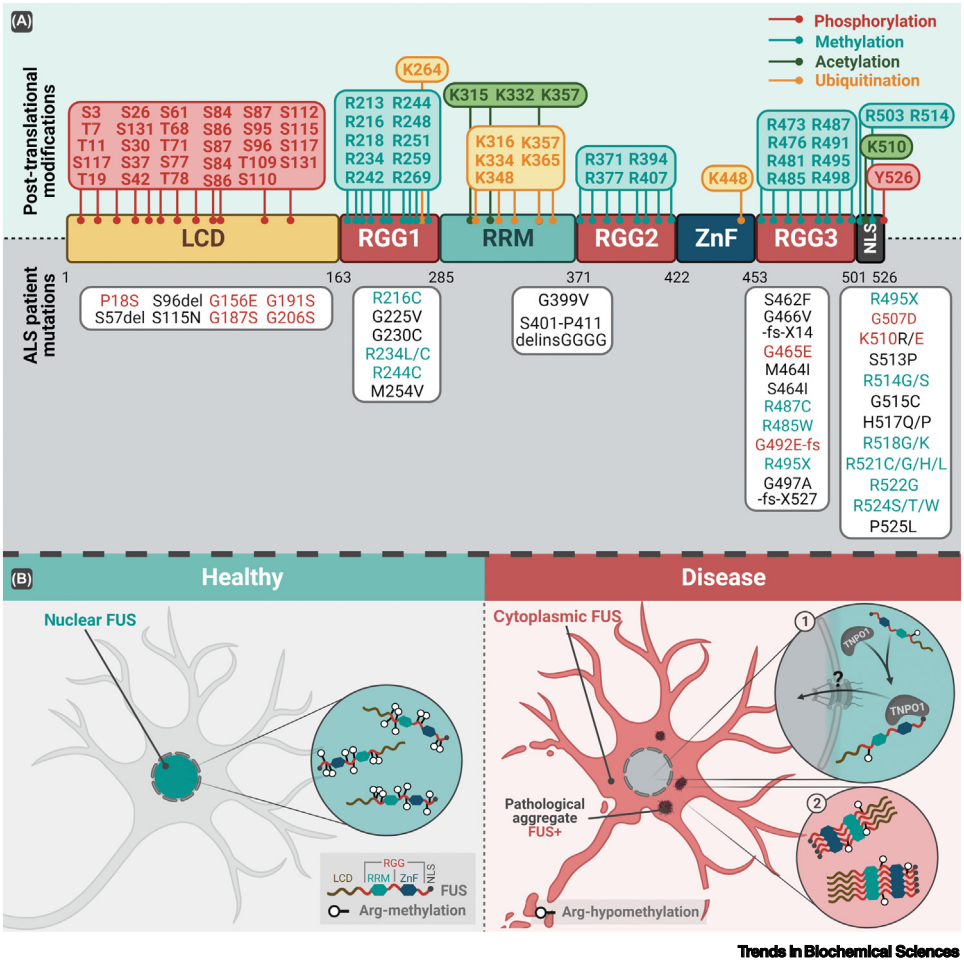

Figure 2. Post-translational modifications (PTMs) of FUS, disease-associated mutations that alter PTM sites, and consequences of FUS hypomethylation in disease. (A) Schematic representation of the FUS protein (526 amino acids) and its functional domains. FUS has an N-terminal low complexity domain (LCD), three RGG/RG motifs (RGG1, RGG2, and RGG3), one RNA recognition motif domain (RRM), one zinc finger domain (ZnF), and a C-terminal nuclear localization signal (NLS). Numbers under the diagram refer to amino acid positions. Top panel displays PTMs that have been mapped on FUS, in both healthy and disease states. Phosphorylation sites are from [42]. Methylation and ubiquitination sites are from www.phosphosite.org. Acetylation sites are from [61] and www.phosphosite.org. Bottom panel displays mutations identified in ALS patients [13,147]. Phosphomimetic mutations and mutations that create potential new phosphorylation sites are highlighted in red. Mutations that remove a methyl-arginine site are shown in blue. (B) FUS methylation status and its consequences under healthy and disease conditions. Under healthy conditions (left), FUS is predominantly found in the nucleus and highly methylated on RGG/RG motif arginines. In postmortem brains of frontotemporal dementia (FTD) patients (right), FUS is found in cytoplasmic aggregates and is no longer highly methylated but hypomethylated instead [39,40]. FUS hypomethylation has ambivalent consequences: (1) its affinity to Transportin-1 (TNPO1) increases, enhancing its nuclear import [39]. This suggests that FUS hypomethylation could be a homeostatic response aimed at restoring the physiological nuclear localization of FUS. However, it remains unclear why this restoration is not observed in patients. (2) FUS hypomethylation enhances phase separation and aggregation of FUS [43,49], suggesting that loss of this PTM may drive formation of cytosolic FUS aggregates.

known to exacerbate the liquid-to-solid state transition of FUS *in vitro* [28,44], but changes in PTMs can also strongly influence the biophysical properties of FUS both *in vitro* and in cells. Serine and threonine phosphorylation of the FUS LCD, as seen after DNA damage [41,42], decreases FUS LLPS and aggregation *in vitro* [29,48], and **phosphomimetic** mutants of FUS

show decreased cytoplasmic aggregation in yeast [48]. Thus, phosphorylation of the FUS LCD during DNA damage may be a cellular response to antagonize FUS insolubility; hence, it would be interesting to explore whether cells utilize this mechanism under physiological conditions to regulate FUS LLPS and function and whether it can be harnessed therapeutically to counteract or reverse FUS aggregation.

Besides phosphorylation, arginine methylation has been shown to increase the liquidity of FUS, as unmethylated FUS shows an increase in LLPS, gelation, and aggregation *in vitro* [43,49]. Likewise, in cells, the presence of asymmetric dimethylation decreases nuclear aggregation of FUS [43], and FUS hypomethylation promotes its association with SGs [49], suggesting that hypomethylated FUS has a higher tendency to accumulate and aggregate in MLOs. Thus, loss of this PTM may be one factor that promotes FUS aggregation through aberrant LLPS in FTD patients that show FUS hypomethylation (Figure 2B).

FUS-PTMs as regulators of protein–protein interactions and FUS localization

Nuclear import of FUS is achieved predominantly through the nuclear import receptor Transportin-1 (TNPO1), also known as Karyopherin-β2, which binds to the C-terminal PY-NLS of FUS [25]. Interestingly, nuclear localization of FUS is regulated by arginine methylation, as TNPO1 binding is enhanced by hypomethylation within the FUS-RGG3 region, which sits adjacent to the PY-NLS and also participates in the TNPO1 interaction [39,40,49].

Binding of TNPO1 to FUS is not only important for nuclear import, but also for chaperoning of FUS and suppressing its LLPS and aggregation in the cytoplasm [49–51]. Hypomethylation of FUS, as seen in FTD-FUS patients, increases TNPO1 binding and thus enhances nuclear import and chaperoning of FUS [39,40]. Considering these data, hypomethylation of FUS should be beneficial and could potentially be a PTM that arises in FTD-FUS patients to offset the TNPO1 pathology observed in these patients [36,37]. In this respect, it is interesting to note that other nuclear import receptors (TNPO3, Importin β, and Importin 7) were recently found to interact with FUS through its RGG/RG regions and, also for these import receptors, hypomethylation enhances binding to FUS [52,53]. Thus, it can be speculated that FUS arginine hypomethylation may arise in patients to allow binding to alternative import receptors and enhance chaperoning and nuclear localization of FUS (Figure 2B). How FUS hypomethylation arises in FTD-FUS patients and why it fails to restore proper nuclear localization of FUS these patients is currently still unknown.

Phosphorylation of FUS has also been shown to influence FUS nuclear localization. One study demonstrated serine/threonine phosphorylation in the N-terminal LCD of FUS by DNA-dependent protein kinase (DNA-PK) following DNA damage, which leads to the translocation of FUS from the nucleus into the cytoplasm [41]. Another study, which confirmed FUS LCD phosphorylation with various DNA damaging agents, however, did not observe cytoplasmic mislocalization of FUS [42], so additional work is necessary to clarify the effects of LCD phosphorylation on nuclear localization of FUS. Finally, it has been shown that C-terminal tyrosine phosphorylation (on Y526 within the PY-NLS) can impair TNPO1 binding and nuclear import of FUS [54]. Under which cellular conditions this modification might arise and whether it occurs in disease, such as in FTD-FUS patients, remains to be addressed.

Other FUS PTMs: potential roles and disease relevance

The presence of ubiquitin-positive FUS inclusions is well documented in ALS and FTD patients [7]. However, it is yet to be shown whether FUS itself is directly ubiquitinated in this context. Proteomic high throughput analysis of various cell lines has shown that FUS ubiquitination can occur within its RRM or ZnF domains [55,56] (Figure 2A), which could aid in FUS degradation.

Additionally, ubiquitination could affect LLPS and aggregation of FUS, as previously reported for other model proteins and the proteasome [57]. Moreover, the high concentration of ubiquitin within FUS inclusions has been shown to disrupt normal ubiquitin homeostasis in cells and thus could lead to misregulation of downstream protein quality control pathways [58] (Box 2).

Lysine acetylation, another common protein modification, has recently been shown to occur within FUS during cellular stress and to influence the phase separation properties of the FUS LCD *in vitro* [59,60]. In addition, acetylation marks have been observed within the RRM and the NLS of FUS and can regulate interactions with RNA and TNPO1, respectively [61]. Treatment of cells with deacetylase inhibitors reduces inclusion formation, and ALS patient-derived fibroblasts show higher levels of lysine acetylation in the NLS [61]. It is yet to be demonstrated whether changes to FUS acetylation are directly tied to mechanisms of disease. Further, FUS was found to undergo Poly-ADP-ribosylation (PARylation) under conditions of genotoxic stress, such as DNA damage or H_20_2 treatment [62]. Additional studies demonstrate that FUS is PARyled *in vitro* by PARP1 [63]; however, the exact sites of PARylation and the functional consequences (e.g., on FUS phase separation, recruitment to SGs, subcellular localization) are still unknown.

TDP-43 pathology in neurodegeneration and disease-linked TDP-43 PTMs

TDP-43 is another disease-linked RBP with numerous roles throughout RNA metabolism [23]. Many of these roles are shared with FUS, including the regulation of splicing, miRNA processing, mRNA transport, and mRNA expression regulation [23]. TDP-43 also overlaps with FUS in its role in the DNA damage response and has recently been demonstrated to act as a DNA repair protein whose function is perturbed in ALS [64,65]. The structure of TDP-43 can be organized into three sections (Figure 3A): the N-terminal domain harbors a classical bipartite NLS and drives dimerization and oligomerization. There is evidence that oligomerization is important for normal physiological function of TDP-43 [66,67]; however, the role of this self-association in pathological aggregation remains unclear. The middle of TDP-43 hosts two RRM domains, responsible for recognition and binding of UG-rich RNA motifs [68]. The C-terminal domain of TDP-43 is an intrinsically disordered LCD that drives LLPS, makes TDP-43 highly aggregation-prone, and can adopt a cross-β sheet amyloid-like conformation [69–72]. Interestingly, almost all ALS-associated mutations in TDP-43 cluster in the C-terminal LCD (Figure 3A). These mutations can alter TDP-43's phase separation and aggregation behavior, its protein–protein interaction profile, its half-life, or its nucleocytoplasmic localization [73]. However, the reported alterations

Box 2. Neurodegenerative disease shares close ties with protein quality control

ALS and FTD both have pathological ties with the protein quality control machinery. Mutations in genes involved in autophagic and proteasomal degradation (*SQSTM1*, *UBQLN2*, *OPTN*, *VCP*, *CHMP2B*, *TBK1*) are genetically linked to ALS and FTD [141,142]. ALS patients with mutations in UBQLN2 present UBQLN2 inclusions that colocalized with ubiquitin, p62, TDP-43, FUS, and OPTN [143,144], and UBQLN2 can impact the RNA-binding and phase separation behavior of FUS and modulate stress granule (SG) dynamics [145]. Moreover, FUS and TDP-43 inclusions are highly enriched in ubiquitin, as well as SQSTM1/p62 [146]. The enrichment of ubiquitin in aggregates is thought to deplete the free ubiquitin pool in cells, which could disrupt protein quality control pathways and exacerbate disease [58]. Another possibility is that polyubiquitin alters the phase separation behavior of the modified RBPs, as it has been previously reported to enhance protein aggregation [112] or phase separation of proteasomes [57]. Similar polyubiquitin-dependent phase separation has been seen with proteins destined to be degraded via the proteasome, where the formation of liquid-like foci allows for the compartmentalization of target proteins and the proteasome machinery [57]. In both cases, polyubiquitination may initially act as a mechanism for the cell to degrade target proteins or concentrate proteins together with the degradation machinery. However, polyubiquitination may then have detrimental side effects, such as enhancing TDP-43 aggregation or trapping and inhibiting components of the degradation machinery. Indeed, TDP-43 CTF inclusions were recently shown to trap stalled proteasomes, as well as additional components of the ubiquitin-proteasome system [92]. Further research is needed to fully understand the links between protein quality control and RBP regulatory pathways.

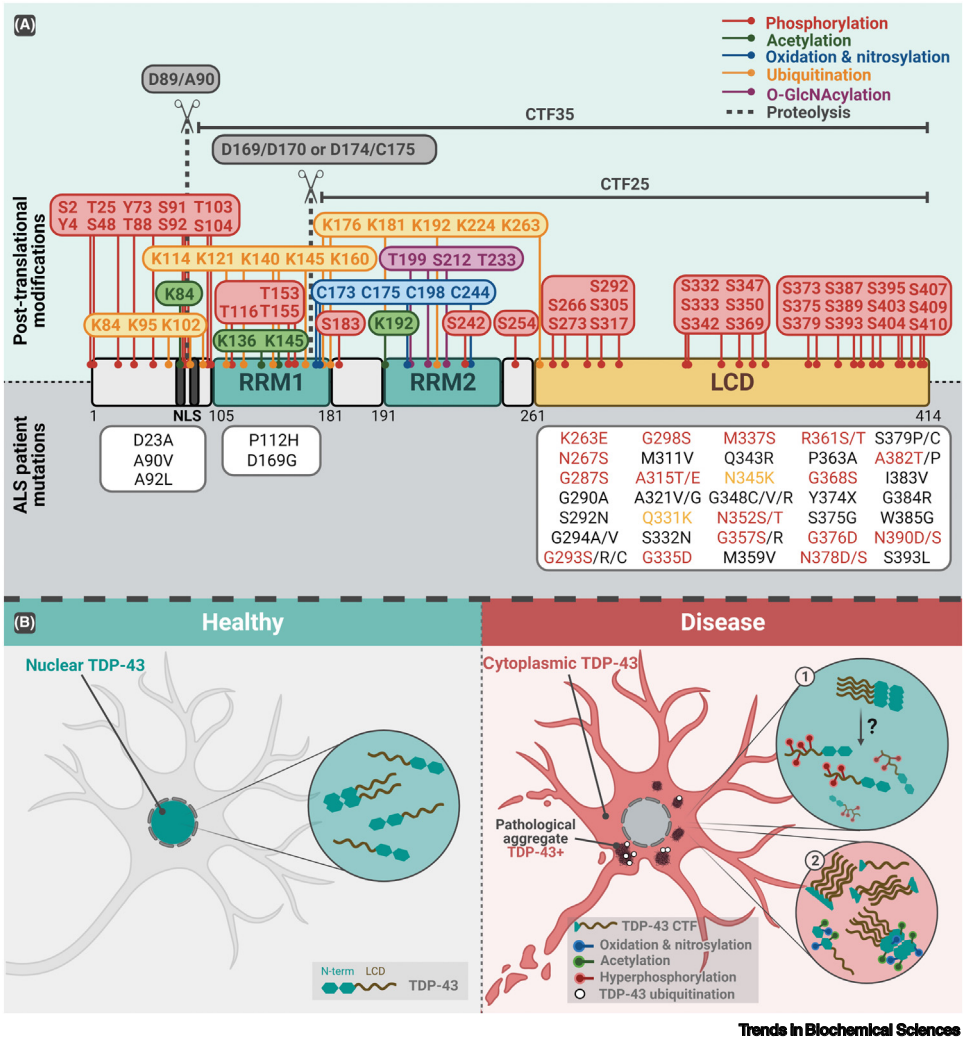

Figure 3. Post-translational modifications (PTMs) of TDP-43, disease-associated mutations that alter PTM sites, and consequences of disease-linked TDP-43 PTMs. (A) Schematic representation of the TDP-43 protein (414 amino acids) and its functional domains. The N-terminal domain harbors a classical bipartite nuclear localization signal (NLS), followed by two RNA recognition motifs (RRM1 and RRM2) and a C-terminal low complexity domain (LCD). Numbers under the diagram refer to amino acid positions. Top panel displays PTMs that have been mapped on TDP-43. Phosphorylation and ubiquitination sites are from www.phosphosite.org. Acetylation sites are from [88,106,107]. Oxidation and nitrosylation sites are from [75,90]. O-GlcNAcylation sites are from [105]. Proteolysis sites are from [91,148]. Most of the displayed PTMs are known to be associated with disease. Bottom panel displays mutations identified in ALS patients [13,76]. Phosphomimetic mutations and mutations that create potential new phosphorylation sites are highlighted in red. Mutations that create a potential new acetylation or ubiquitination site are highlighted in yellow. (B) Disease-associated PTMs on TDP-43 and their consequences. Under physiological conditions, TDP-43 is largely found in the nucleus (left). However, in postmortem brains of ALS, FTD, or Alzheimer's disease patients (right), TDP-43 can be lost from the nucleus and localizes in cytosolic pathological inclusions. In this form, it features several disease-specific PTMs, namely hyperphosphorylation, proteolytic cleavage, and ubiquitination. Like in Fused in sarcoma (FUS), disease-associated PTMs on TDP-43 have ambivalent consequences: (1) C-terminal hyperphosphorylation decreases TDP-43 LLPS and aggregation [96], suggesting that this PTM may possibly arise as a protective mechanism to counteract pathological TDP-43 aggregation. Yet, it remains enigmatic why hyperphosphorylated TDP-43 is detected in pathological aggregates. (2) Proteolytic cleavage leads to the formation of TDP-43 C-terminal fragments (CTF), which are highly aggregation-prone and toxic to cells.

are often subtle and not shared by all mutations, hence, no clear single pathomechanism could be identified so far. Interestingly, many of the mutations alter known or putative PTM sites or generate new ones (Figure 3A), which could contribute to the pathological consequences of these mutations.

Like FUS, TDP-43 is predominately nuclear, but partially translocates to the cytoplasm upon certain types of cellular stress [74,75]. TDP-43 is partially lost from the nucleus and forms cytoplasmic inclusions in the degenerating brain regions of 95% of ALS and ~45% of FTD patients [5]. Mutations in the TDP-43-encoding gene (*TARDBP*) are associated with familial ALS and, very rarely, FTD. However, aggregation of TDP-43 often occurs even when genetic mutations in the gene are absent. Similar to FUS, neurodegeneration is thought to arise through both loss- and gain-of function mechanisms [76]. Upon aberrant aggregation in the cytoplasm, TDP-43 levels are depleted in the nucleus, which can lead to mis-splicing of TDP-43 target RNAs [5,76–78]. Aberrant LLPS of TDP-43 or cytoplasmic TDP-43 aggregates are also thought to be toxic to cells, for example, by sequestering nuclear transport factors [76,79]. TDP-43 oligomers can be released from cells [80] and TDP-43 aggregates from FTD patient tissue can seed new pathological aggregates in cultured neurons or TDP-43 mouse models [81,82]. These observations suggest that TDP-43 pathology may spread from cell to cell and propagate in a prion-like manner, as described for other protein aggregates in neurodegenerative diseases [83].

In ALS and FTD patients with TDP-43 pathology, TDP-43 is known to be hyperphosphorylated, acetylated, ubiquitinated, and proteolytically cleaved [6,84–89] and evidence of cysteine oxidation and nitrosylation of TDP-43 has also been observed in FTD patient brains [75,90] (Figure 3B). C-terminal fragments (CTFs) of ~25 kDa are the most abundant form of TDP-43 found in inclusions in ALS and FTD brains [91], suggesting that proteolytic cleavage is an abundant PTM in these patients. The aggregated CTFs are usually highly phosphorylated and ubiquitinated [91]. Since the C-terminal LCD of TDP-43 is very aggregate-prone, CTFs readily form inclusions in cell or animal models, trap essential cellular factors [79,92], and are highly cytotoxic to cells [93,94]. How various other disease-associated modifications of TDP-43 affect the protein's behavior and thus might influence the process of neurodegeneration is discussed in the following sections.

TDP-43 PTMs as regulators of LLPS and aggregation

TDP-43 readily phase separates both *in vitro* and in cells and several studies have examined how PTMs influence its biophysical properties and LLPS behavior. A single phosphomimetic substitution (S48E) was shown to disrupt the functional dimerization mediated by the globular N-terminal domain and to disrupt LLPS of TDP-43 [95]. Expression of the S48E mutant in cells leads to decreased partitioning into cellular condensates, as well as decreased splicing activity. Under which conditions S48-phosphorylation occurs and whether it occurs in disease is, however, still unclear. Another recent study demonstrated that C-terminal phosphomimetic substitutions in full-length TDP-43 (mimicking hyperphosphorylation in ALS/FTD patients) increased its solubility *in vitro*, suppressed its tendency to phase separate and aggregate, and resulted in more mobile 'liquid-like' TDP-43, in comparison with wild type TDP-43, which forms immobile condensates [96]. In cells, C-terminal phosphomimetic substitutions significantly reduce TDP-43 SG recruitment and aggregation [96–98] and C-terminal phosphorylation precedes aggregation of TDP-43 CTFs [98,99]. Together, these studies suggest that C-terminal phosphorylation of TDP-43 could be a protective cellular mechanism to increase the solubility of TDP-43 and counteract its aggregation, at least in early stages of disease (Figure 3B). Contrasting this hypothesis, phosphorylation of TDP-43 has also been shown to trigger mislocalization, aggregation, and seeding in cells [100], and coexpression of TDP-43 with specific kinases was shown to drive TDP-43

toxicity [101–103] and increase the presence of high molecular weight oligomeric species [104]. In addition, a recent study showed that O-GlcNAcylation of TDP-43 represses its hyperphosphorylation, increases its solubility in cultured cells, and could additionally promote the mRNA splicing activity of TDP-43 [105]. More research is thus needed to determine exactly when in disease progression TDP-43 phosphorylation occurs and how it is linked to pathology.

Aberrant redox signaling through the accumulation of reactive oxygen and nitrogen species can also influence TDP-43 aggregation (Figure 3B). Cellular oxidative stress causes cysteine oxidation within the RRM domains of TDP-43, resulting in the formation of disulfide bridges [75]. Disulfide bridge formation leads to impaired RNA binding and the formation of dithiothreitol (DTT)-sensitive high molecular weight species, which may exacerbate TDP-43 aggregation and loss-of-function phenotypes. DTT-sensitive aggregates have been shown to accumulate within FTD patient brains, alongside DTT-insoluble TDP-43 CTFs. Another recent study reported the presence of S-nitrosylation at cysteine residues in TDP-43 in FTD patient brains, which similarly leads to disulfide bridge formation and the accumulation of high molecular weight species [90]. S-nitrosylated TDP-43 forms in response to elevated nitric oxide (NO) levels, which subsequently leads to aggregation of TDP-43, recruitment to SGs, loss of TDP-43 regulatory activity, and neurotoxicity. Interestingly, aggregated TDP-43 was shown to further trigger reactive oxygen species formation and increased NO levels, leading to a positive feedback loop and promoting further TDP-43 aggregation [90].

TDP-43 PTMs as regulators of protein and RNA interactions and TDP-43 localization

A disease-linked PTM that affects RNA-binding capacity and localization of TDP-43 is lysine acetylation. Acetylation of TDP-43 at K145 increases under oxidative stress conditions and has been identified as a disease-associated modification in ALS patient spinal cords [88,106] (Figure 3B). Interestingly, acetylation within the RRM domains of TDP-43 (on K136, K145, and K192) decrease RNA binding and disrupt regulation of TDP-43 RNA targets [88,107]. The loss of RNA interactions can trigger TDP-43 phase separation in cells and lead to increased aggregation [108,109]. Moreover, lysine acetylation leads to an increase in phosphorylated and ubiquitinated TDP-43 aggregates [106,107], suggesting that these other PTMs might arise as a consequence of TDP-43 acetylation and insolubility, possibly in an attempt to enhance TDP-43 solubility and degradation. Although it is yet to be demonstrated, one could speculate that other PTMs within the RRM domains of TDP-43 could have similar effects on RNA binding and aggregation. Acetylation of K84, located within the NLS of TDP-43, was shown to reduce nuclear import and increase cytoplasmic mislocalization [107], however, it remains to be seen whether this modification arises in disease.

TDP-43 PTMs as regulators of protein quality control

The presence of ubiquitinated TDP-43 in pathological aggregates suggests that the protein quality control machinery may be playing a role in disease (Box 2). Several studies have shown a role for autophagy and the proteasome in clearing TDP-43 and inhibition of either can increase TDP-43 aggregation [110,111]. It can be speculated that some of the various PTMs that are added to TDP-43 during disease influence its polyubiquitination and thus trigger its degradation by the proteasome or autophagy, although this remains to be demonstrated. The addition of polyubiquitin chains may also directly contribute to the aggregation of TDP-43, as polyubiquitin chains have been shown to promote protein aggregation [112]. One could also speculate that, as shown for FUS [58], the increased concentration of ubiquitin in TDP-43 aggregates could deplete cellular ubiquitin levels and lead to improper control of other ubiquitin-dependent pathways. Roles for ubiquitination independent of protein quality control may also be at play. Ubiquitination is an important signal for the DNA damage response, endocytosis, and inflammatory signaling, all of

which have intersecting roles with neurodegeneration [113]. Misregulation of ubiquitin-dependent endocytosis may be particularly detrimental to neurons, as it plays an important role in synaptic plasticity and maintenance [114].

Role of PTMs in regulating other disease-associated RBPs

There is evidence that PTMs also play an important role in regulating other RBPs linked to neurodegenerative diseases. Two examples are the **heterogeneous nuclear ribonucleoproteins (hnRNPs)** hnRNPA1 and hnRNPA2, which are both genetically linked to ALS and multisystem proteinopathy [115,116]. hnRNPA1 was also shown to be partially mislocalized from the nucleus to the cytoplasm in the cortex of FTD-FUS patients [117] as well as in multiple sclerosis patients [118]. Several studies have shown that PTMs can impact the biophysical properties, localization, and function of the two hnRNPs. In cells, tyrosine phosphorylation within the LCD of hnRNPA2 leads to its dissociation from transport granules and also decreases its phase separation propensity [119]. Arginine methylation of the hnRNPA2 LCD also reduces its phase separation *in vitro* [120]. hnRNPA1 phosphorylation occurs upon osmotic stress, resulting in decreased binding to TNPO1 and subsequent relocalization of hnRNPA1 to the cytoplasm [121,122]. Interestingly, O-GlcNAcylation of hnRNPA1 has the opposite effect and increases TNPO1 binding [122]. Further investigation into the PTM status of hnRNPA1 and hnRNPA2 in patients may provide further insight into the role of PTMs in the disease process.

FUS belongs to the **FET protein family**, which includes two other closely related proteins, Ewing's sarcoma (EWS) and TATA Box-binding protein-associated factor 15 (TAF15). Like FUS, EWS and TAF15 are normally imported into the nucleus through TNPO1, but become cytoplasmically mislocalized and aggregated in the cortex of FTD-FUS patients [38,123], possibly promoted by a TNPO1 dysfunction that appears to exist in the affected brain region of these patients [36–38]. This effect is somewhat specific to the FET proteins, as other TNPO1 cargos are not disrupted in FTD-FUS [39]. However, some additional hnRNPs, such as hnRNP-Q and R, have also been shown to be mislocalized and aggregated in these patients [117,124], suggesting a broader misregulation of RBPs in this disease. While the cause of this selective mislocalization of certain RBPs is not yet known, it is worth noting that both hnRNP-Q/R and the FET proteins contain extended RGG/RG motifs and are highly methylated [125]. One could speculate that changes in methylation activity in cells could lead to hypomethylation of the affected RGG/RG-containing proteins, which may drive their pathological phase separation and aggregation, although this is yet to be determined. Finally, O-GlcNAcylation was recently shown to reduce phase separation and aggregation of EWS *in vitro* and in cells [126]. This PTM seems to be specific to EWS, as it is not shared by the other FET family members [127]. Interestingly, FUS and TAF15 are consistently found to be aggregated in FTD patients, but EWS is found more variably, suggesting that EWS aggregation is somehow distinct from FUS and TAF15 [38,123], possibly due to its distinct PTM pattern.

Concluding remarks

Different mechanisms regarding how PTMs can influence protein function within the scope of normal cellular physiology as well as pathology are becoming increasingly clear. These include effects on the biophysical properties, macromolecular interactions, localization, and stability of the modified protein (Figure 4, Key figure) and all of these mechanisms could play an important role in RBP-linked neurodegenerative diseases, as discussed earlier. In many cases, the cellular conditions in which specific PTMs are added to or removed from a protein are not well understood (see Outstanding questions). In the case of FUS RGG/RG methylation, evidence suggests that asymmetric dimethylation is common under normal conditions, but through unknown mechanisms this PTM is missing in the disease state [39,40]. Other modifications, such as C-terminal

Outstanding questions

At what point in the progression of neurodegenerative disease are different disease-linked PTMs introduced or removed? Which factors or signals trigger addition or removal of disease-linked PTMs?

Specifically, when and how is FUS arginine methylation lost in FTD patients; are defects in protein arginine methylation at play, or are arginine demethylases involved?

Specifically, when and by which kinase is TDP-43 hyperphosphorylated in ALS/FTD patients? Can TDP-43 aggregates be hyperphosphorylated and does this lead to dissolution of the aggregates? Does TDP-43 phosphorylation trigger further changes to the PTM pattern (e.g., enhanced ubiquitination and degradation of TDP-43)?

How does (poly)-ubiquitination of disease-linked RBPs affect the phase separation and aggregation behavior? Does it alter RNP granule dynamics, as recently reported for polyubiquitinated G3BP1 [136]?

How do disease-associated mutations in RBPs alter the PTM landscape? Do some of them create novel PTM sites, or alter the interaction with PTM-modifying enzymes?

Which other PTM changes on RBPs, besides the known ones, occur in neurodegenerative diseases? For instance, do PARylation, GlcNAcylation, or SUMOylation occur and play a role in the disease course? Do aberrant PTMs play a role in other neurological diseases (e.g., diseases linked to FMRP dysregulation)?

What combinatorial effects exist between different PTMs on the same protein?

How do PTMs regulate the normal physiological functions and lifecycle of disease-linked RBPs? What cellular pathways are involved in sensing and responding to PTMs on RBPs? Do changes in the PTM landscape of RBPs correlate with broader changes in the proteome or RBP interactome?

Key figure

How post-translational modifications (PTMs) can regulate RNA-binding protein (RBP) performance in cells

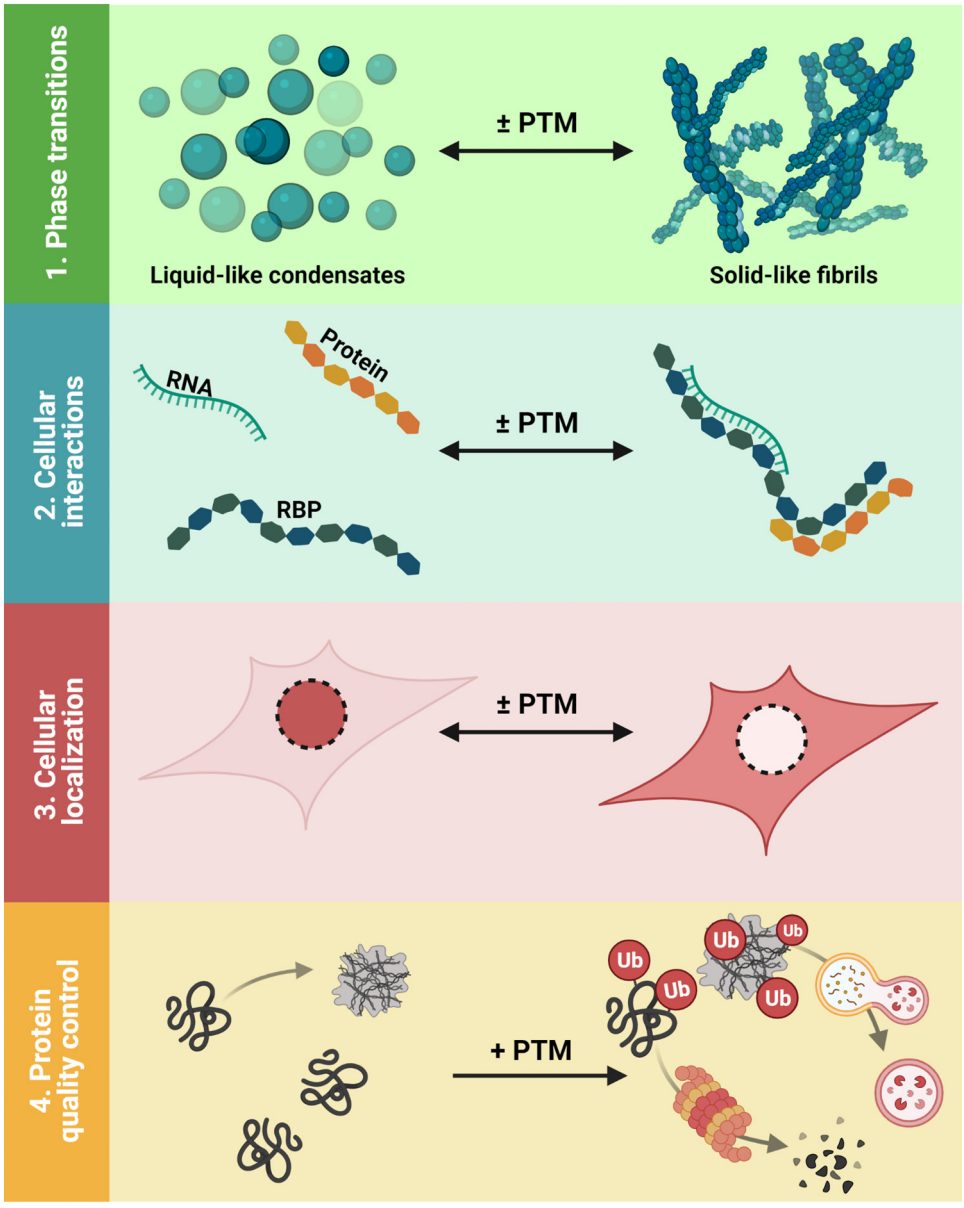

Figure 4. (1) PTMs can influence multivalent interactions of phase separating RBPs, either with themselves or with other cellular molecules, and thus can alter the RBP phase separation behavior or alter the material properties of RBP-containing condensates. (2) PTMs can regulate RBP–protein or RBP–RNA interactions. Altered RBP interactions can in turn affect its phase separation behavior (1) or subcellular localization (3). (3) PTMs can alter the nucleocytoplasmic localization of RBPs, either through changes to the nuclear import/export rate or through

(Figure legend continued at the bottom of the next page.)

TDP-43 hyperphosphorylation, are only present in the disease state. However, it is still unclear at what stage of disease and in response to which signal these modifications are altered. It also remains to be determined whether the activity of the PTM-modifying enzymes themselves is altered in disease.

Moreover, the influence of these PTMs on disease progression is still unclear and we can only speculate on their impact based on mechanistic studies in simple *in vitro* or cellular models. Based on such studies, it appears that some of the PTMs observed in the end stage of disease (i.e., in patients' postmortem brains) could be protective modifications that arise in order to counteract a cellular problem (e.g., protein aggregation or mislocalization) and thus act as 'brakes' in the disease process. Over time this fix may no longer be sufficient or could lead to detrimental secondary effects. Other PTMs observed specifically in postmortem brains appear to accelerate disease progression and thus may be 'drivers' of pathology, for instance, by promoting aberrant phase separation and aggregation, altering protein or RNA interactions, causing mislocalization, or impairing protein degradation. Disease-associated mutations in RBPs could contribute to changes in the PTM landscape, either directly through altering a modified amino acid residue or indirectly through altering molecular interactions, such as with PTM-modifying enzymes.

The PTMs on disease-linked RBPs discussed here are by no means exhaustive. PTMs not discussed in detail here (e.g., NEDDylation and SUMOylation) are emerging as significant regulators of RBP dynamics and SG assembly/disassembly [128–130], and ubiquitination has recently been shown to be a major stress-specific regulator of SG disassembly [131]. Tissue-specific patterns of PTMs may explain why an RBP becomes pathological in some tissues but not in others, despite equal expression. Changes to PTMs can also occur during aging, for instance, arginine methylation was found to decline in the ageing mouse brain [132], and reduced protein methylation has been associated with cellular senescence and premature ageing [133]. As proteomics becomes more sensitive and multiplexable, it should become possible to determine the full extent of PTMs in the proteome and in which tissues and under which physiological or pathological conditions they are present. It also remains to be determined how combinatorial effects of PTMs within one protein will impact its function. To this end, semi-synthetic strategies, as recently employed for Tau [134], could become important tools, as they allow for the introduction of multiple different site-specific modifications within certain protein domains. With a more complete picture of the PTMs regulating RBPs, as well as the requirements for their specificity, it may be possible to alter the PTM landscape through targeted drug therapies against specific PTMs or the modifying enzymes themselves. These could act by reversing pathological PTMs that drive disease, or by introducing protective PTMs that put brakes on disease progression.

Beyond the RBPs discussed here, many other RBPs have been linked to human diseases, including cancer and neurological disorders [3,135], and misregulation of their PTMs may play a role in these diseases. One example could be Fragile X Mental Retardation Protein (FMRP), an RBP implicated in autism spectrum disorders, mood disorders, and schizophrenia [136]. Recent studies have shown that PTMs, including arginine methylation and phosphorylation, are important regulators of FMRP phase-separation and RNA processing functions [137,138]; hence, it seems possible that these PTMs play a role in FMRP dysregulation in disease. Beyond disease,

altered interactions with nuclear versus cytoplasmic molecules. (4) Proteasomal or autophagic degradation of soluble or aggregated RBPs, respectively, can be promoted by the presence of PTMs, for example, phosphorylation that subsequently triggers polyubiquitination and degradation by either the proteasome or the autophagy machinery [149].

PTMs are likely to be key regulators of physiological RBP functions. Building a catalog of RBP functions, as well as the PTMs that regulate them, will be an exciting future area of exploration for scientists to uncover.

Acknowledgments

This work was supported by the Peter and Traudl Engelhorn Foundation (Advancement of Life Sciences Postdoctoral fellowship to E.L.S.) and the German Research Foundation (DFG) through Emmy Noether project DO1804/1-2 (to D.D.), project DO1804/3-1 (to D.D.), project DO1804/4-1 within SPP2191 - ID 402723784 (to D.D.), the Munich Cluster for Systems Neurology (EXC2145 SyNergy – ID 390857198 to D.D.) and the Fritz Thyssen Foundation (Az. 10.19.1.001MN) (to D.D.). D.D. also acknowledges support by ReALity – Resilience, Adaptation and Longevity (Forschungsinitiative des Landes Rheinland-Pfalz) and the Gutenberg Forschungskolleg (GFK) of JGU Mainz. The authors would like to thank Dr Saskia Hutten for critical comments on the manuscript. All figures were created with BioRender.com.

Declaration of interests

No interests are declared.

References

1. Hentze, M.W. *et al.* (2018) A brave new world of RNA-binding proteins. *Nat. Rev. Mol. Cell Biol.* 19, 327–341
2. Müller-Mcnicoll, M. and Neugebauer, K.M. (2013) How cells get the message: dynamic assembly and function of mRNA–protein complexes. *Nat. Rev. Genet.* 14, 275–287
3. Gebauer, F. *et al.* (2021) RNA-binding proteins in human genetic disease. *Nat. Rev. Genet.* 22, 185–198
4. Nussbacher, J.K. *et al.* (2019) Disruption of RNA metabolism in neurological diseases and emerging therapeutic interventions. *Neuron* 102, 294–320
5. Ling, S.-C. *et al.* (2013) Converging mechanisms in ALS and FTD: disrupted RNA and protein homeostasis. *Neuron* 79, 416–438
6. Neumann, M. *et al.* (2006) Ubiquitinated TDP-43 in frontotemporal lobar degeneration and amyotrophic lateral sclerosis. *Science* 314, 130–133
7. Neumann, M. *et al.* (2009) A new subtype of frontotemporal lobar degeneration with FUS pathology. *Brain* 132, 2922–2931
8. Kwiatkowski, T.J. *et al.* (2009) Mutations in the FUS/TLS gene on chromosome 16 cause familial amyotrophic lateral sclerosis. *Science* 323, 1205–1208
9. Vance, C. *et al.* (2009) Mutations in FUS, an RNA processing protein, cause familial amyotrophic lateral sclerosis type 6. *Science* 323, 1208–1211
10. Ikenaka, K. *et al.* (2020) Characteristic features of FUS inclusions in spinal motor neurons of sporadic amyotrophic lateral sclerosis. *J. Neuropathol. Exp. Neurol.* 79, 370–377
11. Mackenzie, I.R. *et al.* (2010) TDP-43 and FUS in amyotrophic lateral sclerosis and frontotemporal dementia. *Lancet Neurol.* 9, 995–1007
12. Hutten, S. and Dormann, D. (2020) Nucleocytoplasmic transport defects in neurodegeneration - cause or consequence? *Semin. Cell Dev. Biol.* 99, 151–162
13. Dormann, D. and Haass, C. (2011) TDP-43 and FUS: a nuclear affair. *Trends Neurosci.* 34, 339–348
14. Nedelsky, N.B. and Taylor, J.P. (2019) Bridging biophysics and neurology: aberrant phase transitions in neurodegenerative disease. *Nat. Rev. Neurol.* 15, 272–286
15. Alberti, S. and Dormann, D. (2019) Liquid–liquid phase separation in disease. *Annu. Rev. Genet.* 53, 171–194
16. Bah, A. and Forman-Kay, J.D. (2016) Modulation of intrinsically disordered protein function by post-translational modifications. *J. Biol. Chem.* 291, 6696–6705
17. Hofweber, M. and Dormann, D. (2019) Friend or foe—post-translational modifications as regulators of phase separation and RNP granule dynamics. *J. Biol. Chem.* 294, 7137–7150
18. Schaffert, L.N. and Carter, W.G. (2020) Do post-translational modifications influence protein aggregation in neurodegenerative diseases: a systematic review. *Brain Sci.* 10, 232
19. Alquezar, C. *et al.* (2021) Tau post-translational modifications: dynamic transformers of Tau function, degradation, and aggregation. *Front. Neurol.* 11, 595532
20. Levine, P.M. *et al.* (2019) α-Synuclein O-GlcNAcylation alters aggregation and toxicity, revealing certain residues as potential inhibitors of Parkinson's disease. *Proc. Natl. Acad. Sci. U. S. A.* 116, 1511–1519
21. Haj-Yahya, M. *et al.* (2020) Site-specific hyperphosphorylation inhibits, rather than promotes, Tau fibrillization, seeding capacity, and its microtubule binding. *Angew. Chem. Int. Ed.* 59, 4059–4067
22. Yuzwa, S.A. *et al.* (2014) O-GlcNAc modification of tau directly inhibits its aggregation without perturbing the conformational properties of tau monomers. *J. Mol. Biol.* 426, 1736–1752
23. Ratti, A. and Buratti, E. (2016) Physiological functions and pathobiology of TDP-43 and FUS/TLS proteins. *J. Neurochem.* 138, 95–111
24. Hill, S.J. *et al.* (2016) Two familial ALS proteins function in prevention/repair of transcription-associated DNA damage. *Proc. Natl. Acad. Sci. U. S. A.* 113, E7701–E7709
25. Dormann, D. *et al.* (2010) ALS-associated Fused in sarcoma (FUS) mutations disrupt Transportin-mediated nuclear import. *EMBO J.* 29, 2841–2857
26. Kino, Y. *et al.* (2011) Intracellular localization and splicing regulation of FUS/TLS are variably affected by amyotrophic lateral sclerosis-linked mutations. *Nucleic Acids Res.* 39, 2781–2798
27. Bosco, D.A. *et al.* (2010) Mutant FUS proteins that cause amyotrophic lateral sclerosis incorporate into stress granules. *Hum. Mol. Genet.* 19, 4160–4175
28. Patel, A. *et al.* (2015) A liquid-to-solid phase transition of the ALS protein FUS accelerated by disease mutation. *Cell* 162, 1066–1077
29. Murray, D.T. *et al.* (2017) Structure of FUS protein fibrils and its relevance to self-assembly and phase separation of low-complexity domains. *Cell* 171, 615–627
30. Tsai, Y.-L. *et al.* (2020) ALS/FTD-associated protein FUS induces mitochondrial dysfunction by preferentially sequestering respiratory chain complex mRNAs. *Genes Dev.* 34, 785–805
31. Kamelgarn, M. *et al.* (2018) ALS mutations of FUS suppress protein translation and disrupt the regulation of nonsense-mediated decay. *Proc. Natl. Acad. Sci. U. S. A.* 115, E11904–E11913
32. López-Erauskin, J. *et al.* (2018) ALS/FTD-linked mutation in FUS suppresses intra-axonal protein synthesis and drives disease without nuclear loss-of-function of FUS. *Neuron* 100, 816–830
33. Birsa, N. *et al.* (2021) FUS-ALS mutants alter FMRP phase separation equilibrium and impair protein translation. *Sci. Adv.* 7, eabf8660
34. Sama, R.R.K. *et al.* (2013) FUS/TLS assembles into stress granules and is a prosurvival factor during hyperosmolar stress. *J. Cell. Physiol.* 228, 2222–2231
35. Hock, E.M. *et al.* (2018) Hypertonic stress causes cytoplasmic translocation of neuronal, but not astrocytic, FUS due to impaired transportin function. *Cell Rep.* 24, 987–1000

36. Brelstaff, J. *et al.* (2011) Transportin1: a marker of FTLD-FUS. *Acta Neuropathol.* 122, 591–600
37. Neumann, M. *et al.* (2012) Transportin 1 accumulates specifically with FET proteins but no other transportin cargos in FTLD-FUS and is absent in FUS inclusions in ALS with FUS mutations. *Acta Neuropathol.* 124, 705–716
38. Davidson, Y.S. *et al.* (2013) Nuclear carrier and RNA-binding proteins in frontotemporal lobar degeneration associated with Fused in sarcoma (FUS) pathological changes. *Neuropathol. Appl. Neurobiol.* 39, 157–165
39. Dormann, D. *et al.* (2012) Arginine methylation next to the PY-NLS modulates Transportin binding and nuclear import of FUS. *EMBO J.* 31, 4258–4275
40. Suárez-Calvet, M. *et al.* (2016) Monomethylated and unmethylated FUS exhibit increased binding to Transportin and distinguish FTLD-FUS from ALS-FUS. *Acta Neuropathol.* 131, 587–604
41. Deng, Q. *et al.* (2014) FUS is phosphorylated by DNA-PK and accumulates in the cytoplasm after DNA damage. *J. Neurosci.* 34, 7802–7813
42. Rhoads, S.N. *et al.* (2018) The prionlike domain of FUS is multiphosphorylated following DNA damage without altering nuclear localization. *Mol. Biol. Cell* 29, 1786–1797
43. Qamar, S. *et al.* (2018) FUS phase separation is modulated by a molecular chaperone and methylation of arginine cation-π interactions. *Cell* 173, 720–734
44. Wang, J. *et al.* (2018) A molecular grammar governing the driving forces for phase separation of prion-like RNA binding proteins. *Cell* 174, 688–699
45. Bogaert, E. *et al.* (2018) Molecular dissection of FUS points at synergistic effect of low-complexity domains in toxicity. *Cell Rep.* 24, 529–537
46. Murthy, A.C. *et al.* (2019) Molecular interactions underlying liquid–liquid phase separation of the FUS low-complexity domain. *Nat. Struct. Mol. Biol.* 26, 637–648
47. Vernon, R.M. *et al.* (2018) Pi-Pi contacts are an overlooked protein feature relevant to phase separation. *eLife* 7, e31486
48. Monahan, Z. *et al.* (2017) Phosphorylation of the FUS low-complexity domain disrupts phase separation, aggregation, and toxicity. *EMBO J.* 36, 2951–2967
49. Hofweber, M. *et al.* (2018) Phase separation of FUS is suppressed by its nuclear import receptor and arginine methylation. *Cell* 173, 706–719
50. Yoshizawa, T. *et al.* (2018) Nuclear import receptor inhibits phase separation of FUS through binding to multiple sites. *Cell* 173, 693–705
51. Guo, L. *et al.* (2018) Nuclear-import receptors reverse aberrant phase transitions of RNA-binding proteins with prion-like domains. *Cell* 173, 677–692
52. Baade, I. *et al.* (2021) The RNA-binding protein FUS is chaperoned and imported into the nucleus by a network of import receptors. *J. Biol. Chem.* 296, 100659
53. Gonzalez, A. *et al.* (2021) Mechanism of karyopherin-β2 binding and nuclear import of ALS variants FUS(P525L) and FUS (R495X). *Sci. Rep.* 11, 3754
54. Darovic, S. *et al.* (2015) Phosphorylation of C-terminal tyrosine residue 526 in FUS impairs its nuclear import. *J. Cell Sci.* 128, 4151–4159
55. Mertins, P. *et al.* (2013) Integrated proteomic analysis of post-translational modifications by serial enrichment. *Nat. Methods* 10, 634–637
56. Akimov, V. *et al.* (2018) UbiSite approach for comprehensive mapping of lysine and N-terminal ubiquitination sites. *Nat. Struct. Mol. Biol.* 25, 631–640
57. Yasuda, S. *et al.* (2020) Stress- and ubiquitylation-dependent phase separation of the proteasome. *Nature* 578, 296–300
58. Farrawell, N.E. *et al.* (2020) Ubiquitin homeostasis is disrupted in TDP-43 and FUS cell models of ALS. *iScience* 23, 101700
59. Bock, A.S. *et al.* (2021) N-terminal acetylation modestly enhances phase separation and reduces aggregation of the low-complexity domain of RNA -binding protein FUS. *Protein Sci.* 30, 1337–1349
60. Perdikari, T.M. *et al.* (2020) A predictive coarse-grained model for position-specific effects of post-translational modifications on disordered protein phase separation. *Biophys. J.* 120, 1187–1197
61. Arenas, A. *et al.* (2020) Lysine acetylation regulates the RNA binding, subcellular localization and inclusion formation of FUS. *Hum. Mol. Genet.* 29, 2684–2697
62. Jungmichel, S. *et al.* (2013) Proteome-wide identification of poly(ADP-ribosyl)ation targets in different genotoxic stress responses. *Mol. Cell* 52, 272–285
63. Singatulina, A.S. *et al.* (2019) PARP-1 activation directs FUS to DNA damage sites to form PARG-reversible compartments enriched in damaged DNA. *Cell Rep.* 27, 1809–1821
64. Konopka, A. *et al.* (2020) Impaired NHEJ repair in amyotrophic lateral sclerosis is associated with TDP-43 mutations. *Mol. Neurodegener.* 15, 51
65. Mitra, J. *et al.* (2019) Motor neuron disease-associated loss of nuclear TDP-43 is linked to DNA double-strand break repair defects. *Proc. Natl. Acad. Sci. U. S. A.* 116, 4696–4705
66. Afroz, T. *et al.* (2017) Functional and dynamic polymerization of the ALS-linked protein TDP-43 antagonizes its pathologic aggregation. *Nat. Commun.* 8, 45
67. Jiang, L.-L. *et al.* (2017) The N-terminal dimerization is required for TDP-43 splicing activity. *Sci. Rep.* 7, 6196
68. Buratti, E. and Baralle, F.E. (2001) Characterization and functional implications of the RNA binding properties of nuclear factor TDP-43, a novel splicing regulator ofCFTR exon 9. *J. Biol. Chem.* 276, 36337–36343
69. Guenther, E.L. *et al.* (2018) Atomic structures of TDP-43 LCD segments and insights into reversible or pathogenic aggregation. *Nat. Struct. Mol. Biol.* 25, 463–471
70. Li, Q. *et al.* (2021) Cryo-EM structure of amyloid fibrils formed by the entire low complexity domain of TDP-43. *Nat. Commun.* 12, 1620
71. Babinchak, W.M. *et al.* (2019) The role of liquid–liquid phase separation in aggregation of the TDP-43 low-complexity domain. *J. Biol. Chem.* 294, 6306–6317
72. Conicella, A.E. *et al.* (2016) ALS mutations disrupt phase separation mediated by α-helical structure in the TDP-43 low-complexity C-terminal domain. *Structure* 24, 1537–1549
73. Buratti, E. (2015) Functional significance of TDP-43 mutations in disease. *Adv. Genet.* 91, 1–53
74. Dewey, C.M. *et al.* (2011) TDP-43 is directed to stress granules by sorbitol, a novel physiological osmotic and oxidative stressor. *Mol. Cell. Biol.* 31, 1098–1108
75. Cohen, T.J. *et al.* (2012) Redox signalling directly regulates TDP-43 via cysteine oxidation and disulphide cross-linking. *EMBO J.* 31, 1241–1252
76. Tziortzouda, P. *et al.* (2021) Triad of TDP43 control in neurodegeneration: autoregulation, localization and aggregation. *Nat. Rev. Neurosci.* 22, 197–208
77. Ling, J.P. *et al.* (2015) TDP-43 repression of nonconserved cryptic exons is compromised in ALS-FTD. *Science* 349, 650–655
78. Polymenidou, M. *et al.* (2011) Long pre-mRNA depletion and RNA missplicing contribute to neuronal vulnerability from loss of TDP-43. *Nat. Neurosci.* 14, 459–468
79. Chou, C.-C. *et al.* (2018) TDP-43 pathology disrupts nuclear pore complexes and nucleocytoplasmic transport in ALS/FTD. *Nat. Neurosci.* 21, 228–239
80. Feiler, M.S. *et al.* (2015) TDP-43 is intercellularly transmitted across axon terminals. *J. Cell Biol.* 211, 897–911
81. Laferrière, F. *et al.* (2019) TDP-43 extracted from frontotemporal lobar degeneration subject brains displays distinct aggregate assemblies and neurotoxic effects reflecting disease progression rates. *Nat. Neurosci.* 22, 65–77
82. Porta, S. *et al.* (2018) Patient-derived frontotemporal lobar degeneration brain extracts induce formation and spreading of TDP-43 pathology in vivo. *Nat. Commun.* 9, 4220
83. Jucker, M. and Walker, L.C. (2018) Propagation and spread of pathogenic protein assemblies in neurodegenerative diseases. *Nat. Neurosci.* 21, 1341–1349
84. Neumann, M. *et al.* (2009) Phosphorylation of S409/410 of TDP-43 is a consistent feature in all sporadic and familial forms of TDP-43 proteinopathies. *Acta Neuropathol.* 117, 137–149

85. Neumann, M. *et al.* (2007) TDP-43 in the ubiquitin pathology of frontotemporal dementia with VCP gene mutations. *J. Neuropathol. Exp. Neurol.* 66, 152–157
86. Hasegawa, M. *et al.* (2008) Phosphorylated TDP-43 in frontotemporal lobar degeneration and amyotrophic lateral sclerosis. *Ann. Neurol.* 64, 60–70
87. Arai, T. *et al.* (2006) TDP-43 is a component of ubiquitin-positive tau-negative inclusions in frontotemporal lobar degeneration and amyotrophic lateral sclerosis. *Biochem. Biophys. Res. Commun.* 351, 602–611
88. Cohen, T.J. *et al.* (2015) An acetylation switch controls TDP-43 function and aggregation propensity. *Nat. Commun.* 6, 5845
89. Buratti, E. (2018) TDP-43 post-translational modifications in health and disease. *Expert Opin. Ther. Targets* 22, 279–293
90. Pirie, E. *et al.* (2021) S-nitrosylated TDP-43 triggers aggregation, cell-to-cell spread, and neurotoxicity in hiPSCs and in vivo models of ALS/FTD. *Proc. Natl. Acad. Sci.* 118, e2021368118
91. Igaz, L.M. *et al.* (2008) Enrichment of C-terminal fragments in TAR DNA-binding protein-43 cytoplasmic inclusions in brain but not in spinal cord of frontotemporal lobar degeneration and amyotrophic lateral sclerosis. *Am. J. Pathol.* 173, 182–194
92. Riemenschneider, H. *et al.* (2021) Gel-like inclusions of C-terminal fragments of TDP-43 sequester and inhibit proteasomes in neurons. *bioRxiv* Published online March 16, 2021. https://doi.org/10.1101/2021.03.15.435268
93. Zhang, Y.J. *et al.* (2009) Aberrant cleavage of TDP-43 enhances aggregation and cellular toxicity. *Proc. Natl. Acad. Sci. U. S. A.* 106, 7607–7612
94. Yang, C. *et al.* (2010) The C-terminal TDP-43 fragments have a high aggregation propensity and harm neurons by a dominant-negative mechanism. *PLoS One* 5, e15878
95. Wang, A. *et al.* (2018) A single N-terminal phosphomimic disrupts TDP-43 polymerization, phase separation, and RNA splicing. *EMBO J.* 37, e97452
96. Gruijs da Silva, L.A. *et al.* (2021) Disease-linked TDP-43 hyperphosphorylation suppresses TDP-43 condensation and aggregation. *bioRxiv* Published online April 30, 2021. https://doi.org/10.1101/2021.04.30.442163, 2021.04.30.442163
97. Brady, O.A. *et al.* (2011) Regulation of TDP-43 aggregation by phosphorylation andp62/SQSTM1. *J. Neurochem.* 116, 248–259
98. Li, H.-Y. *et al.* (2011) Hyperphosphorylation as a defense mechanism to reduce TDP-43 aggregation. *PLoS One* 6, e23075
99. Dormann, D. *et al.* (2009) Proteolytic processing of TAR DNA binding protein-43 by caspases produces C-terminal fragments with disease defining properties independent of progranulin. *J. Neurochem.* 110, 1082–1094
100. Nonaka, T. *et al.* (2016) Phosphorylation of TAR DNA-binding protein of 43 kDa (TDP-43) by truncated casein kinase 1δ triggers mislocalization and accumulation of TDP-43. *J. Biol. Chem.* 291, 5473–5483
101. Liachko, N.F. *et al.* (2010) Phosphorylation promotes neurotoxicity in a *Caenorhabditis elegans* model of TDP-43 proteinopathy. *J. Neurosci.* 30, 16208–16219
102. Liachko, N.F. *et al.* (2014) The Tau tubulin kinases TTBK1/2 promote accumulation of pathological TDP-43. *PLoS Genet.* 10, e1004803
103. Liachko, N.F. *et al.* (2013) CDC7 inhibition blocks pathological TDP-43 phosphorylation and neurodegeneration. *Ann. Neurol.* 74, 39–52
104. Choksi, D.K. *et al.* (2014) TDP-43 phosphorylation by casein kinase Iε promotes oligomerization and enhances toxicity in vivo. *Hum. Mol. Genet.* 23, 1025–1035
105. Zhao, M.J. *et al.* (2021) O-GlcNAcylation of TDP-43 suppresses proteinopathies and promotes TDP-43's mRNA splicing activity. *EMBO Rep.* 22, e51649
106. Wang, P. *et al.* (2017) Acetylation-induced TDP-43 pathology is suppressed by an HSF1-dependent chaperone program. *Nat. Commun.* 8, 82
107. Morato, J.G. *et al.* (2020) Lysine acetylation of TDP-43 drives phase separation and pathological aggregation. *bioRxiv* Published online May 26, 2020. https://doi.org/10.1101/2020.05.26.104356
108. Mann, J.R. *et al.* (2019) RNA binding antagonizes neurotoxic phase transitions of TDP-43. *Neuron* 102, 321–338
109. Maharana, S. *et al.* (2018) RNA buffers the phase separation behavior of prion-like RNA binding proteins. *Science* 360, 918–921
110. Van Eersel, J. *et al.* (2011) Cytoplasmic accumulation and aggregation of TDP-43 upon proteasome inhibition in cultured neurons. *PLoS One* 6, e22850
111. Urushitani, M. *et al.* (2009) Synergistic effect between proteasome and autophagosome in the clearance of polyubiquitinated TDP-43. *J. Neurosci. Res.* 88, 784–797
112. Morimoto, D. *et al.* (2015) The unexpected role of polyubiquitin chains in the formation of fibrillar aggregates. *Nat. Commun.* 6, 6116
113. Schmidt, M.F. *et al.* (2021) Ubiquitin signalling in neurodegeneration: mechanisms and therapeutic opportunities. *Cell Death Differ.* 28, 570–590
114. Schreij, A.M.A. *et al.* (2016) Endocytic membrane trafficking and neurodegenerative disease. *Cell. Mol. Life Sci.* 73, 1529–1545
115. Kim, H.J. *et al.* (2013) Mutations in prion-like domains in hnRNPA2B1 and hnRNPA1 cause multisystem proteinopathy and ALS. *Nature* 495, 467–473
116. Le Ber, I. *et al.* (2014) hnRNPA2B1 and hnRNPA1 mutations are rare in patients with "multisystem proteinopathy" and frontotemporal lobar degeneration phenotypes. *Neurobiol. Aging* 35, 934
117. Gami-Patel, P. *et al.* (2016) The presence of heterogeneous nuclear ribonucleoproteins in frontotemporal lobar degeneration with FUS-positive inclusions. *Neurobiol. Aging* 46, 192–203
118. Salapa, H.E. *et al.* (2020) Neuronal RNA-binding protein dysfunction in multiple sclerosis cortex. *Ann. Clin. Transl. Neurol.* 7, 1214–1224
119. Ryan, V.H. *et al.* (2020) Tyrosine phosphorylation regulates hnRNPA2 granule protein partitioning and reduces neurodegeneration. *EMBO J.* 40, e105001
120. Ryan, V.H. *et al.* (2018) Mechanistic view of hnRNPA2 low-complexity domain structure, interactions, and phase separation altered by mutation and arginine methylation. *Mol. Cell* 69, 465–479
121. Allemand, E. *et al.* (2005) Regulation of heterogenous nuclear ribonucleoprotein A1 transport by phosphorylation in cells stressed by osmotic shock. *Proc. Natl. Acad. Sci.* 102, 3605–3610
122. Roth, S. and Khalaila, I. (2017) The effect of O -GlcNAcylation on hnRNP A1 translocation and interaction with transportin1. *Exp. Cell Res.* 350, 210–217
123. Neumann, M. *et al.* (2011) FET proteins TAF15 and EWS are selective markers that distinguish FTLD with FUS pathology from amyotrophic lateral sclerosis with FUS mutations. *Brain* 134, 2595–2609
124. Gittings, L.M. *et al.* (2019) Heterogeneous nuclear ribonucleoproteins R and Q accumulate in pathological inclusions in FTLD-FUS. *Acta Neuropathol. Commun.* 7, 18
125. Woodsmith, J. *et al.* (2018) Interaction modulation through arrays of clustered methyl-arginine protein modifications. *Life Sci. Alliance* 1, e201800178
126. Nosella, M.L. *et al.* (2021) O-GlcNAcylation reduces phase separation and aggregation of the EWS N-terminal low complexity region. *bioRxiv* Published online May 11, 2021. https://doi.org/10.1101/2021.05.11.443654
127. Kamemura, K. (2017) O-GlcNAc glycosylation stoichiometry of the FET protein family: only EWS is glycosylated with a high stoichiometry. *Biosci. Biotechnol. Biochem.* 81, 541–546
128. Marmor-Kollet, H. *et al.* (2020) Spatiotemporal proteomic analysis of stress granule disassembly using APEX reveals regulation by SUMOylation and links to ALS pathogenesis. *Mol. Cell* 80, 876–891
129. Keiten-Schmitz, J. *et al.* (2020) The nuclear SUMO-targeted ubiquitin quality control network regulates the dynamics of cytoplasmic stress granules. *Mol. Cell* 79, 54–67
130. Jayabalan, A.K. *et al.* (2016) NEDDylation promotes stress granule assembly. *Nat. Commun.* 7, 12125
131. Gwon, Y. *et al.* (2021) Ubiquitination of G3BP1 mediates stress granule disassembly in a stress-specific manner. *bioRxiv* https://doi.org/10.1101/2021.04.22.440930

132. Simandi, Z. *et al.* (2018) Arginine methyltransferase PRMT8 provides cellular stress tolerance in aging motoneurons. *J. Neurosci.* 38, 7683–7700
133. Blanc, R.S. and Richard, S. (2017) Arginine methylation: the coming of age. *Mol. Cell* 65, 8–24
134. Haj-Yahya, M. and Lashuel, H.A. (2018) Protein semisynthesis provides access to Tau disease-associated post-translational modifications (PTMs) and paves the way to deciphering the Tau PTM code in health and diseased states. *J. Am. Chem. Soc.* 140, 6611–6621
135. Lukong, K.E. *et al.* (2008) RNA-binding proteins in human genetic disease. *Trends Genet.* 24, 416–425
136. Fernández, E. *et al.* (2013) The FMRP regulon: from targets to disease convergence. *Front. Neurosci.* 7, 191
137. Kim, T.H. *et al.* (2019) Phospho-dependent phase separation of FMRP and CAPRIN1 recapitulates regulation of translation and deadenylation. *Science* 365, 825–829
138. Tsang, B. *et al.* (2019) Phosphoregulated FMRP phase separation models activity-dependent translation through bidirectional control of mRNA granule formation. *Proc. Natl. Acad. Sci.* 116, 4218–4227
139. Alberti, S. (2017) Phase separation in biology. *Curr. Biol.* 27, R1097–R1102
140. Thandapani, P. *et al.* (2013) Defining the RGG/RG motif. *Mol. Cell* 50, 613–623
141. Weishaupt, J.H. *et al.* (2016) Common molecular pathways in amyotrophic lateral sclerosis and frontotemporal dementia. *Trends Mol. Med.* 22, 769–783
142. Guerreiro, R. *et al.* (2015) SnapShot: genetics of ALS and FTD. *Cell* 160, 798
143. Deng, H.-X. *et al.* (2011) Mutations in UBQLN2 cause dominant X-linked juvenile and adult-onset ALS and ALS/dementia. *Nature* 477, 211–215
144. Williams, K.L. *et al.* (2012) UBQLN2/ubiquilin 2 mutation and pathology in familial amyotrophic lateral sclerosis. *Neurobiol. Aging* 33, 2527
145. Alexander, E.J. *et al.* (2018) Ubiquilin 2 modulates ALS/FTD-linked FUS–RNA complex dynamics and stress granule formation. *Proc. Natl. Acad. Sci.* 115, E11485–E11494
146. Mackenzie, I.R.A. and Neumann, M. (2016) Molecular neuropathology of frontotemporal dementia: insights into disease mechanisms from postmortem studies. *J. Neurochem.* 138, 54–70
147. Shang, Y. and Huang, E.J. (2016) Mechanisms of FUS mutations in familial amyotrophic lateral sclerosis. *Brain Res.* 1647, 65–78
148. Igaz, L.M. *et al.* (2009) Expression of TDP-43 C-terminal fragments in vitro recapitulates pathological features of TDP-43 proteinopathies. *J. Biol. Chem.* 284, 8516–8524
149. Carpenter, K. *et al.* (2018) Phosphorylation-mediated clearance of amyloid-like assemblies in meiosis. *Dev. Cell* 45, 392–405

6 Discussion

Remarkably, the collected data suggests that C-terminal TDP-43 hyperphosphorylation, as observed on pathological TDP-43 aggregates (Neumann *et al,* 2006; Neumann *et al,* 2009a; Hasegawa *et al,* 2008), reduces TDP-43 condensation and makes the protein more soluble and less aggregation prone *in vitro* (see Figure 17 for a graphical summary). Moreover, my results revealed that C-terminal TDP-43 phosphorylation diminishes or even eradicates the recruitment of TDP-43 into MLOs in cells (Figure 17), without affecting TDP-43 main functional properties. These results contradict the so far general belief that TDP-43 phosphorylation is pathological and triggers aggregation of TDP-43. However, our findings go in line with two previous reports where TDP-43 C-terminal fragments harboring phosphomimetic mutations were shown to reduce aggregation and cytotoxicity in cell and *Drosophila* models (Li *et al,* 2011; Brady *et al,* 2011).

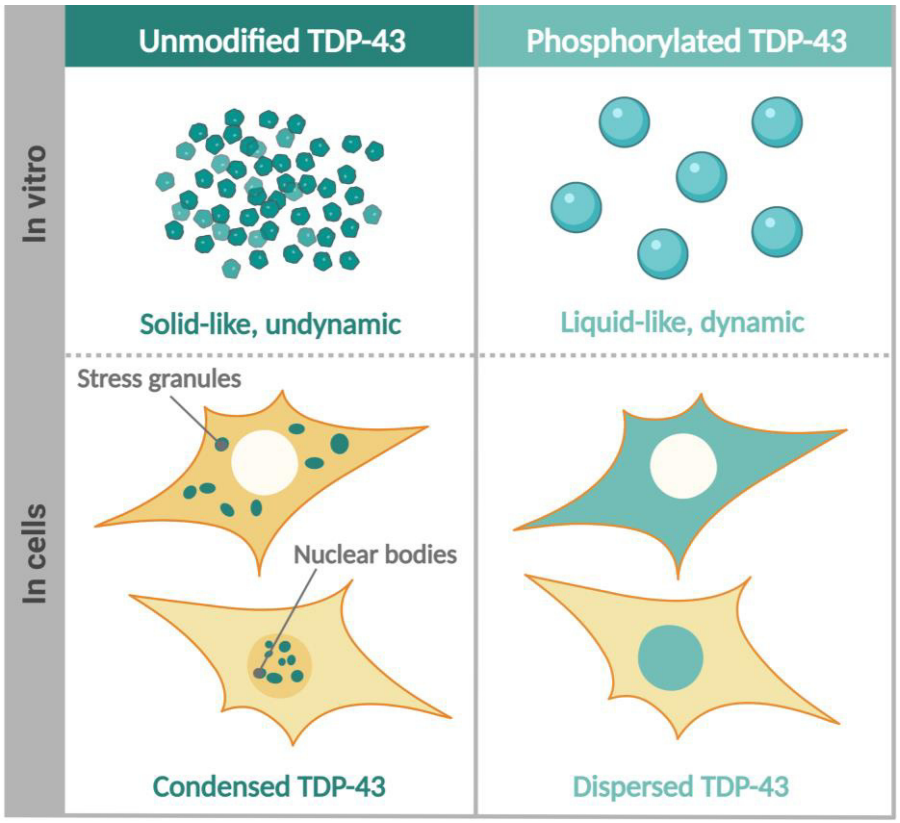

Figure 17. Impact of C-terminal TDP-43 hyperphosphorylation in vitro and in cells.
Recombinant purified unmodified TDP-43 *in vitro* undergoes phase separation and assembles into undynamic and solid-like condensates, while phosphorylated TDP-43 results in liquid and dynamic assemblies (Top panels). In stressed cells, unmodified TDP-43 is prominently recruited into cytoplasmic or nuclear stress-induced MLOs (e.g., stress granules and stress induced-nuclear bodies), but phosphomimetic TDP-43 remains dispersed (bottom panels).

6.1 The impact of phosphorylation in phase separating proteins and the use of phosphomimetic mutations to mimic phosphorylation

Previous studies of RBP phase separation have shown that certain residues are crucial for driving phase separation (e.g., aromatic and charged residues) and regulating material properties (e.g., polar residues G, S, N, Q) of condensates (Wang *et al,* 2018b). Remarkably many of these residues are frequent targets of PTMs (e.g., phospho-groups on Ser or Tyr or methyl-groups on Arg), hence these PTMs are likely crucial modulators of RBPs phase separation (Hofweber & Dormann, 2019; Sternburg *et al,* 2022). Indeed, some studies have demonstrated that phosphorylation plays an important role in controlling the phase separation behavior of several RBPs *in vitro, either positively or negatively,* and can regulate cellular RNP granules. For instance, phosphorylation by DNA-PK or phosphomimetic mutations across the LCD of FUS have been shown to reduce phase separation of full-length FUS and inhibit its subsequential fibril and aggregate formation *in vitro*. In line with these findings, overexpression of phosphomimetic FUS was shown to be less aggregation-prone in mammalian cells and a yeast model (Monahan *et al,* 2017). Tyrosine phosphorylation within the LCD of hnRNPA2 was also shown to reduce its propensity to phase separate and decrease its recruitment into transport granules in cells (Ryan *et al,* 2021). On the other hand, phosphorylation of Fragile X Mental Retardation Protein (FMRP) LCD has been shown to increase its tendency to phase separate, boosting *in vitro* granule assembly (Tsang *et al,* 2019). Similarly, phosphorylation of serines in the microtubule binding domain of Tau by MARK2 kinase promotes Tau LLPS, indicating that increased multivalent electrostatic interactions, by additional negative charges, drive Tau phase separation (Ambadipudi *et al,* 2017; Wegmann *et al,* 2018). In line with these studies, we have discovered that introduction of negative charges in the LCD of TDP-43 by both *in vitro* phosphorylation and phosphomimetic mutations modulates TDP-43 LLPS by reducing TDP-43 condensation and increasing TDP-43 solubility (Publication II). Such findings were possible by prior successful establishment of an *in vitro* method allowing the analysis of TDP-43 (or other RBP) phase separation based on the solubility of the protein in the presence or absence of a PTM or PTM mimic (Publication I).

In order to study defined disease-linked phosphorylation sites, we made use of phosphomimetic mutations (S-to-D), which has occasionally been shown to be a limiting factor, since these mutations do not always recapitulate the impact of phosphorylation on protein-protein interactions (Durocher *et al,* 1999; Yaffe *et al,* 1997). Nevertheless, our findings reveal that *in vitro* purified protein harboring 12 phosphomimetic S to D mutations (12D) has a similar condensation behavior and recruitment to SGs as CK1δ phosphorylated TDP-43 (Publication II). Additionally, it is important to underscore that phosphomimetic residues (Asp and Glu) underestimate the net charge (net charge of aspartate = −1 instead of −2 for a phospho-group) and do not always accurately mimic the chemistry of a phospho group. This net charge difference had indeed an impact on our simulation experiments, where we could appreciate that the higher negative net charge of 12x phosphorylated TDP-43 LCD has a stronger effect on phase separation disruption than the 12D phosphomimetic variant (Publication II).

6.2 Possible mechanisms by which phosphorylation and phosphomimetic mutations reduce TDP-43 phase separation

Our findings clearly show that C-terminal phosphorylation reduces the tendency of TDP-43 to phase separate and make TDP-43 more dynamic and liquid-like, and we obtained first basic insights into the underlying mechanisms. Based on our findings, it can be speculated that the introduction of multiple phosphorylation sites, and respective negative charges, can have a critical impact on TDP-43 LLPS though bulk electrostatics, as it has been described for other proteins (Serber & Ferrell, 2007; Strickfaden *et al,* 2007). From this idea arises the hypothesis that the number of introduced phosphorylation sites, but not the exact position of the negative charges, may be the critical factor behind the observed changes in TDP-43 phase separation. In fact, our results show that TDP-43 phase separation diminishes with increasing number of negative charge by phosphomimetic residues (2D> 5D> 12D) or phospho groups (5pS > 12pS) (Publication II). We have not addressed the possibility that the location of such negative charges is irrelevant for the observed effects. This could be tested, e.g. by performing *in vitro* phase separation assays using TDP-43 variants with the same negative charge content but distributed differently throughout the LCD of the protein. Further supporting this hypothesis two recent studies have shown that the net charge in low complexity IDRs can determine the phase separation behavior of RBPs. For instance, hnRNP A1 and DdX4 phase separation was shown to get destabilized as the net charge per residue increases either in the positive or negative direction, possibly through repulsive electrostatic long-range interactions (Bremer *et al,* 2021; Crabtree *et al,* 2020). When analyzing the global TDP-43 net charge at physiological conditions, we can appreciate that the Wt protein has a relatively neutral (-4.1) net charge in comparison to the phosphomimetic 12D variant (-16.1) and 12x phosphorylated TDP-43 (-28.1). Thus, it seems possible that the strong increase in negative charge by phosphorylation/phosphomimetic mutations is responsible for the diminished tendency of TDP-43 to self-assemble and form condensates.

Several structural types of assembly have been proposed for TDP-43, yet not all modes of interactions seem to be directly and equally affected by phosphorylation/phosphomimetic mutations. For instance, disruption of LLPS by direct interference with intermolecular interactions of transient α-helical structures (Conicella *et al,* 2016; Conicella *et al,* 2020) is likely not applicable, since none of the phosphomimetic mutations in our experiments fall within this conserved region (aa. 321-340) (Publication II). Nevertheless, to exclude an effect on α-helix formation, one would need to perform structural analysis (e.g., NMR) to address whether the transient α-helix arrangement is indeed not affected by the phosphorylation sites/ phosphomimetic mutations.

The importance of aromatic sticker-sticker interactions in the LCD has also been highlighted as a driving force for TPD-43 phase separation (Li *et al,* 2018b; Schmidt *et al,* 2019) and supported by our simulation experiments for the TDP-43 Wt LCD (Publication II). Also here, C-terminal phosphomimetic mutations appear to not extensively interfere with aromatic interactions at the molecular scale, as observed in the contact maps extracted from the simulations. On the other hand, interactions between S residues, possibly by dipole-dipole interactions,

were far more affected, with a substantial decrease in the number of local contacts in the phosphomimetic 12D mutant in comparison to TDP-43 Wt (Publication II). These results suggest that along with aromatic π-π interactions, other dipole mediated interactions might play along in modulating TDP-43 condensation. Interestingly, a study by Wang and coworkers has shown that modulation of polar residues in phase separating RBPs only has a minor effect on the driving forces for phase separation, but instead change the material properties of the phase separating condensates (Wang *et al,* 2018b). These findings suggest that perhaps TDP-43 phase separation is driven by stronger interactions (e.g., π-π interactions), but short range, weak dipole interactions can contribute to the stabilization of the dense phase. In line with this idea, when we substituted S for A, the material properties of TDP-43 condensates appeared to change into an amorphous and aggregate-like morphology (Publication II). Demonstrating that the conserved LCD pattern of flexible hydrophilic sections rich in polar sequences, interrupted by hydrophobic sections, seems to be critical for preserving TDP-43 condensate properties and provide a barrier to solidification and ultimately aggregation, as noted by (Schmidt *et al,* 2019).

6.3 Timing of TDP-43 phosphorylation

It still remains to be determined when (under which conditions) and where (subcellular localization) phosphorylation of TDP-43 occurs in cells and which species of TDP-43 (soluble, phase separated, aggregated) gets phosphorylated. So far, C-terminal TDP-43 phosphorylation has only been found in the disease state, in which phospho-specific antibodies (specific to S379, S403/S404, S409/S410) detect TDP-43 inclusions in ALS/FTD patients, but not physiological nuclear TDP-43 or TDP-43 in control brains (Neumann *et al,* 2006; Hasegawa *et al,* 2008; Neumann *et al,* 2009a). This fact and our findings that phosphorylation is a strong regulator of TDP-43 phase separation and aggregation, raises the possibility of two related but not exclusive scenarios: (1) TDP-43 may be phosphorylated in physiological conditions, but escapes detection, and/or (2) phosphorylation happens primarily in the aggregate state.

Even though, C-terminal TDP-43 phosphorylation has so far exclusively been detected in the disease state, it is possible that it may also occur under physiological conditions e.g. to control TDP-43 phase transitions and avoid its solidification/aggregation or to regulate certain TDP-43 functions. However, detection of TDP-43 phosphorylation under these conditions might be difficult e.g. due to fast dephosphorylation by phosphatases and/or degradation of soluble, phosphorylated TDP-43. Interestingly, treatment with calyculin A phosphatase inhibitor has been shown to increase TDP-43 phosphorylation in HEK-293FT cells (Gu *et al,* 2018), supporting the idea that TDP-43 phosphorylation may, at least to some extent, also arise physiologically. To further test if TDP-43 phosphorylation escapes detection under normal conditions because of rapid dephosphorylation by phosphatases, neuronal cells could be treated with various phosphatase inhibitors (e.g. calyculin A, okadaic acid) and one could test whether C-terminal TDP-43 phosphorylation can be detected using phospho-specific antibodies. Additionally, TDP-43 phosphorylation could also escape detection under normal conditions because it is fast degraded. This could be directly tested by inhibiting the proteasomal degradation pathway, using specific inhibitors (e.g. MG132), or blocking the autophagy pathway, e.g.

using autophagy deficient cells, and then test whether C-terminal TDP-43 phosphorylation can be detected under this conditions.

A different scenario could be that TDP-43 phosphorylation occurs preferentially in the condensed/ aggregated form of TDP-43, through the recruitment of certain kinases into TDP-43 condensates/aggregates. This way, TDP-43 phosphorylation by such kinases could repress TDP-43 aberrant phase transitions or even disperse TDP-43 aggregates. In line with this idea, a couple of studies have reported that C-terminal TDP-43 phosphorylation arises after TDP-43 insolubility, implying that aggregation may precede TDP-43 phosphorylation (Dormann *et al,* 2009; Zhang *et al,* 2009; Brady *et al,* 2011; Zhang *et al,* 2019). Moreover, a recent cryo-EM structure based on TDP-43 aggregates isolated from ALS/FTD patients shows that the C-terminal region of the protein is not in the fibril core, and that the serines in the fibril core (282 – 360) are mostly buried with exception to S342 (Arseni *et al,* 2022). This TDP-43 fibril model suggests that phosphorylation of C-terminal serines outside of the core fibril, including the phospho-sites identified in pathological aggregates, are accessible, and therefore, can possibly be phosphorylated after fibrillization. On the other hand, another cryo-EM structural analysis of recombinant TDP-43 LCD fibrils has identified that most C-terminal serines are buried inside the fibril core structure (Li *et al,* 2021). If serines are buried, it is likely that they are not accessible for phosphorylation after fibril formation, suggesting that TDP-43 phosphorylation may probably arise before solid TDP-43 fibril formation.

This enigma of whether phosphorylation follows or precedes TDP-43 solidification could be directly tested using stable cell lines expressing solidification-prone vs. more liquid-like mutant versions of TDP-43 to analyze their degree of phosphorylation over time through staining/immunoblotting using phospho-specific TDP-43 antibodies. In parallel, the dynamics of TDP-43 condensates (assessment of liquid-to-solid phase transitions) in relation to the kinetics of TDP-43 phosphorylation could be examined at the different time points, using e.g. cellular sedimentation assays (as described in Publication I) and imaging techniques (fluorescence recovery after photobleaching, FRAP).

Based on the hypothesis that phosphorylation may occur after TDP-43 solidification and our findings that TDP-43 phosphorylation turns TDP-43 more dynamic and liquid-like, by reducing C-terminal LCD-LCD interactions, it can be speculated that TDP-43 phosphorylation could be a defensive cellular mechanism that arises in order to counteract aberrant LLPS by dissolution of subsequent TDP-43 aggregates.

In order to test this hypothesis, it would be important to understand whether (1) kinases can partition into pre-formed TDP-43 condensates and induce TDP-43 phosphorylation, and then test whether (2) phosphorylation can liquidify or even dissolve TDP-43 condensates.

The first hypothesis could be tested by co-expression of kinases known to phosphorylate TDP-43 (e.g. CK 1δ, 1ε and 2α, TTBK1, TTBK2 and CDC7) with solidification-prone TDP-43 variants (e.g. CTFs) and then analyze the co-localization of kinases with TDP-43 cellular condensates. Another complementary approach would be to test the same idea *in vitro* using pre-formed TDP-43 condensates/aggregates from purified protein (as described in Publication II) and then test kinase recruitment/partitioning by addition of purified kinases (e.g. CK1δ) into the solution.

Using the same experimental model, one could also address whether kinases can dissolve TDP-43 condensates. Here, TDP-43 phosphorylation can be monitored by addition/absence of ATP and TDP-43 condensate status (e.g. number and dynamic state) could be addressed by simple condensate imaging, turbidity assays or FRAP to measure condensate material properties.

6.4 Functional consequences of TDP-43 phosphorylation

Apart from reducing self-self interactions, TDP-43 phosphorylation could have several different functional outcomes, such as altered protein stability/degradation, protein-protein interactions, localization, RNA-binding and RNA processing functions.

One speculative mechanism could be that phosphorylation accelerates degradation of TDP-43 by the proteasome, as has been described for the amyloid-like translational repressor Rim4 in yeast cells (Carpenter *et al,* 2018). This mechanism has been shown to be essential for progression of yeast cells though meiosis, as translation repression by amyloid-like Rim4 structures in yeast embryos, during pre-meiotic G1 phase, needs to be released so that meiosis can progress (Berchowitz *et al,* 2015). This is accomplished by multi-site phosphorylation of the Rim4 LCD, triggering Rim4 aggregate disassembly and subsequent proteasomal degradation (Carpenter *et al,* 2018). Therefore, it is tempting to speculate that hyperphosphorylation could be a common mechanism to disaggregate amyloid-like protein inclusions, such as TDP-43 positive aggregates, for subsequent degradation.

How LLPS impacts the behavior of TDP-43 in cells e.g. its interactome, is so far not extensively explored. But differences in the interactome could depend on TDP-43 biophysical state, and therefore, reduced LLPS e.g. by phosphorylation could have a significant impact on TDP-43 interactions with other proteins or RNAs and consequently alter its localization and/or functions.

In the current work we show that C-terminal phosphorylation reduces TDP-43 self-self interaction, however we did not address how it affects global TDP-43 protein-protein interactions. This could be directly tested in cells through TDP-43 pulldown experiments followed by global proteomic analysis, comparing Wt vs phosphomimetic TDP-43 variants.

Strikingly, our findings indicate that cellular localization and import rate of TDP-43 are not affected by C-terminal hyperphosphorylation. Moreover, RNA-binding and RNA processing functions (regulation of splicing of certain mRNAs and TDP-43 autoregulation) were also not affected by TDP-43 phosphorylation. Nevertheless, given that our results were only focused on a few known TDP-43 RNA targets and certain mRNA processing functions, we cannot exclude that other TDP-43 targets and functions are not affected by this PTM. In fact, a recent study has reported that helix-mediated phase separation is required for efficient TDP-43 binding to a subset of RNAs containing long multivalent binding sites (Hallegger *et al,* 2021), giving rise to the hypothesis that reduced LLPS by C-terminal hyperphosphorylation could potentially also disturb TDP-43 binding to certain RNAs. Therefore, our analysis of RNA regulation could be expanded, e.g. by full transcriptomic analysis / CLIP studies.

RNA interactions dependent on TDP-43 LLPS through the conserved helical region, was shown to be required for efficient regulation of the bound transcripts, including 3'end processing/alternative polyadenylation and autoregulation of TDP-43 mRNA levels (Hallegger *et al,* 2021). A second study reported that deficient phase separation variants of TDP-43 are not entirely capable of recapitulating TDP-43 splicing functions in cells (Schmidt *et al,* 2019). Additionally, a knock-in mouse expressing endogenous murine LLPS-deficient TDP-43, through the deletion of the conserved helical region via CRISPR technology, has recently reported that TDP-43 LLPS ablation enhances global protein translation. The increase in protein synthesis was related to an enhanced association of TDP-43 to certain translational factors (Gao *et al,* 2021). These studies indicate that TDP-43 LLPS is essential for proper TDP-43 mRNA processing functions, suggesting that C-terminal hyperphosphorylation could indeed affect the regulation of TDP-43 certain mRNA targets, through altered 3'end processing/alternative polyadenylation, splicing and translation. To address this hypothesis additional research could be performed using cells comprising C-terminally phosphorylated TDP-43 in order to study its impact on additional splicing targets (e.g. pre-mRNAs containing cryptic exons to study the efficiency of TDP43-mediated exon skipping during alternative splicing), alternative polyadenylation of RNAs containing long multivalent regions and global translation.

6.5 Possible reasons for persistence of phosphorylated TDP-43 aggregates in ALS/FTD patients

A question that remains is why phosphorylated TDP-43 is still detected in pathological aggregates and TDP-43 aggregates in patients are not disassembled after phosphorylation. Multiple not exclusive mechanisms could explain such phenotype.

One hypothesis could be that during aging and especially in ALS/FTD (Hipp *et al,* 2019; Yerbury *et al,* 2020), clearance mechanisms may be impaired e.g. through the sequestration and inhibition of proteasomes by protein aggregates (Guo *et al,* 2018b; Riemenschneider *et al,* 2021), causing the accumulation of hyperphosphorylated, polyubiquitinated TDP-43 that then might aggregate due to elevated protein concentration.

Another possible scenario is that additional PTMs, such as ubiquitination, may prevent disassembly of C-terminal hyperphosphorylated TDP-43 from pathological aggregates by altering the phase separation behavior of the protein. In line with this hypothesis, addition of polyubiquitin chains was reported to enhance protein aggregation (Morimoto *et al,* 2015) and to regulate the phase separation of certain proteins meant to be degraded through the proteasome (Yasuda *et al,* 2020). Therefore, polyubiquitination of TDP-43, as observed in ALS/FTD-TDP-43 pathology (Neumann *et al,* 2006; Mackenzie & Neumann, 2016), may have detrimental side effects over TDP-43 phase separation, such as enhancing TDP-43 aggregation, which could overcome the possible attempt of phosphorylation to make TDP-43 more soluble and liquid-like.

Moreover, aberrant interactions of TDP-43 with other cellular molecules or organelles could ambush phosphorylated TDP-43 inside aggregates, as recently described for stalled proteasomes, and additional elements of the ubiquitin-proteasome system that are trapped by TDP-43 CTF inclusion (Riemenschneider *et al,* 2021).

Overall, the detection of C-terminal hyperphosphorylated TDP-43 in pathological aggregates could be explained by multiple mechanisms that may overcome the solubilizing effect of phosphorylation. Hence, future research is required to fully comprehend how TDP-43 hyperphosphorylation could be affected by such mechanisms (e.g. additional PTMs) under pathological conditions.

6.6 Contrasting observations upon kinase overexpression

Intriguingly, a considerable amount of literature has reported contrasting results to ours. Several studies found that TDP-43 phosphorylation by kinase overexpression (TTBK1/2, CK1ε, CK1δ, CDC7, CK2 and GSK-3β) is deleterious for cells because it induces TDP-43 aggregation and cytotoxicity (Liachko *et al,* 2013; Liachko *et al,* 2014; Choksi *et al,* 2014; Carlomagno *et al,* 2014; Nonaka *et al,* 2016; Taylor *et al,* 2018; Martínez-González *et al,* 2021). Thus, the use of kinase inhibitors (CDC7, CK1δ, GSK-3β and TTBK1 inhibitors) to block TDP-43 phosphorylation has been proposed as a potential therapeutic approach for ALS, as they showed cytoprotective effects, such as increased lifespan and reduced neuronal loss, in TDP-43 transgenic mouse, Drosophila and C. elegans models (Liachko *et al,* 2013; Salado *et al,* 2014; Martínez-González *et al,* 2020; Martínez-González *et al,* 2021; Nozal *et al,* 2022). One possible explanation for such paradoxical findings can be the possibility of pleiotropic effects by kinase overexpression, i.e., phosphorylation of many different substrates and thereby changes in many different signaling pathways, which may induce TDP-43 aggregation indirectly and not by direct TDP-43 phosphorylation. In the current study, we did not alter any kinase levels/ activity, instead we specifically changed or mimicked TDP-43 phosphorylation and studied its behavior in *in vitro* and cellular experiments, thereby preventing indirect effects by phosphorylation of other proteins. Our results indicate that the resulting beneficial impact of using kinase inhibitors in ALS / TDP-43 toxicity models might not be directly related to diminished TDP-43 phosphorylation, but may instead be caused by other cellular mechanisms.

6.7 Could TDP-43 phosphorylation have detrimental functions?

Our findings do not exclude the possibility that reduced TDP-43 assembly by phosphorylation could have deleterious consequences and disrupt key functions of TDP-43, which may depend on its ability to condensate or solidify, e.g., specific DNA/RNA processing mechanisms or recruitment of TDP-43 into protective nuclear or cytoplasmic MLOs. For instance, TDP-43 recruitment into NBs has been demonstrated to be protective against TDP-43-mediated cytotoxicity in cell and fly models upon cellular stress (Wang *et al,* 2020). Based on this finding, disruption of TDP-43 recruitment into such stress induced NBs by phosphomimetic mutations, as we observed (Publication II), could have a negative impact on nuclear TDP-43 physiological response to stress. Moreover, some recent studies have reported that recruitment of TDP-43

into SGs, which is also reduced by phosphomimetic mutations (Publication II), prevents TDP-43 aggregation (Mann *et al,* 2019; Gasset-Rosa *et al,* 2019). These reports contrast the current believe that pathological aggregation arises through a solidifications of SGs (Zhang *et al,* 2019; Nedelsky & Taylor, 2019), and propose a model in which aggregation arises outside of SGs and therefore recruitment of TDP-43 into these biomolecular condensates is protective against TDP-43 aggregation (Mann *et al,* 2019; Gasset-Rosa *et al,* 2019). Nevertheless, the impact of TDP-43 phosphorylation over the recruitment of TDP-43 into such protective MLOs may depend certainly on the timing, location and form of TDP-43 that is phosphorylated, which, as mentioned before, is still unknown. Further supporting the idea that phosphorylation may disrupt essential functions of TDP-43 and become pathological, a deep mutagenesis study has recently described that hydrophobic, aggregating TDP-43 variants strongly reduce toxicity while hydrophilic, liquid-like TDP-43 variants increase toxicity in yeast cells (Bolognesi *et al,* 2019), hence further research is essential to investigate this possible scenario. Nonetheless, the data collected in this thesis research indicates that nuclear import/nuclear localization, RNA-binding and some core RNA processing tasks of TDP-43 (e.g., regulation of splicing of certain mRNA targets and autoregulation) are not disturbed by C-terminal hyperphosphorylation in mammalian cells (Publication II), and therefore are not dependent on TDP-43 phase separation and solidification. However, another study has shown that deficient phase separating TDP-43 variants are not entirely capable to reproduce Wt TDP-43 splicing functions in cells (Schmidt *et al,* 2019). As mentioned before, TDP-43 LLPS was also shown to be essential for its binding to specific mRNAs and to efficiently regulate alternative polyadenylation of these targets (Hallegger *et al,* 2021). This suggests that TDP-43 phase separation behavior affects RNA-processing functions, at least of certain targets. Moreover, the recent knock-in murine TDP-43 LLPS deficient mouse model reported that deletion of the conserved helical region, required for TDP-43 phase separation, has a great impact on global translation. In addition, these LLPS-deficient TDP-43 mice reveal impaired neuronal functions and brain related behavioral abnormalities (Gao *et al,* 2021). This suggests that TDP-43 phase separation may be crucial for translational regulation of TDP-43, and that dysregulation of translation through reduced TDP-43 phase separation can have detrimental impact in neuronal functions. Hence, it would be interesting to evaluate if cells comprising C-terminally phosphorylated TDP-43 show a similar phenotype.

6.8 Other PTMs regulating phase separation behavior of TDP-43

Besides the 12 C-terminal sites studied in this research project (Publication II), additional TDP-43 C-terminal sites have also been identified to be phosphorylated in ALS/FTD patients (Kametani *et al,* 2016; Neumann *et al,* 2021) (Figure 9). Interestingly, some of them fall within the conserved α-helix region (aa. 321-340) of TDP-43, suggesting that phosphorylation of these sites could disrupt intermolecular interactions mediated by transient α-helical structures in the LCD and subsequently reduce TDP-43 LLPS.

In my thesis project (Publication II) as well as in a previous study (Kametani *et al,* 2009), mass spectrometry analysis of Casein kinase 1-mediated TDP-43 phosphorylation have identified phosphorylated sites in the NTD region of the protein. The impact of phosphorylation in such

NTD sites on TDP-43 LLPS remains to be uncovered. Curiously, it has been reported that a single phosphomimetic mutation in the NTD (S48E) strongly reduces TDP-43 LLPS (Wang *et al,* 2018a). Phosphorylation of this site has not been reported in disease, nevertheless this data demonstrates that regions outside the low complexity IDR can also regulate the phase separation of TDP-43 through PTMs, more specifically via phosphorylation in the globular NTD of TDP-43. Hence, it can be speculated that phosphorylation of additional putative phosphorylation sites in the NTD may as well modulate TDP-43 phase separation. Interestingly, some of these identified phospho sites in the N-terminal region lie within the bipartite NLS (82-98) of TDP-43, such as S91/S92 (Olsen *et al,* 2006; Kametani *et al,* 2009). Thus, phosphorylation of these sites might affect the binding of Importin α/β, by introducing negative charges and thereby impairing Importin α/β binding to the positively charged lysine/arginine residues in the NLS. It has been shown that importins directly affect phase separation of RBPs, including TDP-43, as they can suppress or even reverse RBP phase separation (Hofweber *et al,* 2018; Qamar *et al,* 2018; Yoshizawa *et al,* 2018; Guo *et al,* 2018a; Hutten *et al,* 2020). Therefore, it is possible that phospho sites in the NLS region impair binding of TDP-43 to Importin α/β and this way reduce chaperoning activity by importins and thus promote TDP-43 phase separation. Additionally, acetylation of lysine 82, which has been identified by mass spectrometry analysis of ALS post-mortem brain (Kametani *et al,* 2016), also lies within the bipartite NLS domain of TDP-43. This PTM might likewise affect the binding of Importin α/β, and this way alter TDP-43 LLPS.

A recent study has revealed that p38α MAPK-mediated phosphorylation, and consequent phosphorylation of S292, S409 and S410, reduces TDP-43 LLPS but promotes TDP-43 aggregation and subsequent TDP-43 proteinopathy (Aikio *et al,* 2021). Interestingly, the authors discovered that the residue R293, adjacent to S292, is methylated by protein arginine methyltransferase 1 (PRMT1) and that R293 methylation enhances TDP-43 LLPS but reduces TDP-43 aggregation. Moreover, methylation at R293 inhibited phosphorylation at S292 and *vice versa*, suggesting a crosstalk mechanism between PRMT1-catalyzed arginine methylation at R293 and p38α MAPK-mediated phosphorylation at the adjacent S292 residue, and their possible contribution to regulating TDP-43 LLPS and aggregation (Aikio *et al,* 2021). In addition, another recent study, has found that O-GlcNAcylation of TDP-43 inhibits its phosphorylation and increases TDP-43 solubility in cells (Zhao *et al,* 2021). These studies suggest that an intricate interplay between different PTMs can regulate TDP-43 LLPS and aggregation.

Additional disease-associated PTMs on TDP-43, such as oxidation, S-nitrosylation and ubiquitination, may also have an impact on TDP-43 LLPS behavior. In fact, oxidation of cysteine residues in the RRM domains of TDP-43 and consequent formation of disulfide bridges, after cellular oxidative stress, was shown to decrease RNA binding and induce the formation of dithiothreitol (DTT)-sensitive high molecular weight species (Cohen *et al,* 2012). Reduced RNA binding could decrease TDP-43 LLPS and aggravate its aggregation (Mann *et al,* 2019) and loss-of-function phenotypes. Moreover, ubiquitination/polyubiquitination of TDP-43, as observed in pathological aggregates (Neumann *et al,* 2006), may possibly modify the phase separation of TDP-43, the same way it has been reported to enhance protein aggregation

(Morimoto *et al,* 2015) or phase separation of proteins destined to be degraded via the proteasome (Yasuda *et al,* 2020).

6.9 Protein hyperphosphorylation in other neurodegenerative disorders

Aberrant hyperphosphorylation is not restricted to TDP-43 in TDP-43 proteinopathies, likewise abnormal phosphorylation of Tau is found in pathological aggregates in post-mortem brain samples in Tauopathies (Alquezar *et al,* 2020). Curiously, though Tau hyperphosphorylation is largely considered to induce both Tau dissociation from microtubules and its subsequent phase separation and aggregation (Augustinack *et al,* 2002; Liu *et al,* 2007; Ambadipudi *et al,* 2017; Wegmann *et al,* 2018), Haj-Yahya and colleagues have recently shown that site-specific phosphorylation in the domain responsible for Tau binding to microtubules prevents, instead of inducing Tau seeding and aggregation (Haj-Yahya *et al,* 2020). Our data clearly show that C-terminal TDP-43 hyperphosphorylation, as observed in ALS/ FTD aggregates, has a similar repressive impact on TDP-43 aggregation. Together, these findings suggest that aberrant PTMs that are observed on neuropathological aggregates are not always causing the formation of such inclusions, but may also rise as a cellular protective mechanism that aims to overrule protein aggregation.

V References

Afroz T, Hock E-M, Ernst P, Foglieni C, Jambeau M, Gilhespy LAB, Laferriere F, Maniecka Z, Plückthun A, Mittl P et al (2017)
Functional and dynamic polymerization of the ALS-linked protein TDP-43 antagonizes its pathologic aggregation.
Nat Commun 8: 45

Aikio M, Wobst HJ, Odeh HM, Lee BL, Class B, Ollerhead TA, Mack KL, Ford AF, Barbieri EM, Cupo RR et al (2021)
Opposing roles of p38α-mediated phosphorylation and arginine methylation in driving TDP-43 proteinopathy.
bioRxiv: 2021.08.04.455154

Alami NH, Smith RB, Carrasco MA, Williams LA, Winborn CS, Han SSW, Kiskinis E, Winborn B, Freibaum BD, Kanagaraj A et al (2014)
Axonal transport of TDP-43 mRNA granules is impaired by ALS-causing mutations.
Neuron 81: 536–543

Alberti S (2017)
Phase separation in biology.
Curr Biol 27: R1097-R1102

Alberti S, Gladfelter A, Mittag T (2019)
Considerations and Challenges in Studying Liquid-Liquid Phase Separation and Biomolecular Condensates.
Cell 176: 419–434

Alberti S, Halfmann R, King O, Kapila A, Lindquist S (2009)
A systematic survey identifies prions and illuminates sequence features of prionogenic proteins.
Cell 137: 146–158

Alberti S, Hyman AA (2016)
Are aberrant phase transitions a driver of cellular aging?
BioEssays 38: 959–968

Alberti S, Hyman AA (2021)
Biomolecular condensates at the nexus of cellular stress, protein aggregation disease and ageing.
Nat Rev Mol Cell Biol 22: 196–213

Alberti S, Mateju D, Mediani L, Carra S (2017)
Granulostasis: Protein Quality Control of RNP Granules.
Front. Mol. Neurosci. 10: 84

Alquezar C, Arya S, Kao AW (2020)
Tau Post-translational Modifications: Dynamic Transformers of Tau Function, Degradation, and Aggregation.
Frontiers in neurology 11: 595532

Al-Sarraj S, King A, Troakes C, Smith B, Maekawa S, Bodi I, Rogelj B, Al-Chalabi A, Hortobágyi T, Shaw CE (2011)
p62 positive, TDP-43 negative, neuronal cytoplasmic and intranuclear inclusions in the cerebellum and hippocampus define the pathology of C9orf72-linked FTLD and MND/ALS.
Acta Neuropathol 122: 691–702

Ambadipudi S, Biernat J, Riedel D, Mandelkow E, Zweckstetter M (2017)
Liquid-liquid phase separation of the microtubule-binding repeats of the Alzheimer-related protein Tau.
Nat Commun 8: 275

Anderson P, Kedersha N (2006)
RNA granules.
J Cell Biol 172: 803–808

Apicco DJ, Ash PEA, Maziuk B, LeBlang C, Medalla M, Al Abdullatif A, Ferragud A, Botelho E, Ballance HI, Dhawan U et al (2018)
Reducing the RNA binding protein TIA1 protects against tau-mediated neurodegeneration in vivo.
Nat Neurosci 21: 72–80

Arai T, Hasegawa M, Akiyama H, Ikeda K, Nonaka T, Mori H, Mann D, Tsuchiya K, Yoshida M, Hashizume Y et al (2006)
TDP-43 is a component of ubiquitin-positive tau-negative inclusions in frontotemporal lobar degeneration and amyotrophic lateral sclerosis.
Biochemical and biophysical research communications 351: 602–611

Arai T, Mackenzie IRA, Hasegawa M, Nonoka T, Niizato K, Tsuchiya K, Iritani S, Onaya M, Akiyama H (2009)
Phosphorylated TDP-43 in Alzheimer's disease and dementia with Lewy bodies.
Acta Neuropathol 117: 125–136

Arseni D, Hasegawa M, Murzin AG, Kametani F, Arai M, Yoshida M, Ryskeldi-Falcon B (2022)
Structure of pathological TDP-43 filaments from ALS with FTLD.
Nature 601: 139–143

Ash PEA, Bieniek KF, Gendron TF, Caulfield T, Lin W-L, DeJesus-Hernandez M, van Blitterswijk MM, Jansen-West K, Paul JW, Rademakers R et al (2013)
Unconventional translation of C9ORF72 GGGGCC expansion generates insoluble polypeptides specific to c9FTD/ALS.
Neuron 77: 639–646

Augustinack JC, Schneider A, Mandelkow E-M, Hyman BT (2002)
Specific tau phosphorylation sites correlate with severity of neuronal cytopathology in Alzheimer's disease.
Acta Neuropathol 103: 26–35

Ayala YM, Conti L de, Avendaño-Vázquez SE, Dhir A, Romano M, D'Ambrogio A, Tollervey J, Ule J, Baralle M, Buratti E et al (2011)
TDP-43 regulates its mRNA levels through a negative feedback loop.
The EMBO journal 30: 277–288

Ayala YM, Pantano S, D'Ambrogio A, Buratti E, Brindisi A, Marchetti C, Romano M, Baralle FE (2005)
Human, Drosophila, and C.elegans TDP43: nucleic acid binding properties and splicing regulatory function.
Journal of Molecular Biology 348: 575–588

Ayala YM, Zago P, D'Ambrogio A, Xu Y-F, Petrucelli L, Buratti E, Baralle FE (2008)
Structural determinants of the cellular localization and shuttling of TDP-43.
J Cell Sci 121: 3778–3785

Babinchak WM, Haider R, Dumm BK, Sarkar P, Surewicz K, Choi J-K, Surewicz WK (2019)
The role of liquid-liquid phase separation in aggregation of the TDP-43 low-complexity domain.
Journal of Biological Chemistry 294: 6306–6317

Bah A, Forman-Kay JD (2016)
Modulation of Intrinsically Disordered Protein Function by Post-translational Modifications.
Journal of Biological Chemistry 291: 6696–6705

Banani SF, Lee HO, Hyman AA, Rosen MK (2017)
Biomolecular condensates: organizers of cellular biochemistry.
Nat Rev Mol Cell Biol 18: 285–298

Baron DM, Kaushansky LJ, Ward CL, Sama RRK, Chian R-J, Boggio KJ, Quaresma AJC, Nickerson JA, Bosco DA (2013)
Amyotrophic lateral sclerosis-linked FUS/TLS alters stress granule assembly and dynamics.
Mol Neurodegeneration 8: 30

Bäumer D, Hilton D, Paine SML, Turner MR, Lowe J, Talbot K, Ansorge O (2010)
Juvenile ALS with basophilic inclusions is a FUS proteinopathy with FUS mutations.
Neurology 75: 611–618

Bentmann E, Haass C, Dormann D (2013)
Stress granules in neurodegeneration--lessons learnt from TAR DNA binding protein of 43 kDa and fused in sarcoma.
The FEBS journal 280: 4348–4370

Bentmann E, Neumann M, Tahirovic S, Rodde R, Dormann D, Haass C (2012)
Requirements for Stress Granule Recruitment of Fused in Sarcoma (FUS) and TAR DNA-binding Protein of 43 kDa (TDP-43).
Journal of Biological Chemistry 287: 23079–23094

Berchowitz LE, Kabachinski G, Walker MR, Carlile TM, Gilbert WV, Schwartz TU, Amon A (2015)
Regulated Formation of an Amyloid-like Translational Repressor Governs Gametogenesis.
Cell 163: 406–418

Boer EMJ de, Orie VK, Williams T, Baker MR, Oliveira HM de, Polvikoski T, Silsby M, Menon P, van den Bos M, Halliday GM et al (2020)
TDP-43 proteinopathies: a new wave of neurodegenerative diseases.
J Neurol Neurosurg Psychiatry

Boeynaems S, Bogaert E, Michiels E, Gijselinck I, Sieben A, Jovičić A, Baets G de, Scheveneels W, Steyaert J, Cuijt I et al (2016)
Drosophila screen connects nuclear transport genes to DPR pathology in c9ALS/FTD.
Sci Rep 6: 20877

Boke E, Ruer M, Wühr M, Coughlin M, Lemaitre R, Gygi SP, Alberti S, Drechsel D, Hyman AA, Mitchison TJ (2016)
Amyloid-like Self-Assembly of a Cellular Compartment.
Cell 166: 637–650

Bolognesi B, Faure AJ, Seuma M, Schmiedel JM, Tartaglia GG, Lehner B (2019)
The mutational landscape of a prion-like domain.
Nat Commun 10: 4162

Bowden HA, Dormann D (2016)
Altered mRNP granule dynamics in FTLD pathogenesis.
Journal of neurochemistry 138 Suppl 1: 112–133

Brady OA, Meng P, Zheng Y, Mao Y, Hu F (2011)
Regulation of TDP-43 aggregation by phosphorylation and p62/SQSTM1.
Journal of neurochemistry 116: 248–259

Brangwynne CP, Eckmann CR, Courson DS, Rybarska A, Hoege C, Gharakhani J, Jülicher F, Hyman AA (2009)
Germline P granules are liquid droplets that localize by controlled dissolution/condensation.
Science 324: 1729–1732

Brangwynne CP, Mitchison TJ, Hyman AA (2011)
Active liquid-like behavior of nucleoli determines their size and shape in Xenopus laevis oocytes.
PNAS 108: 4334–4339

Brangwynne CP, Tompa P, Pappu RV (2015)
Polymer physics of intracellular phase transitions.
Nat Rev Dis Primers 11: 899–904

Bremer A, Farag M, Borcherds WM, Peran I, Martin EW, Pappu RV, Mittag T (2021)
Deciphering how naturally occurring sequence features impact the phase behaviours of disordered prion-like domains.
Nat Chem 14: 196–207

Broe M, Hodges JR, Schofield E, Shepherd CE, Kril JJ, Halliday GM (2003)
Staging disease severity in pathologically confirmed cases of frontotemporal dementia.
Neurology 60: 1005–1011

Brown A-L, Wilkins OG, Keuss MJ, Hill SE, Zanovello M, Lee WC, Bampton A, Lee FCY, Masino L, Qi YA et al (2022)
TDP-43 loss and ALS-risk SNPs drive mis-splicing and depletion of UNC13A.
Nature: 1–8

Buchan JR, Kolaitis R-M, Taylor JP, Parker R (2013)
Eukaryotic stress granules are cleared by autophagy and Cdc48/VCP function.
Cell 153: 1461–1474

Buchan JR, Parker R (2009)
Eukaryotic stress granules: the ins and outs of translation.
Mol Cell 36: 932–941

Buratti E (2015)
Functional Significance of TDP-43 Mutations in Disease. In *Advances in genetics,* Friedmann T, Dunlap JC, Goodwin SF (eds) pp. 1–53. Amsterdam: Academic Press

Buratti E (2018)
TDP-43 post-translational modifications in health and disease.
Expert opinion on therapeutic targets 22: 279–293

Buratti E, Brindisi A, Giombi M, Tisminetzky S, Ayala YM, Baralle FE (2005)
TDP-43 binds heterogeneous nuclear ribonucleoprotein A/B through its C-terminal tail: an important region for the inhibition of cystic fibrosis transmembrane conductance regulator exon 9 splicing.
Journal of Biological Chemistry 280: 37572–37584

Buratti E, Conti L de, Stuani C, Romano M, Baralle M, Baralle F (2010)
Nuclear factor TDP-43 can affect selected microRNA levels.
The FEBS journal 277: 2268–2281

Buratti E, Dörk T, Zuccato E, Pagani F, Romano M, Baralle FE (2001)
Nuclear factor TDP-43 and SR proteins promote in vitro and in vivo CFTR exon 9 skipping.
The EMBO journal 20: 1774–1784

Busch A, Hertel KJ (2012)
Evolution of SR protein and hnRNP splicing regulatory factors.
Wiley Interdiscip Rev RNA 3: 1–12

Cacace R, van Cauwenberghe C, Bettens K, Gijselinck I, van der Zee J, Engelborghs S, Vandenbulcke M, van Dongen J, Bäumer V, Dillen L et al (2013)
C9orf72 G4C2 repeat expansions in Alzheimer's disease and mild cognitive impairment.
Neurobiol Aging 34: 1712.e1-7

Carlomagno Y, Chung D-EC, Yue M, Castanedes-Casey M, Madden BJ, Dunmore J, Tong J, Deture M, Dickson DW, Petrucelli L et al (2017)
An acetylation-phosphorylation switch that regulates tau aggregation propensity and function.
Journal of Biological Chemistry 292: 15277–15286

Carlomagno Y, Zhang Y, Davis M, Lin W-L, Cook C, Dunmore J, Tay W, Menkosky K, Cao X, Petrucelli L et al (2014)
Casein kinase II induced polymerization of soluble TDP-43 into filaments is inhibited by heat shock proteins.
PLOS ONE 9: e90452

Carpenter K, Bell RB, Yunus J, Amon A, Berchowitz LE (2018)
Phosphorylation-Mediated Clearance of Amyloid-like Assemblies in Meiosis.
Developmental cell 45: 392-405.e6

Case LB, Zhang X, Ditlev JA, Rosen MK (2019)
Stoichiometry controls activity of phase-separated clusters of actin signaling proteins.
Science 363: 1093–1097

Chang C, Wu T-H, Wu C-Y, Chiang M, Toh EK-W, Hsu Y-C, Lin K-F, Liao Y, Huang T, Huang JJ-T (2012)
The N-terminus of TDP-43 promotes its oligomerization and enhances DNA binding affinity.
Biochemical and biophysical research communications 425: 219–224

Chen Z, Ma L (2010)
Grey matter volume changes over the whole brain in amyotrophic lateral sclerosis: A voxel-wise meta-analysis of voxel based morphometry studies.
Amyotroph Lateral Scler 11: 549–554

Cherkasov V, Hofmann S, Druffel-Augustin S, Mogk A, Tyedmers J, Stoecklin G, Bukau B (2013)
Coordination of translational control and protein homeostasis during severe heat stress.
Current biology : CB 23: 2452–2462

Chiò A, Mazzini L, D'Alfonso S, Corrado L, Canosa A, Moglia C, Manera U, Bersano E, Brunetti M, Barberis M et al (2018)
The multistep hypothesis of ALS revisited: The role of genetic mutations.
Neurology 91: e635-e642

Choksi DK, Roy B, Chatterjee S, Yusuff T, Bakhoum MF, Sengupta U, Ambegaokar S, Kayed R, Jackson GR (2014)
TDP-43 Phosphorylation by casein kinase Iε promotes oligomerization and enhances toxicity in vivo.
Human molecular genetics 23: 1025–1035

Chong PA, Vernon RM, Forman-Kay JD (2018)
RGG/RG Motif Regions in RNA Binding and Phase Separation.
Journal of Molecular Biology 430: 4650–4665

Chou C-C, Zhang Y, Umoh ME, Vaughan SW, Lorenzini I, Liu F, Sayegh M, Donlin-Asp PG, Chen YH, Duong DM et al (2018)
TDP-43 pathology disrupts nuclear pore complexes and nucleocytoplasmic transport in ALS/FTD.
Nat Neurosci 21: 228–239

Cohen TJ, Hwang AW, Restrepo CR, Yuan C-X, Trojanowski JQ, Lee VMY (2015)
An acetylation switch controls TDP-43 function and aggregation propensity.
Nat Commun 6: 5845

Cohen TJ, Hwang AW, Unger T, Trojanowski JQ, Lee VMY (2012)
Redox signalling directly regulates TDP-43 via cysteine oxidation and disulphide cross-linking.
The EMBO journal 31: 1241–1252

Colombrita C, Onesto E, Buratti E, La Grange P de, Gumina V, Baralle FE, Silani V, Ratti A (2015)
From transcriptomic to protein level changes in TDP-43 and FUS loss-of-function cell models.
Biochimica et biophysica acta 1849: 1398–1410

Conicella AE, Dignon GL, Zerze GH, Schmidt HB, D'Ordine AM, Kim YC, Rohatgi R, Ayala YM, Mittal J, Fawzi NL (2020)
TDP-43 α-helical structure tunes liquid-liquid phase separation and function.
PNAS 117: 5883–5894

Conicella AE, Zerze GH, Mittal J, Fawzi NL (2016)
ALS Mutations Disrupt Phase Separation Mediated by α-Helical Structure in the TDP-43 Low-Complexity C-Terminal Domain.
Structure (London, England : 1993) 24: 1537–1549

Conti L de, Akinyi MV, Mendoza-Maldonado R, Romano M, Baralle M, Buratti E (2015)
TDP-43 affects splicing profiles and isoform production of genes involved in the apoptotic and mitotic cellular pathways.
Nucleic Acids Res 43: 8990–9005

Cook C, Zhang Y, Xu Y-F, Dickson DW, Petrucelli L (2008)
TDP-43 in neurodegenerative disorders.
Expert opinion on biological therapy 8: 969–978

Courchaine EM, Lu A, Neugebauer KM (2016)
Droplet organelles?
The EMBO journal 35: 1603–1612

Crabtree MD, Holland J, Kompella P, Babl L, Turner N, Baldwin AJ, Nott TJ (2020)
Repulsive electrostatic interactions modulate dense and dilute phase properties of biomolecular condensates.
bioRxiv: 2020.10.29.357863

DeJesus-Hernandez M, Mackenzie IR, Boeve BF, Boxer AL, Baker M, Rutherford NJ, Nicholson AM, Finch NA, Flynn H, Adamson J et al (2011)
Expanded GGGGCC hexanucleotide repeat in noncoding region of C9ORF72 causes chromosome 9p-linked FTD and ALS.
Neuron 72: 245–256

Deng H-X, Chen W, Hong S-T, Boycott KM, Gorrie GH, Siddique N, Yang Y, Fecto F, Shi Y, Zhai H et al (2011)
Mutations in UBQLN2 cause dominant X-linked juvenile and adult-onset ALS and ALS/dementia.
Nature 477: 211–215

Dewey CM, Cenik B, Sephton CF, Dries DR, Mayer P, Good SK, Johnson BA, Herz J, Yu G (2011)
TDP-43 is directed to stress granules by sorbitol, a novel physiological osmotic and oxidative stressor.
Molecular and cellular biology 31: 1098–1108

Diekstra FP, van Deerlin VM, van Swieten JC, Al-Chalabi A, Ludolph AC, Weishaupt JH, Hardiman O, Landers JE, Brown RH, van Es MA et al (2014)
C9orf72 and UNC13A are shared risk loci for amyotrophic lateral sclerosis and frontotemporal dementia: a genome-wide meta-analysis.
Annals of Neurology 76: 120–133

Doble A (1996)
The pharmacology and mechanism of action of riluzole.
Neurology 47: S233-41

Dormann D, Capell A, Carlson AM, Shankaran SS, Rodde R, Neumann M, Kremmer E, Matsuwaki T, Yamanouchi K, Nishihara M et al (2009)
Proteolytic processing of TAR DNA binding protein-43 by caspases produces C-terminal fragments with disease defining properties independent of progranulin.
Journal of neurochemistry 110: 1082–1094

Dormann D, Haass C (2011)
TDP-43 and FUS: a nuclear affair.
Trends in neurosciences 34: 339–348

Dormann D, Rodde R, Edbauer D, Bentmann E, Fischer I, Hruscha A, Than ME, Mackenzie IRA, Capell A, Schmid B et al (2010)
ALS-associated fused in sarcoma (FUS) mutations disrupt Transportin-mediated nuclear import.
The EMBO journal 29: 2841–2857

Dreyfuss G, Kim VN, Kataoka N (2002)
Messenger-RNA-binding proteins and the messages they carry.
Nat Rev Mol Cell Biol 3: 195–205

Durocher D, Henckel J, Fersht AR, Jackson SP (1999)
The FHA Domain Is a Modular Phosphopeptide Recognition Motif.
Mol Cell 4: 387–394

Ederle H, Dormann D (2017)
TDP-43 and FUS en route from the nucleus to the cytoplasm.
FEBS letters 591: 1489–1507

Elden AC, Kim H-J, Hart MP, Chen-Plotkin AS, Johnson BS, Fang X, Armakola M, Geser F, Greene R, Lu MM et al (2010)
Ataxin-2 intermediate-length polyglutamine expansions are associated with increased risk for ALS.
Nature 466: 1069–1075

Elia LP, Reisine T, Alijagic A, Finkbeiner S (2020)
Approaches to develop therapeutics to treat frontotemporal dementia.
Neuropharmacology 166: 107948

Feiguin F, Godena VK, Romano G, D'Ambrogio A, Klima R, Baralle FE (2009)
Depletion of TDP-43 affects Drosophila motoneurons terminal synapsis and locomotive behavior.
FEBS letters 583: 1586–1592

Feiler MS, Strobel B, Freischmidt A, Helferich AM, Kappel J, Brewer BM, Li D, Thal DR, Walther P, Ludolph AC et al (2015)
TDP-43 is intercellularly transmitted across axon terminals.
J Cell Biol 211: 897–911

Ferreon JC, Jain A, Choi K-J, Tsoi PS, MacKenzie KR, Jung SY, Ferreon AC (2018)
Acetylation Disfavors Tau Phase Separation.
International journal of molecular sciences 19

Fiesel FC, Voigt A, Weber SS, van den Haute C, Waldenmaier A, Görner K, Walter M, Anderson ML, Kern JV, Rasse TM et al (2010)
Knockdown of transactive response DNA-binding protein (TDP-43) downregulates histone deacetylase 6.
The EMBO journal 29: 209–221

Fiesel FC, Weber SS, Supper J, Zell A, Kahle PJ (2012)
TDP-43 regulates global translational yield by splicing of exon junction complex component SKAR.
Nucleic Acids Res 40: 2668–2682

Forman MS, Farmer J, Johnson JK, Clark CM, Arnold SE, Coslett HB, Chatterjee A, Hurtig HI, Karlawish JH, Rosen HJ et al (2006)
Frontotemporal dementia: clinicopathological correlations.
Annals of Neurology 59: 952–962

Forman MS, Trojanowski JQ, Lee VM-Y (2004)
Neurodegenerative diseases: a decade of discoveries paves the way for therapeutic breakthroughs.
Nat Med 10: 1055–1063

Fratta P, Sivakumar P, Humphrey J, Lo K, Ricketts T, Oliveira H, Brito-Armas JM, Kalmar B, Ule A, Yu Y et al (2018)
Mice with endogenous TDP-43 mutations exhibit gain of splicing function and characteristics of amyotrophic lateral sclerosis.
The EMBO journal 37

Freibaum BD, Chitta RK, High AA, Taylor JP (2010)
Global analysis of TDP-43 interacting proteins reveals strong association with RNA splicing and translation machinery.
Journal of proteome research 9: 1104–1120

Fuhrmann J, Clancy KW, Thompson PR (2015)
Chemical biology of protein arginine modifications in epigenetic regulation.
Chemical Reviews 115: 5413–5461

Fujita K, Ito H, Nakano S, Kinoshita Y, Wate R, Kusaka H (2008)
Immunohistochemical identification of messenger RNA-related proteins in basophilic inclusions of adult-onset atypical motor neuron disease.
Acta Neuropathol 116: 439–445

Furukawa Y, Kaneko K, Watanabe S, Yamanaka K, Nukina N (2011)
A seeding reaction recapitulates intracellular formation of Sarkosyl-insoluble transactivation response element (TAR) DNA-binding protein-43 inclusions.
Journal of Biological Chemistry 286: 18664–18672

Ganassi M, Mateju D, Bigi I, Mediani L, Poser I, Lee HO, Seguin SJ, Morelli FF, Vinet J, Leo G et al (2016)
A Surveillance Function of the HSPB8-BAG3-HSP70 Chaperone Complex Ensures Stress Granule Integrity and Dynamism.
Molecular cell 63: 796–810

Gao J, Wang L, Huntley ML, Perry G, Wang X (2018)
Pathomechanisms of TDP-43 in neurodegeneration.
Journal of neurochemistry

Gao J, Wang L, Ren X, Dunn JR, Peters A, Miyagi M, Fujioka H, Zhao F, Askwith C, Liang J et al (2021)
Translational regulation in the brain by TDP-43 phase separation.
J Cell Biol 220

Gasset-Rosa F, Lu S, Yu H, Chen C, Melamed Z, Guo L, Shorter J, Da Cruz S, Cleveland DW (2019)
Cytoplasmic TDP-43 De-mixing Independent of Stress Granules Drives Inhibition of Nuclear Import, Loss of Nuclear TDP-43, and Cell Death.
Neuron 102: 339-357.e7

Gendron TF, Bieniek KF, Zhang Y, Jansen-West K, Ash PEA, Caulfield T, Daughrity L, Dunmore JH, Castanedes-Casey M, Chew J et al (2013)
Antisense transcripts of the expanded C9ORF72 hexanucleotide repeat form nuclear RNA foci and undergo repeat-associated non-ATG translation in c9FTD/ALS.
Acta Neuropathol 126: 829–844

Gitler AD, Tsuiji H (2016)
There has been an awakening: Emerging mechanisms of C9orf72 mutations in FTD/ALS.
Brain Res 1647: 19–29

Gomes E, Shorter J (2019)
The molecular language of membraneless organelles.
Journal of Biological Chemistry 294: 7115–7127

Grese ZR, Bastos AC, Mamede LD, French RL, Miller TM, Ayala YM (2021)
Specific RNA interactions promote TDP-43 multivalent phase separation and maintain liquid properties.
EMBO Rep: e53632

Gu J, Wang W, Miao S, Chen F, Wu F, Hu W, Iqbal K, Gong C-X, Liu F (2018)
Protein Phosphatase 1 dephosphorylates TDP-43 and suppresses its function in tau exon 10 inclusion.
FEBS letters 592: 402–410

Guenther EL, Cao Q, Trinh H, Lu J, Sawaya MR, Cascio D, Boyer DR, Rodriguez JA, Hughes MP, Eisenberg DS (2018)
Atomic structures of TDP-43 LCD segments and insights into reversible or pathogenic aggregation.
Nature structural & molecular biology 25: 463–471

Guillén-Boixet J, Buzon V, Salvatella X, Méndez R (2016)
CPEB4 is regulated during cell cycle by ERK2/Cdk1-mediated phosphorylation and its assembly into liquid-like droplets.
eLife Sciences Publications, Ltd

Guo L, Kim HJ, Wang H, Monaghan J, Freyermuth F, Sung JC, O'Donovan K, Fare CM, Diaz Z, Singh N et al (2018a)
Nuclear-Import Receptors Reverse Aberrant Phase Transitions of RNA-Binding Proteins with Prion-like Domains.
Cell 173: 677-692.e20

Guo Q, Lehmer C, Martínez-Sánchez A, Rudack T, Beck F, Hartmann H, Pérez-Berlanga M, Frottin F, Hipp MS, Hartl FU et al (2018b)
In Situ Structure of Neuronal C9orf72 Poly-GA Aggregates Reveals Proteasome Recruitment.
Cell 172: 696-705.e12

Hackman P, Sarparanta J, Lehtinen S, Vihola A, Evilä A, Jonson PH, Luque H, Kere J, Screen M, Chinnery PF et al (2013)
Welander distal myopathy is caused by a mutation in the RNA-binding protein TIA1.
Annals of Neurology 73: 500–509

Haeusler AR, Donnelly CJ, Periz G, Simko EAJ, Shaw PG, Kim M-S, Maragakis NJ, Troncoso JC, Pandey A, Sattler R et al (2014)
C9orf72 nucleotide repeat structures initiate molecular cascades of disease.
Nature 507: 195–200

Haj-Yahya M, Gopinath P, Rajasekhar K, Mirbaha H, Diamond MI, Lashuel HA (2020)
Site-Specific Hyperphosphorylation Inhibits, Rather than Promotes, Tau Fibrillization, Seeding Capacity, and Its Microtubule Binding.
Angew Chem Int Ed Engl 59: 4059–4067

Hallegger M, Chakrabarti AM, Lee FCY, Lee BL, Amalietti AG, Odeh HM, Copley KE, Rubien JD, Portz B, Kuret K et al (2021)
TDP-43 condensation properties specify its RNA-binding and regulatory repertoire.
Cell 184: 4680-4696.e22

Hardiman O, Al-Chalabi A, Chio A, Corr EM, Logroscino G, Robberecht W, Shaw PJ, Simmons Z, van den Berg LH (2017)
Amyotrophic lateral sclerosis.
Nat Rev Dis Primers 3: 17071

Hasegawa M, Arai T, Nonaka T, Kametani F, Yoshida M, Hashizume Y, Beach TG, Buratti E, Baralle F, Morita M et al (2008)
Phosphorylated TDP-43 in frontotemporal lobar degeneration and amyotrophic lateral sclerosis.
Annals of Neurology 64: 60–70

Hipp MS, Kasturi P, Hartl FU (2019)
The proteostasis network and its decline in ageing.
Nat Rev Mol Cell Biol 20: 421–435

Hofweber M, Dormann D (2019)
Friend or foe-Post-translational modifications as regulators of phase separation and RNP granule dynamics.
Journal of Biological Chemistry 294: 7137–7150

Hofweber M, Hutten S, Bourgeois B, Spreitzer E, Niedner-Boblenz A, Schifferer M, Ruepp M-D, Simons M, Niessing D, Madl T et al (2018)
Phase Separation of FUS Is Suppressed by Its Nuclear Import Receptor and Arginine Methylation.
Cell 173: 706-719.e13

Hoog CL de, Mann M (2004)
Proteomics.
Annu Rev Genomics Hum Genet 5: 267–293

Hornbeck PV, Kornhauser JM, Tkachev S, Zhang B, Skrzypek E, Murray B, Latham V, Sullivan M (2012)
PhosphoSitePlus: a comprehensive resource for investigating the structure and function of experimentally determined post-translational modifications in man and mouse.
Nucleic acids research 40: D261-70

Hornbeck PV, Zhang B, Murray B, Kornhauser JM, Latham V, Skrzypek E (2015)
PhosphoSitePlus, 2014: mutations, PTMs and recalibrations.
Nucleic acids research 43: D512-20

Hughes MP, Sawaya MR, Boyer DR, Goldschmidt L, Rodriguez JA, Cascio D, Chong L, Gonen T, Eisenberg DS (2018)
Atomic structures of low-complexity protein segments reveal kinked β sheets that assemble networks.
Science 359: 698–701

Hutten S, Dormann D (2020)
Nucleocytoplasmic transport defects in neurodegeneration - Cause or consequence?
Seminars in Cell & Developmental Biology 99: 151–162

Hutten S, Usluer S, Bourgeois B, Simonetti F, Odeh HM, Fare CM, Czuppa M, Hruska-Plochan M, Hofweber M, Polymenidou M et al (2020)
Nuclear Import Receptors Directly Bind to Arginine-Rich Dipeptide Repeat Proteins and Suppress Their Pathological Interactions.
Cell reports 33: 108538

Hutton M, Lendon CL, Rizzu P, Baker M, Froelich S, Houlden H, Pickering-Brown S, Chakraverty S, Isaacs A, Grover A et al (1998)
Association of missense and 5'-splice-site mutations in tau with the inherited dementia FTDP-17.
Nature 393: 702–705

Igaz LM, Kwong LK, Chen-Plotkin A, Winton MJ, Unger TL, Xu Y, Neumann M, Trojanowski JQ, Lee VM-Y (2009)
Expression of TDP-43 C-terminal Fragments in Vitro Recapitulates Pathological Features of TDP-43 Proteinopathies.
Journal of Biological Chemistry 284: 8516–8524

Igaz LM, Kwong LK, Xu Y, Truax AC, Uryu K, Neumann M, Clark CM, Elman LB, Miller BL, Grossman M et al (2008)
Enrichment of C-terminal fragments in TAR DNA-binding protein-43 cytoplasmic inclusions in brain but not in spinal cord of frontotemporal lobar degeneration and amyotrophic lateral sclerosis.
The American Journal of Pathology 173: 182–194

Inukai Y, Nonaka T, Arai T, Yoshida M, Hashizume Y, Beach TG, Buratti E, Baralle FE, Akiyama H, Hisanaga S et al (2008)
Abnormal phosphorylation of Ser409/410 of TDP-43 in FTLD-U and ALS.
FEBS letters 582: 2899–2904

Jain S, Wheeler JR, Walters RW, Agrawal A, Barsic A, Parker R (2016)
ATPase-Modulated Stress Granules Contain a Diverse Proteome and Substructure.
Cell 164: 487–498

Jamison JT, Kayali F, Rudolph J, Marshall M, Kimball SR, DeGracia DJ (2008)
Persistent redistribution of poly-adenylated mRNAs correlates with translation arrest and cell death following global brain ischemia and reperfusion.
Neuroscience 154: 504–520

Jiao B, Guo J, Wang Y, Yan X, Zhou L, Liu X, Zhang F, Zhou Y, Xia K, Tang B et al (2013)
C9orf72 mutation is rare in Alzheimer's disease, Parkinson's disease, and essential tremor in China.
Front. Cell. Neurosci. 7: 164

Jovičić A, Mertens J, Boeynaems S, Bogaert E, Chai N, Yamada SB, Paul JW, Sun S, Herdy JR, Bieri G et al (2015)
Modifiers of C9orf72 dipeptide repeat toxicity connect nucleocytoplasmic transport defects to FTD/ALS.
Nat Neurosci 18: 1226–1229

Jovičić A, Paul JW, Gitler AD (2016)
Nuclear transport dysfunction: a common theme in amyotrophic lateral sclerosis and frontotemporal dementia.
Journal of neurochemistry 138 Suppl 1: 134–144

Kabashi E, Lin L, Tradewell ML, Dion PA, Bercier V, Bourgouin P, Rochefort D, Bel Hadj S, Durham HD, Vande Velde C et al (2010)
Gain and loss of function of ALS-related mutations of TARDBP (TDP-43) cause motor deficits in vivo.
Human molecular genetics 19: 671–683

Kabashi E, Valdmanis PN, Dion P, Spiegelman D, McConkey BJ, Vande Velde C, Bouchard J-P, Lacomblez L, Pochigaeva K, Salachas F et al (2008)
TARDBP mutations in individuals with sporadic and familial amyotrophic lateral sclerosis.
Nat Genet 40: 572–574

Kametani F, Nonaka T, Suzuki T, Arai T, Dohmae N, Akiyama H, Hasegawa M (2009)
Identification of casein kinase-1 phosphorylation sites on TDP-43.
Biochemical and biophysical research communications 382: 405–409

Kametani F, Obi T, Shishido T, Akatsu H, Murayama S, Saito Y, Yoshida M, Hasegawa M (2016)
Mass spectrometric analysis of accumulated TDP-43 in amyotrophic lateral sclerosis brains.
Sci Rep 6: 23281

Kato M, Han TW, Xie S, Shi K, Du X, Wu LC, Mirzaei H, Goldsmith EJ, Longgood J, Pei J et al (2012)
Cell-free formation of RNA granules: low complexity sequence domains form dynamic fibers within hydrogels.
Cell 149: 753–767

Kato M, Lin Y, McKnight SL (2017)
Cross-β polymerization and hydrogel formation by low-complexity sequence proteins.
Methods (San Diego, Calif.) 126: 3–11

Kawahara Y, Mieda-Sato A (2012)
TDP-43 promotes microRNA biogenesis as a component of the Drosha and Dicer complexes.
PNAS 109: 3347–3352

Kayali F, Montie HL, Rafols JA, DeGracia DJ (2005)
Prolonged translation arrest in reperfused hippocampal cornu Ammonis 1 is mediated by stress granules.
Neuroscience 134: 1223–1245

Kedersha N, Ivanov P, Anderson P (2013)
Stress granules and cell signaling: more than just a passing phase?
Trends Biochem Sci 38: 494–506

Kiernan MC, Vucic S, Cheah BC, Turner MR, Eisen A, Hardiman O, Burrell JR, Zoing MC (2011)
Amyotrophic lateral sclerosis.
The Lancet 377: 942–955

Kim HJ, Kim NC, Wang Y-D, Scarborough EA, Moore J, Diaz Z, MacLea KS, Freibaum B, Li S, Molliex A et al (2013)
Mutations in prion-like domains in hnRNPA2B1 and hnRNPA1 cause multisystem proteinopathy and ALS.
Nature 495: 467–473

King OD, Gitler AD, Shorter J (2012)
The tip of the iceberg: RNA-binding proteins with prion-like domains in neurodegenerative disease.
Brain Res 1462: 61–80

Klim JR, Williams LA, Limone F, Guerra San Juan I, Davis-Dusenbery BN, Mordes DA, Burberry A, Steinbaugh MJ, Gamage KK, Kirchner R et al (2019)
ALS-implicated protein TDP-43 sustains levels of STMN2, a mediator of motor neuron growth and repair.
Nat Neurosci 22: 167–179

Kraemer BC, Schuck T, Wheeler JM, Robinson LC, Trojanowski JQ, Lee VMY, Schellenberg GD (2010)
Loss of murine TDP-43 disrupts motor function and plays an essential role in embryogenesis.
Acta Neuropathol 119: 409–419

Krisenko MO, Higgins RL, Ghosh S, Zhou Q, Trybula JS, Wang W-H, Geahlen RL (2015)
Syk Is Recruited to Stress Granules and Promotes Their Clearance through Autophagy.
Journal of Biological Chemistry 290: 27803–27815

Kroschwald S, Maharana S, Mateju D, Malinovska L, Nüske E, Poser I, Richter D, Alberti S (2015)
Promiscuous interactions and protein disaggregases determine the material state of stress-inducible RNP granules.
eLife

Kuo P-H, Chiang C-H, Wang Y-T, Doudeva LG, Yuan HS (2014)
The crystal structure of TDP-43 RRM1-DNA complex reveals the specific recognition for UG- and TG-rich nucleic acids.
Nucleic Acids Res 42: 4712–4722

Kwiatkowski TJ, Bosco DA, Leclerc AL, Tamrazian E, Vanderburg CR, Russ C, Davis A, Gilchrist J, Kasarskis EJ, Munsat T et al (2009)
Mutations in the FUS/TLS gene on chromosome 16 cause familial amyotrophic lateral sclerosis.
Science 323: 1205–1208

Lacomblez L, Bensimon G, Leigh PN, Guillet P, Meininger V (1996)
Dose-ranging study of riluzole in amyotrophic lateral sclerosis. Amyotrophic Lateral Sclerosis/Riluzole Study Group II.
The Lancet 347: 1425–1431

Lancaster AK, Nutter-Upham A, Lindquist S, King OD (2014)
PLAAC: a web and command-line application to identify proteins with prion-like amino acid composition.
Bioinformatics 30: 2501–2502

Laurents DV, Stuani C, Pantoja-Uceda D, Buratti E, Mompeán M (2021)
Aromatic and aliphatic residues of the disordered region of TDP-43 are on a fast track for self-assembly.
Biochemical and biophysical research communications 578: 110–114

Lee EB, Lee VM-Y, Trojanowski JQ (2011)
Gains or losses: molecular mechanisms of TDP43-mediated neurodegeneration.
Nat Rev Neurosci 13: 38–50

Lee K-H, Zhang P, Kim HJ, Mitrea DM, Sarkar M, Freibaum BD, Cika J, Coughlin M, Messing J, Molliex A et al (2016)
C9orf72 Dipeptide Repeats Impair the Assembly, Dynamics, and Function of Membrane-Less Organelles.
Cell 167: 774-788.e17

Lee Y-B, Chen H-J, Peres JN, Gomez-Deza J, Attig J, Stalekar M, Troakes C, Nishimura AL, Scotter EL, Vance C et al (2013)
Hexanucleotide repeats in ALS/FTD form length-dependent RNA foci, sequester RNA binding proteins, and are neurotoxic.
Cell reports 5: 1178–1186

Lemke EA (2016)
The Multiple Faces of Disordered Nucleoporins.
Journal of Molecular Biology 428: 2011–2024

Li H-R, Chen T-C, Hsiao C-L, Shi L, Chou C-Y, Huang J-R (2018a)
The physical forces mediating self-association and phase-separation in the C-terminal domain of TDP-43.
Biochimica et biophysica acta. Proteins and proteomics 1866: 214–223

Li H-R, Chiang W-C, Chou P-C, Wang W-J, Huang J-R (2018b)
TAR DNA-binding protein 43 (TDP-43) liquid-liquid phase separation is mediated by just a few aromatic residues.
J Biol Chem 293: 6090–6098

Li H-Y, Yeh P-A, Chiu H-C, Tang C-Y, Tu BP (2011)
Hyperphosphorylation as a defense mechanism to reduce TDP-43 aggregation.
PLOS ONE 6: e23075

Li P, Banjade S, Cheng H-C, Kim S, Chen B, Guo L, Llaguno M, Hollingsworth JV, King DS, Banani SF et al (2012)
Phase transitions in the assembly of multivalent signalling proteins.
Nature 483: 336–340

Li Q, Babinchak WM, Surewicz WK (2021)
Cryo-EM structure of amyloid fibrils formed by the entire low complexity domain of TDP-43.
Nat Commun 12: 1620

Li YR, King OD, Shorter J, Gitler AD (2013)
Stress granules as crucibles of ALS pathogenesis.
J Cell Biol 201: 361–372

Liachko NF, McMillan PJ, Guthrie CR, Bird TD, Leverenz JB, Kraemer BC (2013)
CDC7 inhibition blocks pathological TDP-43 phosphorylation and neurodegeneration.
Annals of Neurology 74: 39–52

Liachko NF, McMillan PJ, Strovas TJ, Loomis E, Greenup L, Murrell JR, Ghetti B, Raskind MA, Montine TJ, Bird TD et al (2014)
The tau tubulin kinases TTBK1/2 promote accumulation of pathological TDP-43.
PLOS Genetics 10: e1004803

Liachko NF, Saxton AD, McMillan PJ, Strovas TJ, Currey HN, Taylor LM, Wheeler JM, Oblak AL, Ghetti B, Montine TJ et al (2016)
The phosphatase calcineurin regulates pathological TDP-43 phosphorylation.
Acta Neuropathol 132: 545–561

Liao Y-C, Fernandopulle MS, Wang G, Choi H, Hao L, Drerup CM, Patel R, Qamar S, Nixon-Abell J, Shen Y et al (2019)
RNA Granules Hitchhike on Lysosomes for Long-Distance Transport, Using Annexin A11 as a Molecular Tether.
Cell 179: 147-164.e20

Ling JP, Pletnikova O, Troncoso JC, Wong PC (2015)
TDP-43 repression of nonconserved cryptic exons is compromised in ALS-FTD.
Science 349: 650–655

Ling S-C, Polymenidou M, Cleveland DW (2013)
Converging mechanisms in ALS and FTD: disrupted RNA and protein homeostasis.
Neuron 79: 416–438

Liu F, Li B, Tung E-J, Grundke-Iqbal I, Iqbal K, Gong C-X (2007)
Site-specific effects of tau phosphorylation on its microtubule assembly activity and self-aggregation.
The European journal of neuroscience 26: 3429–3436

Liu X, Shen J, Xie L, Wei Z, Wong C, Li Y, Zheng X, Li P, Song Y (2020)
Mitotic Implantation of the Transcription Factor Prospero via Phase Separation Drives Terminal Neuronal Differentiation.
Developmental cell 52: 277-293.e8

Liu-Yesucevitz L, Bilgutay A, Zhang Y, Vanderweyde T, Vanderwyde T, Citro A, Mehta T, Zaarur N, McKee A, Bowser R et al (2010)
Tar DNA binding protein-43 (TDP-43) associates with stress granules: analysis of cultured cells and pathological brain tissue.
PLOS ONE 5: e13250

Logroscino G, Traynor BJ, Hardiman O, Chiò A, Mitchell D, Swingler RJ, Millul A, Benn E, Beghi E (2010)
Incidence of amyotrophic lateral sclerosis in Europe.
J Neurol Neurosurg Psychiatry 81: 385–390

Lomen-Hoerth C, Anderson T, Miller B (2002)
The overlap of amyotrophic lateral sclerosis and frontotemporal dementia.
Neurology 59: 1077–1079

Lukavsky PJ, Daujotyte D, Tollervey JR, Ule J, Stuani C, Buratti E, Baralle FE, Damberger FF, Allain FH-T (2013)
Molecular basis of UG-rich RNA recognition by the human splicing factor TDP-43.
Nature structural & molecular biology 20: 1443–1449

Ma XR, Prudencio M, Koike Y, Vatsavayai SC, Kim G, Harbinski F, Briner A, Rodriguez CM, Guo C, Akiyama T et al (2022)
TDP-43 represses cryptic exon inclusion in the FTD–ALS gene UNC13A.
Nature: 1–7

Mackenzie IR, Nicholson AM, Sarkar M, Messing J, Purice MD, Pottier C, Annu K, Baker M, Perkerson RB, Kurti A et al (2017)
TIA1 Mutations in Amyotrophic Lateral Sclerosis and Frontotemporal Dementia Promote Phase Separation and Alter Stress Granule Dynamics.
Neuron 95: 808-816.e9

Mackenzie IRA, Baker M, Pickering-Brown S, Hsiung G-YR, Lindholm C, Dwosh E, Gass J, Cannon A, Rademakers R, Hutton M et al (2006)
The neuropathology of frontotemporal lobar degeneration caused by mutations in the progranulin gene.
Brain: A Journal of Neurology 129: 3081–3090

Mackenzie IRA, Bigio EH, Ince PG, Geser F, Neumann M, Cairns NJ, Kwong LK, Forman MS, Ravits J, Stewart H et al (2007)
Pathological TDP-43 distinguishes sporadic amyotrophic lateral sclerosis from amyotrophic lateral sclerosis with SOD1 mutations.
Annals of Neurology 61: 427–434

Mackenzie IRA, Neumann M (2016)
Molecular neuropathology of frontotemporal dementia: insights into disease mechanisms from postmortem studies.
Journal of neurochemistry 138 Suppl 1: 54–70

Mackenzie IRA, Rademakers R, Neumann M (2010)
TDP-43 and FUS in amyotrophic lateral sclerosis and frontotemporal dementia.
The Lancet Neurology 9: 995–1007

Maharana S, Wang J, Papadopoulos DK, Richter D, Pozniakovsky A, Poser I, Bickle M, Rizk S, Guillén-Boixet J, Franzmann TM et al (2018)
RNA buffers the phase separation behavior of prion-like RNA binding proteins.
Science 360: 918–921

Mahboubi H, Barisé R, Stochaj U (2015)
5'-AMP-activated protein kinase alpha regulates stress granule biogenesis.
Biochimica et biophysica acta 1853: 1725–1737

Mahboubi H, Koromilas AE, Stochaj U (2016)
AMP Kinase Activation Alters Oxidant-Induced Stress Granule Assembly by Modulating Cell Signaling and Microtubule Organization.
Mol Pharmacol 90: 460–468

Mann JR, Gleixner AM, Mauna JC, Gomes E, DeChellis-Marks MR, Needham PG, Copley KE, Hurtle B, Portz B, Pyles NJ et al (2019)
RNA Binding Antagonizes Neurotoxic Phase Transitions of TDP-43.
Neuron 102: 321-338.e8

Martin EW, Holehouse AS (2020)
Intrinsically disordered protein regions and phase separation: sequence determinants of assembly or lack thereof.
Emerging topics in life sciences 4: 307–329

Martínez-González L, Gonzalo-Consuegra C, Gómez-Almería M, Porras G, Lago E de, Martín-Requero Á, Martínez A (2021)
Tideglusib, a Non-ATP Competitive Inhibitor of GSK-3β as a Drug Candidate for the Treatment of Amyotrophic Lateral Sclerosis.
International journal of molecular sciences 22

Martínez-González L, Rodríguez-Cueto C, Cabezudo D, Bartolomé F, Andrés-Benito P, Ferrer I, Gil C, Martín-Requero Á, Fernández-Ruiz J, Martínez A et al (2020)
Motor neuron preservation and decrease of in vivo TDP-43 phosphorylation by protein CK-1δ kinase inhibitor treatment.
Sci Rep 10: 4449

Mateju D, Franzmann TM, Patel A, Kopach A, Boczek EE, Maharana S, Lee HO, Carra S, Hyman AA, Alberti S (2017)
An aberrant phase transition of stress granules triggered by misfolded protein and prevented by chaperone function.
The EMBO journal 36: 1669–1687

Maxwell BA, Gwon Y, Mishra A, Peng J, Nakamura H, Zhang K, Kim HJ, Taylor JP (2021)
Ubiquitination is essential for recovery of cellular activities after heat shock.
Science 372: eabc3593

McDonald KK, Aulas A, Destroismaisons L, Pickles S, Beleac E, Camu W, Rouleau GA, Vande Velde C (2011)
TAR DNA-binding protein 43 (TDP-43) regulates stress granule dynamics via differential regulation of G3BP and TIA-1.
Human molecular genetics 20: 1400–1410

McGurk L, Lee VM, Trojanowksi JQ, van Deerlin VM, Lee EB, Bonini NM (2014)
Poly-A binding protein-1 localization to a subset of TDP-43 inclusions in amyotrophic lateral sclerosis occurs more frequently in patients harboring an expansion in C9orf72.
Journal of neuropathology and experimental neurology 73: 837–845

Melamed Z, López-Erauskin J, Baughn MW, Zhang O, Drenner K, Sun Y, Freyermuth F, McMahon MA, Beccari MS, Artates JW et al (2019)
Premature polyadenylation-mediated loss of stathmin-2 is a hallmark of TDP-43-dependent neurodegeneration.
Nat Neurosci 22: 180–190

Mészáros B, Erdos G, Dosztányi Z (2018)
IUPred2A: context-dependent prediction of protein disorder as a function of redox state and protein binding.
Nucleic Acids Res 46: W329-W337

Miao L, St Clair DK (2009)
Regulation of superoxide dismutase genes: implications in disease.
Free radical biology & medicine 47: 344–356

Mittag T, Parker R (2018)
Multiple Modes of Protein-Protein Interactions Promote RNP Granule Assembly.
Journal of Molecular Biology 430: 4636–4649

Molliex A, Temirov J, Lee J, Coughlin M, Kanagaraj AP, Kim HJ, Mittag T, Taylor JP (2015)
Phase separation by low complexity domains promotes stress granule assembly and drives pathological fibrillization.
Cell 163: 123–133

Monahan Z, Ryan VH, Janke AM, Burke KA, Rhoads SN, Zerze GH, O'Meally R, Dignon GL, Conicella AE, Zheng W et al (2017)
Phosphorylation of the FUS low-complexity domain disrupts phase separation, aggregation, and toxicity.
The EMBO journal 36: 2951–2967

Morato JG, Hans F, Zweydorf F von, Feederle R, Elsässer SJ, Skodras AA, Gloeckner CJ, Buratti E, Neumann M, Kahle PJ (2020)
Sirtuin-1 Sensitive Lysine-136 Acetylation Drives Phase Separation and Pathological Aggregation of TDP-43.
bioRxiv: 2020.05.26.104356

Moreno JA, Halliday M, Molloy C, Radford H, Verity N, Axten JM, Ortori CA, Willis AE, Fischer PM, Barrett DA et al (2013)
Oral treatment targeting the unfolded protein response prevents neurodegeneration and clinical disease in prion-infected mice.
Science translational medicine 5: 206ra138

Morimoto D, Walinda E, Fukada H, Sou Y-S, Kageyama S, Hoshino M, Fujii T, Tsuchiya H, Saeki Y, Arita K et al (2015)
The unexpected role of polyubiquitin chains in the formation of fibrillar aggregates.
Nat Commun 6: 6116

Murakami T, Qamar S, Lin JQ, Schierle GSK, Rees E, Miyashita A, Costa AR, Dodd RB, Chan FTS, Michel CH et al (2015)
ALS/FTD Mutation-Induced Phase Transition of FUS Liquid Droplets and Reversible Hydrogels into Irreversible Hydrogels Impairs RNP Granule Function.
Neuron 88: 678–690

Nagano S, Jinno J, Abdelhamid RF, Jin Y, Shibata M, Watanabe S, Hirokawa S, Nishizawa M, Sakimura K, Onodera O et al (2020)
TDP-43 transports ribosomal protein mRNA to regulate axonal local translation in neuronal axons.
Acta Neuropathol 140: 695–713

Nedelsky NB, Taylor JP (2019)
Bridging biophysics and neurology: aberrant phase transitions in neurodegenerative disease.
Nat Rev Neurol 15: 272–286

Neumann M, Frick P, Paron F, Kosten J, Buratti E, Mackenzie IR (2021)
Correction to: Antibody against TDP-43 phosphorylated at serine 369 suggests conformational differences of TDP-43 aggregates among FTLD-TDP subtypes.
Acta Neuropathol 141: 137

Neumann M, Kwong LK, Lee EB, Kremmer E, Flatley A, Xu Y, Forman MS, Troost D, Kretzschmar HA, Trojanowski JQ et al (2009a)
Phosphorylation of S409/410 of TDP-43 is a consistent feature in all sporadic and familial forms of TDP-43 proteinopathies.
Acta Neuropathol 117: 137–149

Neumann M, Rademakers R, Roeber S, Baker M, Kretzschmar HA, Mackenzie IRA (2009b)
A new subtype of frontotemporal lobar degeneration with FUS pathology.
Brain: A Journal of Neurology 132: 2922–2931

Neumann M, Sampathu DM, Kwong LK, Truax AC, Micsenyi MC, Chou TT, Bruce J, Schuck T, Grossman M, Clark CM et al (2006)
Ubiquitinated TDP-43 in frontotemporal lobar degeneration and amyotrophic lateral sclerosis.
Science 314: 130–133

Nishimura AL, Župunski V, Troakes C, Kathe C, Fratta P, Howell M, Gallo J-M, Hortobágyi T, Shaw CE, Rogelj B (2010)
Nuclear import impairment causes cytoplasmic trans-activation response DNA-binding protein accumulation and is associated with frontotemporal lobar degeneration.
Brain: A Journal of Neurology 133: 1763–1771

Nonaka T, Suzuki G, Tanaka Y, Kametani F, Hirai S, Okado H, Miyashita T, Saitoe M, Akiyama H, Masai H et al (2016)
Phosphorylation of TAR DNA-binding Protein of 43 kDa (TDP-43) by Truncated Casein Kinase 1δ Triggers Mislocalization and Accumulation of TDP-43.
Journal of Biological Chemistry 291: 5473–5483

Nott TJ, Petsalaki E, Farber P, Jervis D, Fussner E, Plochowietz A, Craggs TD, Bazett-Jones DP, Pawson T, Forman-Kay JD et al (2015)
Phase transition of a disordered nuage protein generates environmentally responsive membraneless organelles.
Mol Cell 57: 936–947

Nozal V, Martínez-González L, Gomez-Almeria M, Gonzalo-Consuegra C, Santana P, Chaikuad A, Pérez-Cuevas E, Knapp S, Lietha D, Ramírez D et al (2022)
TDP-43 Modulation by Tau-Tubulin Kinase 1 Inhibitors: A New Avenue for Future Amyotrophic Lateral Sclerosis Therapy.
Journal of Medicinal Chemistry 65: 1585–1607

Olney RK, Murphy J, Forshew D, Garwood E, Miller BL, Langmore S, Kohn MA, Lomen-Hoerth C (2005)
The effects of executive and behavioral dysfunction on the course of ALS.
Neurology 65: 1774–1777

Olsen JV, Blagoev B, Gnad F, Macek B, Kumar C, Mortensen P, Mann M (2006)
Global, in vivo, and site-specific phosphorylation dynamics in signaling networks.
Cell 127: 635–648

Onyike CU, Diehl-Schmid J (2013)
The epidemiology of frontotemporal dementia.
Int Rev Psychiatry 25: 130–137

Ou SH, Wu F, Harrich D, García-Martínez LF, Gaynor RB (1995)
Cloning and characterization of a novel cellular protein, TDP-43, that binds to human immunodeficiency virus type 1 TAR DNA sequence motifs.
J Virol 69: 3584–3596

Patel A, Lee HO, Jawerth L, Maharana S, Jahnel M, Hein MY, Stoynov S, Mahamid J, Saha S, Franzmann TM et al (2015)
A Liquid-to-Solid Phase Transition of the ALS Protein FUS Accelerated by Disease Mutation.
Cell 162: 1066–1077

Patel A, Malinovska L, Saha S, Wang J, Alberti S, Krishnan Y, Hyman AA (2017)
ATP as a biological hydrotrope.
Science 356: 753–756

Pirie E, Oh C, Zhang X, Han X, Cieplak P, Scott HR, Deal AK, Ghatak S, Martinez FJ, Yeo GW et al (2021)
S-nitrosylated TDP-43 triggers aggregation, cell-to-cell spread, and neurotoxicity in hiPSCs and in vivo models of ALS/FTD.
PNAS 118

Placek K, Baer GM, Elman L, McCluskey L, Hennessy L, Ferraro PM, Lee EB, Lee VMY, Trojanowski JQ, van Deerlin VM et al (2019)
UNC13A polymorphism contributes to frontotemporal disease in sporadic amyotrophic lateral sclerosis.
Neurobiol Aging 73: 190–199

Polymenidou M, Cleveland DW (2011)
The seeds of neurodegeneration: prion-like spreading in ALS.
Cell 147: 498–508

Polymenidou M, Lagier-Tourenne C, Hutt KR, Huelga SC, Moran J, Liang TY, Ling S-C, Sun E, Wancewicz E, Mazur C et al (2011)
Long pre-mRNA depletion and RNA missplicing contribute to neuronal vulnerability from loss of TDP-43.
Nat Neurosci 14: 459–468

Porta S, Xu Y, Restrepo CR, Kwong LK, Zhang B, Brown HJ, Lee EB, Trojanowski JQ, Lee VM-Y (2018)
Patient-derived frontotemporal lobar degeneration brain extracts induce formation and spreading of TDP-43 pathology in vivo.
Nat Commun 9: 4220

Prouteau M, Loewith R (2018)
Regulation of Cellular Metabolism through Phase Separation of Enzymes.
Biomolecules 8: 160

Qamar S, Wang G, Randle SJ, Ruggeri FS, Varela JA, Lin JQ, Phillips EC, Miyashita A, Williams D, Ströhl F et al (2018)
FUS Phase Separation Is Modulated by a Molecular Chaperone and Methylation of Arginine Cation-π Interactions.
Cell 173: 720-734.e15

Rai AK, Chen J-X, Selbach M, Pelkmans L (2018)
Kinase-controlled phase transition of membraneless organelles in mitosis.
Nature 559: 211–216

Ratti A, Buratti E (2016)
Physiological functions and pathobiology of TDP-43 and FUS/TLS proteins.
Journal of neurochemistry 138 Suppl 1: 95–111

Renton AE, Majounie E, Waite A, Simón-Sánchez J, Rollinson S, Gibbs JR, Schymick JC, Laaksovirta H, van Swieten JC, Myllykangas L et al (2011)
A hexanucleotide repeat expansion in C9ORF72 is the cause of chromosome 9p21-linked ALS-FTD.
Neuron 72: 257–268

Riemenschneider H, Guo Q, Bader J, Frottin F, Farny D, Kleinberger G, Haass C, Mann M, Hartl FU, Baumeister W et al (2021)
Gel-like inclusions of C-terminal fragments of TDP-43 sequester and inhibit proteasomes in neurons.
bioRxiv: 2021.03.15.435268

Rigbolt KTG, Prokhorova TA, Akimov V, Henningsen J, Johansen PT, Kratchmarova I, Kassem M, Mann M, Olsen JV, Blagoev B (2011)
System-wide temporal characterization of the proteome and phosphoproteome of human embryonic stem cell differentiation.
Science signaling 4: rs3

Ritson GP, Custer SK, Freibaum BD, Guinto JB, Geffel D, Moore J, Tang W, Winton MJ, Neumann M, Trojanowski JQ et al (2010)
TDP-43 mediates degeneration in a novel Drosophila model of disease caused by mutations in VCP/p97.
J Neurosci (Journal of Neuroscience) 30: 7729–7739

Robberecht W, Philips T (2013)
The changing scene of amyotrophic lateral sclerosis.
Nat Rev Neurosci 14: 248–264

Rohrer JD, Guerreiro R, Vandrovcova J, Uphill J, Reiman D, Beck J, Isaacs AM, Authier A, Ferrari R, Fox NC et al (2009)
The heritability and genetics of frontotemporal lobar degeneration.
Neurology 73: 1451–1456

Rosen DR, Siddique T, Patterson D, Figlewicz DA, Sapp P, Hentati A, Donaldson D, Goto J, O'Regan JP, Deng HX (1993)
Mutations in Cu/Zn superoxide dismutase gene are associated with familial amyotrophic lateral sclerosis.
Nature 362: 59–62

Rowland LP, Shneider NA (2001)
Amyotrophic lateral sclerosis.
N Engl J Med 344: 1688–1700

Ryan VH, Dignon GL, Zerze GH, Chabata CV, Silva R, Conicella AE, Amaya J, Burke KA, Mittal J, Fawzi NL (2018)
Mechanistic View of hnRNPA2 Low-Complexity Domain Structure, Interactions, and Phase Separation Altered by Mutation and Arginine Methylation.
Molecular cell 69: 465-479.e7

Ryan VH, Perdikari TM, Naik MT, Saueressig CF, Lins J, Dignon GL, Mittal J, Hart AC, Fawzi NL (2021)
Tyrosine phosphorylation regulates hnRNPA2 granule protein partitioning and reduces neurodegeneration.
The EMBO journal 40: e105001

Saito M, Hess D, Eglinger J, Fritsch AW, Kreysing M, Weinert BT, Choudhary C, Matthias P (2019)
Acetylation of intrinsically disordered regions regulates phase separation.
Nat Chem Biol 15: 51–61

Salado IG, Redondo M, Bello ML, Perez C, Liachko NF, Kraemer BC, Miguel L, Lecourtois M, Gil C, Martinez A et al (2014)
Protein kinase CK-1 inhibitors as new potential drugs for amyotrophic lateral sclerosis.
Journal of Medicinal Chemistry 57: 2755–2772

Schmid B, Hruscha A, Hogl S, Banzhaf-Strathmann J, Strecker K, van der Zee J, Teucke M, Eimer S, Hegermann J, Kittelmann M et al (2013)
Loss of ALS-associated TDP-43 in zebrafish causes muscle degeneration, vascular dysfunction, and reduced motor neuron axon outgrowth.
PNAS 110: 4986–4991

Schmidt HB, Barreau A, Rohatgi R (2019)
Phase separation-deficient TDP43 remains functional in splicing.
Nat Commun 10: 4890

Sephton CF, Cenik C, Kucukural A, Dammer EB, Cenik B, Han Y, Dewey CM, Roth FP, Herz J, Peng J et al (2011)
Identification of Neuronal RNA Targets of TDP-43-containing Ribonucleoprotein Complexes.
Journal of Biological Chemistry 286: 1204–1215

Sephton CF, Good SK, Atkin S, Dewey CM, Mayer P, Herz J, Yu G (2010)
TDP-43 is a developmentally regulated protein essential for early embryonic development.
J Biol Chem 285: 6826–6834

Serber Z, Ferrell JE (2007)
Tuning bulk electrostatics to regulate protein function.
Cell 128: 441–444

Shiga A, Ishihara T, Miyashita A, Kuwabara M, Kato T, Watanabe N, Yamahira A, Kondo C, Yokoseki A, Takahashi M et al (2012)
Alteration of POLDIP3 splicing associated with loss of function of TDP-43 in tissues affected with ALS.
PLOS ONE 7: e43120

Shin Y, Brangwynne CP (2017)
Liquid phase condensation in cell physiology and disease.
Science 357

Siddique N, Siddique T (2021)
Amyotrophic Lateral Sclerosis Overview.
Gene Reviews

Snead WT, Gladfelter AS (2019)
The Control Centers of Biomolecular Phase Separation: How Membrane Surfaces, PTMs, and Active Processes Regulate Condensation.
Molecular cell 76: 295–305

Solomon DA, Stepto A, Au WH, Adachi Y, Diaper DC, Hall R, Rekhi A, Boudi A, Tziortzouda P, Lee Y-B et al (2018)
A feedback loop between dipeptide-repeat protein, TDP-43 and karyopherin-α mediates C9orf72-related neurodegeneration.
Brain: A Journal of Neurology 141: 2908–2924

Sreedharan J, Blair IP, Tripathi VB, Hu X, Vance C, Rogelj B, Ackerley S, Durnall JC, Williams KL, Buratti E et al (2008)
TDP-43 mutations in familial and sporadic amyotrophic lateral sclerosis.
Science 319: 1668–1672

Stallings NR, Puttaparthi K, Luther CM, Burns DK, Elliott JL (2010)
Progressive motor weakness in transgenic mice expressing human TDP-43.
Neurobiol Dis 40: 404–414

Sternburg EL, Gruijs da Silva, Lara A., Dormann D (2022)
Post-translational modifications on RNA-binding proteins: accelerators, brakes, or passengers in neurodegeneration?
Trends Biochem Sci 47: 6–22

Stewart H, Rutherford NJ, Briemberg H, Krieger C, Cashman N, Fabros M, Baker M, Fok A, DeJesus-Hernandez M, Eisen A et al (2012)
Clinical and pathological features of amyotrophic lateral sclerosis caused by mutation in the C9ORF72 gene on chromosome 9p.
Acta Neuropathol 123: 409–417

Strickfaden SC, Winters MJ, Ben-Ari G, Lamson RE, Tyers M, Pryciak PM (2007)
A mechanism for cell-cycle regulation of MAP kinase signaling in a yeast differentiation pathway.
Cell 128: 519–531

Strong MJ, Volkening K, Hammond R, Yang W, Strong W, Leystra-Lantz C, Shoesmith C (2007)
TDP43 is a human low molecular weight neurofilament (hNFL) mRNA-binding protein.
Molecular and cellular neurosciences 35: 320–327

Tan C-F, Eguchi H, Tagawa A, Onodera O, Iwasaki T, Tsujino A, Nishizawa M, Kakita A, Takahashi H (2007)
TDP-43 immunoreactivity in neuronal inclusions in familial amyotrophic lateral sclerosis with or without SOD1 gene mutation.
Acta Neuropathol 113: 535–542

Tanikawa C, Ueda K, Suzuki A, Iida A, Nakamura R, Atsuta N, Tohnai G, Sobue G, Saichi N, Momozawa Y et al (2018)
Citrullination of RGG Motifs in FET Proteins by PAD4 Regulates Protein Aggregation and ALS Susceptibility.
Cell reports 22: 1473–1483

Taylor LM, McMillan PJ, Liachko NF, Strovas TJ, Ghetti B, Bird TD, Keene CD, Kraemer BC (2018)
Pathological phosphorylation of tau and TDP-43 by TTBK1 and TTBK2 drives neurodegeneration.
Mol Neurodegeneration 13: 7

Tollervey JR, Curk T, Rogelj B, Briese M, Cereda M, Kayikci M, König J, Hortobágyi T, Nishimura AL, Zupunski V et al (2011)
Characterizing the RNA targets and position-dependent splicing regulation by TDP-43.
Nat Neurosci 14: 452–458

Tsang B, Arsenault J, Vernon RM, Lin H, Sonenberg N, Wang L-Y, Bah A, Forman-Kay JD (2019)
Phosphoregulated FMRP phase separation models activity-dependent translation through bidirectional control of mRNA granule formation.
PNAS 116: 4218–4227

Tyedmers J, Mogk A, Bukau B (2010)
Cellular strategies for controlling protein aggregation.
Nat Rev Mol Cell Biol 11: 777–788

van Damme P, Robberech W, van den Bosch L (2017)
Modelling amyotrophic lateral sclerosis: progress and possibilities.
The Company of Biologists

van Engelen M-PE, Gossink FT, Vijlder LS de, Meursing JRA, Scheltens P, Dols A, Pijnenburg YAL (2020)
End Stage Clinical Features and Cause of Death of Behavioral Variant Frontotemporal Dementia and Young-Onset Alzheimer's Disease.
J Alzheimers Dis 77: 1169–1180

van Es MA, Hardiman O, Chio A, Al-Chalabi A, Pasterkamp RJ, Veldink JH, van den Berg LH (2017)
Amyotrophic lateral sclerosis.
The Lancet 390: 2084–2098

van Es MA, Veldink JH, Saris CGJ, Blauw HM, van Vught PWJ, Birve A, Lemmens R, Schelhaas HJ, Groen EJN, Huisman MHB et al (2009)
Genome-wide association study identifies 19p13.3 (UNC13A) and 9p21.2 as susceptibility loci for sporadic amyotrophic lateral sclerosis.
Nat Genet 41: 1083–1087

Vance C, Rogelj B, Hortobágyi T, Vos KJ de, Nishimura AL, Sreedharan J, Hu X, Smith B, Ruddy D, Wright P et al (2009)
Mutations in FUS, an RNA processing protein, cause familial amyotrophic lateral sclerosis type 6.
Science 323: 1208–1211

Vance C, Scotter EL, Nishimura AL, Troakes C, Mitchell JC, Kathe C, Urwin H, Manser C, Miller CC, Hortobágyi T et al (2013)
ALS mutant FUS disrupts nuclear localization and sequesters wild-type FUS within cytoplasmic stress granules.
Human molecular genetics 22: 2676–2688

Vanderweyde T, Apicco DJ, Youmans-Kidder K, Ash PEA, Cook C, Da Lummertz Rocha E, Jansen-West K, Frame AA, Citro A, Leszyk JD et al (2016)
Interaction of tau with the RNA-Binding Protein TIA1 Regulates tau Pathophysiology and Toxicity.
Cell reports 15: 1455–1466

Vanderweyde T, Yu H, Varnum M, Liu-Yesucevitz L, Citro A, Ikezu T, Duff K, Wolozin B (2012)
Contrasting pathology of the stress granule proteins TIA-1 and G3BP in tauopathies.
J Neurosci (Journal of Neuroscience) 32: 8270–8283

Vatsavayai SC, Yoon SJ, Gardner RC, Gendron TF, Vargas JNS, Trujillo A, Pribadi M, Phillips JJ, Gaus SE, Hixson JD et al (2016)
Timing and significance of pathological features in C9orf72 expansion-associated frontotemporal dementia.
Brain: A Journal of Neurology 139: 3202–3216

Volkening K, Leystra-Lantz C, Yang W, Jaffee H, Strong MJ (2009)
Tar DNA binding protein of 43 kDa (TDP-43), 14-3-3 proteins and copper/zinc superoxide dismutase (SOD1) interact to modulate NFL mRNA stability. Implications for altered RNA processing in amyotrophic lateral sclerosis (ALS).
Brain Res 1305: 168–182

Vossenaar ER, Zendman AJW, van Venrooij WJ, Pruijn GJM (2003)
PAD, a growing family of citrullinating enzymes: genes, features and involvement in disease.
BioEssays : news and reviews in molecular, cellular and developmental biology 25: 1106–1118

Vucic S, Higashihara M, Sobue G, Atsuta N, Doi Y, Kuwabara S, Kim SH, Kim I, Oh K-W, Park J et al (2020)
ALS is a multistep process in South Korean, Japanese, and Australian patients.
Neurology 94: e1657-e1663

Wallace EWJ, Kear-Scott JL, Pilipenko EV, Schwartz MH, Laskowski PR, Rojek AE, Katanski CD, Riback JA, Dion MF, Franks AM et al (2015)
Reversible, Specific, Active Aggregates of Endogenous Proteins Assemble upon Heat Stress.
Cell 162: 1286–1298

Wang A, Conicella AE, Schmidt HB, Martin EW, Rhoads SN, Reeb AN, Nourse A, Ramirez Montero D, Ryan VH, Rohatgi R et al (2018a)
A single N-terminal phosphomimic disrupts TDP-43 polymerization, phase separation, and RNA splicing.
The EMBO journal 37

Wang C, Duan Y, Duan G, Wang Q, Zhang K, Deng X, Qian B, Gu J, Ma Z, Zhang S et al (2020)
Stress Induces Dynamic, Cytotoxicity-Antagonizing TDP-43 Nuclear Bodies via Paraspeckle LncRNA NEAT1-Mediated Liquid-Liquid Phase Separation.
Mol Cell 79: 443-458.e7

Wang H-Y, Wang I-F, Bose J, Shen C-K (2004a)
Structural diversity and functional implications of the eukaryotic TDP gene family.
Genomics 83: 130–139

Wang I-F, Wu L-S, Chang H-Y, Shen C-KJ (2008)
TDP-43, the signature protein of FTLD-U, is a neuronal activity-responsive factor.
Journal of neurochemistry 105: 797–806

Wang J, Choi J-M, Holehouse AS, Lee HO, Zhang X, Jahnel M, Maharana S, Lemaitre R, Pozniakovsky A, Drechsel D et al (2018b)
A Molecular Grammar Governing the Driving Forces for Phase Separation of Prion-like RNA Binding Proteins.
Cell 174: 688-699.e16

Wang P, Wander CM, Yuan C-X, Bereman MS, Cohen TJ (2017)
Acetylation-induced TDP-43 pathology is suppressed by an HSF1-dependent chaperone program.
Nat Commun 8: 82

Wang S-J, Wang K-Y, Wang W-C (2004b)
Mechanisms underlying the riluzole inhibition of glutamate release from rat cerebral cortex nerve terminals (synaptosomes).
Neuroscience 125: 191–201

Wang Y, Mandelkow E (2016)
Tau in physiology and pathology.
Nat Rev Neurosci 17: 5–21

Warren JD, Rohrer JD, Rossor MN (2013)
Clinical review. Frontotemporal dementia.
BMJ 347: f4827

Weber SC, Brangwynne CP (2012)
Getting RNA and protein in phase.
Cell 149: 1188–1191

Wegmann S, Eftekharzadeh B, Tepper K, Zoltowska KM, Bennett RE, Dujardin S, Laskowski PR, MacKenzie D, Kamath T, Commins C et al (2018)
Tau protein liquid-liquid phase separation can initiate tau aggregation.
The EMBO journal 37

Wippich F, Bodenmiller B, Trajkovska MG, Wanka S, Aebersold R, Pelkmans L (2013)
Dual specificity kinase DYRK3 couples stress granule condensation/dissolution to mTORC1 signaling.
Cell 152: 791–805

Wootton JC, Federhen S (1993)
Statistics of local complexity in amino acid sequences and sequence databases.
Computers & Chemistry 17: 149–163

Xiao S, Sanelli T, Dib S, Sheps D, Findlater J, Bilbao J, Keith J, Zinman L, Rogaeva E, Robertson J (2011)
RNA targets of TDP-43 identified by UV-CLIP are deregulated in ALS.
Molecular and cellular neurosciences 47: 167–180

Yaffe MB, Rittinger K, Volinia S, Caron PR, Aitken A, Leffers H, Gamblin SJ, Smerdon SJ, Cantley LC (1997)
The Structural Basis for 14-3-3:Phosphopeptide Binding Specificity.
Cell 91: 961–971

Yang C, Tan W, Whittle C, Qiu L, Cao L, Akbarian S, Xu Z (2010)
The C-terminal TDP-43 fragments have a high aggregation propensity and harm neurons by a dominant-negative mechanism.
PLOS ONE 5: e15878

Yasuda S, Tsuchiya H, Kaiho A, Guo Q, Ikeuchi K, Endo A, Arai N, Ohtake F, Murata S, Inada T et al (2020)
Stress- and ubiquitylation-dependent phase separation of the proteasome.
Nature 578: 296–300

Yerbury JJ, Farrawell NE, McAlary L (2020)
Proteome Homeostasis Dysfunction: A Unifying Principle in ALS Pathogenesis.
Trends in neurosciences 43: 274–284

Yoshizawa T, Ali R, Jiou J, Fung HYJ, Burke KA, Kim SJ, Lin Y, Peeples WB, Saltzberg D, Soniat M et al (2018)
Nuclear Import Receptor Inhibits Phase Separation of FUS through Binding to Multiple Sites.
Cell 173: 693-705.e22

Zeng M, Chen X, Guan D, Xu J, Wu H, Tong P, Zhang M (2018)
Reconstituted Postsynaptic Density as a Molecular Platform for Understanding Synapse Formation and Plasticity.
Cell 174: 1172-1187.e16

Zhang K, Daigle JG, Cunningham KM, Coyne AN, Ruan K, Grima JC, Bowen KE, Wadhwa H, Yang P, Rigo F et al (2018)
Stress Granule Assembly Disrupts Nucleocytoplasmic Transport.
Cell 173: 958-971.e17

Zhang K, Donnelly CJ, Haeusler AR, Grima JC, Machamer JB, Steinwald P, Daley EL, Miller SJ, Cunningham KM, Vidensky S et al (2015)
The C9orf72 repeat expansion disrupts nucleocytoplasmic transport.
Nature 525: 56–61

Zhang P, Fan B, Yang P, Temirov J, Messing J, Kim HJ, Taylor JP (2019)
Chronic optogenetic induction of stress granules is cytotoxic and reveals the evolution of ALS-FTD pathology.
eLife

Zhang Y, Xu Y-F, Cook C, Gendron TF, Roettges P, Link CD, Lin W-L, Tong J, Castanedes-Casey M, Ash P et al (2009)
Aberrant cleavage of TDP-43 enhances aggregation and cellular toxicity.
PNAS 106: 7607–7612

Zhao M-J, Yao X, Wei P, Zhao C, Cheng M, Zhang D, Xue W, He W-T, Xue W, Zuo X et al (2021)
O-GlcNAcylation of TDP-43 suppresses proteinopathies and promotes TDP-43's mRNA splicing activity.
EMBO Rep 22: e51649

Zhou H, Huang C, Chen H, Wang D, Landel CP, Xia PY, Bowser R, Liu Y-J, Xia XG (2010)
Transgenic rat model of neurodegeneration caused by mutation in the TDP gene.
PLOS Genetics 6: e1000887

VI Acknowledgements

Firstly, I would like to express my thanks to my supportive supervisor, Dorothee Dormann, who has given me constant advice, guidance and support throughout my PhD project. Her immense knowledge and constant, contagious positive attitude have encouraged me in all the time of my academic research journey.

I would like to thank all my lab colleagues (+ DD alumni) for sharing their knowledge, for all their help in and outside of the lab, for the great team work, and for all the fun moments throughout these last 4 years.

My appreciation also goes out to my family and friends for their encouragement and support. Last but not least I want to thank Patrick for being always there and for making me smile no matter what.

VIII List of publications

Gruijs da Silva LA, Dormann D (In Press)
Sedimentation assays to assess the impact of post-translational modifications on phase separation of RNA-binding proteins in vitro and in cells. In Phase-Separated Biomolecular Condensates.
Huan-Xiang Zhou, Jan-Hendrik Spille, and Priya Banerjee (ed): Springer Nature

Gruijs da Silva LA, Simonetti F, Hutten S, Riemenschneider H, Sternburg EL, Pietrek LM, Gebel J, Dötsch V, Edbauer D, Hummer G et al (2022)
Disease-linked TDP-43 hyperphosphorylation suppresses TDP-43 condensation and aggregation.
The EMBO journal: e108443

Sternburg EL, **Gruijs da Silva LA**, Dormann D (2022)
Post-translational modifications on RNA-binding proteins: accelerators, brakes, or passengers in neurodegeneration?
Trends Biochem Sci 47: 6–22

Bento-Abreu A, Jager G, Swinnen B, Rué L, Hendrickx S, Jones A, Staats KA, Taes I, Eykens C, Nonneman A, Nuyts R, Timmers M, **Silva L**, Chariot A, Nguyen L, Ravits J et al (2018)
Elongator subunit 3 (ELP3) modifies ALS through tRNA modification.
Human molecular genetics 27: 1276–1289

IX Eidesstattliche Versicherung/Affidavit

Lara Aletta Gruijs da Silva

(Studierende / Student)

Hiermit versichere ich an Eides statt, dass ich die vorliegende Dissertation

Driving forces of TDP-43 phase transitions and their physiological and pathological consequences in cells

selbstständig angefertigt habe, mich außer der angegebenen keiner weiteren Hilfsmittel bedient und alle Erkenntnisse, die aus dem Schrifttum ganz oder annähernd übernommen sind, als solche kenntlich gemacht und nach ihrer Herkunft unter Bezeichnung der Fundstelle einzeln nachgewiesen habe.

I hereby confirm that the dissertation

Driving forces of TDP-43 phase transitions and their physiological and pathological consequences in cells

is the result of my own work and that I have only used sources or materials listed and specified in the dissertation.

München / Munich

04.07.2022 Lara Aletta Gruijs da Silva

(Datum / Date) (Unterschrift / Signature)

X Declaration of copyright and contributions

Lara A. Gruijs da Silva wrote the thesis text, performed most experiments, and prepared most of the figures.

As first author of **publication I**, I contributed to the design of the described methods, wrote the manuscript, and performed all the experimental work.

As first author of **publication II**, I contributed to the study design, manuscript writing and conducted the majority of the experimental work. I performed most of the experiments with some exceptions, as described below.

As second author of **publication III**, I contributed to the review design and created all the figures of the manuscript. See below for more details. *Elsevier* holds the copyright (2021) for this article published in *Trends in Biochemical Sciences* and permits its usage in this dissertation.

München / Munich

(Datum / Date) (Unterschrift / Signature)

Prof. Dr. Dorothee Dormann, supervisor and research group leader, developed the design of the project and coordinated involved collaborators (e.g., communication with collaborators and exchange expression vectors). Dorothee Dormann is the senior/corresponding author of the three publications of this PhD thesis and consequently operates as a representative for contributing co-authors, which are listed below.

Publication II, "Disease-linked TDP-43 hyperphosphorylation suppresses TDP-43 condensation and aggregation" published at The EMBO Journal, had contributions of the following researchers/co-authors (for details see table 1 below):

1) Lukas S. Stelzl conducted and analyzed the atomistic and coarse-grained simulations.

2) Francesca Simonetti conducted the aggregation assay, the semi-denaturing detergent agarose gel electrophoresis (SDD-AGE) and some of the experiments with primary hippocampal neurons.

3) Saskia Hutten conducted and analyzed the nuclear import and the semi-permeabilized cell assays.

4) Henrick Riemenschneider prepared lentiviral constructs and conducted most experiments with primary hippocampal neurons.

5) Erin L. Sternburg conducted the electrophoretic mobility shift assays (EMSA).

Figure 2D-F, appendix figure S3	Aggregation assay and Semi-denaturing detergent agarose gel electrophoresis conducted by Francesca Simonetti
Figure 3, EV3, appendix figure S4, S5, Table S1	Atomistic and coarse-grained simulations conducted by Lukas S. Stelzl
Figure 4A, B	Hormone-inducible nuclear import assay conducted and quantified by Saskia Hutten
Figure 4D, EV4B	Electrophoretic mobility shift assays conducted by Erin L. Sternburg
Figure 5C, D, EV5A, B	Stress granule recruitment assay in semi-permeabilized cells conducted and quantified by Saskia Hutten
Figure 6C	Filter trap assay conducted by Henrick Riemenschneider
Figure 6D, E, appendix figure S8	Primary hippocampal neural experiments (localization, and SG recruitment) conducted by Henrick Riemenschneider and Francesca Simonetti

Table X.1: Summary of contributions to publication II by other researchers.

Mainz

(Datum / Date) (Unterschrift / Signature)

Publication III, "Post-translational modifications on RNA-binding proteins: accelerators, brakes, or passengers in neurodegeneration?" a review article published at Trends in Biochemical Sciences, had the contribution of the following researcher/co-author:

1) Erin L. Sternburg, postdoctoral researcher in the research group of Dorothee Dormann, wrote the manuscript and is the first author of this review article.

Mainz

_____ _____

(Datum / Date) (Unterschrift / Signatur